8-2021

Development of Density-Functional Tight-Binding Methods for Chemical Energy Science

Quan Vuong
University of Tennessee, Knoxville, qvuong@vols.utk.edu

To the Graduate Council:

I am submitting herewith a dissertation written by Quan Vuong entitled "Development of Density-Functional Tight-Binding Methods for Chemical Energy Science." I have examined the final electronic copy of this dissertation for form and content and recommend that it be accepted in partial fulfillment of the requirements for the degree of Doctor of Philosophy, with a major in Energy Science and Engineering.

Stephan Irle, Major Professor

We have read this dissertation and recommend its acceptance:

Stephan Irle, David J. Keffer, Hong Guo, Paul R Kent

Accepted for the Council:

Dixie L. Thompson

Vice Provost and Dean of the Graduate School

(Original signatures are on file with official student records.)

Development of Density-Functional Tight-Binding Methods for Chemical Energy Science

A Dissertation Presented for the

Doctor of Philosophy

Degree

The University of Tennessee, Knoxville

Van Quan Vuong

August 2021

Dedication to my family, Caitrang, and Asa

Acknowledgments

I want to give a great appreciation and a special acknowledgment to my supervisor, Dr. Stephan Irle. His guidance has eternally been my most helpful guideline. I would like to thank Jenica Marie L. Madridejos, Dr. Gregory F. Metha, Dr. Balint Aradi for the work collaboration of the Au-P parameterization. I would like to thank Ka Hung Lee and Dr. Victor Fung for the work collaboration of the Pt-(Pt, Ti, O) parameterization. I would like to thank Dr. Yoshio Nishimoto, Dr. Dmitri G. Fedorov, Dr. Thomas A. Niehaus, and Dr. Bobby G. Sumpter for the work collaboration of the FMO-LC-DFTB development. I would also like to acknowledge my Ph.D. committee members, Dr. David Keffer, Hong Guo, and Paul R Kent, for their guidance and intriguing scientific discussions. I also appreciate GS Jung, Rabi Khanal, Ke Yuan, and members of the FIRST Center and the C4WARD project for all the help.

I would like to thank the financial support of the Energy Science and Engineering Fellowship of the Bredesen Center for Interdisciplinary Research and Graduate Education at the University of Tennessee, Knoxville. In addition, I would like to thank the support of the LDRD, FIRST EFRC, and C4WARD programs of Oak Ridge National Laboratory.

Abstract

Density-functional tight-binding (DFTB) method is an approximation to the popular first-principles density functional theory (DFT) method. Recently, DFTB has gained considerable visibility due to its inexpensive computational requirements that confer it the capability of sustaining long-timescale reactive molecular dynamics (MD) simulations while providing an explicit description of electronic structure at all time steps. This capability allows the description of bond formation and breaking processes, as well as charge polarization and charge transfer phenomena, with accuracy and transferability beyond comparable classical reactive force fields. It has thus been employed successfully in the simulation of many complex chemical processes. However, its applications for chemical energy science, particularly for the development of chemical energy storage systems and industry-scale catalysts are limited due to the lack of carefully validated parameters, specially for transition metal elements. In this dissertation, my previously developed DFTBparaopt semi-automatic parameterization was therefore employed for the development of two sets of urgently needed DFTB parameters involving prominent transition metals, (1) for phosphine-stabilized nanoscale gold clusters, and (2) for platinum nanoparticles in the vacuum and on TiO_2 support. Performances of the newly developed DFTB parameters were validated extensively against DFT geometries, binding energies, electronic structure, and chemisorption for gold and platinum clusters. With the new parameters, the DFTB method can be used to investigate Au-cluster or Pt-clusters catalysts, and can be expected to pave the way for the future development of improved catalytic systems. In addition to these parameterizations, I focused on the development of an accurate DFTB-based linear-scaling method capable of describing zwitterionic systems for the simulation of electrolytes. To realize this method, the combination of the fragment molecular orbital (FMO) approach with the recently developed

long-range corrected DFTB (LC-DFTB) method had been selected and implemented. Initial benchmarks and demonstration applications are presented. A satisfactory accuracy and computational performance of FMO-LC-DFTB has been demonstrated. The new method offers advanced capabilities for the first principles-based modeling of large-size ionic liquids, ions interaction with electrodes, and other chemical energy storage systems. The lessons learned in this dissertation point to areas for future improvements of the DFTB method that will enhance its accuracy and the transferability of its parameters even further.

Table of Contents

List of Tables

List of Figures

Chapter 1

Introduction

Notwithstanding recent improvements in modern electrochemical energy storage technologies, addressing the many critical requirements such as achieving simultaneously high energy density (amount of energy stored) and high power density (the rate at which the material can be charged or discharged) remains a challenge.[1–5] Energy science, most notably in the branches related to industrial catalysis and electrochemical energy storage, involves highly complex reactive chemical processes, as well as phenomena related to ion and electron transport.[6] Transformational processes in energy science-related materials often occur on long time and length scales, ranging from the atomic to the macro scale. They typically involve multiple chemical component systems, comprised of transition metal catalysts, substrates, electrolytes and solvents, and chemically reactive species. Experimental design of novel materials that address energy science challenges by trial-and-error requires a tremendous amount of time and resources, including materials cost and manpower. In order to alleviate these issues, computational methods have been developed to provide theoretical insight and predictions for chemically reactive systems at the atomic level, rationalize experimental data, and guide the design of materials at the atomic-scale.[7–10] However, computer-aided design approaches and their underlying methodologies have thus far had relatively limited impact on energy sciences in general, mostly due to the lack of computational chemistry methodology that is both predictive as well as manageable in terms of time to solution and computer resources. For example, classical simulations that are computationally inexpensive are often held back by the lack of accurate interatomic potentials, specifically when metal elements

are involved, whereas first principles-based quantum chemical methods require a tremendous amount of computer resources for large-size and long-timescale simulations.[7,11] Therefore, the development of simpler yet robust computational approaches remains a crucially important area in the field of chemical energy science.

Over the last century, a wide range of computational chemistry and materials sciences atomic-scale simulation methods has been developed, either based on classical molecular mechanics (MM) or quantum mechanics (QM) approaches. Most MM-based force fields (FF) approximate the "covalently bonded" atomic interactions using simple empirical potentials, such as the harmonic potential with no explicit description of electronic structure.[12–16] Consequently, MM-based methods require a set of pre-fitted parameters for different types of atoms, chemical bonds, and bond angles for each system. Due to such simplifications, MM-based methods are typically much faster than QM-based methods and are capable to perform molecular dynamics (MD) simulations for systems consisting of up to several hundred million atoms. They are usually employed to study large-scale non-reactive molecular dynamic processes, such as protein folding or transport through membranes. However, these methods often fail in describing covalent bond breaking or bond formation processes, both of which are essential in chemical processes. Recent advancements in the MM-based FFs include reactive force fields such as ReaxFF,[17] which utilize bond order potentials to enable the simulation of bond breaking and formation processes. Nevertheless, their low transferability and inability to describe charge polarization or electronic charge transfer phenomena, limits their application to systems close to those for which they were trained.[18] On the other side of the spectrum, fully QM-based approaches such as ab initio wave function theory (WFT) or first principles density functional theory (DFT) methods explicitly solve the electronic structure of molecular or solid-state systems based on the time-independent Schrödinger equation. These QM-based methods are capable of simulating reactive chemical processes and dynamics, and can reliably predict electronic properties such as electronic band structures, polarization, and charge transfer. However, the QM-based methods can only be employed for picosecond-scale simulations of systems containing a few hundred in routine applications.[19,20] Reactive dynamics simulations of larger systems and on nanosecond scale are practically out of reach due to the prohibitive computational cost that increases exponentially with the system size.

To address the need for computationally inexpensive yet reliable quantum chemical methods, various semi-empirical quantum mechanical (SQM) approaches based on the Hartree-Fock (HF) method were proposed fifty years ago, such as the complete neglect of differential overlap (CNDO), the intermediate neglect of differential overlap (INDO), the neglect of diatomic differential overlap (NDDO), and the modified neglect of diatomic overlap (MNDO) methods.[21–23] More sophisticated SQM methods have been developed mostly based on the foundation of the MNDO approach for the ground state computations such as AM1,[24] PM3,[25,26] PM6,[27] and PM7,[28] to name a few prominent examples. In addition, OM1,[29] OM2,[30] and OM3[31] methods have been developed to improve excited state computations, based on explicit orthogonalization corrections within the NDDO approach. Generally, these approximated methods are 2-3 orders of magnitude faster than the conventional DFT or HF methods and are capable of describing chemical reactions, but unfortunately often with a lower accuracy.[19,32–34] In parallel to these HF-based SQM methods, the density-functional tight-binding (DFTB) formalism emerged as a very promising family of approximate DFT methods that can be viewed as a semi-empirical incarnation of Kohn-Sham DFT methods. DFTB methods often outperform other HF-based semi-empirical methods with respect to accuracy in both geometries and energies due to their DFT origin that explicitly addresses the issue of electron correlation.[33,35–37] Like HF-based SQM methods, DFTB solves the time-independent Schrödinger equation using a minimum basis set for the valence electrons only. However, a key difference of the DFTB methods to HF-based SQM methods is the employment of pre-tabulated Kohn-Sham Hamiltonian and basis set overlap matrix elements in a two-center approximation. While this approach avoids the explicit computation of expensive integrals, it still improves the accuracy over HF-based SQM approaches which either neglect or approximate the integrals as simple parameters or analytical functions. Since the three-center terms can often be neglected to good accuracy in the construction of the Hamiltonian and the four-center integrals can be approximated by way of self-consistent charge (SCC) extensions, the DFTB method can often reach the accuracy level found in conventional DFT methods.[32,38] With these features, DFTB extends the time scale of DFT-quality MD simulations of systems containing 400 atoms to nanoseconds.[39] Ultimately, in combination with recently implemented massively parallel linear-scaling approaches

such as the fragment molecular orbital (FMO) method,[40–45] the divide-and-conquer (DC) method[46–48] or modified DC (mDC) method,[49] geometry optimization for a system consist of a million atoms or MD simulations at the nanosecond-scale for system up to several thousand atoms have also become feasible.[41,45]

Over the last 25 years, several different formulations for the DFTB methods have been developed. Based on the Foulkes-Haydock approach,[50] the Kohn & Sham (KS)-DFT energy[51,52] is expanded in terms of electron density fluctuation $\Delta\rho$ around a reference density, using a Taylor series expansion. The individual terms of the Taylor series give rise to a hierarchical series of DFTB methods, starting with the simplest version, DFTB1,[53,54] which is accurate to the first-order expansion. It is identical to the method that was historically called DFTB, since the first-order term of the Taylor series vanishes. The latest iteration of the approach, called DFTB3, contains the full third-order term of the Taylor series.[55] Also, it is worth mentioning that a simplified version of this DFTB3 method was recently developed by Grimme et al., named GFN-xTB.[56] In the following, these DFTB versions will be explained in some more detail.

DFTB1 is a non-self-consistent-charge (NCC)-DFTB method because its Hamiltonian is independent of the electron density fluctuation $\Delta\rho$, which makes it the fastest among the DFTB versions. Yet, it is suitable only for systems with small interatomic charge transfer and cannot be applied to systems where charge transfer is a dominant feature.[38,57] DFTB2 extends the applicability of DFTB to such systems by including the second-order term of the Taylor expansion, which explicitly covers long-range Coulomb interactions and on-site charge interaction energies.[58] Because the DFTB2 Hamiltonian depends on electron density differences $\Delta\rho$ from the reference density used to construct the DFTB1 Hamiltonian, the second-order term can only be determined after solving the (KS)-DFT equation. This implies that the DFTB2 Kohn-Sham problem must be solved iteratively, since its Hamiltonian explicitly depends on the difference charge. Therefore, the DFTB2 method was originally called self-consistent charge DFTB or SCC-DFTB. The DFTB2 method significantly improved the accuracy of the DFTB method, making it more suitable to describe polar systems.[38,57] However, problems persisted related to important proton transfer barriers

and proton affinities, as well as the description of anionic systems, and therefore the third-order term of the Taylor expansion was explicitly considered. This led to the development of the DFTB3 method, in which the third-order term allows the atomic chemical hardness (incorporated in DFTB as the so-called "Hubbard" parameter) to variate depending on the charge state at the respective atom.[33,38,55,59] Finally, the GFN-xTB simplifies DFTB3 in the sense that it replaces explicit parameterization of the two-center Hamiltonian matrix elements and binary repulsive potentials based on combinations of carefully fitted mono-elemental equivalents. Therefore, it is less accurate when it comes to the description of interaction energies, particularly for transition states and activation energies, which are essential for catalysis and ion transport phenomena under investigation in this dissertation.

Despite the many advantages mentioned above, the applicability of the DFTB method in chemical energy sciences remains limited due to the lack of transferable and carefully validated parameters for different chemical element combinations across the periodic table. Currently, optimized parameters for most DFTB methods are available only for a handful of bio and organic elements, and a few incomplete sets of parameters available for selected transition metal elements like Sc, Ti, Fe, Co, and Ni in the "trans3d" set,[60] Au in the "auorg" set,[61] and Ti in the "tiorg" set.[62] Among the many missing parameters for transition metal elements, two notable chemical elements, Au and Pt are particularly valuable in catalysis applications. Nanoscale gold clusters have demonstrated high catalytic activity and selectivity for certain reactions at low temperatures, such as the oxidation of carbon monoxide, propene, alcohols, or the hydrogenation of acetylene.[63–66] On the other hand, platinum is well-known for its highly effective and selective catalytic behaviour in both heterogeneous and homogeneous systems, for instance, the catalytic reforming of straight-run naphthas, hydrogen evolution reactions, the decomposition of hydrogen peroxide, or the reduction of oxygen. Particularly, platinum nanoparticles (Pt-NPs) supported on titania surfaces are often used as effective heterogeneous catalysts in industrial processes. In order to capture and understand the chemical reaction mechanisms of these complex catalytic systems, it is vital to understand and be able to predict the variation of electronic structure, chemical bond breaking and formation that occur during the dynamic processes. The practically infinite number of possible side reactions and other dynamic processes are able to

exert a significance, adverse effect on the catalytic performance.[67,68] In order to employ DFTB methods for the theoretical studies of these systems, it is thus necessary to provide accurate parameters for all binary chemical element interactions found in the systems. In the case of ligated nanoscale Au clusters, the most prominent ligands are thiols and phophines, that complex the metal nanoclusters via Au-S and Au-P interactions. While the Au-S interaction was included in the "auorg" parameter set for gold-thiolate clusters,[61,69] the parameters for the Au-P interaction had previously not been developed. In the case of Pt, only pure Pt-Pt parameters were available, for the description of platinum clusters in the gas phase.[70–72] However, even in these cases, the existing DFTB parameters either severely overestimate or underestimate Pt-Pt interactions and lack transferability.

The fundamental difficulty associated with the parameterization is related to finding a meaningful balance between DFTB accuracy and parameter transferability for a wide range of elements, molecular systems, and condensed systems. Historically, the parameterization procedure required significant human effort. In realizing the need, several groups had already developed a number of "semi-automatic" DFTB parameterization schemes.[73–76] However, none of these efforts was able to significantly impact the DFTB parameterization efforts, due a number of factors, such as: (1) the lack of a user-friendly interface, (2) computational inefficiencies, (3) rapidly converging search algorithms that would trap the algorithm in local minima,[74,75] or (4) a combination of these factors. To address these issues, I developed as part of my Master Thesis a robust automatic genetic algorithm (GA)-based parameterization program, the so-called DFTBparaopt.[77] The program is based of a semi-automatic scheme that solves for a set of linear equations, developed originally by Gaus et al.[78] The GA was employed to optimize the remaining non-linear parameters and to reduce the dependence on the initial guess while increasing the chances for finding the global minimum in the scoring function, i.e. the errors for reproducing the target fitting quantities. The parameterization protocol was successfully employed to optimize long-range corrected (LC)-DFTB parameters for C, H, N, and O chemical elements simultaneously. In this Ph.D. dissertation, the GA-based parameterization protocol was further improved and used to extend the "auorg" parameter set for Au to include the Au-P interaction. The Pt-X (X = Pt, Ti, O) interactions were also parameterized using the same GA-based protocol to describe platinum clusters with

an emphasis on Pt atom and clusters on TiO_2 support. The parameterization for Pt was based on a previous titania parameterization.[62] The accuracy of these new DFTB parameters in terms of geometries, energetic properties, and electronic structures was validated against full DFT and available experimental results. The DFTBparaopt code is now publicly available on github and it is hoped that it will enable more rapid parameterization of additional chemical element combinations for any of the DFTB methods currently available.

In addition to the lack of parameters, all traditional DFTB methods and their linear-scaling incarnations, which are derived from local-density approximations (LDA) or generalized gradient approximations (GGA) DFT functionals, can fail to describe zwitterionic systems containing opposite electric charges, such as ionic liquids or metalloprotein enzyme. This failure is inherited from DFT on which DFTB is founded, and is due to the so-called self-interaction error (SIE).[79,80] The spurious repulsion of an electron with its own electron density artificially stabilizes delocalized states, leading to a variety of computational artifacts, such as charge equilibration, underestimation of frontier orbital energy gaps in molecules and band gaps in bulk materials, and charge-transfer excitation energies. Similarily, the overestimation of conductance, incorrect description of activation energies for chemical reactions, and binding energies in charge-transfer complexes could also be attribute to these artifacts.[79,81–88] Recently, a long-range corrected (LC) version of the second-order DFTB[58] has been developed to overcome these drawbacks.[89,90] Analogous to the long-range corrected DFT methods,[91–94] the LC-DFTB2 splits electron-electron interactions into short-range and long-range contributions. The short-range interaction is computed by a DFT exchange-correlation functional, while the long-range interaction is computed by the HF exchange, which is sometimes also called "exact exchange".[89] The LC-DFTB2 method systematically corrects the underestimation of the DFTB HOMO-LUMO gap for small molecules and zwitterionic proteins in ground-state calculations and thereby enables the correct description of zwitterions.[77,90] Furthermore, the LC-DFTB2 method can be used to provide correct thermochemistry, geometries, and vibrational frequencies.[77] The computational cost of the LC-DFTB2 method is more expensive than traditional DFTB methods due to the additional calculations needed to compute the long-range HF exchange term, nevertheless, it is still orders of magnitude faster than traditional LC-DFT methods.[90] To expand the applicability

of the LC-DFTB2 method, it is necessary to achieve linear scaling with system size. Therefore, in this dissertation, the linear-scaling LC-DFTB2 method was introduced on top of the FMO framework, referred to as FMO-LC-DFTB. The FMO-LC-DFTB method was implemented in the GAMESS-US program.[95,96] Its performance was assessed for various ionic systems, including ionic liquids and proteins. The development of FMO-LC-DFTB enables large and longtime scale simulations of ionic liquids and metalloprotein enzymes, which are important material components in energy science.

The rest of the dissertation is organized as follows. In Chapter 2, the theoretical background of WFT, DFT, DFTB, FMO, and ReaxFF methods are briefly presented. In Chapter 3, the parameterization and benchmark of DFTB for phosphine-stabilized nanoscale gold clusters are presented. A case study for a large cluster $Au_{108}S_{24}(PPh_3)_{16}$ using DFTB with the optimized parameters is also mentioned to highlight the predictive capabilities of the new parameter set. In Chapter 4, the parameterization and benchmark of DFTB for Pt nanoparticles and bulk in vacuum and on TiO_2 support are presented. The dynamics of Pt atom on TiO_2 surface are demonstrated and discussed. In Chapter 5, the combination of the FMO approach with the LC-DFTB method and its applicability are presented. Finally, Chapter 6 concludes with a summary and future prospects of these works.

Chapter 2

Background Theories

2.1 Introduction to Quantum Chemistry

Quantum chemistry (QC) is a sub-field in quantum mechanics (QM) developed to understand the electronic structure of atoms, molecules, and solids from first principles. The central equation in QC is the Schrödinger equation,[97] from which the wave function of a system can be obtained. In QM, the state of a system can be completely described by Schrödinger's "wave function", and all observable properties of a system can be calculated from it. In the scope of this dissertation, we will only consider the non-relativistic and time-independent Schrödinger equation

$$\mathcal{H}\Psi = \varepsilon\Psi, \tag{2.1}$$

where $\mathcal{H}$ is the Hamiltonian operator of the system, Ψ is the wave function describing the state of the system, and ε is the energy of the system. In atomic units, the Hamiltonian operator for a system consisting of nuclei and electrons can be written as

$$\mathcal{H} = -\frac{1}{2}\sum_{i=1}^{N}\nabla_i^2 - \frac{1}{2}\sum_{A=1}^{M}\frac{1}{M_A}\nabla_A^2 - \sum_{i=1}^{N}\sum_{A=1}^{M}\frac{Z_A}{r_{iA}} + \sum_{i=1}^{N}\sum_{j>i}^{N}\frac{1}{r_{ij}} + \sum_{A=1}^{M}\sum_{B>A}^{M}\frac{Z_A Z_B}{R_{AB}}. \tag{2.2}$$

Here, N and M are the numbers of electrons and nuclei respectively, M_A is the mass of nucleus A in atomic unit, Z_A is the atomic number of nucleus A, r_{ij}, r_{iA}, and R_{AB} are the distance between the ith and jth electrons, the ith electrons and Ath nucleus, and Ath and Bth

nucleus, respectively. Since the nuclei are much heavier than the electrons, they move much slower than the other. Thus, one can consider electrons as particles moving in the field of fixed nuclei. The kinetic energy of the nuclei can thus be neglected, and the nuclear repulsive term can be considered as a constant for a given molecular or crystal geometry. This concept of electrons in a field of fixed nuclei is known as the Born-Oppenheimer approximation. The remaining Hamiltonian operator is called the electronic Hamiltonian

$$\mathcal{H}^{elec} = -\frac{1}{2}\sum_{i=1}^{N}\nabla_i^2 - \sum_{i=1}^{N}\sum_{A=1}^{M}\frac{Z_A}{r_{iA}} + \sum_{i=1}^{N}\sum_{j>i}^{N}\frac{1}{r_{ij}}. \tag{2.3}$$

Equation 2.1 could then be rewritten for a given atomic configuration as

$$\mathcal{H}^{elec}\Psi^{elec} = \varepsilon^{elec}\Psi^{elec}, \tag{2.4}$$

where Ψ^{elec} is the electronic wave function describing the motion of electrons in the field of the fixed nuclei. Unfortunately, in most cases, the analytical solution of equation 2.4 is unknown. Over the last century, since the birth of QM, two main quantum approaches have been established to provide approximate solutions to the Schrödinger equation, namely ab initio wave function theory (WFT) and first-principles density functional theory (DFT). In the following, I will describe the foundations of WFT, namely Hartree-Fock theory, DFT, an approximation to DFT called density-functional tight-binding (DFTB), a linear-scaling approach called the fragment molecular orbital (FMO), and a popular, computationally less expensive simulation method capable to describe chemical reactions without explicitly describing wave function or electron density, namely the reactive force field method.

2.2 Hartree-Fock Theory

The foundations of WFT-based methods lies in the Hartree-Fock (HF) method.[98] In HF theory, $\mathcal{H}^{elec}$ is approximated as a sum of effective one-electron Hamiltonians

$$\mathcal{H}^{elec} = \sum_{i=1}^{N} h(i), \tag{2.5}$$

where $h(i)$ is an effective one-electron operator describing the potential energy and the kinetic energy of electron i. The effect of electron-electron repulsion is averaged together as a "mean field approximation". The eigenfunctions of $h(i)$ are called one-electron spatial orbitals, $\{\phi_i\}$, which can be taken to form a set of one-electron spin orbitals, $\{\chi_i\}$, by multiplying $\{\phi_i\}$ by a spin function, $\alpha(\omega)$ or $\beta(\omega)$. The simplest of N-electron wave functions, called the Hartree product (HP), can be constructed as a product of spin orbitals for each electron

$$\Psi^{HP}(x_1, x_2, \cdots, x_N) = \chi_i(x_1)\chi_j(x_2)\cdots\chi_k(x_N). \tag{2.6}$$

However, the Hartree product does not satisfy the antisymmetry principle, more commonly known as the Pauli exclusion principle. It was found that a properly antisymmetrized version of the Hartree N-electron wave function (one that properly obeys the Pauli exclusion principle) can be arranged as the so-called Slater determinant,

$$\begin{aligned}\Psi(x_1, x_2, \cdots, x_N) &= \frac{1}{\sqrt{N!}}\begin{vmatrix} \chi_i(x_1) & \chi_j(x_1) & \cdots & \chi_k(x_1) \\ \chi_i(x_2) & \chi_j(x_2) & \cdots & \chi_k(x_2) \\ \vdots & \vdots & \ddots & \vdots \\ \chi_i(x_N) & \chi_j(x_N) & \cdots & \chi_k(x_N) \end{vmatrix} \\ &= |\chi_i(x_1)\chi_j(x_2)\cdots\chi_k(x_N)|.\end{aligned} \tag{2.7}$$

Considering the ground state of an N-electron system as a single Slater determinant

$$|\Psi_0\rangle = |\chi_1\chi_2\cdots\chi_a\chi_b\cdots\chi_N\rangle, \tag{2.8}$$

the expectation value for the total electronic energy of the system can be expressed as

$$\begin{aligned}E_0 &= \langle\Psi_0|\mathcal{H}|\Psi_0\rangle \\ &= \sum_a \langle a|h|a\rangle + \frac{1}{2}\sum_{ab}[aa|bb] - \frac{1}{2}\sum_{ab}[ab|ba],\end{aligned} \tag{2.9}$$

where the first term is the one-electron Hamiltonian integral, the second term is the two-electron integral representing the Coulomb repulsion between electrons, and the last term, a

two-electron integral known as the QM exchange which arises as a consequence of $|\Psi_0\rangle$ that satisfies the Pauli exclusion principle.

By applying the variation principle, one can find the optimal spin orbitals, which minimize E_0. The solution is the eigenfunction of an equation called the HF equation

$$f(i)\chi(x_i) = \epsilon\chi(x_i), \tag{2.10}$$

where $f(i)$ is the Fock operator

$$f(i) = -\frac{1}{2}\nabla_i^2 - \sum_{A=1}^{M}\frac{Z_A}{r_{iA}} + v^{HF}(i). \tag{2.11}$$

Here $v^{HF}(i)$ is the average potential experienced by the ith electron due to the presence of the other electrons. Since the Fock operator depends on the entire electronic structure of the system, which can only be determined after solving the Hartree-Fock equation itself, the solution to the equation must be solved iteratively. This process of iterative solving for the orbitals of the Fock equation in a self-consistent manner is therefore called the self-consistent-field (SCF) method.

The HF method approximately solves the Schrödinger equation by ignoring explicit electron correlation between electrons with opposite spin, while the Pauli exclusion principle eliminates the possibility of finding two electrons of the same spin in the same position by way of the "exchange energy" term. Nevertheless, even the latter term only accounts for spin-spin interaction and does not consider the explicit Coulomb repulsion between electrons. Therefore, HF as a mean-field approach is severely affected by the so-called "electron correlation" error. Neglect of explicit Coulomb electron correlation can cause significant deviations from experimental results. Therefore, a number of methods have been devised to take the electron correlation into account based on the wave functions obtained by HF. These approaches are collectively called post-Hartree-Fock (post-HF) methods. Post-HF methods are, in general, more accurate methods compared to HF as they attempt to account for the neglected electron correlation. They accomplish this in a variety of ways, such as extending the HF wave function by a linear combination of Slater determinants (so-called configuration

interaction or CI method)[99] or by employing Møller-Plesset perturbation theory (MPn)[100,101] to the HF wave function. Unfortunately, these methods scale unfavorably with the number of electrons, thus requiring tremendous computer resources. Therefore, albeit more accurate than HF, post-HF methods are typically only applicable for very small molecular systems.

2.3 Density Functional Theory

As postulated in QM, knowledge of the N-electron wave function, $\Psi(x_1, x_2, \cdots, x_N)$, of a system implies knowledge of all observable properties of the system in the corresponding state. However, the wave function of a system was not the only way observable properties of a system could be obtained. Hohenberg and Kohn famously proved that knowing the electron density, $\rho(r)$, of a system could also be used to know all observable properties of the system in the ground state.[51] Thus, the description of the N-electron system by a wave function can instead be replaced by the electron density of the system with an equivalent theory to WFT, now called density functional theory (DFT). The formalism of DFT was based on their two theorems.[51] The first theorem states that the ground-state properties of a many-electron system can be uniquely determined by an electron density, $\rho(r)$. The total energy of the system, within the Born-Oppenheimer approximation, thus becomes a functional of the electron density

$$E[\rho(r)] = T[\rho(r)] + V^{ee}[\rho(r)] + \int \rho(r) v^{ext}(r) dr, \tag{2.12}$$

where T and V^{ee} are the kinetic and electron interaction energies, respectively, and $v^{ext}(r)$ is the external potential. The second theorem states that the energy $E[\rho(r)]$ of this system takes its minimum value when the electron density is the ground-state electron density $\rho^0(r)$. Therefore, the ground state energy and its corresponding electron density can be obtained by solving the minimization problem of $E[\rho(r)]$ with respect to $\rho(r)$. However, the original DFT method possesses a serious challenge that has yet to be overcome, the analytical formulation of T and V^{ee}, both of which remain unknown to date.

This practical limitation notwithstanding, approximations to the true density functional have been implemented and employed in DFT calculations, starting with the precisely-known energy functional for a hypothetical system, the free-electron gas. With an approximate functional, Kohn and Sham have then suggested a practical procedure using an orbital-based approach to perform DFT calculations using the SCF method in a process analogous to HF theory.[52] The main contribution of kinetic and electron interaction energies is evaluated by the non-interacting kinetic energy, T^0, and the classical Coulomb interaction energy, $E^H[\rho(r)]$, respectively

$$T^0 = -\frac{1}{2}\sum_{i=1}^{N}\int \phi_i(r)\nabla_i^2\phi_i(r)dr, \tag{2.13}$$

$$E^H[\rho(r)] = \int \frac{\rho(r)\rho(r')}{|r-r'|}drdr'. \tag{2.14}$$

The Equation 2.12 can be rewritten as

$$\begin{aligned} E[\rho(r)] &= T^0 + E^H[\rho(r)] + \int \rho(r)v^{ext}(r)dr + T[\rho(r)] - T^0 + V^{ee}[\rho(r)] - E^H[\rho(r)] \\ &= T^0 + E^H[\rho(r)] + \int \rho(r)v^{ext}(r)dr + E^{xc}[\rho(r)], \end{aligned} \tag{2.15}$$

where $E^{xc}[\rho(r)]$ is called the exchange-correlation energy, which includes the difference between interacting and non-interacting kinetic energies and the non-classical electron-electron interaction energy.

The electron density is expressed as a sum of one-electron orbitals, $\phi(r)$,

$$\rho(r) = \sum_{i=1}^{N}|\phi_i(r)|^2. \tag{2.16}$$

By substituting Equation 2.16 into Equation 2.15, and then minimizing the equation with respect to a set of orbitals, one can obtain the Kohn-Sham equations

$$\left(-\frac{1}{2}\nabla^2 + \int \frac{\rho(r')}{|r-r'|}dr' + v^{ext}(r) + v^{xc}[\rho(r)]\right)\phi_i(r) = \epsilon_i\phi_i(r). \tag{2.17}$$

Here $v^{xc}[\rho(r)]$ is the derivative of the exchange-correlation energy with respect to the fluctuation of the electron density

$$v^{xc}[\rho(r)] = \frac{\delta E^{xc}}{\delta \rho(r)}. \tag{2.18}$$

Since the equation depends on the electronic structure of the system, $\rho(r)$, the equation must be solved iteratively in a similar SCF fashion to the Hartree-Fock method.

If the expression of the exchange-correlation functional is given, the system's electron density and ground state energy can be obtained by solving the Kohn-Sham equation. Unfortunately, the exact formulation of E^{xc} is unknown. Over time, numerous versions of the approximate E^{xc} have been reported. In this section, the two main types of approximation for E^{xc}, namely the local density approximation (LDA) and the generalized gradient approximation (GGA), are briefly reviewed.

LDA is a class of approximations to the exchange-correlation energy functional that are based only on the description of the electron density value at a given evaluation point. Within LDA, E^{xc} is expressed as

$$E^{xc}_{LDA} = \int \epsilon^{xc}_{LDA}[\rho(r)]\rho(r)dr, \tag{2.19}$$

where $\epsilon^{xc}_{LDA}[\rho(r)]$ is the exchange-correlation energy per particle of a homogeneous electron gas of density $\rho(r)$. $\epsilon^{xc}_{LDA}[\rho(r)]$ consists of the exchange part, $\epsilon^{x}_{LDA}[\rho(r)]$, and the correlation part, $\epsilon^{c}_{LDA}[\rho(r)]$

$$\epsilon^{xc}_{LDA}[\rho(r)] = \epsilon^{x}_{LDA}[\rho(r)] + \epsilon^{c}_{LDA}[\rho(r)]. \tag{2.20}$$

The $\epsilon^{x}_{LDA}[\rho(r)]$ is derived from a homogeneous electron gas model[102]

$$\epsilon^{x}_{LDA}[\rho(r)] = \frac{3}{4}\left(\frac{3}{\pi}\right)^{1/3}\rho(r)(r)^{1/3}, \tag{2.21}$$

while $\epsilon^{c}_{LDA}[\rho(r)]$ can be parameterized from highly accurate approaches like numerical quantum Monte-Carlo.[103]

Apart from LDA methods, GGA methods uses not only the electron density but also its gradients. The general GGA exchange-correlation energy can be expressed as

$$E_{GGA}^{xc} = \int \epsilon_{GGA}^{xc}[\rho(r), \nabla\rho(r)]\rho(r)dr. \tag{2.22}$$

The GGA exchange-correlation energy is a functional of the electron density and its gradient. The gradients provide more information about how the energy varies with changes in electron density around the evaluation point. Thus, GGA functionals would offer a significant qualitative improvement over LDA functionals. In a similar footing, the second derivative of electron density can be included to provide more information about how the energy varies with electron density variation around the evaluation point, leading to a class of functionals called meta-GGA.[104,105]

The aforementioned LDA, GGA, and meta-GGA functionals are categorized as a family of "pure" DFT functionals because their functionals depends only on the electron density and its derivatives. These pure DFT functionals can exhibit remarkable failures such as underestimation of the frontier orbital energy gap in molecules, bandgap in materials, and charge-transfer excitation energies, as well as the overestimation of charge-transfer and conductance, incorrect description of activation energies for chemical reactions and binding energies in charge-transfer complexes, and absence of the Rydberg series.[79,81,83–88] The failures of these pure DFT functionals can be attributed to the self-interaction error (SIE), also known as the delocalization problem. Lately, hybrid functionals and range-separated functionals have been developed to correct the SIE by combining the traditional DFT exchange with the HF exchange.[106–111] These hybrid/range-separated DFT functionals fix many of the failures found in pure DFT functionals and usually give very accurate results in a wide range of properties.

In general, DFT approximates for electron correlation by introducing an empirical energy functional of the electron density, through a term called the "electron exchange-correlation" (xc) functional. In practical applications, DFT can be comparable to post-HF methods in terms of accuracy but at remarkably reduced computational cost, more commensurate with the HF approach. For these reasons, DFT is currently considered as the most popular

method in computational chemistry and solid-state physics.[87] Nowadays, with the rapid increase in computing power, the calculation of molecular structures of systems containing several hundred atoms by DFT became routine. However, large-scale systems like proteins or nano-materials remain beyond the scope of HF or DFT. Therefore, further approximation is needed to reduce the amount of computational time.

2.4 Density-Functional Tight-Binding (DFTB)

2.4.1 From DFT to DFTB

The central idea of the DFTB method is that the "electrons are tightly bound to atoms".[112] Only valence electrons are considered explicitly in a minimal atomic basis set, while core electrons are treated in an empirical manner using two-center repulsive potentials. The derivation of DFTB from DFT was described in great detail by Michael Gaus.[113] Here, only important equations of the derivation are discussed.

Considering a system of electrons and nuclei, the external potential experienced by electrons, $v^{ext}(r)$, is defined by the nucleus potential, $v^{ne}(r)$,

$$v^{ext}(r) = v^{ne}(r) = -\sum_{a} \frac{Z_a}{|r - R_a|}. \tag{2.23}$$

The DFT electronic energy of the system can be obtained by solving Equation 2.17. The total energy of the system can be obtained by adding the nucleus-nucleus interaction energy, E^{nn}, to the electronic energy

$$\begin{aligned} E^{DFT}[\rho(r)] = \sum_{i}^{occ} \int \psi_i^*(r) \Big(-\frac{1}{2}\nabla^2 + \int \frac{\rho(r')}{|r - r'|} dr' + v^{ne}(r) + v^{xc}[\rho(r)] \Big) \psi_i(r) dr \\ - \frac{1}{2} \int \int \frac{\rho(r')\rho(r)}{|r - r'|} dr' dr - \int v^{xc}[\rho(r)]\rho(r) dr + E^{xc}[\rho(r)] + E^{nn}, \end{aligned} \tag{2.24}$$

where E^{nn} is defined as

$$E^{nn} = -\frac{1}{2} \sum_{a \neq b} \frac{Z_a Z_b}{|R_a - R_b|}. \tag{2.25}$$

The electron density, $\rho(r)$, is expanded to include small fluctuations, $\Delta\rho(r)$, from a reference electron density, $\rho^0(r)$,

$$\rho(r) = \rho^0(r) + \Delta\rho(r). \tag{2.26}$$

Substituting $\rho(r)$ from Equation 2.26 into Equation 2.24, the DFT total energy can be rewritten as

$$\begin{aligned}
E^{DFT}[\rho^0(r) + \Delta\rho(r)] &= \sum_i^{occ} \int \psi_i^*(r) \Big(-\frac{1}{2}\nabla^2 + \int \frac{\rho^0(r')}{|r-r'|} dr' + v^{ne}(r) + v^{xc}[\rho^0(r)] \Big) \psi_i(r) dr \\
&- \frac{1}{2} \int\int \frac{\rho^0(r')\rho^0(r)}{|r-r'|} dr' dr - \int v^{xc}[\rho^0(r)]\rho^0(r) dr + E^{nn} \\
&+ \frac{1}{2} \int\int \left(\frac{1}{|r-r'|} \right) \Delta\rho(r')\Delta\rho(r) dr' dr + E^{xc}[\rho^0(r) + \Delta\rho(r)] \\
&= \sum_i^{occ} \langle \psi_i | H^0 | \psi_i \rangle - \frac{1}{2} \int\int \frac{\rho^0(r')\rho^0(r)}{|r-r'|} dr' dr - \int v^{xc}[\rho^0(r)]\rho^0(r) dr + E^{nn} \\
&+ \frac{1}{2} \int\int \left(\frac{1}{|r-r'|} \right) \Delta\rho(r')\Delta\rho(r) dr' dr + E^{xc}[\rho^0(r) + \Delta\rho(r)],
\end{aligned} \tag{2.27}$$

where H^0 represents the Hamiltonian generated with the reference electron density, $\rho^0(r)$.

$$H^0 = -\frac{1}{2}\nabla^2 + \int \frac{\rho^0(r')}{|r-r'|} dr' + v^{ne}(r) + v^{xc}[\rho^0(r)] \tag{2.28}$$

.

Further approximations can be made, where the exchange-correlation energy $E^{xc}[\rho^0(r) + \Delta\rho(r)]$ is substituted by its Taylor series expansion with respect to the fluctuation of election density

$$\begin{aligned}
E^{DFT}[\rho^0(r) + \Delta\rho(r)] &= \sum_i^{occ} \langle \psi_i | H^0 | \psi_i \rangle - \frac{1}{2} \int\int \frac{\rho^0(r')\rho^0(r)}{|r-r'|} dr' dr \\
&- \int v^{xc}[\rho^0(r)]\rho^0(r) dr + E^{xc}[\rho^0(r)] + E^{nn} \\
&+ \frac{1}{2} \int\int \left(\frac{1}{|r-r'|} + \frac{\delta^2 E^{xc}[\rho(r)]}{\delta\rho(r')\delta\rho(r)} \Big|_{\rho^0(r')\rho^0(r)} \right) \Delta\rho(r')\Delta\rho(r) dr' dr \\
&+ \frac{1}{6} \int\int\int \left(\frac{\delta^3 E^{xc}[\rho(r)]}{\delta\rho(r'')\delta\rho(r')\delta\rho(r)} \Big|_{\rho^0(r'')\rho^0(r')\rho^0(r)} \right) \Delta\rho(r'')\Delta\rho(r')\Delta\rho(r) dr'' dr' dr + \ldots.
\end{aligned} \tag{2.29}$$

Different levels of approximations can be introduced by truncating of this Talyor series.[50,53,55,58,114] The second, third, fourth, and fifth terms of Equation 2.29 depend only on the reference electron density, $\rho^0(r)$, and distance of atoms. Thus, one can approximate these terms into a term called E^{rep}

$$\begin{aligned} E^{rep} &\approx \frac{1}{2}\int\int \frac{\rho^0(r')\rho^0(r)}{|r-r'|}dr'dr - \int v^{xc}[\rho^0(r)]\rho^0(r)dr + E^{xc}[\rho^0(r)] + E^{nn} \\ &= \frac{1}{2}\sum_{a,b} V_{ab}^{rep}(R_{ab}), \end{aligned} \tag{2.30}$$

where $V_{ab}^{rep}(R_{ab})$ is an atom-pair potential depending on distance, R_{ab}, between atom "a" and atom "b". Therefore, one could express the general form of DFTB energy expressed as

$$\begin{aligned} E = &\sum_{i}^{occ}\langle\psi_i|H^0|\psi_i\rangle + E^{rep} \\ &+ \frac{1}{2}\int\int\left(\frac{1}{|r-r'|} + \frac{\delta^2 E^{xc}[\rho(r)]}{\delta\rho(r')\delta\rho(r)}\Big|_{\rho^0(r')\rho^0(r)}\right)\Delta\rho(r')\Delta\rho(r)dr'dr \\ &+ \frac{1}{6}\int\int\int\left(\frac{\delta^3 E^{xc}[\rho(r)]}{\delta\rho(r'')\delta\rho(r')\delta\rho(r)}\Big|_{\rho^0(r'')\rho^0(r')\rho^0(r)}\right)\Delta\rho(r'')\Delta\rho(r')\Delta\rho(r)dr''dr'dr + \ldots \end{aligned} \tag{2.31}$$

2.4.2 Non-Self-Consistent-Charge (NCC) DFTB

The NCC-DFTB[50,53,114] neglects the second- and higher-order terms of the Talyor series expansion found in Equation 2.31 leading to a simple equation of energy

$$E^{NCC-DFTB} = \sum_{i}^{occ}\langle\psi_i|H^0|\psi_i\rangle + E^{rep}. \tag{2.32}$$

By introducing a minimal basis set $|\phi_\mu\rangle$ within the linear combination of atomic orbitals (LCAO) framework,

$$\psi_i(r) = \sum_{\mu} c_{\mu i}\phi_\mu(r), \tag{2.33}$$

and applying the variational principle to Equation 2.32, one can obtain an eigenvalue problem

$$\sum_{\nu}^{AO} c_{\nu i}(H^0_{\mu\nu} - \epsilon_i S_{\mu\nu}) = 0. \tag{2.34}$$

Here, $H^0_{\mu\nu}$ and $S_{\mu\nu} = \langle\phi_\mu|\phi_\nu\rangle$ are the Hamiltonian and overlap matrix elements, respectively. In DFTB, the Hamiltonian matrix elements, $H^0_{\mu\nu}$, are defined as

$$H^0_{\mu\nu} = \begin{cases} \left\langle \phi_\mu \right| -\frac{1}{2}\nabla^2 + V[\rho^0_a + \rho^0_b] \left| \phi_\nu \right\rangle & \text{if } a \neq b \\ \epsilon^{\text{free atom}} & \text{if } a = b, \mu = \nu \\ 0 & \text{if } a = b, \mu \neq \nu. \end{cases} \tag{2.35}$$

Since the Hamiltonian matrix element does not depend on the electronic structure, the iterative SCF procedure is not necessary. This leads to a non-self-consistent-charge (NCC) scheme. Because the Hamiltonian of NCC-DFTB does not depend on the electron density fluctuation $\Delta\rho$, it makes NCC-DFTB the fastest among DFTB variants, but is suitable only for systems with small interatomic charge transfer, such as homoatomic systems.[38,57]

2.4.3 Self-Consistent-Charge (SCC) DFTB

The second-order term in the density fluctuation becomes important in the case of heteroatomic compounds when the charge transfer among atoms becomes non-negligible. In order to preserve computational efficiency, SCC-DFTB[58] (or DFTB2) approximates the second-order terms

$$\begin{aligned} E^{2nd} &= \frac{1}{2}\int\int \left(\frac{1}{|r-r'|} + \frac{\delta^2 E^{xc}[\rho(r)]}{\delta\rho^0(r')\delta\rho^0(r)}\Big|_{\rho^0(r')\rho^0(r)} \right) \Delta\rho^0(r')\Delta\rho^0(r) dr' dr \\ &\approx \frac{1}{2}\sum_{a,b} \gamma_{ab}(R_{ab})\Delta q_a \Delta q_b, \end{aligned} \tag{2.36}$$

where $\gamma_{ab}(R_{ab})$ is a function that depends only on the distance between atom a and b and their chemical hardness and Δq_a which is the deviation of the Mulliken population on atom a from that in the neutral atom, q^0_a,

$$\Delta q_a = \frac{1}{2}\sum_i n_i \sum_{\mu\in a}\sum_\nu (c_{\mu i}c_{\nu i}S_{\mu\nu} + c_{\nu i}c_{\mu i}S_{\nu\mu}) - q^0_a. \tag{2.37}$$

The total energy of SCC-DFTB is defined as

$$E^{SCC-DFTB} = \sum_{i}^{occ} \langle \psi_i | H^0 | \psi_i \rangle + E^{rep} + \frac{1}{2} \sum_{a,b} \gamma_{ab}(R_{ab}) \Delta q_a \Delta q_b. \tag{2.38}$$

Similar to NCC-DFTB, one can apply the variational principle to Equation 2.38 to obtain an eigenvalue problem

$$\sum_{\nu}^{AO} c_{\nu i}(H_{\mu\nu} - \epsilon_i S\mu\nu) = 0, \tag{2.39}$$

where the Hamiltonian matrix element, $H_{\mu\nu}$, is

$$H_{\mu\nu} = H^0_{\mu\nu} + \frac{1}{2} S_{\mu\nu} \sum_{c} (\gamma_{ac} + \gamma_{bc}) \Delta q_c. \tag{2.40}$$

Since Δq_c depends on MO coefficients, $c_{\mu i}$, which can only be determined after solving Equation 2.39, the equation must be solved iteratively, hence is called the self-consistent-charge (SCC), a process analogous to the SCF in DFT. The SCC-DFTB method systematically improves the charge-charge interaction, making it more suitable to describe polar systems.[38,57]

2.4.4 Long-Range Corrected (LC) DFTB

The traditional DFTB methods, which were derived from a local-density approximations (LDA) or generalized gradient approximations (GGA) DFT functionals, inherits not only its advantages but also its most infamous shortcoming, the so-called self-interaction error (SIE).[79,86,115] The spurious repulsion between an electron with its own electron density artificially stabilizes delocalized states, leading to a variety of computational artifacts. These artifacts include: the underestimation of the frontier orbital energy gap in molecules, bandgap in materials, and charge-transfer excitation energies, as well as the overestimation of charge-transfer and conductance, the incorrect description of activation energies for chemical reactions and binding energies in charge-transfer complexes.[79,81,83–88] The long-range corrected (LC) version of the SCC-DFTB has recently been developed in order to overcome the inherited SIE.[89,90] The derivation of LC-DFTB from DFT was described in

detail by Niehaus et al.[89] Here, only the important equations of LC-DFTB are shown. The total energy of LC-DFTB is

$$E^{LC-DFTB} = \sum_{\mu\nu} D_{\mu\nu} H^0_{\mu\nu} + \frac{1}{2}\sum_{ab} \gamma_{ab}\Delta q_a \Delta q_b + \sum_{a>b} E^{rep}_{ab} - \frac{1}{4}\sum_{\mu\nu\alpha\beta} \Delta D_{\mu\nu}\Delta D_{\alpha\beta}(\mu\alpha|\beta\nu)^{lr}, \tag{2.41}$$

where "a" and "b" denote atoms; and μ, ν, α, and β are indices for atomic orbital (AO). The $D_{\mu\nu}$ and $\Delta D_{\mu\nu}$ are elements of the electron density matrix and the deviation electron density matrix, which are defined as

$$D_{\mu\nu} = n_i \sum_{i}^{occ} c_{\mu i} c^*_{\nu i}, \tag{2.42}$$

$$\Delta D_{\mu\nu} = D_{\mu\nu} - D^0_{\mu\nu}. \tag{2.43}$$

The $c_{\mu i}$ is the expansion coefficients of the i^{th} molecular orbital (MO) in an AO basis set; D^0 represents the electron density matrix of the reference system; and Δq_a is the deviation of the Mulliken population on atom a from that in the neutral atom, q^0_a,

$$\Delta q_a = \frac{1}{2}\sum_i n_i \sum_{\mu\in a}\sum_{\nu} (c_{\mu i} c_{\nu i} S_{\mu\nu} + c_{\nu i} c_{\mu i} S_{\nu\mu}) - q^0_a. \tag{2.44}$$

Here $S_{\mu\nu} = \langle \phi_\mu | \phi_\nu \rangle$ are the overlap matrix elements. The four center integral, the last term of Equation 2.41, is simplified by applying the Mulliken approximation.[116,117]

After some manipulation, the total energy could be rewritten as

$$\begin{aligned} E^{LC-DFTB} = &\sum_{\mu\nu} D_{\mu\nu} H^0_{\mu\nu} + \frac{1}{2}\sum_{ab} \gamma_{ab}\Delta q_a \Delta q_b + \sum_{a>b} E^{rep}_{ab} \\ &- \frac{1}{16}\sum_{\mu\nu\alpha\beta} \Delta D_{\mu\nu}\Delta D_{\alpha\beta} S_{\mu\alpha} S_{\beta\nu} (\gamma^{lr}_{\mu\beta} + \gamma^{lr}_{\mu\nu} + \gamma^{lr}_{\alpha\beta} + \gamma^{lr}_{\alpha\nu}), \end{aligned} \tag{2.45}$$

where $\gamma_{\mu\nu} = \gamma_{ab}$ and $\gamma^{lr}_{\mu\nu} = \gamma^{lr}_{ab}$ if $\mu \in a$ and $\nu \in b$, γ_{ab} and γ^{lr}_{ab} are functions dependent on the distance between atoms and their chemical hardness. It is worth mentioning that the γ^{lr} also depends on a range separation parameter ω, which regulates the "long-range distance". Similar to SCC-DFTB, one can obtains an eigenvalue problem by employing the variational

principle to Equation 2.45,

$$\sum_{\nu}^{AO} c_{\nu i}(H_{\mu\nu} - \epsilon_i S_{\mu\nu}) = 0. \tag{2.46}$$

Within the LC-DFTB method, the Hamiltonian matrix elements, $H_{\mu\nu}$, are defined as

$$H_{\mu\nu} = H^0_{\mu\nu} + \frac{1}{2} S_{\mu\nu} \sum_c (\gamma_{ac} + \gamma_{bc}) \Delta q_c - \frac{1}{8} \sum_{\alpha\beta} \Delta D_{\alpha\beta} S_{\mu\alpha} S_{\beta\nu} (\gamma^{lr}_{\mu\beta} + \gamma^{lr}_{\mu\nu} + \gamma^{lr}_{\alpha\beta} + \gamma^{lr}_{\alpha\nu}). \tag{2.47}$$

The evaluation of the last term of $H_{\mu\nu}$ is computationally heavy. Lutsker et al. have proposed a cutoff algorithm to save computing effort.[90] Here, they have consider

$$\begin{aligned} K_{\mu\nu} &= -\frac{1}{8} \sum_{\alpha\beta} S_{\mu\alpha} \Delta D_{\alpha\beta} S_{\beta\nu} (\gamma^{lr}_{\mu\beta} + \gamma^{lr}_{\mu\nu} + \gamma^{lr}_{\alpha\beta} + \gamma^{lr}_{\alpha\nu}) \\ &= -\frac{1}{8} \sum_{cd} \Gamma_{abcd} \sum_{\alpha\in c} \sum_{\beta\in d} S_{\mu\alpha} \Delta D_{\alpha\beta} S_{\beta\nu} \\ &= -\frac{1}{8} \sum_{cd} \Gamma_{abcd} \sum_{\alpha\in c} \sum_{\beta\in d} Q^{cd}_{\mu\nu} \qquad \text{with} \qquad \mu \in a, \nu \in b. \end{aligned} \tag{2.48}$$

Of which,

$$\begin{aligned} Q^{cd}_{\mu\nu} &\leq \sum_{\alpha\in c} \sum_{\beta\in d} |S_{\mu\alpha}||\Delta D_{\alpha\beta}||S_{\beta\nu}| \\ &\leq \bar{S}_{ac} \overline{\Delta D} \bar{S}_{db} \sum_{\alpha\in c} \sum_{\beta\in d} 1, \end{aligned} \tag{2.49}$$

where $\bar{S}_{ac}$=max($|S_{\mu\alpha}|$) with $\mu \in a$, $\alpha \in c$, and $\overline{\Delta D}$=max($|D_{\alpha\beta}|$). By comparing $\bar{S}_{ac}\overline{\Delta D}\bar{S}_{db}$ to a threshold value, $\epsilon_{threshold}$, one can avoid evaluation of the negligible small contribution,

$$\bar{S}_{ac} \overline{\Delta D} \bar{S}_{db} \leq \epsilon_{threshold}. \tag{2.50}$$

The LC-DFTB method corrects the systematic underestimation of the DFTB HOMO-LUMO gap for small molecules and zwitterionic proteins in ground-state calculations.[77,90] It was found that the LC-DFTB method also has great performance for thermochemistry, geometries, and vibrational frequencies. Furthermore, the performance for intramolecular charge transfer and excited states by the time-dependent (TD)-LC-DFTB method is also quite auspicious.[90,118]

2.5 Fragment Molecular Orbital (FMO)

The FMO method is a linear-scaling approach for computing large-sized chemical systems.[119] The central concept of the FMO method is dividing these large-sized systems into sets of smaller fragments. The properties of these systems can be recovered by summing up values calculated from the fragments. For instance, the total energy of the whole system in the simplest version of the FMO method, called one-body FMO (or FMO1) expansion, is

$$E^{\mathrm{FMO1}} = \sum_{I}^{N} E_I, \tag{2.51}$$

where N is the number of fragments, E_I is the energy of a monomer (fragment) I. The calculation of each fragment must be done in the presence of an electrostatic potential (ESP) generated by surrounding fragments. The FMO1 approach fails to describe charge transfer between fragments due to its simplicity. To describe the charge transfer between fragments and improve the accuracy of the approach, the two-body FMO (or FMO2) expansion[120] was introduced. In FMO2, the total energy of the whole system is defined as

$$E^{\mathrm{FMO2}} = \sum_{I}^{N} E_I + \sum_{(I>J)}^{N} \Delta E_{IJ}, \tag{2.52}$$

where

$$\Delta E_{IJ} = E_{IJ} - E_I - E_J, \tag{2.53}$$

and E_{IJ} is the energy of a dimer consisting of fragments I and J. Since the number of dimer calculations scales quadratically with the size of systems, the computational time generally also scales quadratically. To achieve a near-linear-scaling, the electrostatic dimer (ES-DIM) approximation[119,121] is typically used for far separated dimers, in which the amount of charge transfer between fragments becomes negligibly small. In a similar footing, the three-body FMO (or FMO3) expansion was also introduced to include the three-body quantum

effects.[44,122,123] In FMO3, the total energy is defined as

$$E^{\mathrm{FMO3}} = \sum_{I}^{N} E_I + \sum_{I>J}^{N} \Delta E_{IJ} + \sum_{I>J>K}^{N} \big(\Delta E_{IJK} - \Delta E_{IJ} - \Delta E_{IK} - \Delta E_{JK}\big), \tag{2.54}$$

In order to preserve computational efficiency, the three-body quantum effects of far separated trimers can also be neglected using the I-TRIM algorithm.[44,124] In this dissertation, A combination of the FMO2 and FMO3 with the LC-DFTB method will be discussed in more detail in Chapter 5.

2.6 Reactive Force Field

Alternatively, to DFTB or other semi-empirical QM (SQM) methods that are derived from QM, reactive force field (ReaxFF)[17,125] is a method based on classical molecular mechanics, utilizing bond-order potentials that has been developed to describe the bond formation and bond breaking during chemical reactions. The ReaxFF potential is defined as

$$E^{ReaxFF} = E^{bond} + E^{angle} + E^{tors} + E^{over} + E^{under} + E^{lp} + E^{vdw} + E^{coul} + E^{specific}, \tag{2.55}$$

where E^{bond}, E^{angle}, and E^{tors} are the bond, angle, dihedral contributions, respectively; E^{under} and E^{over} are the energy-penalty terms that prevents the under-coordination and over-coordination of atoms, respectively; E^{lp} is the energy of lone-pair electrons; E^{vdw} and E^{coul} are the dispersive and electrostatic contributions, respectively; and $E^{specific}$ represents additional energy corrections for a particular system of interest. The six first terms are bond-order dependent. In ReaxFF, the bond-order (BO) is estimated from interatomic distances using the following definition:

$$\begin{aligned} BO_{ij} &= BO_{ij}^{\sigma} + BO_{ij}^{\pi} + BO_{ij}^{\pi\pi} \\ &= \exp\left[p_{bo1}\left(\frac{r_{ij}}{r_{ij}^{\sigma}}\right)^{p_{bo2}}\right] + \exp\left[p_{bo3}\left(\frac{r_{ij}}{r_{ij}^{\pi}}\right)^{p_{bo4}}\right] + \exp\left[p_{bo5}\left(\frac{r_{ij}}{r_{ij}^{\pi\pi}}\right)^{p_{bo6}}\right], \end{aligned} \tag{2.56}$$

where BO_{ij} and r_{ij} are the bond order and interatomic distance between atoms i and j. r_0 is the equilibrium bond length, and $p_{bo(1-6)}$ are empirical fitting parameters. Generally,

the ReaxFF method is 1 to 2 orders of magnitude faster than DFTB. Nevertheless, a recent benchmark shows that the ReaxFF can lead to many unphysical mechanisms for chemical reactions.[125] Similarly, ReaxFF's low transferability limits its applications to only systems resembling their training data.[18]

Chapter 3

Density-Functional Tight-Binding for Phosphine-Stabilized Nanoscale Gold Clusters

A version of this chapter was originally published by Vuong, V. Q.; Madridejos, J. M. L.; Aradi, B.; Sumpter, B. G.; Metha, G. F.; Irle, S. "Density-Functional Tight-Binding for Phosphine-Stabilized Nanoscale Gold Clusters" *Chem. Sci.* **2020**, *11*, 13113–13128.

3.1 Abstract

We report a parameterization of the second-order density-functional tight-binding (DFTB2) method for the quantum chemical simulation of phosphine-ligated nanoscale gold clusters, metalloids, and gold surfaces. Our parameterization extends the previously released DFTB2 "auorg" parameter set by connecting it to the electronic parameter of phosphorus in the "mio" parameter set. Although this connection could technically simply be accomplished by creating only the required additional Au-P repulsive potential, we found that the Au 6p and P 3d virtual atomic orbital energy levels exert a strong influence on the overall performance of the combined parameter set. Our optimized parameters are validated against density functional theory (DFT) geometries, ligand binding and cluster isomerization energies, ligand

dissociation potential energy curves, and molecular orbital energies for relevant phosphine-ligated Au_n clusters ($n = 2 - 70$), as well as selected experimental X-ray structures from the Cambridge Structural Database. In addition, we validate DFTB simulated far-IR spectra for several posphine- and thiolate-ligated gold clusters against experimental and DFT spectra. The transferability of the parameter set is evaluated using DFT and DFTB potential energy surfaces resulting from the chemisorption of a PH_3 molecule on the gold (111) surface. To demonstrate the potential of the DFTB method for quantum chemical simulations of metalloid gold clusters that are challenging for traditional DFT calculations, we report the predicted molecular geometry, electronic structure, ligand binding energy, and IR spectrum of $Au_{108}S_{24}(PPh_3)_{16}$.

3.2 Introduction

Atomically precise ligated gold clusters of nanometer dimension receive continued attention due to their unique catalytic properties[66,126,127] and well-defined discrete electronic energy levels[128] that potentially offer greater flexibility and control over the more metal-like states of the corresponding bare gold nanoparticles and complexes.[66,129] Nanoscale gold clusters have shown high catalytic activity and selectivity for certain reactions at low temperature, such as the oxidation of carbon monoxide, propene and alcohols, or the hydrogenation of acetylene.[63–66] Commonly chosen "capping ligands" employed to stabilize atomically precise nanoscale gold clusters are typically thiolates and phosphines, which prevent aggregation, coalescence and unlimited growth during synthesis.[130] Post-treatment is usually required to remove some (or all) of the ligands to allow interaction with the substrate or reactants.[131–135] To achieve control over such complex catalytic systems it is vitally important to understand the relationship between molecular and electronic structure, often studied by a combination of experimental and theoretical approaches.[67,68] In addition, a better knowledge of the energetics associated with ligand removal is required to identify how post-treatment can be done without inducing concomitant side-effects such as agglomeration. Density functional theory (DFT) methods are most often employed in theoretical investigations, as they are capable to accurately describe electronic, geometrical, and vibrational structure of

gold clusters and nanoparticles.[68,136–148] In particular, the DFT-based simulation of IR, Raman, and UV-vis spectra has been achieved for a range of gold clusters, thus providing useful theoretical fingerprints to distinguish between bonding arrangements and orientations between gold atoms and ligands, and ligand-ligand interactions within clusters.[142,149–153]

Unfortunately, DFT calculations can become prohibitively expensive with system size,[19] and routine theoretical investigations are limited to moderate system sizes. One way of reducing the computational cost is to entirely neglect the ligands and only perform DFT calculations on the gold cores. An alternative way is to employ simplified ligand models where e.g. triphenylphosphine (PPh_3) is replaced by phosphine (PH_3) or trimethylphosphine (PMe_3).[136,137,141,144,145,147,148,154] This, as with the complete ligand removal approach, has the additional benefit that conformational searching is simplified, as the torsions of the three phenyl groups per ligand give rise to a large number of local minima with similar energies. Nevertheless, it is well known that the electronic effects of the larger ligands are different from those of the smaller ones, for instance inductive effects,[154–157] and a computational truncation of the ligands will influence the chemistry and therefore description of the catalytic properties in calculations. Integrated schemes such as ONIOM[158] may be used to capture such electronic effects in calculations on the untruncated "real" systems; however, the choice for high and low levels of theory and the definition of the interface between them is not straightforward. A rigorous ONIOM study requires benchmarks of the selected methods against a high-level calculation for the "real" system,[159] which is often computationally unfeasible. In practice therefore, integrated methods are often difficult to employ in the context of ligated nanoscale metal clusters. Besides the computational effort related to the proper modeling of the ligands, the size of the metal cluster itself can become problematic for conventional DFT studies, severely impacting the size range of gold clusters to be investigated for property control and fine-tuning. Exacerbating this problem is the recent emergence of larger, so called metalloid, clusters such as $Au_{108}S_{24}(PPh_3)_{16}$.[144] To make matters even worse, interactions of deposited gold clusters with substrate surfaces such as SiO_2 and TiO_2 may play an important role in the catalytic reaction,[131–135,160] which further increases the computational expense of DFT studies. A recent review on connections between theory and experiment for gold nanoclusters

has thus posed the question as to how theoretical calculations can be expanded to treat larger sizes and length scales.[67]

Semi-empirical electronic structure methods offer the capability to simulate large systems with explicit inclusion of electronic structure by introducing empirical parameters and methodological approximations to rigorous *ab initio* or first principles methods.[32–34,161–163] Among them, density-functional tight-binding (DFTB),[53–55,58,89,161] an approximation to DFT formulated in the framework of non-orthogonal tight binding, has emerged as one of the most accurate, and potentially versatile choices. DFTB is capable of simulating systems containing many thousands of atoms with an accuracy comparable to traditional DFT methods.[33,59,164] As the DFTB method takes advantage of the two-center approximation, tabulated Hamiltonian and overlap integrals within the Slater-Koster scheme,[58,112] it is two to three orders of magnitudes faster than DFT. In order to apply DFTB into the theoretical study of ligated gold clusters, it is necessary to provide accurate parameters for all binary chemical element interactions, most notably Au-S and Au-P. The Au-S interaction in combination with the "mio" parameter set[55,58,165] was included in the "auorg" parameter set for gold-thiolates clusters,[61,69] but the parameters for the Au-P interaction have not been developed.

In this work, we report a parameterization of the Au-P interactions for the second-order DFTB (DFTB2) method for the sake of compatibility with the previously developed parameters. The accuracy of these new DFTB parameters is probed by comparing the corresponding properties against DFT-calculated values and available experimental results in terms of: (1) root mean square deviations of optimized geometries, (2) energetic properties, i.e. ligand binding energies, relative isomer energies, and ligand dissociation energy profiles, (3) electronic structure, (4) normal vibrational modes of Au-P containing clusters, and (5) the adsorption of a PH_3 molecule on the gold (111) surface. Finally, we present DFTB-based predictions for structural, energetic, and vibrational properties of the recent experimentally reported metalloid gold cluster $Au_{108}S_{24}(PPh_3)_{16}$.[144]

3.3 Methodology and computational details

3.3.1 Brief overview of DFTB2

A comprehensive review of DFTB methods can be found elsewhere[38] and will not be repeated here. In this work, we only focus on generating parameters for the DFTB2 method, which is also referred to as self-consistent-charge (SCC)-DFTB.[58] The DFTB2 total energy can be viewed as a 2nd order Taylor expansion of the Kohn-Sham energy with respect to a reference initial electron density ρ_0 and electron density fluctuations $\Delta\rho$

$$E = \sum_{i}^{occ.} \langle \Psi_i | \hat{H}_0 | \Psi_i \rangle + \frac{1}{2} \sum_{AB}^{atoms} \gamma_{AB} \Delta q_A \Delta q_B + \sum_{A>B}^{atoms} E_{AB}^{\text{rep}} \quad , \tag{3.1}$$

where $\hat{H}_0$ is the initial Hamiltonian constructed from the superposition of neutral atomic densities in a two-center approximation,[53] and the $|\Psi_i\rangle$ are occupied valence molecular orbitals (MOs), expanded as a linear combination of optimized pseudo-atomic orbitals $|\phi_\mu\rangle$. The optimization of these pseudo-atomic valence orbitals and orbital densities for a given chemical element constitutes the determination of the electronic parameters. Δq_A is a point charge[166] on atom A, and $\gamma_{AB}\Delta q_A \Delta q_B$ represents the Coulomb interaction energy between the two point charges;[58] when $A = B$, γ_{AA} is the chemical hardness or second derivative of the total energy with respect to the charge on atom A. γ_{AB} is defined as

$$\gamma_{AB} = \frac{1}{r_{AB}} - S(r_{AB}, U_A, U_B), \tag{3.2}$$

where S is an exponentially decaying short-range function that depends on the distance between the two atoms $r_{AB} = |r_A - r_B|$ and their chemical hardness, given in form of the so-called Hubbard parameter U. The latter is calculated prior to molecular DFTB calculations for each chemical element using the DFT method, typically employing the Perdew-Burke-Ernzerhof (PBE) functional.[167]

In the framework of the two-center approximation, the Hamiltonian integrals $\langle \phi_\mu | \hat{H}_0 | \phi_\nu \rangle$ and the overlap integrals $\langle \phi_\mu | \phi_\nu \rangle$ are pre-tabulated for each chemical element pair. As in all

tight binding approaches, the DFTB2 total energy consists of an electronic energy, which is the sum of the first two terms in eq 3.1, and a summation over all unique repulsive potentials between two atoms E_{AB}^{rep}. The latter are formulated as a two-center term that depends only on the chemical element type of atoms A and B and their interatomic distance r_{AB}.[38] In principle, these pairwise repulsive potentials can be pre-calculated analytically from DFT for diatomic molecules. However, it was found that the performance of such DFT-based repulsive potentials is usually not sufficiently accurate for general purposes.[69] Therefore, in practice, one computes DFT- or wave function theory (WFT)-based reference relative energies for model systems that contain various bond lengths of the chemical element pair in question, and fits the total repulsive energy such as to minimize the difference between reference and resulting DFTB relative energies. For this purpose, the repulsive potentials are approximated by a combination of exponential and spline functions

$$E_{AB}^{rep}(r_{AB}) = \begin{cases} e^{-a_1 * r_{AB} + a_2} + a_3 & r_{AB} < r_{AB,0}^0; \\ \sum_{i=0}^{4} a_{AB,n,i}(r_{AB} - r_{AB,n}^0)^i & r_{AB,n}^0 \leq r_{AB} < r_{AB,n+1}^0; \\ 0 & r_{AB,cutoff}^0 \leq r_{AB}, \end{cases} \tag{3.3}$$

where "$r_{AB,n}^0$" is a spline knot at the nth interval, and the "a$_{AB,n}$" are the polynomial spline coefficients. These variables are considered the free empirical parameters and optimized either by hand or automatically[75,77,78] to minimize the difference between reference and DFTB relative energy for a series of training systems. In addition to relative energies, repulsive potentials can also be optimized to fit molecular geometries by minimizing the difference between the reference DFT or WFT energy gradient and the DFTB energy gradient for a set of equilibrium and non-equilibrium geometries in the training set. The possible constraints on the repulsive potentials include a cutoff radius, a limit on the number of allowable extrema, and a continuity requirement up to a given derivative order.

3.3.2 Gold-phosphorus parameterization

As indicated above, there are two groups of DFTB2 parameters that need to be determined: (1) the electronic parameters, and (2) the repulsive potentials for pairs of chemical elements.

The electronic parameters are comprised of the radii r^{wf} used in the definition of atomic confinement potentials for generating pseudo-atomic orbitals $|\phi_\mu\rangle$ as well as the confinement radii r^{dens} for the atomic density; additional electronic parameters are the atomic orbital energies and the atomic Hubbard parameters U for each chemical elements.[58] While the AO energies and the Hubbard parameters U are normally taken from DFT calculations of the free atom, the other electronic parameters and pairwise repulsive potentials are subject to optimization with the goal to reproduce certain desired properties; for instance, electronic band structure, atomization energies, reaction energies, and geometries (energy gradients). In order to parameterize the Au and P interactions for DFTB2, we adopted the Au electronic parameters from the "auorg" set published by Fihey et al. (referred to as auorg$^\alpha$),[61] and a modified version of "auorg" by Oliveiria et al. (referred to as auorg$^\chi$).[69] The difference between these two parameter sets lies in the Au 6p-orbital energy; in the auorg$^\alpha$ set it was taken as the true PBE orbital energy, while in the auorg$^\chi$ set it was empirically shifted upward by $\approx +0.0279$ Hartree. The main purpose for this orbital energy shift was to obtain improved values for cohesive energies of pure gold nanoclusters with respect to PBE.[69] Following the work of "auorg", only 5d and 6s valence electrons are considered, in total 11 valence electrons per Au atom. The parameters of the other elements in the auorg$^\alpha$ and auorg$^\chi$ sets were taken from the "mio" parameter set.[55,58] Consequently, we adopted the electronic parameters for P taken from the "mio" parameter set as well. It is important to mention that the 3d orbital energy of the P atom had been shifted by +0.5 Hartree from its PBE-calculated value of 0.02044 Hartree, according to Gaus et al. to reduce the overbinding in phosphate compounds, as the shift had also been adopted in the "3ob" parameter set for the DFTB3 method.[55,168] However, in the case of Au-P interactions, such a drastic shift of the P 3d virtual orbital energy introduces significant underbinding. We therefore decided to investigate the effect of the P 3d orbital energy level in detail. We systematically increased the value of the P 3d orbital energy by increments of 0.1 Hartree from its PBE computed and the "mio" shifted value, and used our genetic algorithm (GA) optimization tool[77] to automatically generate repulsive potentials for the Au-P interaction with these orbital energy shifts. In this way we tested the performance of the resulting Au-P parameterization with special consideration of geometries and binding energies for the adsorption of a PH_3 on Au (111). An energy value of

0.12044 Hartree was determined as the optimal compromise for the P 3d orbital. We refer to Table A.1 in the Supporting Information for the performance of DFTB2/mio with different P 3d orbital energies for a selected test set of chemical reactions involving H, C, N, O, P, and S containing compounds.

We decided to introduce a nomenclature for denoting the different choices of Au 6p and P 3d orbital energies in our parameters. Following Oliveira et al.[69] we denote the original PBE Au 6p energy value by 'α' and its modified value by 'χ'. The shifted "mio" P 3d energy will leave these notations unchanged, while the use of our new optimized P 3d orbital energy value of 0.12044 Hartree will be denoted with a prime, '$\prime$'. Hence, auorg$^{\alpha}$ coupled with the original "mio" P is unchanged, while the auorg$^{\alpha}$ and auorg$^{\chi}$ coupled with the new P 3d-orbital energy are referred to as auorg$^{\alpha\prime}$ and auorg$^{\chi\prime}$, respectively. Because auorg$^{\chi}$ exhibits the largest underestimation of the Au-P electronic binding energy (both Au 6p and P 3d virtual orbital energies are shifted upwards from PBE values), we did not generate Au-P repulsive potential for this orbital energy combination. Table 3.1 summarizes the nomenclature of the three different parameter sets and the relationship with their employed Au and P virtual atomic orbital energies.

The Au-P repulsive potentials were optimized on the basis of shell-resolved self-consistent charge electronic energies to fit ligand binding energies and forces for the training set listed in Table 3.2 using our in-house genetic algorithm (GA)-based parameterization tool.[77] After several preliminary tests, we employed a cutoff radius of 4 Å and 5 spline knots (the maximum for n in eq 3.3 was equal to 5), one allowable extremum, and a continuity requirement up to the third derivative. For the GA optimization, population sizes of 3000 and 5000 generations were employed with two-point crossover and random mutation rates of 0.9 and 0.2, respectively. The GA was used to minimize a scoring function F^{score} defined as the fitness of the parameter sets with respect to DFTB values and reference data according to the formula

$$F^{score} = \frac{1}{N_{eq}}\Big[\sum_i W_i^{bind}\left(\Delta E_i^{bind}\right)^2 + \sum_i W_i^{force}\sum_{j\in 3N_i}\left(\Delta F_{i,j}^{force}\right)^2\Big], \tag{3.4}$$

Table 3.1: Energies in Hartree for Au 6p and P 3d virtual atomic orbitals in different parameter sets

	auorg$^{\alpha}$	auorg$^{\alpha\prime}$	auorg$^{\chi\prime}$
ϵ_{Au}^{6p}	-0.02786	-0.02786	-0.00001
ϵ_{P}^{3d}	0.52044	0.12044	0.12044

where $\Delta E^{bind} = E^{bind}_{eDFTB} - E^{bind}_{ref}$ is the deviation in ligand binding energies, $\Delta F^{force} = F^{force}_{eDFTB} - F^{force}_{ref}$ is the deviation in forces, W^{bind}_i and W^{force}_i are weight factors of the i^{th} binding energy and the force of the i^{th} structure, respectively, N_{eq} is the number of fitting data points, N_i is the number of atoms in the i^{th} compound, and $eDFTB$ stands for the DFTB energy without repulsive potential term. In the training, we empirically shifted the reference ligand binding energies of PH_3 by -24 kcal/mol for auorg$^{\alpha\prime}$ and -22 kcal/mol for the auorg$^{\chi\prime}$ to better reproduce ligand binding energies of larger ligands and the adsorption of PH_3 on the Au (111) surface. Surprisingly, auorg$^{\alpha\prime}$ and auorg$^{\chi\prime}$ optimized Au-P repulsive potentials are almost identical, see Figure A.1 in the Supporting Information. In principle, the Au-P repulsive potential for auorg$^{\alpha}$ can also be optimized in a similar way to maximize its performance, however, for the sake of simplicity and transferability we decided to use the same Au-P repulsive potential for auorg$^{\alpha\prime}$ and auorg$^{\alpha}$.

3.3.3 Computational details

In the original parameterization of the auorg set,[61] the generalized gradient approximation (GGA) PBE density functional was selected to generate reference geometries and cluster binding energies. In this work, we opted for the TPSS density functional[104] because it was noted by Kepp[169] and Goel *et al.*[137] that this meta-GGA functional reproduces experimental or high-level theory bond energies and ligand-gold distances better than the standard GGA PBE functional. For the training set of small clusters in Table 3.2, the reference data were computed by the TPSS in combination with Ahlrich's triple-zeta valence polarized basis set (def2-TZVP).[170] No dispersion correction was employed in the calculations generating the training set in order to avoid complications originating from a possible convolution of DFTB repulsive energy terms and the long-distance dispersion term.

In order to benchmark the accuracy of the new parameters, ligand binding energies and optimized geometries were compared to their TPSS counterparts for various complexes of PH_3, PMe_3, PPh_3 and small- to moderate-sized gold clusters. For the larger complexes, which are listed in Table 3.3, the experimental structures from the Cambridge Structural Database (CSD) were used as the reference geometries. The different phosphorus-containing ligands considered in this test set are triphenylphosphine (PPh_3),

Table 3.2: Training set for Au-P repulsive potential fitting and weights for each complex used in the fitting with eq 3.4.

Forces (Equilibrium Geometries)

Complexes	Structures	Weights
Au_1-PH_2	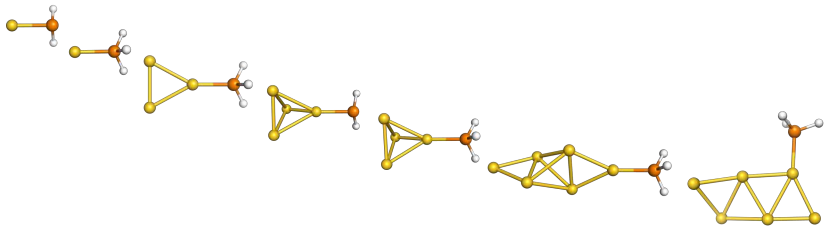	1.0
$[Au_1-PH_3]^+$		1.0
$[Au_3-PH_3]^+$		1.0
$[Au_4-PH_2]^+$		1.0
$[Au_4-PH_3]^{2+}$		1.0
$[Au_6-PH_3]^{2+}$		1.0
$[Au_6(planar)-PH_3]^{2+}$		1.0

Forces (Distorted Geometries)

Complexes	ΔR_{Au-P}(Å)	Weights
$[Au_1-PH_3]^+$	-0.3	0.5
$[Au_1-PH_3]^+$	-0.2	0.5
$[Au_1-PH_3]^+$	-0.1	0.5
$[Au_3-PH_3]^+$	+0.1	0.5
$[Au_3-PH_3]^+$	+0.2	0.3
$[Au_3-PH_3]^+$	+0.3	0.1

Ligand Binding Energies

Reactions							ΔE (kcal/mol)	Weights
$[Au_3]^+$	+	PH_3	=	$[Au_3-PH_3]^+$	⇒		-55.53	1.0
$[Au_4]^{2+}$	+	PH_3	=	$[Au_4-PH_3]^{2+}$	⇒		-76.27	1.0
$[Au_6]^{2+}$	+	PH_3	=	$[Au_6-PH_3]^{2+}$	⇒		-65.01	1.0
$[Au_6(planar)]^{2+}$	+	PH_3	=	$[Au_6(planar)-PH_3]^{2+}$	⇒		-64.58	1.0

1,1-bis(diphenylphosphino) propane (dppm), 1,3-bis(diphenylphosphino) propane (dppp), methyldiphenylphosphine ($PMePh_2$), tris(2-(diphenylphosphino) ethyl) phosphine (PP_3) and 1,8-bis(diphenylphosphino) octane (dppo). Additionally, there are thiol-containing ligands in some clusters comprised of reduced S_2^- and meta-methylbenzenethiol (m-MBT). For these test sets, the reference calculations were performed at the TPSS/def2-SVP[170] level of theory. Here we included the empirical D3 dispersion contribution[171,172] in both DFT and DFTB2 calculations.[173] The D3 dispersion correction was used to improve description of ligand-ligand interactions and ligand effects which are deemed to be important factors on the structural, electronic, and vibrational properties of ligated gold clusters.[142] In the DFT calculations we employed an effective core potential (ECP)[174] for the Au atoms. In order to accelerate the DFT calculations, we employed the resolution-of-the-identity (RI) approximation with the corresponding auxiliary basis sets.[175] All non-periodic DFT calculations were carried out using the implementation of the ORCA code.[176] DFTB2 single point energy and geometry optimization calculations were performed with the DFTB+ code.[177] All DFTB calculations were carried out with the shell-resolved SCC option "OrbitallyResolvedSCC = Yes". The auorg parameter was designed such that this option mostly affects the charge distribution on the gold atoms themselves and their interactions with the other elements.

To test the accuracy of the DFTB parameters for the prediction of vibrational spectroscopic data, we compared DFTB- and PBE-calculated far-IR spectra to the experimental spectra for $[Au_6(dppp)_4]^{2+}$, $[Au_8(PPh_3)_8]^{2+}$ and $[Au_9(PPh_3)_8]^{3+}$ clusters. The DFTB2 IR vibrational spectroscopy calculations were computed using the GAMESS-US code.[96,178] The simulated IR spectra were obtained by convoluting the calculated stick spectra using a Lorentzian line shape function with 3 cm^{-1} full width at half maximum.

The transferability of the DFTB parameters was evaluated by comparing DFT and DFTB energy landscapes of PH_3 adsorption on the Au(111) surface. A 4x4 supercell consisting of 4 layers of Au atoms was cut from bulk and a vacuum layer of 20 Å was added to effectively suppress through-space slab-slab interactions. For the adsorption energy scans, all Au atoms were fixed. Selective geometry relaxation was used by constraining the P atom of the PH_3 molecule in all but the z-direction, while the H atoms the were fully optimized. For the DFT calculations, the PBE functional was used with the projector augmented wave

Table 3.3: Experimental crystal structures taken from the CSD database for the test set

Complexes	CSD codes
$[Au_6(dppp)_4]^{2+}$	BOTSOS[179]
$[Au_6(PPh_3)_6]^{2+}$	CATPAO10[180]
$[Au_7(PPh_3)_7]^{+}$	BIXZAK[181]
$[Au_8(PPh_3)_7]^{2+}$	BASWUN10[181]
$[Au_8(PPh_3)_8]^{2+}$	OPAUPF[182]
$[Au_8S_2(dppm)_4]^{2+}$	LEVKIJ[146]
$[Au_9(PPh_3)_8]^{3+}$ (D_{2h})	MIVPOX[183]
$[Au_{11}(PMePh_2)_{10}]^{3+}$ (C_{3v})	ZUCMAL[184]
$[Au_{11}(PMePh_2)_{10}]^{3+}$ (D_{4d})	ZUCMEP[184]
$[Au_{13}(dppm)_6]^{5+}$	LEVKAB[146]
$[Au_{20}(PP_3)_4]^{4+}$	POFPUX[185]
$Au_{22}(dppo)_6$	TOCFIC[186]
$[Au_{38}(m\text{-}MBT)_{20}(PPh_3)_4]^{2+}$	CEMZIG[187]
$Au_{70}S_{20}(PPh_3)_{12}$	TELMUV[145]

(PAW) approach,[188] the kinetic energy cutoff was 450 eV, and k-point grids were generated dynamically using a 3x3x1 Monkhorst-Pack scheme. The DFT calculations were carried out with the Vienna Ab initio simulation package (VASP) program in conjunction with the provided "PAW_PBE" pseudopotentials.[189,190] The convergence criteria were set to 10^{-6} eV for achieving self-consistent field energies, and 0.005 eV/Å for the maximum force in case of geometry optimizations.

For the demonstration application, a case study on the large $Au_{108}S_{24}(PPh_3)_{16}$ metalloid was performed. The initial positions of Au, S, and P atoms were taken from the experimental crystal structure (CSD code: DAFLOO). The PH_3 and PPh_3 ligands were added based on the position of the P atoms in the CIF file. Then, these complexes went through a two-step geometry optimization: First, only C and H atoms were optimized while Au, S and P atoms were fixed, and second, all atoms were optimized. The fully relaxed complexes were used to calculate binding energy, electronic properties and the IR spectrum.

3.4 Results and discussion

3.4.1 Performance for small- and moderate-sized clusters

Small-Sized Clusters: The differences between DFTB and TPSS/def2-SVP levels of theory for optimized geometries and ligand binding energies were evaluated for nine model complexes, which were constructed from three small-sized gold clusters Au_n (n = 2, 3, and 4) with three phosphorus-based donor ligands, including PH_3, PMe_3 and PPh_3. Overall, Figure 3.1 shows that all three parameter sets are performing very well, as measured by the root mean square deviation (RMSD) over Au and P atom positions, with all values below 0.13 Å. auorg$^{\alpha}$ is superior among the three sets with a maximum RMSD of only 0.09 Å, while auorg$^{\alpha'}$ produces typically the largest error. The averaged and normalized DFTB ligand binding energy generally shows overbinding for these small-sized complexes relative to the reference TPSS/def2-TZVP level of theory, strongest for auorg$^{\alpha'}$ and least for auorg$^{\alpha}$ (see Figure 3.1 and Table A.2 in the Supporting Information). We note that the deviation in ligand binding energies decreases with the size of gold clusters as well as the size of the

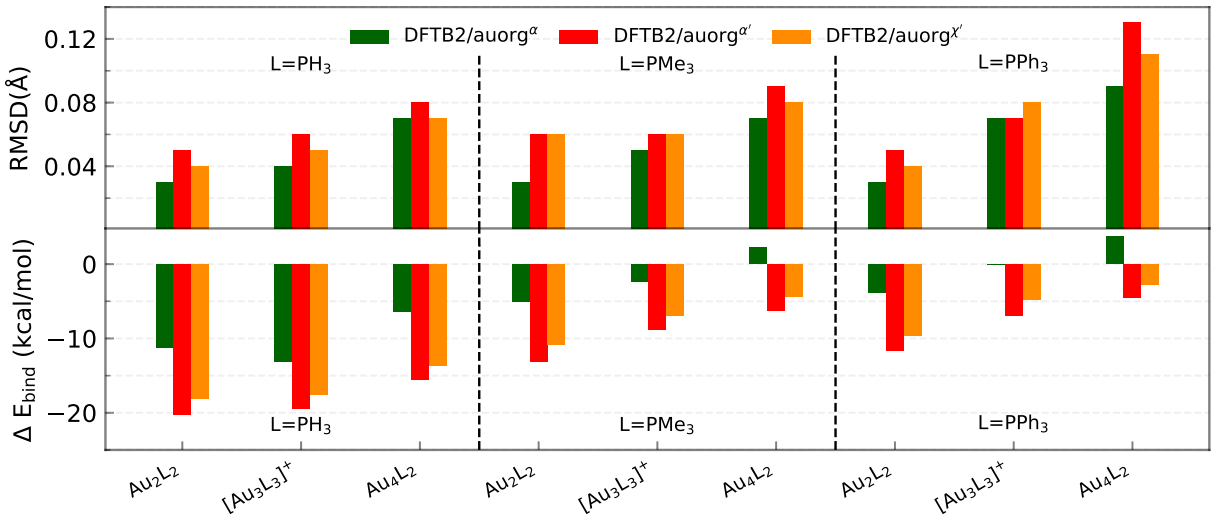

Figure 3.1: RMSD over atomic positions (upper panel), and deviation in averaged and normalized ligand binding energies (lower panel) for the small-sized gold clusters with different phosphine ligands (L = PH_3, PMe_3, and PPh_3). The RMSD over atomic positions only considers Au and P atoms.

ligands: Errors are largest for the PH_3 ligand and smallest for the PPh_3 ligand. The variation of the binding energy deviation can be attributed to the electronic interaction rather than the repulsive potential: while all Au-P bond lengths in these complexes are almost the same, ≈ 2.35 Å, the averaged and normalized ligand binding energies increase with the Au cluster size as well as ligand size. For instance, the ligand binding energies of PH_3, PMe_3, PPh_3 with Au_4 cluster are -33.91, -46.44, and -48.69 kcal/mol respectively. Since the overbinding can be caused by low virtual orbital energies, it makes sense that the auorg$^{\alpha\prime}$ is mostly affected by it. As for the ranking in performance for averaged and normalized ligand binding energies, we find the same order as for the geometries: auorg$^{\alpha}$ is the best parameter in terms of binding energy, while auorg$^{\alpha\prime}$ performs the worst.

Moderate-Sized Clusters: Figure 3.2 displays the same performance data for moderate-sized clusters Au_n ($n = 6 - 22$) with phosphine or trimethylphosphine ligands. The DFTB optimized geometries agree acceptably well with those from TPSS/def2-SVP, with RMSDs less than 0.5 Å in most cases. Exceptionally, three cases of $[Au_7(PH_3)_7]^+$, $Au_{22}(PH_3)_{12}$ and $[Au_{20}(PMe_3)_{16}]^{4+}$ complexes exhibit RMSD values larger than 0.7 Å. While the RMSD of auorg$^{\alpha\prime}$ and auorg$^{\chi\prime}$ for these three clusters, and auorg$^{\alpha}$ for $Au_{22}(PH_3)_{12}$ $[Au_{20}(PMe_3)_{16}]^{4+}$ remain in an acceptable range around $\approx$0.7 Å, the auorg$^{\alpha}$ RMSD value of 1.18 Å appears problematic for $[Au_7(PH_3)_7]^+$. After closer inspection, we conclude that this large value results from a strongly distorted Au_7 core shape that can only be stabilized when larger ligands such as PMe_3 or PPh_3 are used. It is worth mentioning that these model systems are experimentally not stable in general, because the gold core prefers a planar structure rather than a 3D geometry, unless ligands are present.[191,192] The model geometries here were constructed by replacing the experimentally used ligands (listed in Table 3.3) with PH_3 or PMe_3 ligands. For these hypothetical models, large RMSDs are expected because the presence of many local minima on the potential energy surfaces complicates the geometry optimization, and can cause the DFT and DFTB geometry optimization to converge to different local minima. For the $[Au_7(PH_3)_7]^+$ cluster, lower RMSDs were observed for auorg$^{\alpha\prime}$ and auorg$^{\chi\prime}$ because these two parameters increase the contribution of the P 3d-orbital in stabilizing the complex due to its lower orbital energy.

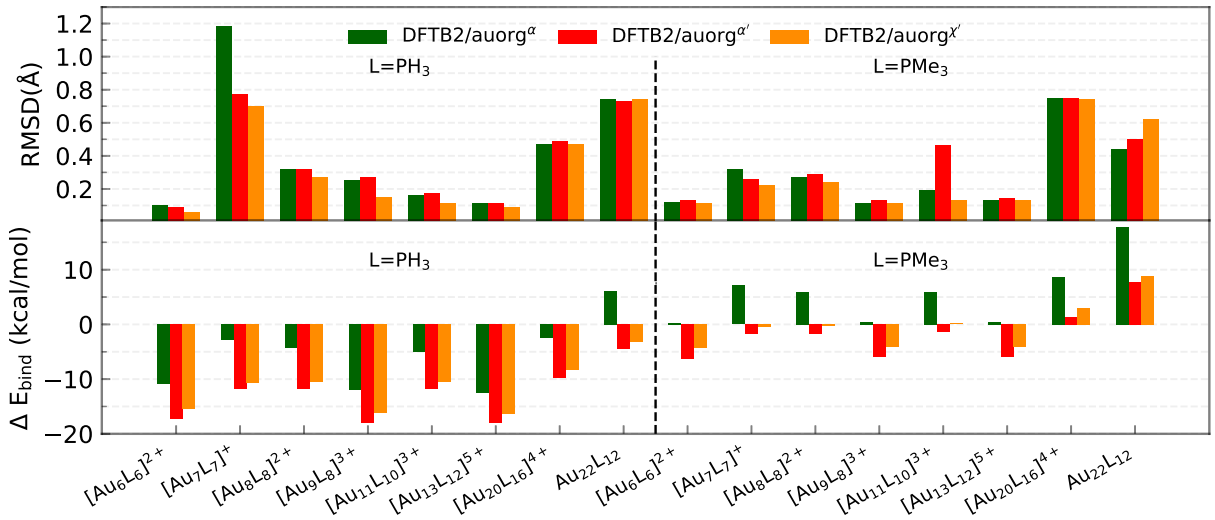

Figure 3.2: RMSD over atomic positions (upper panel), and deviation in averaged and normalized ligand binding energies (lower panel) for the moderate-sized phosphine-stabilized gold clusters with phosphine ligands (L = PH_3 and PMe_3). The RMSD over atom positions only considers Au and P atoms.

Compared to the situation in small-sized clusters, ligand overbinding is less prominent in the medium-sized systems for both auorg$^{\alpha\prime}$ and auorg$^{\chi\prime}$ parameters, with energy deviations as high as -18 kcal/mol for the smallest PH_3-ligated clusters (see Figure 3.2 and Table A.3 in the Supporting Information). Again we find generally that the averaged and normalized ligand binding energy deviations become smaller when the larger PMe_3 ligands are used. Again, auorg$^{\alpha}$ has smaller overbinding than the other two parameters for PH_3 ligands, and this tendency turns to underbinding when the larger PMe_3 ligands are used. The performance ranking for the three parameter sets is less clear-cut as in the case of the small-sized clusters, but especially in terms of ligand binding energies we find the tendency confirmed that auorg$^{\alpha}$ tends towards least overbinding and auorg$^{\alpha\prime}$ towards greatest overbinding, with auorg$^{\chi\prime}$ somewhere in between but closer to auorg$^{\alpha\prime}$. Since small ligands themselves consistenly tend to increase overbinding, we find that auorg$^{\alpha}$ performs best for small ligands and small Au clusters, while auorg$^{\alpha\prime}$ or auorg$^{\chi\prime}$ parameters are better for larger ligands and larger gold clusters.

3.4.2 Performance for large-sized clusters

The accuracy of the new DFTB2 parameters for geometries and ligand binding energies was further assessed for a series of gold clusters (Au_n, $n = 6 - 70$) in complexes with their experimentally used larger ligands including PPh3, $PMePh_2$, PP_3, dppp, dppm, dppo, and m-MBT, see Table 3.3. In this test, the experimental crystal structures were used as the reference geometry for RMSD evaluation, rather than DFT geometries. In both DFT and DFTB calculations, all counterions were removed and no symmetry constrains were applied. In this section, only the performance of auorg$^{\alpha}$ and auorg$^{\alpha\prime}$ parameters is presented and discussed in the main text. The performance of the auorg$^{\chi\prime}$ parameter is presented in the Supporting Information.

Geometry: The RMSDs between experimental and computed cluster geometries shown in Figure 3.3 demonstrate that the DFTB2 methods are able to reproduce X-ray structures, with maximum RMSDs equal to 0.46 Å and 0.37 Å for auorg$^{\alpha}$ and auorg$^{\alpha\prime}$, respectively. The same RMSDs of auorg$^{\chi\prime}$ are shown in Figure A.2 in the Supporting Information. In fact, the DFTB2 geometries even outperform TPSS/def2-SVP geometries for many clusters in the test

set, as for instance in the case of $[Au_6(dppp)_4]^{2+}$ (BOTSOS), $[Au_6(PPh_3)_6]^{2+}$ (CATPAO10), and $[Au_8S_2(dppm)_4]^{2+}$ (LEVKIJ). In the previous section, $[Au_7(PH_3)_7]^+$, $Au_{22}(PH_3)_{12}$ and $[Au_{20}(PMe_3)_{16}]^{4+}$ model clusters were found to be the most problematic cases. Here, with the experimentally used ligands, DFTB-optimized structures of $[Au_7(PPh_3)_7]^+$, $[Au_{20}(PP_3)_4]^{4+}$, and $Au_{22}(dppo)_6$ have lower RMSD values than their previously described truncated model clusters with PH_3 and PMe_3. auorg$^{\alpha\prime}$ slightly outperforms auorg$^{\alpha}$ in most of the cases (by only up to 0.1 Å for the $[Au_{22}(dppo)_6]$) neutral complex). It is important to keep in mind that the RMSDs over atom position convolutes deviations in angles and torsions with the bond lengths. If one only considers bond length comparison, Au-Au and Au-P deviations are within 0.06 Å from experimental values.

In order to graphically illustrate the differences between experimental and computed DFT and auorg$^{\chi\prime}$ geometries, Figure 3.4 shows X-ray and optimized structures for the following ligated Au clusters: $[Au_6(dppp)_4]^{2+}$ (BOTSOS), $[Au_7(PPh_3)_7]^+$ (BIXZAK), $[Au_8(PPh_3)_8]^{2+}$ (OPAUPF), and $[Au_9(PPh_3)_8]^{3+}$ (MIVPOX-D_{2h}). The analogous comparison for auorg$^{\alpha}$ and auorg$^{\chi\prime}$ is shown in Figure A.3 in the Supporting Information. The overlapped structures were determined by a minimization procedure, which includes recentering and rotation to minimize the RMSD using the quaternion algorithm.[193] The figure highlights the good performance of the theoretical methods in the description of the cluster core geometries relative to experiment. We note that ligand orientations can be strongly impacted by crystal field effects that are not present in our gas phase theoretical calculations, and thus we will not discuss differences in ligand geometries.

Binding Energy: The evaluation of predicted averaged and normalized ligand binding energies follows the schemes used above for the smaller-sized and moderate-sized clusters. The ligand binding energies are listed in Table A.4 in the Supporting Information, the relative deviations of the DFTB methods from TPSS/def2-SVP data are shown in Figure 3.5 for auorg$^{\alpha}$ and auorg$^{\alpha\prime}$, and Figure A.4 in the Supporting Information for auorg$^{\chi\prime}$. All predictions by DFTB tend towards underbinding, with only three minor exceptions. From the smallest $[Au_6(dppp)_4]^{2+}$ up to $[Au_{13}(dppm)_6]^{5+}$, the auorg$^{\alpha\prime}$ binding energy deviations of ≤ 5 kcal/mol are in very good agreement with the DFT reference. auorg$^{\alpha}$ trends towards strong underbinding in all cases. In the case of clusters with more core Au atoms ($n \geq 20$),

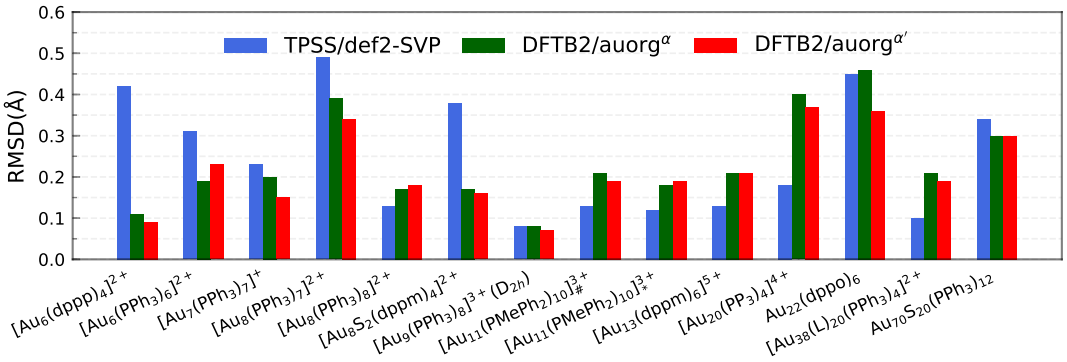

Figure 3.3: RMSD over atomic positions for the large-sized phosphine-stabilized gold clusters. The RMSD of atomic positions considers Au, and P atoms for all large-sized phosphine-based gold clusters, $[Au_{11}(PMePh_2)_{10}]^{3+}_{\#}$ denotes $[Au_{11}(PMePh_2)_{10}]^{3+}$ (C_{3v}), $[Au_{11}(PMePh_2)_{10}]^{3+}_{*}$ denotes $[Au_{11}(PMePh_2)_{10}]^{3+}$ (D_{4d}), $[Au_{38}(L)_{20}(PPh_3)_4]^{2+}$ denotes $[Au_{38}(m\text{-}MBT)_{20}(PPh_3)_4]^{2+}$.

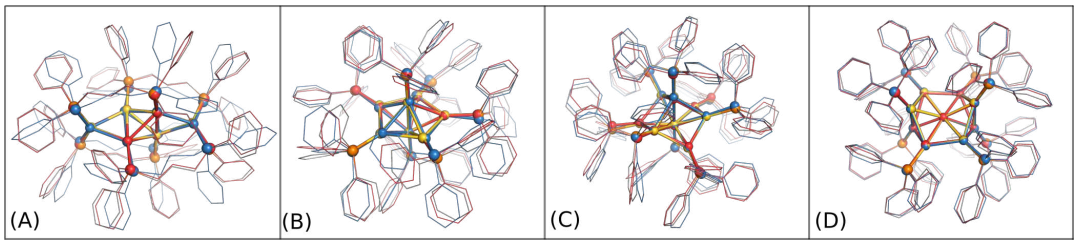

Figure 3.4: Overlap of experimental crystal structure (Au in gold, P in orange and C in grey) and optimized auorg$^{\alpha\prime}$ and DFT structures. auorg$^{\alpha\prime}$ and DFT structures are represented by light red and sky blue, respectively. The gold nanoclusters considered in this figure are (A) $[Au_6(dppp)_4]^{2+}$ (BOTSOS), (B) $[Au_7(PPh_3)_7]^{+}$ (BIXZAK), (C) $[Au_8(PPh_3)_8]^{2+}$ (OPAUPF), and (D) $[Au_9(PPh_3)_8]^{3+}$ (MIVPOX-D_{2h}).

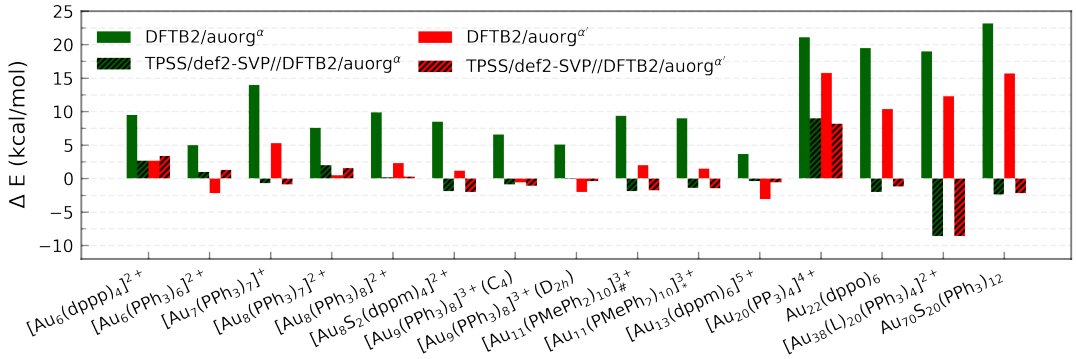

Figure 3.5: Deviation in averaged and normalized ligand binding energies for the large-sized phosphine-stabilized gold clusters in reference to the TPSS/def2-SVP binding energies, $[Au_{11}(PMePh_2)_{10}]^{3+}_{\#}$ denotes $[Au_{11}(PMePh_2)_{10}]^{3+}$ (C_{3v}), $[Au_{11}(PMePh_2)_{10}]^{3+}_{*}$ denotes $[Au_{11}(PMePh_2)_{10}]^{3+}$ (D_{4d}), $[Au_{38}(L)_{20}(PPh_3)_4]^{2+}$ denotes $[Au_{38}(m\text{-}MBT)_{20}(PPh_3)_4]^{2+}$.

auorg$^{\alpha}$ and auorg$^{\alpha\prime}$ have both noticeable underbinding as high as 20 and 15 kcal/mol, respectively. The results are consistent with the overall trend that was already seen in the small-sized and moderate-sized ligand complexes above. To further investigate the effect of geometry on the ligand binding energies, TPSS single point energy calculation using the DFTB optimized geometries were carried out, and the corresponding deviations in ligand binding energies are shown in Figure 3.5 and Figure A.4 in the Supporting Information, indicated as usual by the at-the-geometry-of symbol "//" symbol. It becomes immediately obvious that the deviation of ligand binding energies with TPSS single point energy refinement is reduced in all cases, with a maximum absolute deviation of ≤ 9 kcal/mol. It follows that, if highly accurate ligand binding energies are required, DFTB geometry optimizations followed by TPSS single point energy calculations can provide a reasonable "shortcut" over straightforward DFT calculations. In addition to the binding energies, DFTB isomerization energies are compared to the DFT values as well for $[Au_9(PPh_3)_8]^{3+}$ and $[Au_{11}(PMePh_2)_{10}]^{3+}$ clusters, see Figure A.5 in the Supporting Information for more details.

3.4.3 Gold cluster-ligand bond dissociation energy curves for the $[Au_8(PPh_3)_8]^{2+}$ complex

Ligand removal of nanoscale gold clusters is a key step in making the clusters catalytically more active by increasing the gold core interaction with the substrate or reactants. Previous studies have reported the partial removal of ligands of atomically-precise gold clusters $Au_n(PPh_3)_m$ (n = 8, 9, 11, and 101) on titania after undergoing different treatments such as calcination and acid-washing.[131,132] One of the primary applications of the DFTB methodology developed here is the theoretical study of cluster fragmentation and the catalytic reaction mechanisms of clusters with dissociated ligands. For validation against DFT, we therefore compare rigid energy scans for Au-P bond dissociation between TPSS/def-SVP and DFTB2 methods for the aforementioned $[Au_8(PPh_3)_8]^{2+}$ cluster as a representative for the experimentally relevant complexes with larger ligands. Starting from the DFT optimized geometries of the cluster, the Au-P bond of the ligand in question was simply stretched up to a distance of 20 Å. The relative energy ΔE of this practically dissociated

geometry was defined in all methods as 0 kcal/mol. In reality, complex structural relaxation of the cluster and ligand would occur obscuring methodological differences, which is the reason for presenting rigid scans. Figure 3.6 shows four different bond dissociation energy curves that correspond to four ligand detachment scans.

Overall, the DFTB curves mimic the TPSS curves closely in both energy of the binding region and the shape of the energy curves. The rigid scan does not include a barrier and converges within about 12 Å to the dissociation limit. As for the DFTB curves, we observe underbinding in the region from 2.5 to 6 Å in all of the plots (cf. Figure 3.5). DFTB is strongly underbinding in the case of one ligand by more than 30 kcal/mol (upper right curve in Figure 3.6). Here, the Au atom involved in the Au-P bond has a more "surface"-like binding with the other Au atoms as opposed to a pyramidal shape as in the other ligand cases. For more "cluster"-like detached Au atoms, the deviations are in the range of $\approx$ 5-10 kcal/mol. In all cases, DFTB2/auorg$^{\alpha\prime}$ and DFTB2/auorg$^{\chi\prime}$ are very similar to each other and outperform DFTB2/auorg$^{\alpha}$. As is typical for the DFTB method in general, the entrance region of the binding well, here around 6 Å, is underbinding since the atomic orbitals are compressed with fixed electronic confinement radii optimized to describe geometries and binding energies.[194] The underestimation of phosphine ligands binding to gold "surface" will be discussed further below regarding the adsorption of a PH_3 molecule on the gold (111) surface.

3.4.4 Electronic structures of phosphine-stabilized gold clusters

To evaluate the ability of DFTB to accurately describe electronic structures of phosphine-stabilized gold clusters, we investigated the frontier orbital energies (HOMO-1, HOMO, LUMO, LUMO+1) and HOMO-LUMO gaps (HLGs) of a number of medium-sized gold clusters using DFT and DFTB methods. In this discussion, we concentrate on the auorg$^{\alpha\prime}$ parameter, but show the corresponding performance of the other parameters in the Supporting Information. Figure 3.7 shows the TPSS/def2-SVP and DFTB/auorg$^{\alpha\prime}$ calculated energy levels of the frontier molecular orbitals for selected gold clusters. The plots showing frontier orbitals computed with auorg$^{\alpha\prime}$ and auorg$^{\chi\prime}$ are shown in Figure A.6 in the Supporting Information. The total charge in the selected clusters changes from +1 to

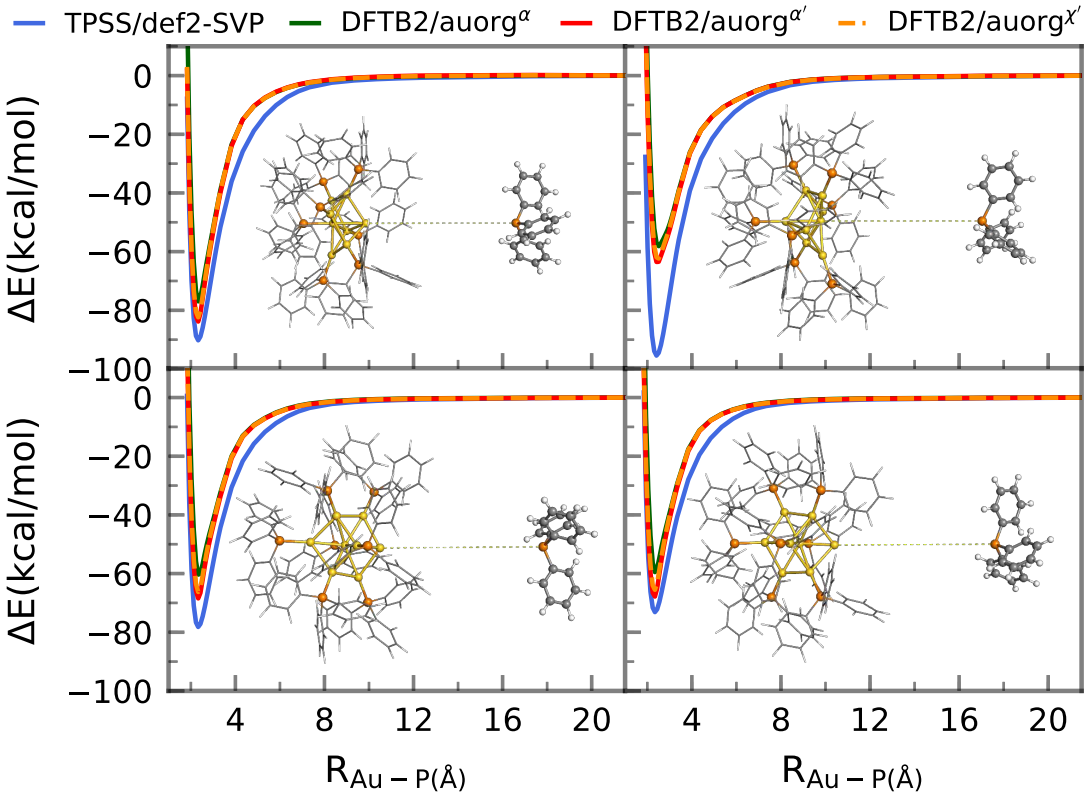

Figure 3.6: Gold cluster-ligand rigid bond dissociation energy curves of $[Au_8(PPh_3)_8]^{2+}$.

+3, with the orbitals of the least charged clusters being highest in absolute orbital energies, and the highest charged clusters having lowest absolute orbital energies. Within the energy range spanned by these four orbitals among these clusters, the DFTB orbital energy levels reproduce TPSS orbital energy levels very well, as indicated by the dashed lines to mark the changes of electronic structure with molecular structure and total charge. Individual orbital energy level shifts are appreciable and may reach ≈0.9 eV (see Table A.6), with a general trend towards lower energies. Regarding HLGs, DFTB/auorg$^{\alpha\prime}$ tends to underestimate those for the singly charged $[Au_7(PPh_3)_7]^+$ (BIXZAK), the doubly charged $[Au_8(PPh_3)_8]^{2+}$ (OPAUPF), and the triply charged $[Au_{11}(PMePh_2)_{10}]^{3+}$ (ZUCMEP) clusters. In these particular three clusters, the DFTB HOMO energy shifts are -0.28, -0.32, and -0.40 eV for Au_7, Au_8 and Au_{11} respectively, while their LUMO shifts are -0.63, -0.89, -0.92 eV, obviously quantitatively larger. This imbalance results in their smaller HOMO-LUMO gap values. Nonetheless, the HLG values of DFTB/auorg$^{\alpha\prime}$ are quantitatively close to the TPSS calculated values with deviations no greater than 0.6 eV.

Figure A.7, in the Supporting Information, displays the HOMO and LUMO orbital shapes for $[Au_6(dppp)_4]^{2+}$, $[Au_7(PPh_3)_7]^+$ (BIXZAK), $[Au_8(PPh_3)_8]^{2+}$ (OPAUPF) and $[Au_9(PPh_3)_8]^{3+}$ (MIVPOX-D_{2h}) clusters for the TPSS and DFTB2/auorg$^{\alpha\prime}$ methods. Despite some inevitable quantitative differences in the orbital topology, the amplitudes of the HOMO and LUMO orbitals obtained with the DFTB2/auorg$^{\alpha\prime}$ method are very close to the ones obtained by TPSS/def2-SVP. Noticeable qualitative differences are the LUMOs of Au_7 and Au_8 where DFTB both overestimated the contribution from the gold core and less contributions from the phosphine ligands, possibly providing a rationale for the previously discussed large LUMO energy shifts of Au_7 and Au_8. The HOMO and LUMO plots of DFTB2/auorg$^{\alpha}$ and DFTB2/auorg$^{\chi\prime}$ are shown in Figures A.8 and A.9 in the Supporting Information. Both of these two sets of molecular orbitals have similar shapes with DFTB2/auorg$^{\alpha\prime}$ orbitals; with DFTB2/auorg$^{\alpha}$ also overestimating contribution from the gold core while DFTB2/auorg$^{\chi\prime}$ underestimates the gold and overestimates the contribution from phosphine ligands in Au_7. We note that these differences within the different DFTB parameter sets originate mostly from the different choices of the virtual orbital energies (see Table 3.1) and a minor degree from the different geometries.

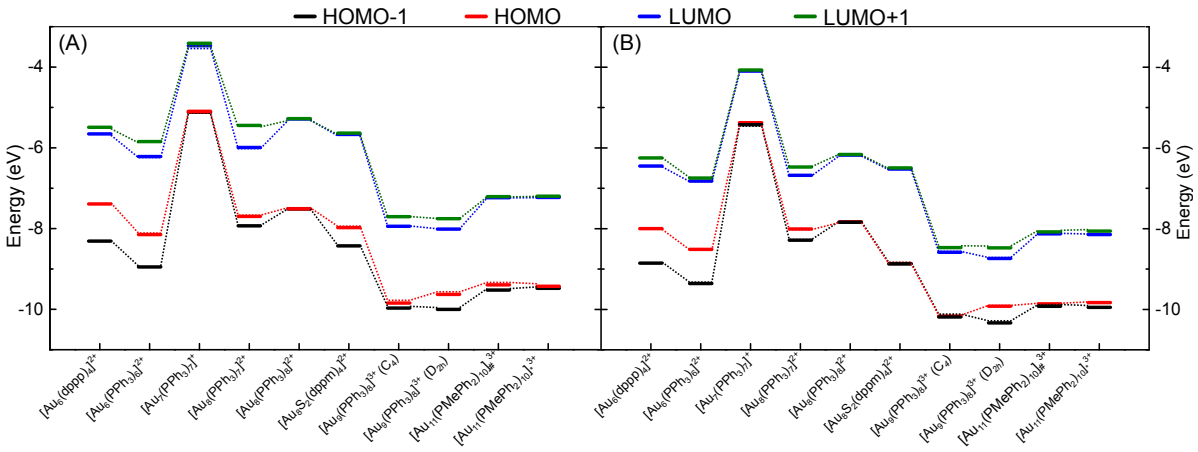

Figure 3.7: Energy level diagram for the frontier orbitals of various clusters as calculated by (A) TPSS/def2-SVP and (B) DFTB2/auorg$^{\alpha\prime}$, $[Au_{11}(PMePh_2)_{10}]^{3+}_{\#}$ denotes $[Au_{11}(PMePh_2)_{10}]^{3+}$ (C_{3v}), $[Au_{11}(PMePh_2)_{10}]^{3+}_{*}$ denotes $[Au_{11}(PMePh_2)_{10}]^{3+}$ (D_{4d}). Dashed lines are included to guide the eye.

3.4.5 IR spectra of $[Au_6(dppp)_4]^{2+}$, $[Au_8(PPh_3)_8]^{2+}$ and $[Au_9(PPh_3)_8]^{3+}$ clusters

The IR spectra of $[Au_6(dppp)_4]^{2+}$ (BOTSOS), $[Au_8(PPh_3)_8]^{2+}$ (OPAUPF), and $[Au_9(PPh_3)_8]^{3+}$ (MIVPOX-D_{2h}) clusters have been studied previously both experimentally and computationally using DFT[138] and therefore represent good choices for the performance of our DFTB parameters for predicting vibrational spectra. The calculated DFTB IR spectra were evaluated by comparing them with experimental data and DFT-calculated IR, see Figure 3.8 and Figure A.10 in the Supporting Information. The experimental far-IR spectra of the three clusters consists of two main parts: gold core distortion between the range 90-250 cm^{-1} and Au-P modes above 400 cm^{-1}. Both PBE/def2-SVP and DFTB2/auorg$^{\alpha'}$-calculated IR spectra match the previously reported experimental and M06/LANL2DZ predicted spectra, having the same mode description for each vibration. Also, the DFTB and PBE normalized spectral shapes are in good agreement, especially concerning the main peaks involving Au-P interactions. A noticeable difference between the experimental and calculated spectra of Au_8 and Au_9 is the presence of an experimentally distinct peak at 398 cm^{-1}. While all DFT and DFTB methods are able to predict peaks that are comparable with the position of this feature, the calculated intensities in DFTB are considerably weaker. Nevertheless, both methods have shown that this peak can be attributed to phenyl group twisting vibrations. Another difference is the presence of a peak at 317 cm^{-1} in the Au_8 and Au_9 DFTB calculated spectra that is missing in the DFT spectra. The DFTB peak matches a seemingly broad experimental peak in the same region. In the previous study,[138] this peak was not assigned to any vibrational mode, as DFT was not able to predict this feature. DFTB revealed that these peaks near 317 cm^{-1} of Au_8 are related to vibrations with weaker intensity assigned to a phenyl rocking vibration that is attached to protruding Au_1-P_8. In the case of Au_9, this peak has several contributing vibrations that are also assigned to a phenyl rocking of the complex's several phosphine ligands. The summary of contributing transitions for all clusters are given in Tables A.7 to A.9 in the Supporting Information. We conclude that DFTB is very useful in the prediction of vibrational spectra for nanoscale gold clusters with stabilizing ligands; this had not been discussed in the previous auorg parameterization work.[61,69]

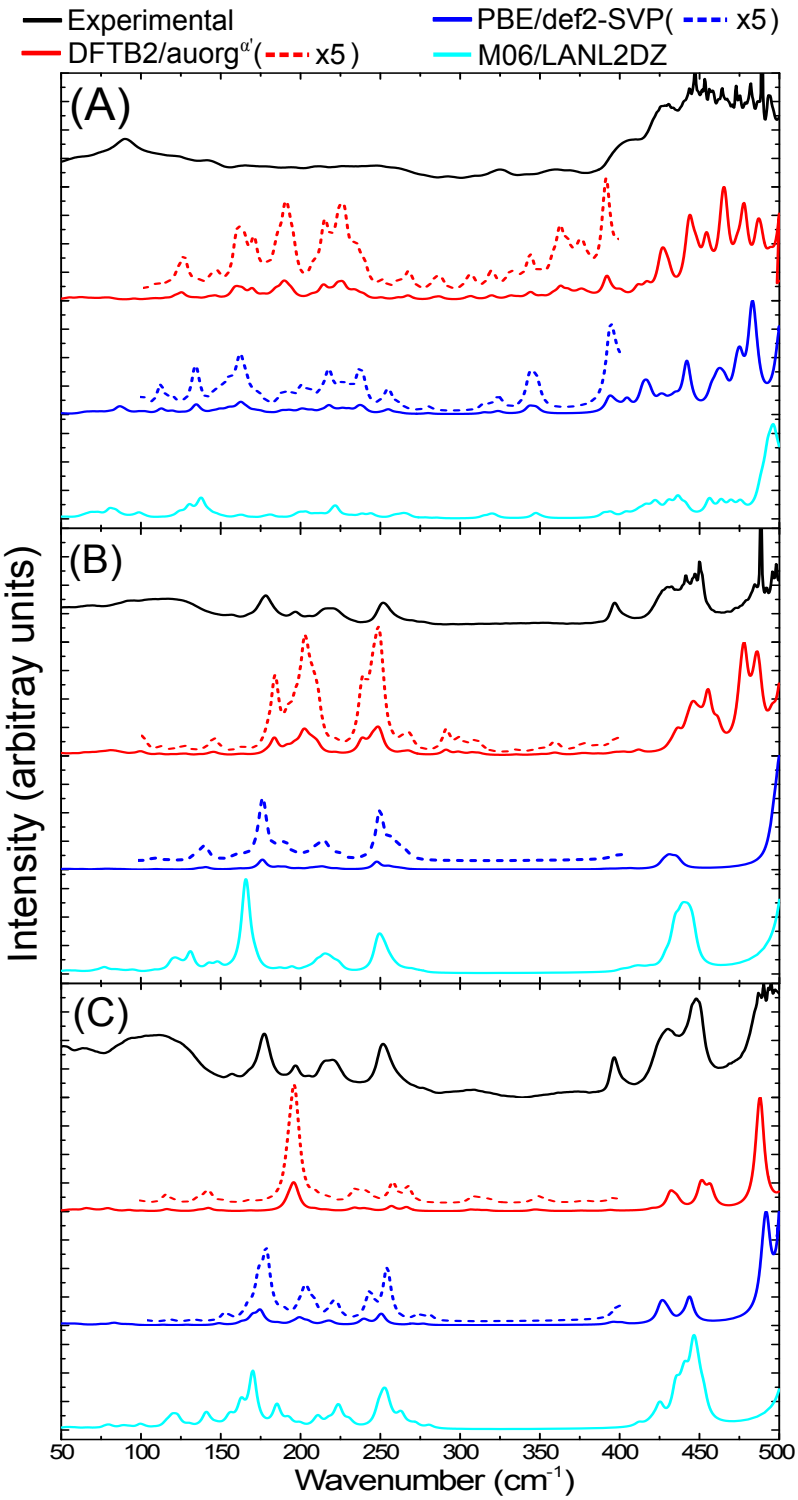

Figure 3.8: Experimental (in black),[138] computed DFTB2/auorg$^{\alpha\prime}$ (in red), PBE/def2-SVP (in blue) and M06/LANL2DZ (in cyan) far-IR spectra for (A) $[Au_6(dppp)_4]^{2+}$, (B) $[Au_8(PPh_3)_8]^{2+}$, and (C) $[Au_9(PPh_3)_8]^{3+}$ clusters. The additional red and blue dashed lines are for the scaled up plots of the region 100-400 cm^{-1} for DFTB2/auorg$^{\alpha\prime}$ and PBE/def2-SVP.

3.4.6 Chemisorption of PH_3 on the Au (111) surface

To evaluate the transferability of the new DFTB parameters, we explored the energy landscape of PH_3 chemisorption on the Au (111) surface and compared it to DFT with the PBE functional, which is popular in the solid state community to simulate surface processes. The computed DFTB2/auorg$^{\alpha}$, DFTB2/auorg$^{\alpha\prime}$, DFTB2/auorg$^{\chi\prime}$ and PBE energy landscapes are shown in Figure 3.9. In this Au (111) surface model, there are three important adsorption locations: top, hollow fcc, and hollow hcp (see Figure A.11 in the Supporting Information). The corresponding top and hollow adsorption sites are marked in Figure 3.9 for reference. This test is particularly useful for evaluating the transferability of the new parameters, as the number of Au atoms coordinating with the P atom of PH_3 molecule varies from one at the top site, to two at the bridge sites (see Figure A.11 in the Supporting Information), to three at the hollow sites. Figure 3.9 shows that the adsorption energies vary in a range of approximately 5 kcal/mol, and both auorg$^{\alpha\prime}$ and auorg$^{\chi\prime}$ parameters are able to reproduce qualitatively the relative PBE energy landscape. The top site is the most preferred adsorption location of PH_3 adsorption on the Au (111) surface according to PBE, DFTB2/auorg$^{\alpha\prime}$ and DFTB2/auorg$^{\chi\prime}$. However, DFTB2/auorg$^{\alpha}$ predicts the most preferred adsorption location is somewhere in the middle of top, hollow fcc, and hollow hcp positions.

Considering the absolute binding energy, all three DFTB parameter sets underestimate the Au-P interaction energy compared to the PBE method. Among them, the underestimation is smallest with the deviation $\Delta E \approx 4.6 - 7.4$ kcal/mol for auorg$^{\alpha\prime}$, the deviation $\Delta E \approx 7.6 - 9.8$ kcal/mol for auorg$^{\chi\prime}$, and largest with $\Delta E \approx 8.9 - 9.8$ for auorg$^{\alpha}$. The trends in the deviations can again be rationalized by correlating them with the orbital energies of the virtual Au 6p and P 3d orbitals: The larger the upward shift, the greater the underbinding. This test shows that DFTB2/auorg$^{\alpha\prime}$ is the best option to study phosphine ligands chemisorbed on Au surfaces, and that our parameter has difficulties for the interaction of phosphines with flat Au surfaces, as mentioned above in Section 3.4.3.

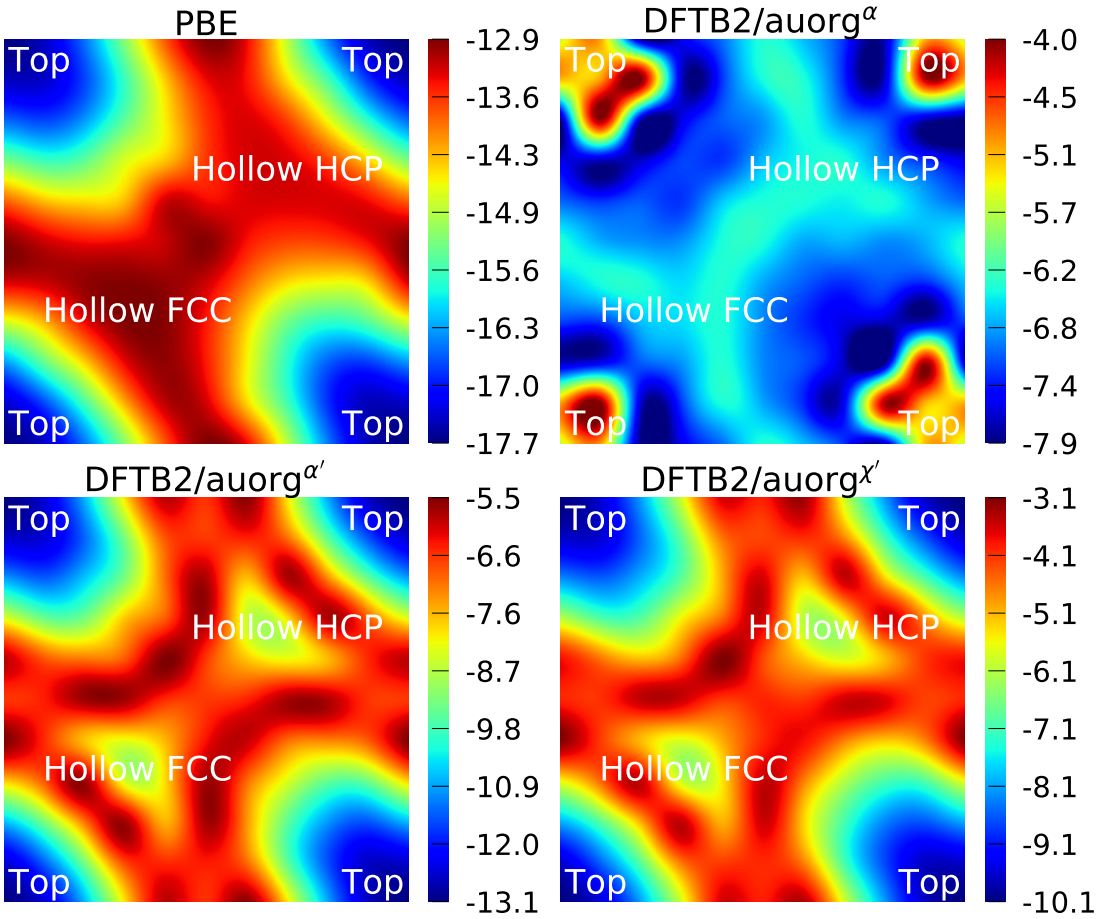

Figure 3.9: Energy landscape in kcal/mol of PH_3 adsorption on the Au (111) surface obtained at the PBE and DFTB2 methods. The energy profiles show the three important adsorption locations of the Au (111) surface for clear comparison.

3.4.7 Case study for $Au_{108}S_{24}(PPh_3)_{16}$: geometry, ligand binding energy, frontier orbitals, and IR spectra

In order to demonstrate the capability of the new DFTB parameters for the study of large-scale phosphine-stabilized gold clusters, we performed a case study for the recently synthesized metalloid complex $Au_{108}S_{24}(PPh_3)_{16}$.[144] The core of the metalloid consists of a Russian doll motif with an Au_6 inner octahderon enclosed by a second-shell Au_{38} octahedron. This core is then capped at its six tips by novel Au_4S_4 planar rings, which are then connected by 4 more gold atoms, resulting in a $(Au_2S)_{24}$ outer shell motif. Finally, sixteen $Au(PPh_3)$ groups complete this metalloid and are bound to each side of the Au_{44} octahedral Russian-doll core. The available experimental crystal structure (CSD code: DAFLOO) provides a clear picture of Au, S and P atomic positions in 3D. However, it does not depict the positions of C atoms well due to overlapping rings of the triphenylphosphine groups, with unreasonable C-C distances in the CIF file, sometimes being shorter than 0.2 Å. To prepare the initial geometrical inputs for our DFTB geometry optimization, we constructed the initial structure based on the experimental positions of Au, S and P atoms, and then added manually the sixteen PPh_3 ligands. The geometry was then optimized using the DFTB2/auorg$^{\alpha\prime}$ method. Figure 3.10 compares the final DFTB optimized geometry to the initial, experimental crystal structure. DFTB2/auorg$^{\alpha\prime}$ predicts the averaged and normalized ligand binding energies of $Au_{108}S_{24}(PPh_3)_{16}$ to be -63.2 kcal/mol, in good agreement with TPSS/def2-SVP single point energies performed using our DFTB optimized geometries, which predicts the averaged ligand binding energy to be -72.9 kcal/mol. We note that a single point energy+gradient calculation on 16 "Intel Xeon E5-2697 2.30GHz CPU cores" took 39935 s (11.09 h) with DFT and only 27 s with DFTB, corresponding to a speed-up factor of nearly 1500x. The DFTB method is therefore the only practical option if one considers routinely carrying out geometry optimizations of large nanoscale gold clusters, or a more challenging molecular dynamics (MD) simulation with a few million steps to reach nanosecond time scales.

Computationally, the electronic structure of this cluster has been approximately investigated previously at the BP86/TZVPP level of theory, using a simplified model in which the triphenylphosphine ligands were replaced by PH_3 groups, and the entire structure assumed to

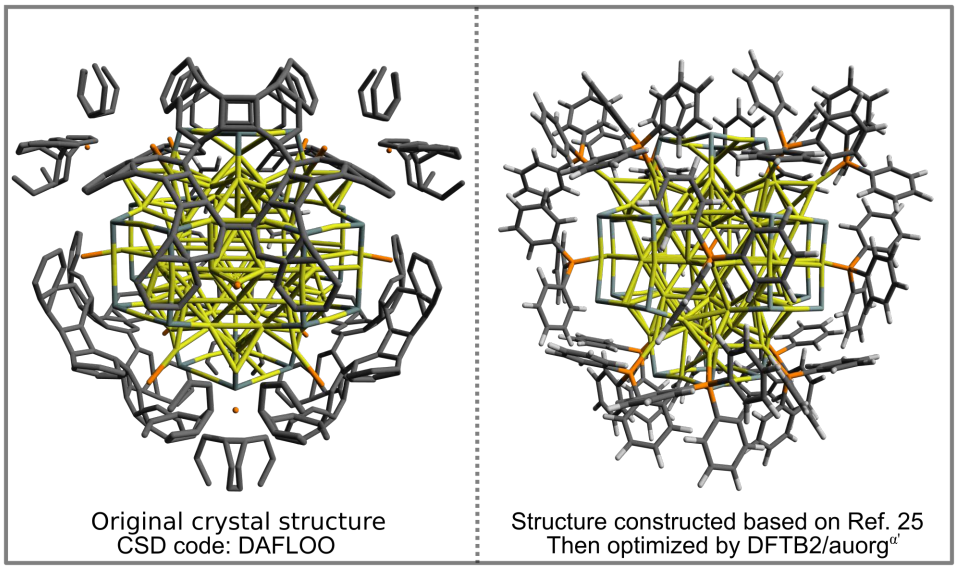

Figure 3.10: X-ray experimental structure of $Au_{108}S_{24}(PPh_3)_{16}$ taken from Cambridge Crystallographic Database (CSD code DAFLOO) with overlapping of the phenyl rings, caused by short ≈0.2 Å C-C bond lengths between triphenylphosphine groups, and DFTB2/auorg$^{\alpha'}$ optimized structure without overlapping of the phenyl rings.

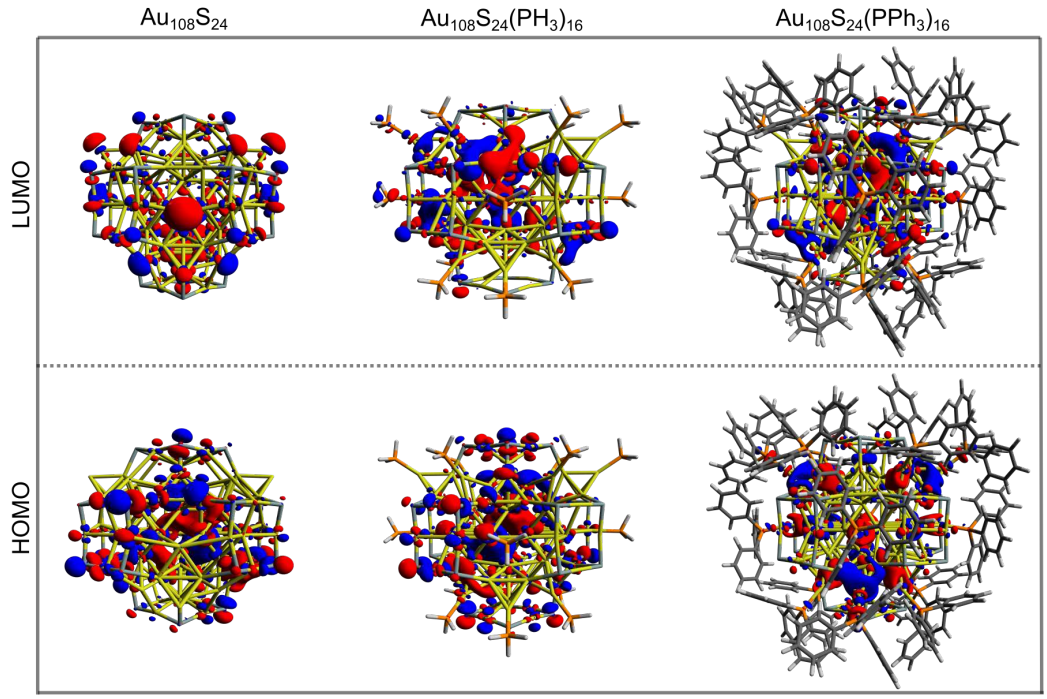

Figure 3.11: HOMO and LUMO plots of $Au_{108}S_{24}$, $Au_{108}S_{24}(PH_3)_{16}$, and $Au_{108}S_{24}(PPh_3)_{16}$ clusters as calculated by DFTB2/auorg$^{\alpha'}$; isosurface value = 0.015 a.u.

take T_d point group symmetry. The HOMO-LUMO gap of this simplified $Au_{108}S_{24}(PH_3)_{16}$ cluster was found to be 0.68 eV. Figure 3.11 shows the DFTB2/auorg$^{\alpha\prime}$ HOMO and LUMO plots of $Au_{108}S_{24}$, $Au_{108}S_{24}(PH_3)_{16}$, and $Au_{108}S_{24}(PPh_3)_{16}$ clusters. The calculated HOMO-LUMO gaps for these three clusters are 0.200 eV, 0.681 eV, and 0.634 eV, respectively. The increase in the HLG from the $Au_{108}S_{24}$ core to fully ligated cluster denotes that the phosphine groups stabilize the core, much like in $Au_{70}S_{20}(PPh_3)_{12}$.[145] The quantitative difference in the energy gaps between $Au_{108}S_{24}(PH_3)_{16}$ and $Au_{108}S_{24}(PPh_3)_{16}$ clusters are smaller than 0.05 eV. However, it is worth noting that partial density of state (PDOS) plots, see Figure 3.12, portray that there is an undeniable difference of sulfur-orbital contribution in the bonding of the $Au_{108}S_{24}(PH_3)_{16}$ and $Au_{108}S_{24}(PPh_3)_{16}$ clusters. In addition, both HOMO and LUMO are shifted by $\approx$ -0.80 eV when PPh_3 ligands are replaced by PH_3 ligands. In the case of the HLG, employing the simplified model $Au_{108}S_{24}(PH_3)_{16}$ yields a similar value to the HLG of the $Au_{108}S_{24}(PPh_3)_{16}$ cluster, however, the Fermi level has shifted dramatically by -0.8 eV! Our calculations therefore indicate that the use of a simplified model is inadequate and can indeed significantly affect the electronic properties of nanoclusters.

The calculation of IR spectra of large-scale systems within the normal mode approximation, requiring the calculation of the Hessian matrix, is beyond the capability of most contemporary DFT codes on current computer systems within a reasonable amount of time. In this case, DFTB can be particularly useful as it has been shown in the benchmark sections that DFTB can reproduce the experimental IR spectra very well. In this case study, we carried out DFTB2/auorg$^{\alpha\prime}$ Hessian calculations to predict the IR spectrum for the $Au_{108}S_{24}(PPh_3)_{16}$ cluster. Since the performance of DFTB in simulating infrared spectra of thiolate-ligated gold nanoclusters has not been tested before, in this work, we validated the accuracy of DFTB in predicting IR spectra for various thiolated gold clusters. We compare the DFTB simulated IR spectra of $Au_4(SCH_3)_4$, $[Au_{25}(SCH_3)_{18}]^-$ clusters, and six Au_{18} clusters protected with various types of ligands to the corresponding DFT and experimental spectra in the case of $Au_{18}(S-c\text{-}C_6H_{11})_{14}$.[142,150,151] The comparison is presented in the Supporting Information, Figure A.13 and Figure A.14. In summary, similar to phosphine-stabilized nanoclusters in Section 3.4.5, the DFTB-calculated IR spectra for thiolate-protected gold clusters agree well with previous DFT simulations and experimental

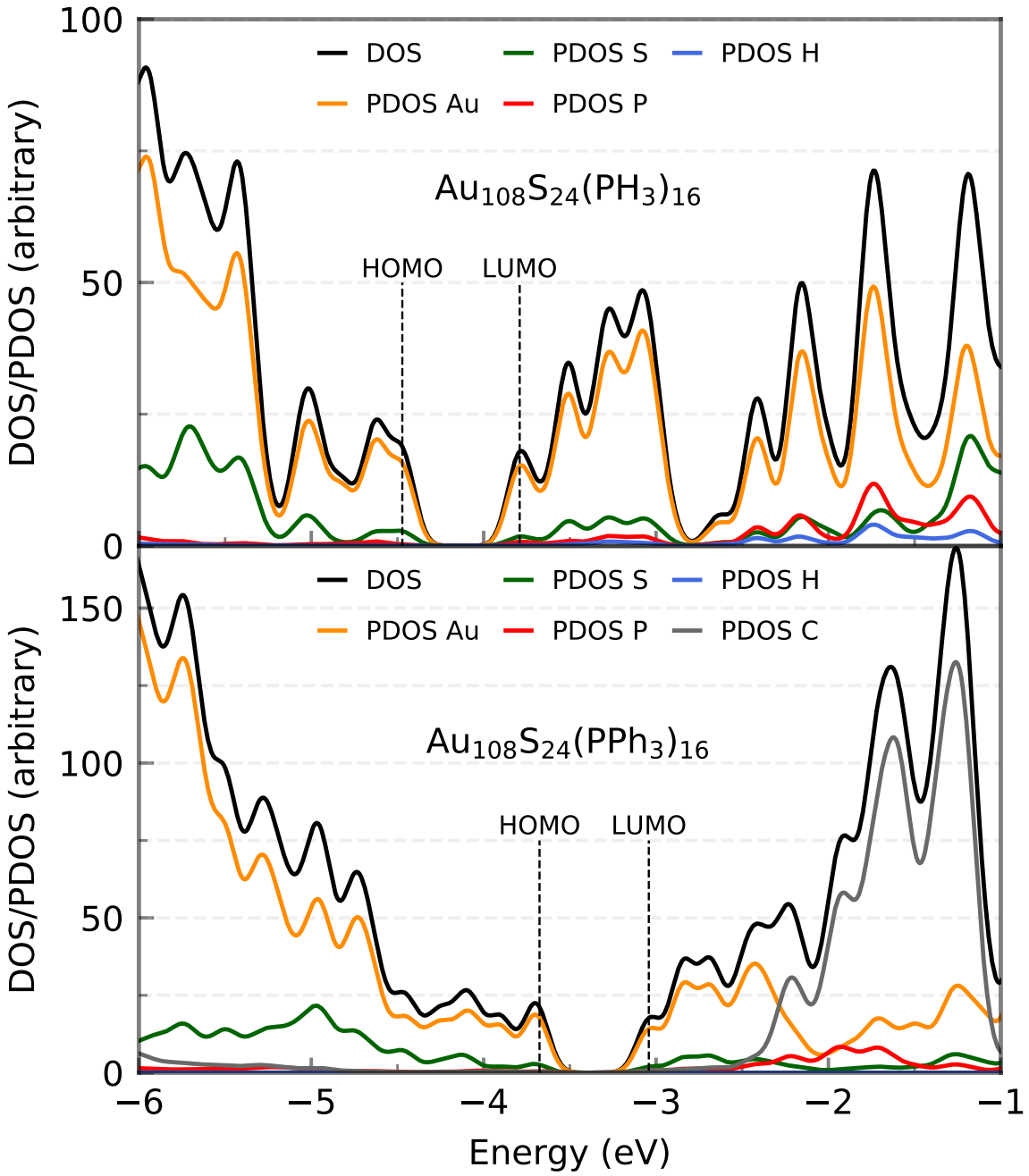

Figure 3.12: Density of states (DOS) and partial density of states (PDOS) of $Au_{108}S_{24}(PH_3)_{16}$ (top) and $Au_{108}S_{24}(PPh_3)_{16}$ (bottom) clusters as calculated by DFTB2/auorg$^{\alpha\prime}$.

IR spectra. These new results, in combination with the results presented in Section 3.4.5, indicate that DFTB is a reliable method in predicting IR spectra of thiolate- and phosphine-stabilized gold nanoclusters. Figure 3.13 shows the DFTB calculated far-IR spectrum of $Au_{108}S_{24}(PPh_3)_{16}$. We focus our attention on the far-IR region because it is of particular interest in understanding the core vibrations of Au, S, and P atoms. The calculated IR spectrum has several large peaks in the 500-600 cm^{-1} region which are attributed to PPh_3 distortions. The multiple peaks in the 200-350 cm^{-1} region are caused by various normal modes of both Au-P and Au-S vibrations (see Table A.10, Table A.11 and Table A.12 in the Supporting Information), the peaks labelled in the figure are the normal modes related to the novel Au_4S_4 planar rings: (1) Au-S stretching at 241.1 cm^{-1}, (2) S-Au-S-Au-S symmetric stretching at 277.2 cm^{-1} and (3) S-Au-S symmetric stretch at 517.05 cm^{-1}. The inset of Figure 3.13 shows several peaks < 150 cm^{-1} which are mostly attributed to Au_{44} core distortion.

Since the novel Au_4S_4 planar ring motif of $Au_{108}S_{24}(PPh_3)_{16}$ has not yet been studied using IR spectroscopy, there are no experimental validations so far about its normal modes. The calculated Au-S stretches found in this planar ring motif are compared with that of the $Au_4(SCH_3)_4$, $[Au_{25}(SCH_3)_4]^-$ and $[Au_{37}(PPh_3)_{10}(SR)_{10}Cl_2]^+$ clusters.[150–152] The S-Au-S-Au-S asymmetric and symmetric stretching values are found to be 274 cm^{-1} and 277 cm^{-1} (see Peak 2 of the inset in Figure 3.13). The S-Au-S-Au-S symmetric stretching value is similar to the DFT-calculated breathing mode (293 cm^{-1}) of $Au_4(SCH_3)_4$ cluster. Other IR studies of thiolate-containing Au nanoclusters such as $[Au_{25}(SCH_3)_{18}]^-$ and $[Au_{37}(PPh_3)_{10}(SR)_{10}Cl_2]^+$ have reported their Au-S symmetric stretches at 293 cm^{-1} and 239 cm^{-1}, respectively, which are relatively close to our DFTB-calculated Au-S stretch values; 241 cm^{-1} as shown as Peak 1 in the inset of Figure 3.13, and 287 cm^{-1} as presented in Table A.11 and Table A.12, for the $Au_{108}S_{24}(PPh_3)_{16}$ cluster. Peak 3 in the inset of Figure 3.13 shows another peak at 514 cm^{-1}, which is another characteristic S-Au-S symmetric stretch. One can depict the similarity of the Au-S stretches in the 200-300 cm^{-1} regions with that of other sulfur-capped Au clusters.[139,142,150–152,195,196] Based on the good agreement between our DFTB calculated IR spectra with DFT calculated as well as the experimental spectra for gold clusters in the

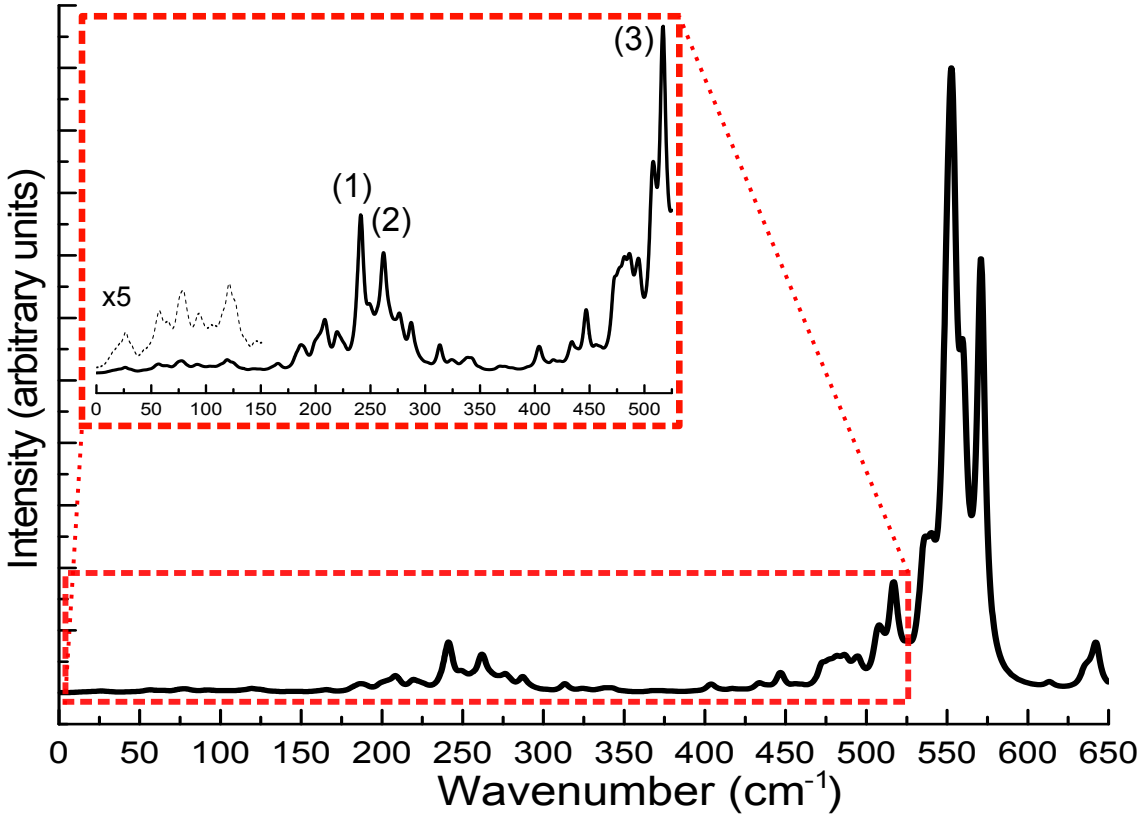

Figure 3.13: Predicted far-IR spectra for $Au_{108}S_{24}(PPh_3)_{16}$ clusters calculated using DFTB2/auorg$^{\alpha\prime}$. The inset of the figure shows the scaled up plots of the region 0-550 cm^{-1} with labelled peaks pertaining to normal modes of Au_4S_4 planar rings. The additional black dashed line in the inset are for the scaled up plots of the region 0-150 cm^{-1}.

benchmark, the predicted IR spectrum of $Au_{108}S_{24}(PPh_3)_{16}$ is reliable and provides a useful fingerprint to identify this cluster in future studies.

3.5 Conclusions

Parameters for the density-functional tight-binding (DFTB) method were generated to describe gold-phosphorus interactions for simulations of phosphine-stabilized nanoscale gold clusters. We build on preceding works reporting second-order DFTB (DFTB2) parameters for hybrid gold–thiolates compounds,[61,69] which were based on the mio parameter set.[55,58,165] The present effort thus expands the applicability of the DFTB2 method to organometallic gold complexes with ligands containing the full set of chemical elements contained in the mio parameter set: H, C, N, O, P, and S. In the construction of the repulsive potentials we considered three different combinations of the gold 6p and phosphorus 3d virtual atomic orbital energies. The performance of our parameters was evaluated using density functional theory (DFT) geometries, ligand binding and cluster isomerization energies, ligand dissociation potential energy curves, molecular orbital energies, and simulated far-IR spectra. We further compare predicted geometries with X-ray crystallographic structures and experimental far-IR spectra, and evaluate parameter transferability for phosphine chemisorption on a gold surface.

In general it is found that the absolute ligand binding energies increase with decreased virtual orbital energies, i.e. $\text{auorg}^{\alpha} < \text{auorg}^{\chi\prime} \approx \text{auorg}^{\alpha\prime}$. The total ligand binding energy increases both with cluster and ligand size. This means that for a given gold cluster, the variation in the ligand binding energy in DFTB needs to be almost completely described by the electronic energy, as the Au-P bond distances only marginally change with different ligands. However, the current DFTB electronic parameters are not flexible enough to accurately describe the variations in the electronic ligand binding energies. Similarly, the same trend holds for increasing gold cluster size. According to the benchmark results, we found that DFTB2/auorg^{α} is the best option to study small ligands and small Au clusters. DFTB2/$\text{auorg}^{\alpha\prime}$ is the best option to study large ligands, large Au clusters, or Au surfaces. For the moderate-sized ligands or gold clusters, both DFTB2/auorg^{α} and DFTB2/$\text{auorg}^{\alpha\prime}$

are good options to be used. The performance of auorg$^{\chi\prime}$ for Au-P interactions is similar to that of auorg$^{\alpha\prime}$ because the effects of shifting the Au 6p orbital energy from -0.02786 to -0.00001 Hartree is less significant than shifting the P 3d orbital energy from 0.12044 to 0.52044 Hartree. However, the effect of shifting the Au 6p orbital energy has not been investigated for Au-(C, H, N, O and S) interactions, thus the use of auorg$^{\alpha\prime}$ is more preferable over auorg$^{\chi\prime}$. Besides consideration of cluster and ligand sizes, the geometrical environment of the Au-P bond also influences the performance of our parameters. Surface-like Au atoms present a challenge while more pyramidalized Au atoms are better described. Possible reasons are the minimum basis set or the missing multipolar charge contribution. Such situations are rare, however, and our auorg$^{\alpha\prime}$ parameter performs overall well in theoretical studies of relevant nanoscale gold clusters that experimentally feature large capping ligands. In particular, our DFTB parameterization enables the simulation of ligand dissociation, reliably predicting how post-treatment can be done in experiment without inducing concomitant side-effects such as agglomeration. The auorg$^{\alpha\prime}$ parameter set will be publicly distributed via the http://www.dftb.org website. To switch from DFTB2/auorg$^{\alpha\prime}$ to DFTB2/auorg$^{\alpha}$, one can simply modify the P 3d-orbital energy according to Table 3.1.

We employed the new DFTB parameters to determine the geometric structure of $Au_{108}S_{24}(PPh_3)_{16}$ nanocluster[144] and investigate its molecular and electronic structure. The optimized Cartesian coordinates of $Au_{108}S_{24}(PPh_3)_{16}$ are provided in the Supporting Information. We found that for large ligand-protected gold clusters, using a simplified model in simulations is inadequate and can substantially affect the bonding and electronic structures of the clusters. Finally, we predicted the IR spectrum of the cluster. Both optimized geometric structure and the simulated IR spectrum of the $Au_{108}S_{24}(PPh_3)_{16}$ nanocluster will serve as useful reference for future studies.

DFTB approaches with appropriately developed parameters for the description of molecular and electronic structure and energetics as well as vibrational spectra are promising to provide insight as to how to tune catalyst reactivity for both product selectivity and reaction specificity. Further development of DFTB parameters for the interaction of gold clusters with various substrate surfaces will advance the development of transformative

catalytic systems. This work is vital to herald the promised potential of unprecedented reaction tunability using cluster-based catalysts.

Chapter 4

Density-Functional Tight-Binding for Platinum Nanoparticles in Vacuum and on TiO_2 Support

A version of this chapter will be submitted to a peer reviewd journal for publication by Vuong, V. Q.; Lee, K. H.; Irle, S. "Density-Functional Tight-Binding for Platinum Nanoparticles in Vacuum and on TiO_2 Support", In preparation.

4.1 Abstract

Platinum nanoparticles (Pt-NPs) supported on titania surfaces are often employed in heterogeneous catalysis. Density functional theory (DFT) is frequently used to explore theoretical minimum energy reaction pathways on static potential energy surfaces of small model systems with clusters of only a few-atoms. Density-functional tight-binding (DFTB) is an approximation to DFT which allows for more realistic investigations of mechanisms and dynamics in systems containing several hundred atoms, including defect structures and dynamic changes in particle shape. Here, we present the parameterization for Pt-X (X = Pt, Ti, O) interactions in the framework of the second-order DFTB method, using a previous parameterization for titania as a basis. The optimized DFTB parameters were validated by

comparing the corresponding properties of geometries, energetic properties, and electronic structures against those computed by DFT. The test set includes Pt_n ($n = 2-116$) clusters, $\approx$ 20,000 conformations of Pt_n ($n = 10, 11, 12, 13$) clusters, bulk Pt (SC, BCC, HCP, and FCC), and the chemisorption of Pt_n ($n = 1-8$) clusters on the TiO_2 rutile (110) and anatase (101) surfaces. The parameter set with the best overall performance was used to simulate the surface diffusion of a single platinum atom (Pt_1) and the nucleation of Pt_6 from Pt_5 and Pt_1 on the rutile (110) surface, using the steered molecular dynamics (SMD) method. The temperature effects on the dynamics of Pt atoms and clusters on the titania surface were also investigated at three separate temperatures (T = 400K, 600K, 800K).

4.2 Introduction

The noble transition metal platinum (Pt) is well-known not only for its uses in refined jewellery but it is also known for its highly effective and highly selective catalytic properties in both homogeneous and heterogeneous catalysis. Pt-based heterogeneous catalysts are an indispensable part of automobile exhaust gas treatment, fertilizer manufacturing, hydrogen production, and fuel cells. However, due to its rarity on the planet, Pt is an expensive metal, making its application very costly. Therefore, the creation of new, durable Pt-based catalysts with reduced platinum remains paramount.

Generally, the effectiveness of heterogeneous catalysts is governed by their surface's atomic and electronic structures. The size of a heterogeneous catalyst, which can be used to control the catalyst's surface area and electronic structures, was found to be critical in controlling its catalytic performance. With the advancement of nanoscience over the past decades, the use of size-tunable Pt-nanoparticles (Pt-NPs), which have a significantly higher specific surface area than their bulk counterparts, has been greatly increased. Notably, Pt-NPs supported on titania surfaces were often used as effective heterogeneous catalysts in industrial processes. In order to capture the chemical reaction mechanisms for such complex systems and to further optimize its catalytic properties, it is vital to understand and predict changes in electronic structures, chemical bond-breaking, and bond-forming that occurs from their dynamic processes.[67,68]

Density functional theory (DFT) is currently the method of choice to theoretically explore catalytic properties of Pt-NPs and their supported complexes on titania surfaces. However, its tremendously high computational cost often requires an adaption of small nanoclusters to represent Pt-NPs. This drawback can impose severe limitations on the studies of numerous longtime scale dynamic processes that may occur during catalysis at high temperatures, such as particle diffusion, nucleation, Ostwald ripening/NP sintering, particle-phase transformations, surface reconstructions, etc. Therefore, in order to capture more realistic chemical reaction mechanisms, the effects of Pt-NPs size, or changes to catalytic properties with temperature, it is necessary to employ a more computationally efficient method for systems with larger sizes.

The density-functional tight-binding (DFTB) approximation to DFT is a viable candidate for more realistic investigations of dynamics and chemical reaction mechanisms, allowing for the computation of systems containing thousands of atoms. Combined with molecular dynamics (MD) simulations, it is an ideal method for predicting complex dynamic processes in heterogeneous catalysts, such as surface reconstruction or NP sintering at the nanometer-scale and long-timescales. However, the application of DFTB Pt-NPs in the vacuum and on titania support is limited due to the lack of well-optimized parameters. While there are not DFTB parameters for the Pt-X (X = Ti, O) available, the existing DFTB parameters for pure Pt systems either severely overestimates or underestimates Pt-Pt interactions.[70–72] In this work, the DFTB electronic parameters of Pt were optimized, and the Pt-X (X = Pt, Ti, O) repulsive potentials were parameterized in the framework of the second-order DFTB method, leveraging a previous parameterization of titania.[62] The optimized DFTB parameters were validated by comparing the corresponding properties against DFT: geometries, energetic properties, and electronic structures. The test set includes Pt_n ($n = 2 - 116$) clusters, $\approx$ 20,000 conformations of Pt_n ($n = 10, 11, 12, 13$) clusters, bulk Pt (SC, BCC, HCP, and FCC), and the chemisorption of Pt_n ($n = 1 - 8$) cluster on the TiO_2 rutile (110) and anatase surfaces. The overall best performing parameter set, based on our benchmark, was employed to simulate the diffusion of Pt_1 atom, and the nucleation of Pt_6 from Pt_5 and Pt_1 on rutile (110) surface using the steered molecular dynamics (SMD) method. The effects of temperature on the dynamics of Pt particles on the titania surface were also investigated.

4.3 Methodology and Computational Details

4.3.1 Overview of DFTB2

The density-functional tight-binding (DFTB) method is an approximation to the density functional theory (DFT) based on the Taylor expansion of DFT energy $E[\rho]$, a two-center approximation, and empirical fitted pairwise potentials.[50] For a given molecule, its electron density can be written as a sum of a reference/initial electron density ρ_0 and an electron density fluctuation $\delta\rho$. By employing the Taylor expansion, the DFT energy can be approximated as

$$E[\rho] = E^0[\rho_0] + E^1[\rho_0, \delta\rho] + E^2[\rho_0, (\delta\rho)^2] + E^3[\rho_0, (\delta\rho)^3] + \dots \quad , \tag{4.1}$$

where $\rho = \rho_0 + \delta\rho$. In the framework of DFTB, the expansion of DFT energy can be truncated at each energy term (E^1, E^2 or E^3) to formulate the corresponding energy for the first-order DFTB1, the second-order DFTB2, and the third-order DFTB3, respectively.[59]

Detailed derivations and comprehensive review of the DFTB methods can be found elsewhere.[38,58,59] In this work, we will only focus on the DFTB2 method, which is also referred to as self-consistent-charge-DFTB, or (SCC)-DFTB.[58] The DFTB2 total energy is defined as

$$E = \sum_i n_i \langle \Psi_i | \hat{H}[\rho_0] | \Psi_i \rangle + \frac{1}{2} \sum_{AB} \gamma_{AB} \Delta q_A \Delta q_B + \sum_{A>B} E_{AB}^{\text{rep}} \quad , \tag{4.2}$$

where $\hat{H}[\rho_0]$ is the initial Hamiltonian, $|\Psi_i\rangle$ is the occupied valence molecular orbitals (MOs), n_i is the occupation numbers, Δq_A is the Mulliken point charge[166] on atom A, $\gamma_{AB}\Delta q_A \Delta q_B$ representing the Coulomb interaction energy between the two point charges,[58] and E_{AB}^{rep} is the repulsive potential between two atoms A and B. The MO $|\Psi\rangle$ can be expanded as a linear combination of optimized atomic orbitals (AOs) $|\phi_\mu\rangle$.

To obtain a reasonable pseudo-atomic basis set and initial atomic electron density for the molecular environment in DFTB, an external confinement was introduced to the Kohn-Sham

equation of the free atom

$$\left[-\frac{1}{2}\nabla^2 + v^{\text{eff}}[\rho^{\text{atom}}] + \left(\frac{|\mathbf{r}|}{r_0}\right)^2 \right] \phi_\mu(\mathbf{r}) = \epsilon_\mu \phi_\mu(\mathbf{r}), \tag{4.3}$$

where r_0 is the empirical confinement radius parameter and ϕ_μ is the atom-centered pseudo-atomic Slater type orbitals. By solving the eq 4.3, one can obtain various atomic orbital and electron density depending on confining radii r_0. Because the atomic orbital and electron density can be optimized separately, there are two types of confinement radii - one for the wavefunction, r^{wf}, and one for density, r^{dens}. They are responsible for confining the atomic orbitals (basis set) and the atomic reference electron densities, respectively.

In the framework of the two-center approximation and the pseudo-atomic basis set, the initial Hamiltonian $\hat{H}_0[\rho_0]$ is defined as

$$H^0_{\mu\nu} = \langle \phi_\mu | \hat{H}[\rho_0] | \phi_\nu \rangle \approx \begin{cases} \epsilon_\mu^{\text{neutral free atom}} & \mu = \nu; \\ \langle \phi_\mu | \hat{T} + V^{AB} | \phi_\nu \rangle & \mu \in A, \nu \in B, \mu \neq \nu; \\ 0 & \text{otherwise}, \end{cases} \tag{4.4}$$

where $V^{AB} = V[\rho_0^A + \rho_0^B]$ in the density superposition approach or $V^{AB} = V[\rho_0^A] + V[\rho_0^B]$ in the potential superposition approach. The repulsive potential between two atoms E_{AB}^{rep} is formulated as a two-center term that depends only on the chemical element type of atoms A and B and their interatomic distance r_{AB}.[38] Practically, the repulsive potentials can be defined as a combination of exponential and spline functions, and the total repulsive energy is fitted to minimize the difference between DFTB electronic relative energies and reference relative energies for a training set of molecular systems.[75,77,78] The reference energies are usually computed by high-level methods like wave function theory (WFT) or DFT methods.

4.3.2 Parameterization

For the parametrization of DFTB methods, there are two groups of parameters that needs to be determined: (1) the electronic parameters (which includes the confinement radii r^{wf} for the AOs basis set, the confinement radii r^{dens} for the atomic densities, and the atomic

orbital energies) and (2) the pairwise repulsive potentials. While the occupied atomic orbital energies are computed from DFT, the unoccupied atomic orbital energies, other electronic parameters, and pairwise repulsive potentials are optimized in order to reproduce certain desired properties, for instance, electronic structures, energies, and geometries.

Pt-Pt interactions: Given their similar sizes at the atomic scale, we adopted the confining radii for the electron density r^{dens} and atomic wave functions r^{wf} of occupied atomic orbitals of Au from the "auorg" parameter set[61] for the electronic parameters of Pt. The atomic orbital energy and confinement radius r^{wf} of the virtual orbital $6p$ were empirically explored. We found that shifting up the energy of $6p$ virtual orbital by 0.0345 a.u. from the PBE-computed value or by employing a larger confinement radius r^{wf} for the virtual orbital can reduce the over-binding of Pt-Pt interactions. The combination of the two options for the virtual orbital energy ϵ_{Pt}^{6p} and the two option for the confinement radius r_{6p}^{wf} results in four sets of Pt-electronic parameter sets listed in table 4.1.

The Pt-Pt repulsive potential was optimized for each set of electronic parameters using the genetic algorithm (GA) optimization tool that we had recently developed.[77] We employed a similar automatic parameterization protocol developed previously for other DFTB parameters.[77,197] The repulsive potentials were optimized on the basis of DFTB2 electronic energies to fit atomization energies, forces, and reaction energies for the training set listed in Table B.1, B.2, and B.4 in the Supporting Information. The GA was also used to minimize a scoring function F^{score} defined as the fitness of the parameter sets with respect to DFTB values and reference data according to the formula

$$F^{score} = \frac{1}{N_{eq}}\Big[\sum_i W_i^{at}\left(\Delta E_i^{at}\right)^2 + \sum_i W_i^{react.}\left(\Delta E_i^{react.}\right)^2 + \sum_i W_i^{force}\sum_{j\in 3N_i}\left(\Delta F_{i,j}^{force}\right)^2\Big], \tag{4.5}$$

where $\Delta E^{at} = E_{eDFTB}^{at} - E_{ref}^{at}$ is the deviation in atomization energies, $\Delta E^{react.} = E_{eDFTB}^{react.} - E_{ref}^{react.}$ is the deviation in reaction energies, $\Delta F^{force} = F_{eDFTB}^{force} - F_{ref}^{force}$ is the deviation in forces, W_i^{at}, $W_i^{react.}$, and W_i^{force} are the weight factors of the i^{th} atomization energy, reaction energy, and the force of the i^{th} structure, respectively, N_{eq} is the number of fitting data points, N_i is the number of atoms in the i^{th} compound, and $eDFTB$ stands for DFTB energy without the repulsive potential term. We employed a cutoff radius of 3.5 Å and 6

Table 4.1: Atomic orbital energy and compression radii of Pt in a.u. for different optimized parameter sets.

	pt^{α}	pt^{β}	pt^{κ}	pt^{χ}
ϵ_{Pt}^{6p}	-0.0305	0.0040	-0.0305	0.0040
r_{6p}^{wf}	4.51	4.51	6.50	6.50
r_{6s}^{wf}	6.50	6.50	6.50	6.50
r_{5d}^{wf}	6.50	6.50	6.50	6.50
r^{dens}	9.41	9.41	9.41	9.41

spline knots for the repulsive potential term with one allowable extremum and a continuity requirement up to the second derivative. For the GA optimization, population sizes of 1000 and 3000 generations were employed with two-point crossover and random mutation rates of 0.9 and 0.2, respectively.

Pt-Ti and Pt-O interactions: As we will show in the "Results and Discussion" section below, the pt$^{\alpha}$ parameter set has the poorest performance for the Pt bulk system, thus was dropped in the parameterization for Pt-Ti and Pt-O interactions. The DFTB confinement radii for Ti and O as well as their Ti-Ti, Ti-O, and O-O repulsive potentials were taken from the "tiorg" parameter set.[62] In combination with three new Pt parameter sets (pt$^{\beta}$ pt$^{\kappa}$ pt$^{\chi}$), three corresponding pt$^{\beta}$-tiorg, pt$^{\kappa}$-tiorg, pt$^{\chi}$-tiorg sets were created. We employed a similar fitting strategy for the Pt-Ti and Pt-O repulsive potentials as we did for the fitting of the Pt-Pt repulsive potential. The training set listed in Table B.3, B.5, and B.6 in the Supporting Information. In addition, we applied three additional constraints on the Pt-Ti repulsive potential and empirically shifted the reference reaction energies of two reactions in Table B.6 by -11 kcal/mol to improve the adsorption of Pt atoms (Pt_1) on the rutile (110) surface. We employed a cutoff radius of 3.7 Å and 3.4 Å for Pt-Ti and Pt-O potentials, respectively. The same six spline knots, one allowable extremum, and a continuity requirement up to the second derivative constraints were also used. For the GA optimization, population sizes of 2000 and 3000 generations were employed with two-point crossover and random mutation rates of 0.9 and 0.2, respectively. The two potentials Pt-Ti and Pt-O were optimized simultaneously.

4.3.3 Computational details

In this work, all DFTB2 calculations were carried out using the DFTB+ program.[177] For reference data, the Perdew-Burke-Ernzerhof (PBE) density functional was chosen as the reference method. For the DFT calculations, the projector augmented wave (PAW) was used approach,[188] with the kinetic energy cutoff set at 450 eV and carried out using the Vienna ab-initio simulation package (VASP) program in conjunction with the provided "PAW_PBE" pseudo-potentials.[189,190] The convergence criteria were set to 10^{-6} eV for achieving self-consistent field energies, and 0.005 eV/Å for the maximum force in case of geometry optimizations.

4.4 Results and Discussion

4.4.1 Performance for pure Pt clusters and bulk Pt

To evaluate the accuracy of DFTB with our new Pt parameters, we compared DFTB-computed binding energies, optimized geometries, and band-structures to their corresponding reference values computed by the PBE functional for a series of Pt clusters and bulk systems. The performance of our four parameter sets pt^{α}, pt^{β}, pt^{κ}, and pt^{χ}, was also compared to previously developed Pt parameters pt^{Shi} reported by Shi et al.,[70] pt^{Lee} reported by Lee et al.,[71] and the parameter sets pt^{VdB13} and pt^{VdB55} reported by Bossche.[72]

Pt_2 to Pt_{116} clusters. Figure 4.1 shows the DFTB performance in predicting binding energy for pure Pt clusters ranging from Pt_2 to Pt_{116}. The root mean square error (RMSE), mean unsigned error (MUE), mean signed error (MSE), and maximum of absolute error (Max) of DFTB normalized binding energies reference to their corresponding DFT-computed values for the test are listed in Table 4.2. While every parameter set in question can mimic the increase in normalized binding energy with the size of Pt clusters using DFTB, their accuracy varies drastically. DFTB/pt^{VdB13} and DFTB/pt^{VdB55} severely overestimates binding energies, particularly for large clusters, with a MSE of 0.47 and 1.32 eV/at, respectively. The large overestimation of binding energies in these parameters can be attributed to their parameterization, which focused only on relative energies. DFTB/pt^{Lee} also shows significant over-binding with a MSE of 0.18 eV/at, while DFTB/pt^{Shi} shows significant under-binding with a MSE of -0.22 eV/at. These four new parameter sets generally outperform the existing parameter sets with a MSE ≈0.01 eV/at, and RMSE less than 0.1 eV/at. Among the four new parameter sets, pt^{β} shows the best performance with a RMSE of 0.05 eV/at.

To assess the accuracy of DFTB in predicting the structure of Pt clusters, DFTB-optimized geometries were compared to the DFT-optimized one. The root mean square (RMS), mean, and max of root mean square deviation (RMSD) over atomic positions of the test set are listed in Table 4.2. Similar to the performance of predicting binding energies, pt^{VdB13} and pt^{VdB55} shows significantly large deviations with the mean of RMSD

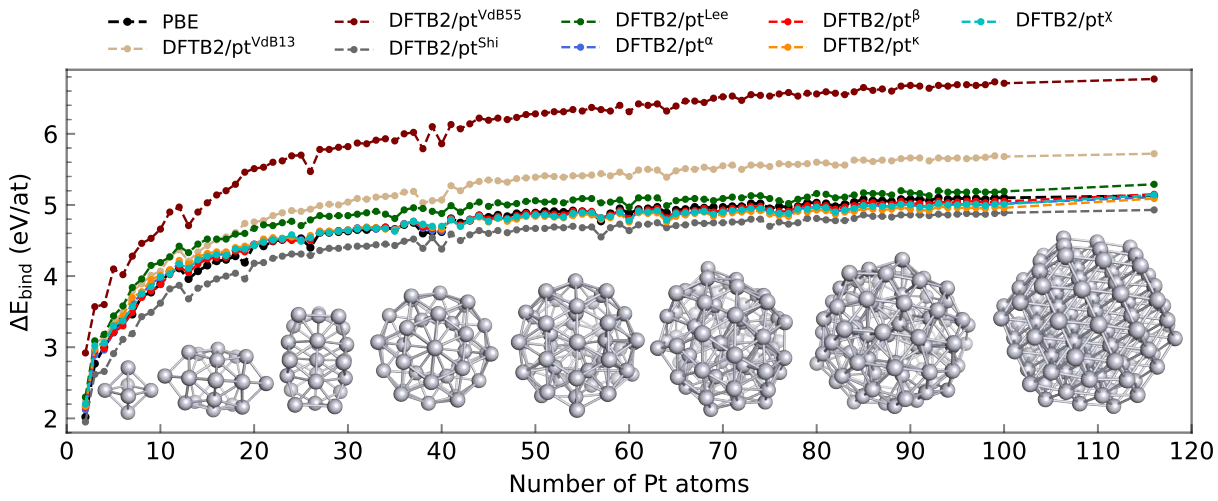

Figure 4.1: DFTB normalized binding energies computed with different parameter sets in comparison to the PBE normalized binding energies for Pt_2 to Pt_{116} clusters.

approximating to 0.44 and 0.39 Å, respectively. pt^{Shi} shows a similar level of accuracy with a large mean of RMSD of 0.34 Å. In terms of geometry, pt^{Lee} and our new four parameter sets outperforms the other parameters with a mean of RMSD less than 0.17 Å. pt^{Lee} is slightly better than the new parameter sets with a mean of RMSD of 0.14 Å. Among the four new parameter sets, pt^{β} shows the best performance with the smallest RMS of RMSD being 0.17 Å, compared to the RMS of RMSD equaling 0.18 Å in the case of pt^{α}, pt^{κ}, and pt^{χ}.

Large-set of Pt_{10}, Pt_{11}, Pt_{12}, and Pt13 isomers. To further assess the accuracy of our new parameters with DFTB, their performance was evaluated for a large-set of 5000 Pt_{10} isomers, 5000 Pt_{11} isomers, 5000 Pt_{12} isomers, and 4950 Pt_{13} isomers. The test set was originally reported by Fung et al. and was used to test DFTB in the work of Lee et al. These geometries were taken from the work by Fung et al., and single-point energy calculations were carried out using DFTB with the different parameters. The DFT single-point energies were recomputed using PBE functional with a high energy cutoff of 450 eV in order to get a more accurate reference data. Figure 4.2 compares the DFTB-computed normalized binding energies with pt^{Shi}, pt^{Lee}, pt^{α}, and pt^{β} parameters to the DFT-computed normalized binding energies. The same comparison of DFTB energies with pt^{VdB13}, pt^{VdB55}, pt^{κ}, and pt^{χ} is shown in Figure B.1 in the Supporting Information. In terms of absolute binding energies, similar to the "Pt_2 to Pt_{116}" test set, the new parameters outperforms existing parameters. Significant over-binding was observed for pt^{VdB55} and pt^{Lee}, while under-binding was observed for pt^{Shi}. It is interesting to note that pt^{VdB13} shows reasonably small over-binding for Pt clusters in this range. This is likely due to the fact that the parameter was originally optimized for Pt_{13} clusters. In terms of relative binding energies, pt^{VdB13} and pt^{VdB55} outperforms all other parameters, with a R^2 higher than 0.88. This is especially true in the case of pt^{VdB13} where R^2 is higher than 0.95. This is to be expected as these parameters were optimized to predicted not binding energies but the relative energy of isomers. pt^{Shi} shows the poorest correlation with R^2 ranging from 0.45 to 0.63, whereas the four new parameter sets and pt^{Lee} show a reasonably high correlation, varying from 0.74 to 0.91 for R^2.

As these ≈20,000 structures were only partially optimized in the work by Fung et al., they are not suitable to test the accuracy of DFTB in predicting geometry. Thus, we selected 70 isomers of Pt_{10}, 80 isomers of Pt_{11}, 90 isomers of Pt_{12}, and 100 isomers of Pt_{13} to formulate

Table 4.2: Root mean square error (RMSE), mean unsigned error (MUE), mean signed error (MSE), and maximum of absolute error (Max) of DFTB normalized binding energies comparing to PBE normalized binding energies, root mean square (RMS), mean, and max of root mean square deviation (RMSD) over atomic positions of DFTB geometries comparing to PBE optimized geometries for Pt_2 to Pt_{116} clusters.

Names	Energy (eV/at)				RMSD (Å)		
	RMSE	MUE	MSE	Max	RMS	Mean	Max
pt^{VdB13}	0.48	0.47	0.47	0.67	0.44	0.37	1.09
pt^{VdB55}	1.35	1.32	1.32	1.64	0.39	0.31	1.09
pt^{Shi}	0.23	0.22	-0.22	0.34	0.37	0.34	1.01
pt^{Lee}	0.20	0.18	0.18	0.41	0.15	0.14	0.30
pt^{α}	0.07	0.06	-0.01	0.19	0.18	0.16	0.36
pt^{β}	0.05	0.04	-0.01	0.18	0.17	0.16	0.36
pt^{κ}	0.10	0.09	-0.02	0.24	0.18	0.17	0.36
pt^{χ}	0.08	0.06	-0.01	0.25	0.18	0.16	0.43

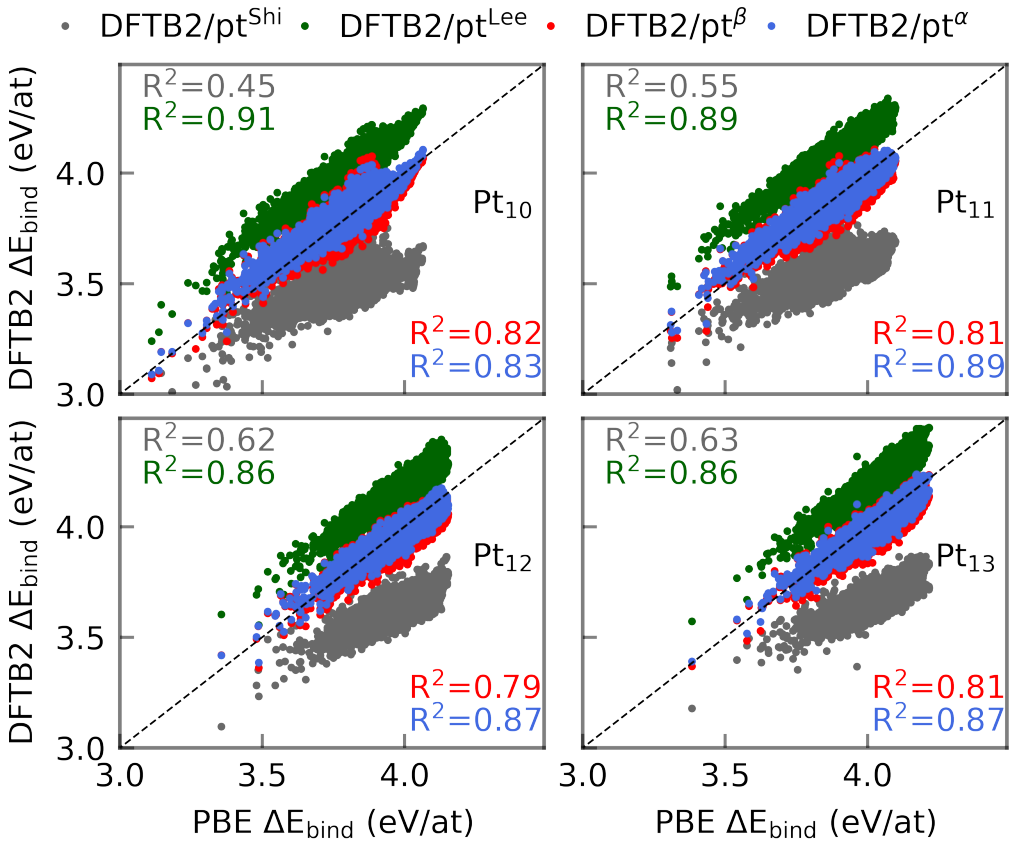

Figure 4.2: DFTB2 normalized binding energies ΔE_{bind} comparing to PBE normalized binding energies ΔE_{bind} for $\approx$ 20,000 conformations of Pt_{10}, Pt_{11}, Pt_{12}, and Pt_{13}, clusters.

a new test set of 340 isomers of Pt_{10} to Pt_{13}. These clusters were fully reoptimized using PBE with our higher energy cutoff of 450 eV. Table 4.3 shows the accuracy of DFTB with all parameters with regards to binding energy and geometry. Overall, the accuracy among all DFTB parameters is similar to the accuracy observed in the cases above for the "Pt_2 to Pt_{116}" test set. Nevertheless, in terms of geometry, all four new parameter sets and pt^{Lee} show a slightly larger mean of RMSD when compared to the previous test set. This can be attributed to the fact that the test set includes a large number of high-energy isomers, which have long Pt-Pt bond lengths. The high-energy structures with long-bond are generally more difficult to obtain with DFTB which utilizes a minimal basis set.

Bulk systems. To complete the evaluation of DFTB with our new parameters for Pt-Pt interactions, we assess their accuracy for various bulk systems. To test this, we compared DFTB-computed cohesive energies, lattice constants, and band structures bulk systems to their corresponding values computed by PBE for simple cubic (SC), body-centered cubic (BCC), hexagonal closest packed (HCP), and face-centered cubic (FCC) unit cells. The computed cohesive energies, and lattice constants are listed in Table 4.4. Overall, all DFTB parameters can reproduce PBE-computed lattice constants well with the largest deviation being less than 0.15 Å. On the other hand, the accuracy in predicting the cohesive energies varies wildly from parameter to parameter. Among the four new parameters, all except pt^{α} were able to predict the order of cohesive energies increasing from SC to FCC unit cells (SC < BCC < HCP < FCC). For pt^{β}, pt^{κ}, and pt^{χ}, a significantly large underestimation of 0.5-0.7 eV in cohesive energy was observed in the case of SC and BCC unit cells. Smaller deviations of 0.1-0.2 eV were observed for HCP and FCC unit cells. In general, DFTB is more accurate for denser and lower-energy unit cells, due to its usage of a minimum basis set. The results highlights the limit of the method for higher energy systems.

Figure 4.3 shows a comparison of DFTB/pt^{β}-computed band structures to PBE-computed band structures for SC, BCC, HCP, and FCC unit cells. The same comparison of DFTB with pt^{α}, pt^{κ}, and pt^{χ} are shown in Figure B.2, B.3, B.4, B.5, B.6, B.7, and B.8 in the Supporting Information. Overall, DFTB with the new parameters mimics closely PBE-computed band structures for all unit cell in the range of -5 to 5 eV. Larger deviations were observed in the range for the range of -10 to -5 eV and 5 to 10 eV.

Table 4.3: Root mean square error (RMSE), mean unsigned error (MUE), mean signed error (MSE), and maximum of absolute error (Max) of DFTB normalized binding energies comparing to PBE normalized binding energies, root mean square (RMS), mean, and max of root mean square deviation (RMSD) over atomic positions of DFTB geometries comparing to PBE optimized geometries for 340 isomers of Pt_{10} to Pt_{13} clusters.

Names	Energy (eV/at)				RMSD (Å)		
	RMSE	MUE	MSE	Max	RMS	Mean	Max
pt^{VdB13}	0.27	0.27	0.27	0.46	0.41	0.33	1.31
pt^{VdB55}	0.96	0.96	0.96	1.82	0.37	0.31	1.09
pt^{Shi}	0.20	0.19	-0.19	0.34	0.38	0.35	1.10
pt^{Lee}	0.25	0.25	0.25	0.41	0.22	0.18	0.71
pt^{α}	0.07	0.06	0.05	0.17	0.25	0.20	0.95
pt^{β}	0.08	0.06	0.05	0.22	0.26	0.21	0.94
pt^{κ}	0.07	0.07	0.06	0.24	0.23	0.19	0.97
pt^{χ}	0.09	0.07	0.06	0.23	0.26	0.22	0.95

Table 4.4: Cohesive energies ΔE_{coh} and lattice constants computed by DFTB2 with different parameters in comparison to the corresponding values computed by PBE for Pt simple cubic (SC), body-centered cubic (BCC), hexagonal closest packed (HCP), and face-centered cubic (FCC) unit cells.

	PBE	DFTB2							
		pt^{VdB13}	pt^{VdB55}	pt^{Shi}	pt^{Lee}	pt^{α}	pt^{β}	pt^{κ}	pt^{χ}
SC									
a (Å)	2.63	2.58	2.56	2.82	2.73	2.73	2.72	2.73	2.72
ΔE_{coh} (eV/at)	5.42	6.17	7.38	5.32	5.07	5.13	5.16	4.91	4.98
BCC									
a (Å)	3.17	3.15	3.14	3.35	3.06	3.20	3.15	3.14	3.08
ΔE_{coh} (eV/at)	5.78	6.72	8.08	5.49	5.52	5.10	5.21	4.96	5.13
HCP									
a (Å)	2.77	2.75	2.73	2.92	2.81	2.80	2.78	2.79	2.77
b (Å)	2.77	2.73	2.73	2.92	2.81	2.80	2.78	2.79	2.77
c (Å)	4.78	4.78	4.73	4.81	4.82	4.70	4.68	4.67	4.65
ΔE_{coh} (eV/at)	5.82	6.79	8.23	5.56	5.82	5.59	5.72	5.52	5.67
FCC									
a (Å)	3.98	3.93	3.92	4.14	4.05	3.99	3.97	3.97	3.96
ΔE_{coh} (eV/at)	5.87	6.69	8.29	5.63	5.87	5.66	5.79	5.59	5.74

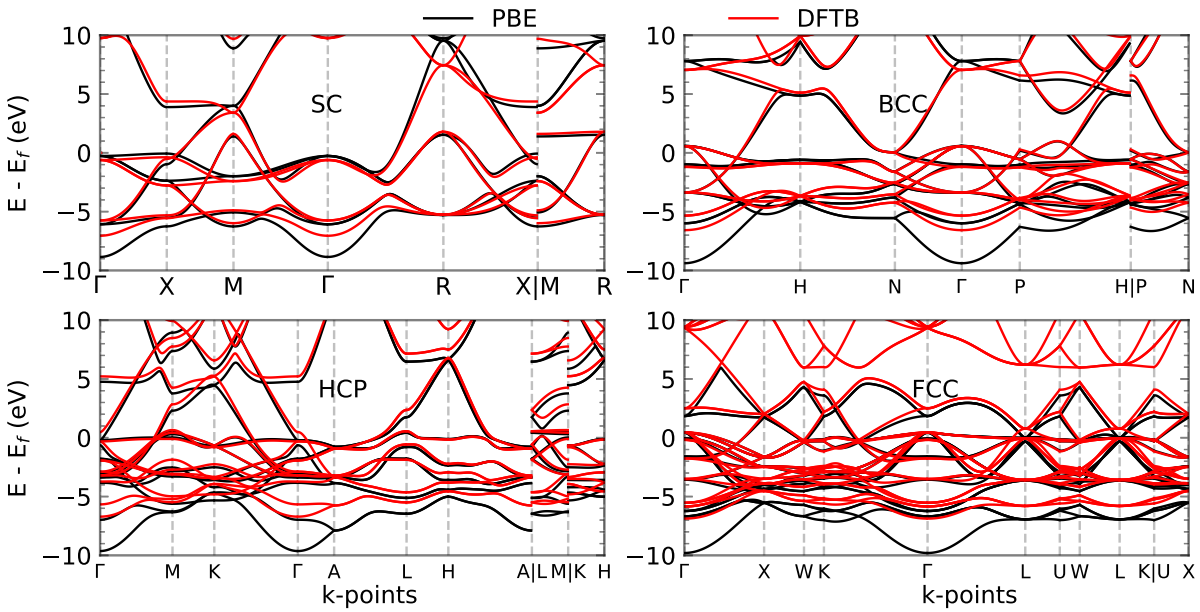

Figure 4.3: Band structures computed by DFTB2/pt$^{\beta}$ in comparison to the band structures computed by PBE for Pt simple cubic (SC), body-centered cubic (BCC), hexagonal closest packed (HCP), and face-centered cubic (FCC) unit cells.

4.4.2 Performance for Pt clusters on titania support

As previously mentioned in the "Parameterization" section, only three parameter sets (pt$^{\beta}$, pt$^{\kappa}$, and pt$^{\chi}$) were incorporated with the "tiorg" parameter set. To evaluate the accuracy of DFTB with the newly combined pt$^{\beta}$-tiorg, pt$^{\kappa}$-tiorg, pt$^{\chi}$-tiorg sets, we compared their binding energies, optimized and geometries computed by DFTB to their corresponding reference values computed by the PBE functional for a series of Pt_1 to Pt_8 clusters on the TiO_2 rutile (110) surface, and Pt_1 to Pt_4 clusters on the TiO_2 anatase (101) surface. Additionally, the energy landscape of Pt atom adsorption on the TiO_2 rutile (110) surface was also used to assess the new parameters.

Pt_1 to Pt_8 clusters on the TiO_2 rutile (110) surface and Pt_1 to Pt_4 clusters on the TiO_2 anatase (101) surface. Figure 4.4 shows the performance of DFTB for the three parameter sets in predicting adsorption energy for Pt clusters on titania support. The RMSE, MUE, MSE, and Max of DFTB normalized binding energies reference to their corresponding DFT-computed values for the test are listed in Table 4.5. Overall, DFTB can decently reproduce the change of PBE-computed adsorption energy with Pt cluster size. While the level of accuracy is impressively high for all sets, around the same level of accuracy for the rutile (110) surface with RMSE varying from 0.12 eV/at to 0.14 eV/at, pt$^{\beta}$-tiorg is superior when it comes to the case of the anatase (101) surface with a RMSE of 0.16 compared to a RMSE of 0.24 eV/at and 0.28 eV/at of pt-tiorg$^{\kappa}$ and pt-tiorg$^{\chi}$, respectively.

The RMS, mean, and max of RMSDs between DFTB-optimized and PBE-optimized geometries for Pt clusters on the two surfaces are listed in Table 4.5. Overall, all three parameter sets show excellent accuracy in terms of geometry, especially in the case of the anatase surface with all RMS of RMSDs being less than 0.13 Å. In the case of the rutile surface, the RMS of RMSDs of 0.16 Å for pt$^{\beta}$-tiorg is slightly better than the other two, which values are 0.18 and 0.19 Å for pt$^{\chi}$-tiorg and pt$^{\kappa}$-tiorg, respectively. In order to illustrate visually the differences between PBE-optimized and DFTB-optimized geometries, Figure 4.5 shows the overlay of Pt clusters optimized by PBE and DFTB/pt$^{\beta}$-tiorg. Similar comparisons for structures optimized by DFTB/pt$^{\kappa}$-tiorg and DFTB/pt$^{\chi}$-tiorg are shown in in Figures B.9 and B.10 in the Supporting Information. The overlaid structures were determined by a

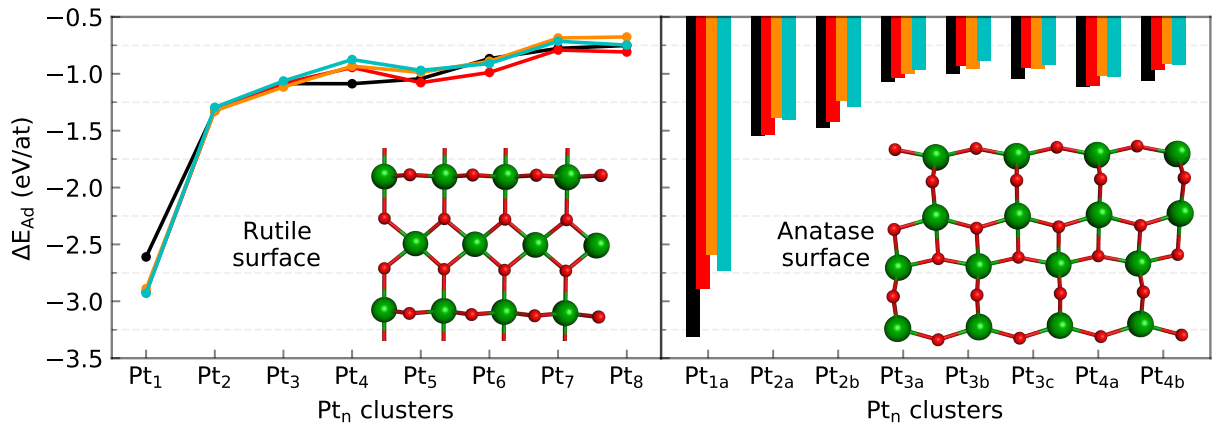

Figure 4.4: Normalized adsorption energies computed by DFTB2 with three different parameter sets in comparison to the corresponding values computed by PBE for Pt_1 to Pt_8 clusters on the TiO_2 rutile (110) surface, and Pt_1 to Pt_4 clusters on the TiO_2 anatase (101) surface.

Table 4.5: Root mean square error (RMSE), mean unsigned error (MUE), mean signed error (MSE), and maximum of absolute error (Max) of DFTB normalized binding energies comparing to PBE normalized binding energies, root mean square (RMS), mean, and max of root mean square deviation (RMSD) over atomic positions of DFTB geometries comparing to PBE optimized geometries for for Pt_1 to Pt_8 clusters on the TiO_2 rutile (110) surface, and Pt_1 to Pt_4 clusters on the TiO_2 anatase (101) surface. The RMSD over atomic positions were calculated over the Pt atoms and their directly bonded Ti and O atoms, cutoffs of 2.8 Å and 2.5 Å were used to determined bonding of Pt-Ti and Pt-O, respectively.

Names	Energy (eV/at)				RMSD (Å)		
	RMSE	MUE	MSE	Max	RMS	Mean	Max
Rutile							
pt$^{\beta}$-tiorg	0.13	0.08	-0.05	0.31	0.16	0.15	0.22
pt$^{\kappa}$-tiorg	0.12	0.09	0.00	0.28	0.19	0.18	0.27
pt$^{\chi}$-tiorg	0.14	0.09	0.00	0.32	0.18	0.17	0.27
Anatase							
pt$^{\beta}$-tiorg	0.16	0.10	0.10	0.42	0.12	0.10	0.27
pt$^{\kappa}$-tiorg	0.28	0.20	0.20	0.72	0.13	0.10	0.28
pt$^{\chi}$-tiorg	0.24	0.19	0.19	0.58	0.12	0.10	0.27

minimization procedure, which includes recentering and rotation to minimize the RMSD over all Pt atoms and the Ti and O atoms directly bonded to them. These structures highlights the excellent performance of DFTB in the description of Pt cluster geometries on rutile and anatase surfaces.

Energy landscape of single Pt atom adsorption on the TiO_2 rutile (110) surface. To evaluate the transferability of the new DFTB parameters, we further explored the energy landscape of a single Pt atom adsorption on the TiO_2 rutile (110) surface and compared it to their corresponding PBE-computed energy landscape. The computed DFTB/pt$^{\beta}$-tiorg and PBE energy landscapes are shown in Figure 4.6. Similar comparisons for energy landscapes computed by DFTB/pt$^{\kappa}$-tiorg, and DFTB/pt$^{\chi}$-tiorg are shown in Figures B.11 and B.12, respectively in the Supporting Information. As discussed in a previous work for the parameterization of Au-P interactions,[197] this test is particularly useful for evaluating the transferability of the new parameters, as the varying number of Ti and O atoms coordinating with the Pt atom on the surface simulates a change in chemical bonding environment. DFTB/pt$^{\beta}$-tiorg is able to qualitatively reproduce the relative PBE energy landscape in the strongly bonding "valley" on the rutile surface. However, a significant deviation is observed in the high-energy region outside this valley. Even though the significant deviation in the high-energy region implies a limit to the transferability of these parameters, it is important to note that DFTB/pt$^{\beta}$-tiorg can mimic the change of PBE energy landscape between with and without constraint. This suggests that the parameters can describe changes in the support surface, which is crucial in dynamic simulations.

4.4.3 Diffusion of Pt atom on the TiO_2 rutile (110) surface

In order to demonstrate the applicability of our new DFTB parameters for Pt on TiO_2 support, we employed our "best" set (DFTB/pt$^{\beta}$-tiorg) to investigate the diffusion of Pt atom on the TiO_2 rutile (110) surface as well as temperature effects on the dynamics of the Pt atom on the surface. The free energy barrier of the diffusion and temperature effects were estimated using the steered molecular dynamics (SMD) method. The simulation was carried out by pulling a single Pt atom along the "value" of the rutile (110) surface. The potential of mean force (PMF) was computed from the calculated work of pulling of over 100

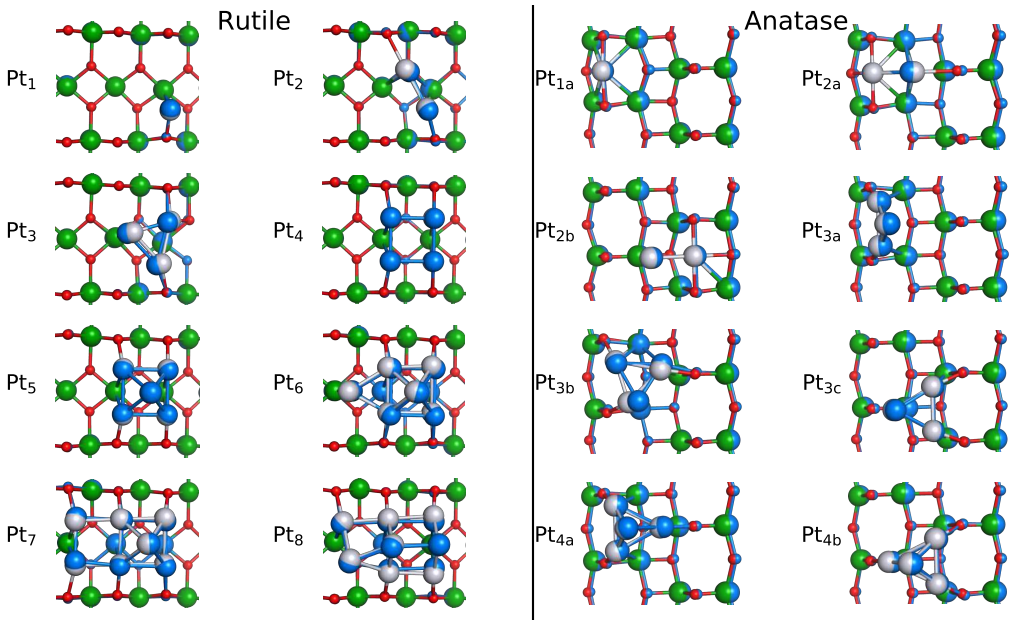

Figure 4.5: Overlap of PBE-optimized structures (Pt in grey, Ti in green and O in red) and DFTB/pt$^{\beta}$-tiorg optimized structures (in sky blue) for Pt_1 to Pt_8 clusters on the TiO_2 rutile (110) surface, and Pt_1 to Pt_4 clusters on the TiO_2 anatase (101) surface.

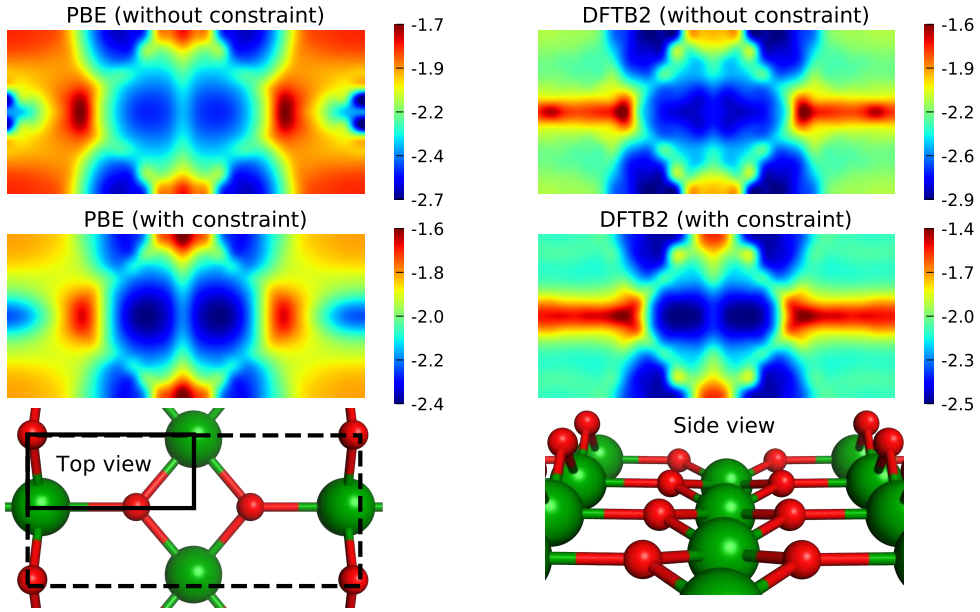

Figure 4.6: Energy landscape in eV of Pt atom adsorption on the TiO_2 rutile (110) surface obtained at PBE and DFTB2/pt$^{\beta}$-tiorg methods. "Without constraint" refers to the geometry optimization with the top two layers of TiO_2 surface were fully optimized, "with constraint" refers to the geometry optimization with only few selected Ti and O atoms nearby the Pt single atom were optimized.

SMD trajectories using Jarzynski's equality. The SMD simulation is illustrated in Figure 4.7. The same Figure shows that the free energy of the diffusion barrier is dependent on the temperature. When the temperature increases from 400 K to 800 K, the energy barrier reduces from 11 kcal/mol to only 7 kcal/mol. This results agree with experimental data showing that the sintering procedure of a single Pt atom or small Pt clusters occurs much faster in increased temperatures.

4.4.4 Nucleation of Pt_6 from Pt_5 and Pt_1 on the TiO_2 rutile (110) surface

To further understand the sintering event and the effect of temperature, we employ DFTB/pt$^{\beta}$-tiorg to investigate the nucleation of Pt_6 from Pt_5 and Pt_1 on the TiO_2 rutile (110) surface. Similar to the study of Pt diffusion, the SMD method was used to accelerate the event. The single Pt atom was pulled toward the Pt_5 cluster as illustrated in Figure 4.8. Again, the potential of mean force (PMF) was computed from the pulling work of over 100 SMD trajectories using Jarzynski's equality. While the effects of temperature on the amplitude of the first barrier is similar to the case of single Pt atom diffusion on the surface, the second barrier changed drastically with the temperature. The second barrier was reduced from 11 kcal/mol at 400 K to ≈ 0 kcal/mol at 800 K. By analyzing the SMD trajectories, we had found that the lowering second energy barrier is due to the dynamics of the Pt_5 cluster as it distorts toward the Pt single atom at the position of the second energy barrier. This distortion of the Pt_5 cluster induces the early formation of Pt_5+Pt_1 complex, stabilizing the transition state. Nevertheless, because of the distortion of Pt_5 and the early formation of the Pt_5+Pt_1 complex, the PMF of pulling the single Pt atom after crossing the second energy barrier does not reflect the free energy of formation for Pt_6 from Pt_5 and Pt_1.

To estimate the effect of temperature on the free energy of formation for Pt_6 from Pt_5 and Pt_1, we employed an additional restrain on two Pt atoms of Pt_5 in order to restrict the movement of the cluster toward the single Pt atom and preventing it from distorting. The simulation is illustrated in Figure B.14. With the extra restrain on the Pt_5 cluster, the drastic changes found previously in the second energy barrier at high temperatures were eliminated.

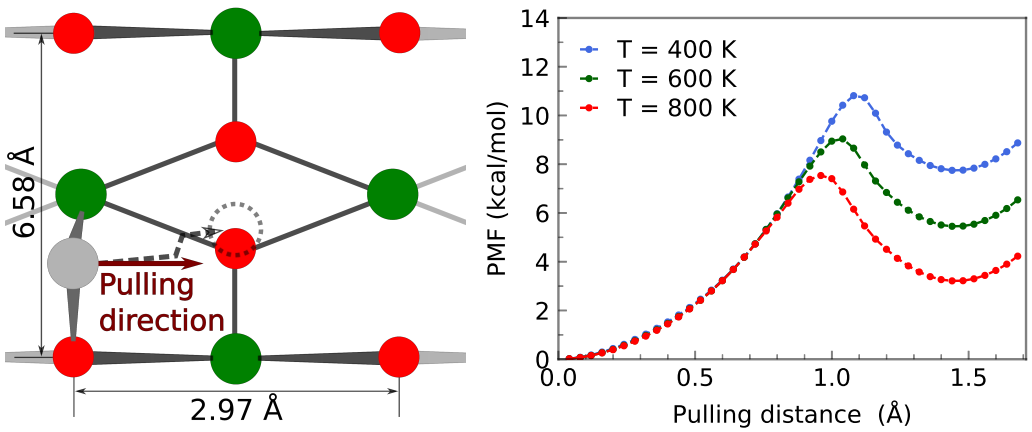

Figure 4.7: Potential of mean force (PMF) of single Pt atom transport on the TiO_2 rutile (110) surface at three different temperatures computed by the steered molecular dynamics (SMD) method with pulling speed of 0.02 Å/ns.

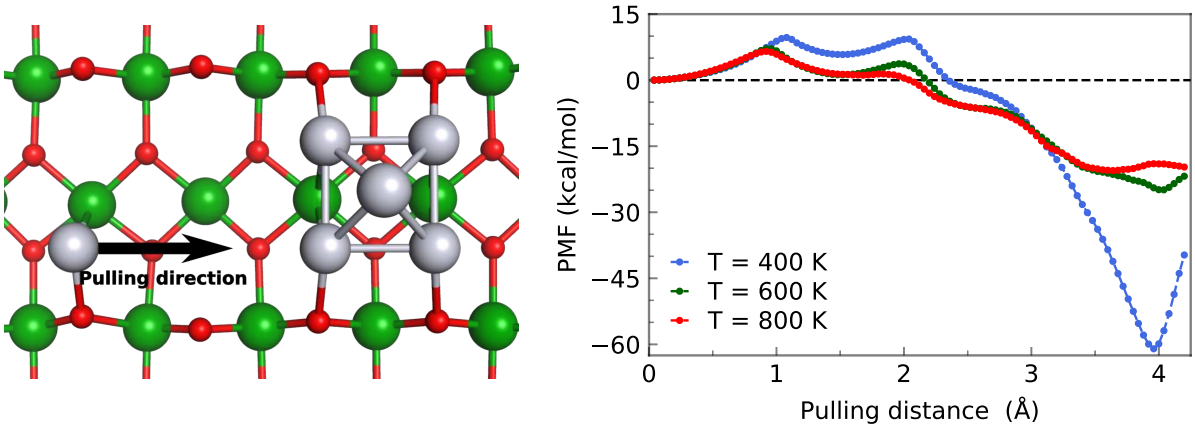

Figure 4.8: Potential of mean force (PMF) of a nucleation of Pt_6 from Pt_5 and nearby single Pt atom on the TiO_2 rutile (110) surface at three different temperatures computed by the steered molecular dynamics (SMD) method.

This result confirms that the decrease in energy originated from the distortion of the Pt_5 cluster. The total free energy of ≈30 kcal/mol was observed. The increase in temperature also affects the total free energy of formation for Pt_6 from Pt_5 and Pt_1. However, the change in amplitude of a few kcal/mol is small compared to the total formation energy of ≈30 kcal/mol. In conclusion, increasing temperatures significantly reduces the energy barrier of Pt atom transport on TiO_2 surface and the TS of its nucleation, while having a minimal effect on the total nucleation energy. Therefore, enhances the sintering event.

4.5 Conclusions

New parameters for the density-functional tight-binding (DFTB) method were generated to simulate platinum particles in vacuum, bulk Pt, and Pt clusters on TiO_2 support. New Pt electronic and repulsive potentials were developed using a protocol we have previously devised and connected with the tiorg parameter set. The optimized DFTB parameters were validated by comparing corresponding geometries, energetic properties, and electronic structures against DFT. The test set includes Pt_n ($n = 2 - 116$) clusters, ≈ 20,000 conformations of Pt_n ($n = 10, 11, 12, 13$) clusters, bulk Pt unit cells (SC, BCC, HCP, and FCC), and the chemisorption of Pt_n ($n = 1-8$) clusters on the TiO_2 rutile (110) and anatase (101) surfaces.

We employed the new DFTB parameters to simulate the diffusion of Pt_1 atom and the nucleation of Pt_6 from Pt_5 and Pt_1 on rutile (110) surface using the steered molecular dynamics (SMD) method. While increasing temperatures were found to have a minimal effect on the total nucleation energy, it significantly reduces the free energy barrier of Pt atom migration on the TiO_2 surface and the transition state (TS) of its nucleation. We expect that with our new parameters, the DFTB method will be able to contribute to simulations that involves nanoparticle sintering in catalytic systems and pave the way for future improvements in these systems.

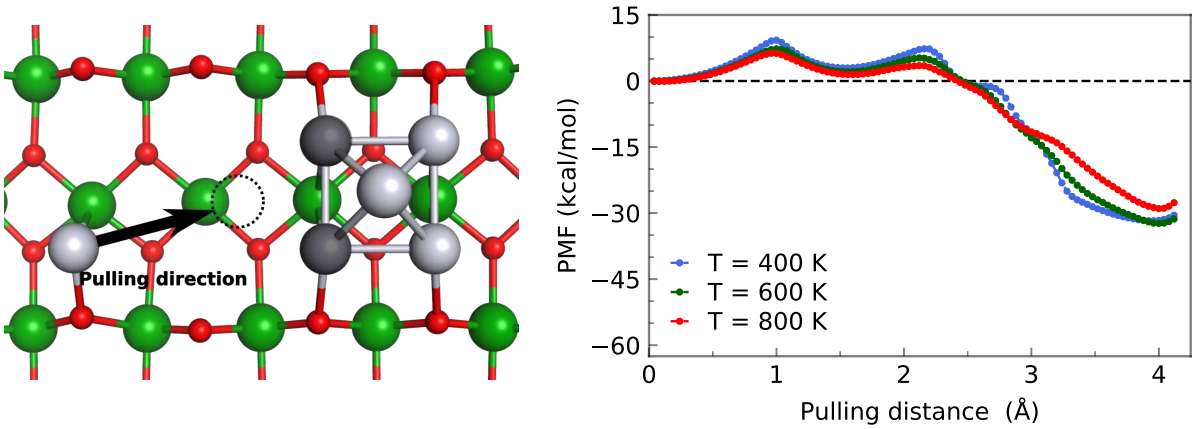

Figure 4.9: Potential of mean force (PMF) of a nucleation of Pt_6 from Pt_5 and nearby single Pt atom on the TiO_2 rutile (110) surface at three different temperatures computed by the steered molecular dynamics (SMD) method. An additional restraint was applied on the Pt_5 cluster to reduce its dynamic along the reaction coordinate, pulling speed $v = 0.02$ Å/ns.

Chapter 5

The Fragment Molecular Orbital Method Based on Long-Range Corrected Density-Functional Tight-Binding

A version of this chapter was originally published by Vuong, V. Q.; Nishimoto, Y.; Fedorov, D. G.; Sumpter, B. G.; Niehaus, T. A.; Irle, S. "The Fragment Molecular Orbital Method Based on Long-Range Corrected Density-Functional Tight-Binding" *J. Chem. Theory Comput.* **2019**, *15*, 3008–3020.

5.1 Abstract

The presently available linear scaling approaches to density-functional tight-binding (DFTB) based on the fragment molecular orbital (FMO) method are severely impacted by the problem of artificial charge transfer due to the self-interaction error (SIE), hampering the simulation of zwitterionic systems such as biopolymers or ionic liquids. We here report an extension of FMO-DFTB where we included a long-range corrected (LC) functional designed to mitigate the DFTB SIE, called the FMO-LC-DFTB method, resulting in a robust method which succeeds in simulating zwitterionic systems. Both energy and analytic gradient are developed for the gas phase and the polarizable continuum model of solvation. The scaling of FMO-LC-DFTB with system size N is shown to be almost linear, $O(N^{1.13-1.28})$ and its

numerical accuracy is established for a variety of representative systems including neutral and charged polypeptides. It is shown that pair interaction energies between fragments for two mini-proteins are in excellent agreement with results from long-range corrected density functional theory. The new method was employed in long timescale (1 nanosecond) molecular dynamics simulations of the tryptophan cage protein (PDB: 1L2Y) in the gas phase for four different protonation states, and in stochastic global minimum structure searches for 1-ethyl-3-methylimidazolium nitrate ionic liquid clusters containing up to 2300 atoms.

5.2 Introduction

Dynamic chemical processes in zwitterionic systems, such as bio-polymers, ionic liquids, salt solutions, or metal-organic frameworks, have received considerable attention due to their fundamental importance in diverse fields such as energy conversion, medical applications, and catalysis.[198–203] Detailed atomic-level understanding of ion transport reactive dynamics is needed to allow the rational design of a material to enhance its ionic conductivity.[204,205] While the application of classical mechanics to study these processes is usually limited because of the lack of parameters and polarization in most force fields, a fully quantum chemical study of these reactive processes is difficult due to the required long simulation timescale and large system size, often ranging in the tens of thousands of atoms.[200,204] Ab initio wave function or density functional theory (DFT) methods are capable of describing reactive dynamics in quantum mechanics (QM)-based molecular dynamics (MD) simulations. However, these methods are only capable of simulating systems containing a few hundred atoms on the order of hundreds of picoseconds, due to their tremendous computational cost even when modern supercomputers are used.[19,20]

Semi-empirical approximations based on wave function methods or DFT have been proposed to tackle the size and time scale issue. Among them, the density-functional tight-binding (DFTB) method,[50,53–55,58] an approximation to DFT, has emerged as a promising approach.[161] DFTB often outperforms other Hartree–Fock-based semi-empirical methods like AM1,[24] PM3,[25,26] PM6,[27] or OMx[206] because its DFT roots allow for implicit inclusion of dynamic electron correlation effects,[33,35,36,207] and in principle all terms in the DFTB

energy expression can be computed from regular DFT.[208] At the same time, its tight-binding framework dramatically reduces the computational cost of DFTB, potentially expanding the applicability of this quantum-chemical method by several orders of magnitude.[33,161] The computational efficiency of DFTB originates from the use of a two-center approximation, minimal valence electron atomic basis set, and pre-tabulated DFT integrals. On a single central processing unit (CPU), DFTB allows the geometry optimization of a system containing several thousand atoms. DFTB enables MD simulations on a nanosecond timescale for systems containing many hundreds of atoms.[39]

Even though DFTB is several orders of magnitude faster than conventional Hartree–Fock (HF) or DFT methods, a computational bottleneck remains related to solving the Schrödinger equation as a generalized eigenvalue problem requiring the diagonalization of the DFTB Hamiltonian matrix. This step incurs cubic scaling of computer time with system size[209] and limits the practical application of DFTB to systems containing a few thousand atoms.[38] Linear-scaling approaches such as the fragment molecular orbital method (FMO),[40,41,43–45,210] divide-and-conquer (DC)[46–48] or modified DC (mDC)[49] have been developed for DFTB to address the scaling problem. These approaches significantly broaden the applicable scope of DFTB, and, for instance, it is possible for FMO-DFTB to perform full quantum-chemical geometry optimization of systems containing up to 1,000,000 atoms on 128 CPU cores in ∼4 days,[41] as well as an MD simulation for a nanoscale system of a similar size.[45]

DFTB, and necessarily all of its linear-scaling incarnations, inherit not only the advantages of DFT, but also its deficiencies, most prominently its self-interaction error (SIE).[79,86,115] The spurious interaction of an electron with itself artificially stabilizes delocalized states, leading to a variety of problematic issues including the underestimation of the band gap in materials and charge transfer excitation energies, the overestimation of charge transfer and conductance, and the incorrect description of activation energies for chemical reactions, as well as the binding energies in charge transfer complexes.[79,81–88]

The underestimation of the energy gap between the highest occupied molecular orbital (HOMO) and the lowest unoccupied molecular orbital (LUMO) in zwitterionic systems, such as proteins with charged residues, or ionic liquids, results in oscillation of orbital

occupations during self-consistency cycles, which in turn prevents convergence in self-consistent field (SCF) procedures including self-consistent-charge (SCC) approaches as employed in DFTB.[79,84,115] Although the convergence problem of nearly metallic systems can be circumvented by using a finite electronic temperature, e.g. in the Fermi–Dirac fractional orbital occupation distribution function,[211] this solution can only be regarded as technical workaround that simply allows one to gain convergence without solving the electronic state problem itself.[90]

FMO-DFTB calculations can fail for systems containing multiple charged fragments in the gas phase, as previously discussed by Nishimoto et al.[80] who demonstrated that artificial charge transfer occurs in such systems because of the nearly metallic electronic state; adding solvent in the polarizable continuum model (PCM) tends to stabilize occupied orbitals and thus increases the HOMO-LUMO gap, stabilizing the calculations. However, enzymatic catalysis relies heavily on the destabilizing effect of charges in the interior of proteins,[212] where implicit solvent models are not generally suitable to stabilize zwitterionic charge states. Moreover, the SIE still present in FMO-DFTB/PCM methods significantly affects the description of inter-fragment interactions in dimer calculations containing opposite charges. Clearly, a more fundamental solution to these problems is highly desirable.

Della Sala and Niehaus have developed a DFTB method with a long-range correction (LC) in analogy to long-range corrected DFT functionals,[91–94] aimed at correcting the SIE in DFTB.[89] The LC-DFTB exchange–correlation functional splits the electron–electron interaction into short-range and long-range contributions, where the long-range exchange part is computed by HF and the short-range part is computed by the DFT exchange–correlation functional.[89] The HF exchange integrals are computed in LC-DFTB using products of the single electron density matrices to construct the required two-electron density matrix. The onset of the 'long-range interaction' is regulated by a parameter ω in the Yukawa potential.[90] It was found that LC-DFTB succeeds to correct the systematic underestimation of the DFTB HOMO-LUMO gap and the SCF convergence problem for small molecules and zwitterionic proteins in ground state calculations.[77,90]

Furthermore, LC-DFTB has recently been utilized to compute excited states by way of a time-dependent (TD) approach,[213] showing that the method can reproduce LC-DFT

results for optical properties of small molecules, polyacenes, and nucleobases, as well as charge-transfer excited states in molecular dimers.[118] In addition, Humeniuk and Mitric also introduced an alternative LC approach for TD-DFTB.[214,215] Due to the additional calculation of the long-range HF exchange contribution to construct the Hamiltonian matrix, LC-DFTB is significantly slower than traditional DFTB, but remains faster than LC-DFT by several orders of magnitude.[90]

Because of the artificial charge transfer in FMO-DFTB caused by the nearly metallic character of systems with multiple oppositely charged fragments, and the high computational cost and poor scaling of LC-DFTB, the development of a linear-scaling approach for it is indispensable to study large zwitterionic systems. In this work, the nearly linear-scaling FMO approach is interfaced with the LC-DFTB developed by Della Sala and Niehaus, referred to as FMO-LC-DFTB, in the implementation in the GAMESS-US program package.[95,216] The development of FMO-LC-DFTB aims to enable MD simulations for large-scale zwitterionic systems such as proteins or ionic liquids, which are currently out of the scope of applicability for the standard FMO-DFTB method.

5.3 Methodology

5.3.1 Overview of LC-DFTB

The derivation of LC-DFTB from DFT has been described in detail by Della Sala and Niehaus.[89,90] The total energy of LC-DFTB is defined as

$$\begin{aligned} E = &\sum_{\mu\nu} D_{\mu\nu} H^0_{\mu\nu} + \frac{1}{2}\sum_{ab} \gamma_{ab} \Delta q_a \Delta q_b + \sum_{a>b} E^{\mathrm{rep}}_{ab} \\ &- \frac{1}{16}\sum_{\mu\nu\alpha\beta} \Delta D_{\mu\nu} \Delta D_{\alpha\beta} S_{\mu\alpha} S_{\beta\nu} \left(\gamma^{\mathrm{lr}}_{\mu\beta} + \gamma^{\mathrm{lr}}_{\mu\nu} + \gamma^{\mathrm{lr}}_{\alpha\beta} + \gamma^{\mathrm{lr}}_{\alpha\nu}\right), \end{aligned} \tag{5.1}$$

where 'a' and 'b' are indices for atoms; μ, ν, α, and β are indices for atomic orbital (AO); $\gamma_{\mu\nu} = \gamma_{ab}$ and $\gamma^{\mathrm{lr}}_{\mu\nu} = \gamma^{\mathrm{lr}}_{ab}$ if $\mu \in a$ and $\nu \in b$; γ_{ab} and $\gamma^{\mathrm{lr}}_{ab}$ are functions depending on the distance between atoms and their chemical hardness. The γ^{lr} also depends on the range-separation parameter ω, which regulates the onset of the 'long-range interaction'. In eq 5.1,

the electron density matrix, $\mathbf{D}$, and difference electron density matrix, $\Delta\mathbf{D}$, are respectively defined as

$$\begin{aligned} D_{\mu\nu} =& \sum_{i}^{\text{occ.}} n_i c_{\mu i} c_{\nu i}, \\ \Delta D_{\mu\nu} =& D_{\mu\nu} - D^0_{\mu\nu}, \end{aligned} \tag{5.2}$$

where $c_{\mu i}$ is the expansion coefficient of the ith molecular orbital (MO) in an AO basis and $\mathbf{D}^0$ is the electron density matrix of a reference system. The orbital occupation number n_i is 2 and 0 for occupied (occ.) and virtual (vir., for later use) orbitals, respectively. The atomic charge or deviation of the Mulliken population, Δq_a, on atom 'a' from that in the neutral atom is defined as

$$\Delta q_a = \sum_{i}^{\text{occ.}} n_i \sum_{\mu\in a} \sum_{\nu} c_{\mu i} c_{\nu i} S_{\mu\nu} - q^0_a, \tag{5.3}$$

where $S_{\mu\nu} = \langle \phi_\mu | \phi_\nu \rangle$ is the overlap matrix element and q^0_a is the number of valence electrons of atom 'a' in the neutral state. For LC-DFTB, the Hamiltonian matrix $\mathbf{H}$ is

$$\begin{aligned} H_{\mu\nu} = & H^0_{\mu\nu} + \frac{1}{2} S_{\mu\nu} \sum_c (\gamma_{ac} + \gamma_{bc}) \Delta q_c \\ & - \frac{1}{8} \sum_{\alpha\beta} \Delta D_{\alpha\beta} S_{\mu\alpha} S_{\beta\nu} (\gamma^{\text{lr}}_{\mu\beta} + \gamma^{\text{lr}}_{\mu\nu} + \gamma^{\text{lr}}_{\alpha\beta} + \gamma^{\text{lr}}_{\alpha\nu}). \end{aligned} \tag{5.4}$$

The derivative of the energy with respect to the coordinate r_a (r can be x, y or z in the Cartesian coordinate system) of atom 'a' is

$$\begin{aligned} \frac{\partial E}{\partial r_a} = & \sum_{a\neq b} \sum_{\mu\in a} \sum_{\nu\in b} \Bigg[2 D_{\mu\nu} \frac{\partial H^0_{\mu\nu}}{\partial r_a} - 2 W_{\mu\nu} \frac{\partial S_{\mu\nu}}{\partial r_a} \\ & + D_{\mu\nu} \frac{\partial S_{\mu\nu}}{\partial r_a} \sum_c (\gamma_{ac} + \gamma_{bc}) \Delta q_c - \frac{1}{4} \frac{\partial S_{\mu\nu}}{\partial r_a} \\ & \sum_{\alpha\beta} \Delta D_{\mu\alpha} \Delta D_{\beta\nu} S_{\alpha\beta} (\gamma^{\text{lr}}_{a\alpha} + \gamma^{\text{lr}}_{a\beta} + \gamma^{\text{lr}}_{b\alpha} + \gamma^{\text{lr}}_{b\beta}) \\ & - \frac{1}{4} \frac{\partial \gamma^{\text{lr}}_{ab}}{\partial r_a} \sum_{\alpha\beta} S^X_{\mu\beta} S^X_{\nu\alpha} \big(\Delta D_{\mu\alpha} \Delta D_{\beta\nu} + \Delta D_{\mu\nu} \Delta D_{\alpha\beta} \big) \Bigg] \\ & + \Delta q_a \sum_{c\neq a} \Delta q_c \frac{\partial \gamma_{ac}}{\partial r_a} + \sum_{a\neq b} \frac{\partial E^{\text{rep}}_{ab}}{\partial r_a}, \end{aligned} \tag{5.5}$$

where $\mathbf{W}$ is the energy-weighted density matrix,

$$W_{\mu\nu} = \sum_{i}^{\text{occ.}} n_i c_{\mu i} c_{\nu i} \epsilon_i, \tag{5.6}$$

where ϵ_i is the ith eigenvalue of $\mathbf{H}$ after diagonalization.

5.3.2 Two- and Three-Body Expansions of FMO combined with LC-DFTB

The FMO method[217] is a fragmentation approach[218–224] described in detail in the reviews.[40,225–227] Here, it is briefly summarized for completeness. A molecular system is divided into fragments; then SCC calculations of each fragment are performed in the embedding potential due to the whole system. After all fragments converge, pairs of fragments are calculated also in the embedding field; for higher accuracy, triples of fragments are also computed. The highest level of conglomeration is the order of the FMO expansion, equal to 2 and 3 if the largest conglomerate is a dimer or trimer, respectively.

In this work, two- and three-body expansions of the FMO method[41,43,44,210] are combined with LC-DFTB. In the two-body FMO expansion (FMO2),[41,120] the total energy is defined as

$$E^{\text{FMO2}} = \sum_{I}^{N} E_I + \sum_{I>J}^{N} (E_{IJ} - E_I - E_J), \tag{5.7}$$

where N is the number of fragments, E_I and E_{IJ} are the energies of monomer (fragment) I and fragment dimer IJ, respectively. They are defined as

$$E_X = E_X^{'} + E_{X,X}^{V}. \tag{5.8}$$

The internal energy, $E_X^{'}$, of a fragment X ($X = I, J$ or IJ) is

$$\begin{aligned} E_X^{'} = &\sum_{\mu\nu\in X} D_{\mu\nu}^X H_{\mu\nu}^{0,X} + \frac{1}{2}\sum_{ab\in X}\gamma_{ab}\Delta q_a^X \Delta q_b^X \\ &- \frac{1}{16}\sum_{\mu\nu\alpha\beta\in X}\Delta D_{\mu\nu}^X \Delta D_{\alpha\beta}^X S_{\mu\alpha}S_{\beta\nu} \\ &(\gamma_{\mu\beta}^{\mathrm{lr}} + \gamma_{\mu\nu}^{\mathrm{lr}} + \gamma_{\alpha\beta}^{\mathrm{lr}} + \gamma_{\alpha\nu}^{\mathrm{lr}}) + \sum_{a>b,ab\in X} E_{ab}^{\mathrm{rep}}. \end{aligned} \tag{5.9}$$

In analogy to FMO-HF, the HF exchange contribution is neglected in the embedding potential.[228,229] The embedding energy $E_{X,Y}^V$ is therefore defined in exactly the same way as in FMO-DFTB without LC

$$E_{X,Y}^V = \sum_{a\in X}\sum_{K\neq Y}^{N}\sum_{c\in K}\gamma_{ac}\Delta q_a^X \Delta q_c^K, \tag{5.10}$$

where Δq_a^X is the charge on atom a in a fragment X.

By substituting eqs 5.8, 5.9 and 5.10 into eq 5.7, one can rewrite the total FMO2 energy as

$$\begin{aligned} E^{\mathrm{FMO2}} =& \sum_{I}^{N} E_I^{'} + \sum_{I>J}^{N}\Delta E_{IJ} \\ \Delta E_{IJ} =& E_{IJ}^{'} - E_I^{'} - E_J^{'} + \Delta E_{IJ}^V \end{aligned} \tag{5.11}$$

The coupling of the charge transfer to the embedding potential ΔE_{IJ}^V is

$$\Delta E_{IJ}^V = \sum_{a\in IJ}\sum_{K\neq I,J}^{N}\sum_{c\in K}\gamma_{ac}\Delta\Delta q_a^{IJ}\Delta q_c^K \ , \tag{5.12}$$

where $\Delta\Delta q_a^{IJ}$ is the difference between the charge of atom a in monomer and dimer calculations

$$\Delta\Delta q_a^{IJ} = \Delta q_a^{IJ} - \Delta q_a^I \delta_{a\in I} - \Delta q_a^J \delta_{a\in J} \tag{5.13}$$

and $\delta_{a\in I} = 1$ if atom a belongs to fragment I, and otherwise it is zero. Because the inter-fragment charge transfer is short-ranged, $\Delta\Delta q_a^{IJ} \approx 0$ for dimers that are far apart from each other. Following the earlier approach,[41] the electrostatic dimer (ES-DIM) approximation[121]

is employed for the calculation of dimers separated farther than a certain cutoff,

$$E'_{IJ} \approx E'_I + E'_J + \sum_{a\in I}\sum_{b\in J} \gamma_{ab}\Delta q_a^I \Delta q_b^J. \tag{5.14}$$

In case of the three-body FMO expansion (FMO3),[44,122,123] the total energy is defined as

$$\begin{aligned} E^{\mathrm{FMO3}} =& \sum_I^N E'_I + \sum_{I>J}^N \Delta E_{IJ} \\ &+ \sum_{I>J>K}^N \big(\Delta E_{IJK} - \Delta E_{IJ} - \Delta E_{IK} - \Delta E_{JK}\big), \end{aligned} \tag{5.15}$$

where

$$\Delta E_{IJK} = E'_{IJK} - E'_I - E'_J - E'_K + \Delta E^V_{IJK} \tag{5.16}$$

and

$$\Delta E^V_{IJK} = E^V_{IJK,IJK} - E^V_{I,IJK} - E^V_{J,IJK} - E^V_{K,IJK}. \tag{5.17}$$

In FMO3, the three-body quantum effects of far separated trimers are negligible, and these energy contributions are ignored for separated trimers using the I-TRIM algorithm.[44,124]

5.3.3 Analytic Gradients for FMO combined with LC-DFTB

For FMO2, the derivative of energy with respect to an atomic coordinate r_a is obtained from the derivative of eq 5.11

$$\begin{aligned} \frac{\partial E^{\mathrm{FMO2}}}{\partial r_a} =& \sum_I^N \frac{\partial E'_I}{\partial r_a} + \sum_{I>J}^N \left(\frac{\partial E'_{IJ}}{\partial r_a} - \frac{\partial E'_I}{\partial r_a} - \frac{\partial E'_J}{\partial r_a}\right) \\ &+ \sum_{I>J}^N \frac{\partial(\Delta E^V_{IJ})}{\partial r_a}. \end{aligned} \tag{5.18}$$

By taking the derivative of eq 5.9, one obtains the contribution of the internal energy term. For a closed shell fragment,

$$\begin{aligned}\frac{\partial E_X^{'}}{\partial r_a} = \sum_{(a\neq b)\in X}\sum_{\mu\in a}\sum_{\nu\in b}\Bigg[& 2D^X_{\mu\nu}\frac{\partial H^{0,X}_{\mu\nu}}{\partial r_a} - 2W^{'X}_{\mu\nu}\frac{\partial S^X_{\mu\nu}}{\partial r_a} \\ & + D^X_{\mu\nu}\frac{\partial S^X_{\mu\nu}}{\partial r_a}\sum_{c\in X}(\gamma_{ac}+\gamma_{bc})\Delta q^X_c - \frac{1}{4}\frac{\partial S^X_{\mu\nu}}{\partial r_a} \\ & \sum_{\alpha\beta\in X}\Delta D^X_{\mu\alpha}\Delta D^X_{\beta\nu}S^X_{\alpha\beta}(\gamma^{\mathrm{lr}}_{a\alpha}+\gamma^{\mathrm{lr}}_{a\beta}+\gamma^{\mathrm{lr}}_{b\alpha}+\gamma^{\mathrm{lr}}_{b\beta}) \\ & - \frac{1}{4}\frac{\partial \gamma^{\mathrm{lr}}_{ab}}{\partial r_a}\sum_{\alpha\beta\in X}S^X_{\mu\beta}S^X_{\nu\alpha}\big(\Delta D^X_{\mu\alpha}\Delta D^X_{\beta\nu} \\ & + \Delta D^X_{\mu\nu}\Delta D^X_{\alpha\beta}\big)\Bigg] + \Delta q^X_a\sum_{(c\neq a)\in X}\Delta q^X_c\frac{\partial\gamma_{ac}}{\partial r_a} \\ & + \sum_{(a\neq b)\in X}\frac{\partial E^{\mathrm{rep}}_{ab}}{\partial r_a} - \sum_{m\in X}^{\mathrm{vir.}}\sum_{i\in X}^{\mathrm{occ.}}4U^{r_a,X}_{mi}V^X_{mi},\end{aligned} \tag{5.19}$$

where $W^{'X}_{\mu\nu}$ is the internal energy-weighted density matrix of a fragment X defined earlier[41] and $D^X_{\mu\nu}$ is the density matrix element of the fragment X. In eq 5.19, the derivatives of the MO coefficient, $c_{\mu i}$, with respect to the coordinate r_a are expanded as

$$\frac{\partial c^X_{\mu i}}{\partial r_a} = \sum_m^{\mathrm{all}} c^X_{\mu m}U^{r_a,X}_{mi}\ , \tag{5.20}$$

where $U^{r_a,X}_{mi}$ are the orbital responses. The response contribution (the last term) in eq 5.19 arises because of the non-variational formulation of the FMO2 (and FMO3) energy (i.e., the use of the embedding potential of fragments in SCC calculations of dimers and trimers).

Because the HF exchange contribution is neglected in the embedding calculation, the derivative of the embedding energy is obtained as described earlier.[41] Following the definition

of the integral derivative of ΔE_{IJ}^{V},[45] the derivative of ΔE_{IJ}^{V} can be written as

$$\begin{aligned}\frac{\partial \Delta E_{IJ}^{V}}{\partial r_a} &= \Delta E_{IJ}^{V,r_a} + \overline{U}^{r_a,IJ,IJ} - \overline{U}^{r_a,I,IJ} - \overline{U}^{r_a,J,IJ} \\ &+ \sum_{K\neq I,J} \sum_{m\in K}^{\text{vir.}} \sum_{i\in K}^{\text{occ.}} U_{mi}^{r_a,K} L_{mi}^{IJ,K},\end{aligned} \tag{5.21}$$

where $\Delta E_{IJ}^{V,r_a}$ are the integral derivatives in the embedding dimer energies,[41] and $L_{mi}^{IJ,K}$ are the Lagrangian contributions of the embedding energy.[43,45] $\overline{U}^{r_a,X,Y}$ is defined as

$$\overline{U}^{r_a,X,Y} = 4 \sum_{m\in X}^{\text{vir.}} \sum_{i\in X}^{\text{occ.}} U_{mi}^{r_a,X} V_{mi}^{Y}, \tag{5.22}$$

where V_{mi}^{Y} is the ESP matrix of fragment Y in the MO basis.

By collecting all U^{r_a} terms for the total gradient of E, one obtains the total response contribution (see earlier work for details[43])

$$R^{r_a} = \sum_{K}^{N} \sum_{m\in K}^{\text{vir.}} \sum_{i\in K}^{\text{occ.}} U_{mi}^{r_a,K} \sum_{I>J(I,J\neq K)} L_{mi}^{IJ,K}. \tag{5.23}$$

Responses $U^{r_a,K}mi$ can be obtained by solving the coupled-perturbed (CP) LC-DFTB (CP-LC-DFTB) equations:

$$\sum_{K}^{N} \sum_{k\in K}^{\text{vir.}} \sum_{l\in X}^{\text{occ.}} A_{ij,kl}^{X,K} U_{kl}^{r_a,K} = B_{ij}^{r_a,X} \ , \tag{5.24}$$

where $A_{ij,kl}^{X,K}$ and $B_{ij}^{r_a,X}$ are defined in the Supporting Information. Also in the Supporting Information is given the derivation of the CP-LC-DFTB equation. As in the case of the standard FMO-DFTB method, the response contribution is evaluated via the self-consistent Z-vector (SCZV) method.[43,230]

The analytic gradient for FMO3 is obtained following the earlier work[44] and explicit equations are omitted for brevity. Likewise, an interface of LC-DFTB to PCM for FMO[44,80] is essentially identical to that for the conventional DFTB, so detailed derivations are omitted.

5.3.4 Validation, Benchmarks, and Demonstration Applications

The accuracy and scaling of the implemented FMO-LC-DFTB energy and gradient was evaluated for two fragmentation choices and various system sizes. Following the validation, three applications were carried out (1) electronic structure and pair interaction energies (PIE)[231] for two mini-proteins, (2) MD simulation for Trp-cage protein in gas phase, (3) stochastic search for the optimal structure and cluster energy of ionic liquid model clusters.

The energy accuracy was evaluated for a polyalanine (COMe–$(Ala)_n$–NHMe, $n = 10, 20, \ldots, 200$) α-helix and extended (unfolded) structure. The precision of the implemented FMO-LC-DFTB analytic gradient was examined via the slope of the total energy fluctuations as a function of the MD time step for a $(H_2O)_{64}$ cluster. Microcanonical ensemble (NVE) FMO2-LC-DFTB/MD simulations were performed for 1 ps (time step 0.1 fs) using velocities initiated at 300 K for relaxation, and the following 10,000 steps were used to compute the slope. The accuracy of the gradient was evaluated by comparison of optimized geometrical parameters of α-helix and extended polyalanine COMe–$(Ala)_{20}$–NHMe. Geometry optimizations were performed until the maximum gradient values became smaller than 10^{-4} Hartree/Bohr.

The accuracy of the solvation energy computed with FMO-LC-DFTB was examined for two mini-proteins: Chignolin and the Tryptophan (Trp) cage. The input geometries and residue protonation states were taken from the first configuration of nuclear magnetic resonance (NMR)-derived structures obtained in aqueous solution; (PDB: 1UAO) for the Chignolin protein[232] and (PDB: 1L2Y) for the Trp-cage protein.[233] The PCM calculations were carried out with the following options: 'SOLVNT=H2O', 'ICAV=1', 'IDISP=1', and for FMO also 'IFMO=-1' was added signifying PCM⟨1⟩.[234] All PCM calculations were performed using 60 initial tesserae per atom with the keyword 'NTSALL=60' and the default van-der-Waals atomic radii.

The scaling of the FMO-LC-DFTB computing time with respect to the system size was evaluated for series of water clusters $(H_2O)_n$, $n \in [517, 3191]$, ethanol clusters $(C_2H_5OH)_n$, $n \in [184, 1044]$ and glucose clusters $(C_6H_{12}O_6)_n$, $n \in [80, 416]$. All input geometries in the scaling tests were prepared by spherically cutting amorphous structures for various radii.

The wall-clock time of single point energy and gradient for these clusters was measured. All computations of the scaling tests were performed using one CPU core of 'Intel Xeon E5-2697' at 2.30GHz.

For the first application, the energy levels of HOMO and LUMO, and the gaps in each fragment residue of two small proteins Chignolin and Trp-cage in the gas phase were investigated using FMO1 based DFTB, LC-DFTB, and LC-BLYP[235] methods. The input geometries were prepared in analogy to the aforementioned PCM test. DFTB2 was used with the MIO Slater-Koster parameter set[58] for DFTB and 6-31G(d) basis set for DFT. Besides the gaps, PIEs in these proteins were obtained with FMO2 based LC-DFTB, LC-BLYP and CAM-B3LYP.[107] All LC-BLYP and CAM-B3LYP calculations were carried out with their default range-separation parameters.

For the second application, MD simulations of the Trp-cage protein were carried out to determine the stable zwitterionic structure of the protein in the gas phase. Four protonation states RCK, RDK, RCQ and RDQ of the Trp-cage protein were prepared in the same way they were proposed by Patriksson et al.[236] as described in the Supporting Information. The initial structure was taken from the first configuration of solvated NMR-derived structure (PDB: 1L2Y). For a short relaxation and sampling, FMO-LC-DFTB/MD simulations of 1 ns were carried out for each protonation state at 300 K with a time step of 1 fs. The potential energy and geometries were collected every 100 fs. RATTLE[237] was applied to constrain the length of H–C, H–O and H–N bonds. For each protonation state, the most stable snapshots were further optimized to rank their stability in the gas phase.

For the last application, a stochastic search for the optimal structure of 1-ethyl-3-methylimidazolium (EMIM) nitrate clusters was performed. The cluster size varies from 1 to 100 pairs of ions. For each cluster size, 1000 initial structures of the clusters were randomly generated using a modification of the Kick[3] program.[238,239] Then, each structure was relaxed for 1 ps MD simulation at 300 K with the time step of 1 fs. The RATTLE algorithm was also applied to constrain H–C bonds. A snapshot was extracted from MD trajectories every 100 steps. In total, 10,000 structures were obtained for each cluster size. The 100 lowest potential energy structures were further optimized to determine the most stable structure for each cluster size.

For all LC-DFTB calculations, the OB2 (shift) Slater-Koster parameter set[77] were used with a range-separation parameter ω=0.3. The Pulay's DIIS interpolation combined with second order SCF (SOSCF) orbital optimization methods were used for the SCF procedure with the following options: 'DIIS=.T.', 'ETHRSH=2.0', 'SWDIIS=0.005' and 'FDIFF=.F.' The ES-DIM approximation was applied with the cutoff value (unitless) of 2.0 for FMO2 and 3.25 for FMO3 as recommended earlier.[44] For FMO3, the three trimer I-TRIM thresholds were 1.25,-1,2. Covalent bond fragmentation was performed at the sp^3 C_α carbon atoms, and hybrid orbital projection (HOP) method was used to treat fragment boundaries across covalent bonds. Hybrid orbitals for sp^3 carbons were determined by the Pipek–Mezey localization analysis[240] using LC-DFTB MOs of a methane molecule in its equilibrium geometry optimized by the same method (the coefficients are provided in the Supporting Information). In all validations, input geometries were pre-optimized using the 'minimize' modules of the TINKER package,[241] unless stated otherwise. The same package was used to generate the α-helix and extended structure of polyalanines.

5.4 Results and Discussion

Although the use of a dispersion correction for FMO-LC-DFTB is straightforward, as such corrections are typically independent from the electronic structure and readily available in the GAMESS package, we selected not to employ dispersion corrections in any of our demonstrations. According to the earlier parametrization work and benchmarks of the D3(BJ) dispersion correction[171] for LC-DFTB, D3(BJ) does not generally improve LC-DFTB results. It does significantly improve the performance of LC-DFTB-D3(BJ) for the S66 and WATER27 test sets, but has detrimental effects in the IDISP and BHPERI test sets.[77] In particular the IDISP test set is currently accepted as a key performance check for intramolecular dispersion interactions. It is therefore necessary to carefully investigate the effect of the dispersion correction on the system of interest before selecting a particular one. For this reason, we decided not to use any dispersion correction and present only results for the pure LC-DFTB method, even though dispersion corrections are available for FMO-LC-DFTB in our GAMESS-US implementation.

5.4.1 Accuracy of FMO-LC-DFTB

In order to assess the accuracy of FMO-LC-DFTB, its energies and optimized geometries were compared to corresponding full LC-DFTB (without fragmentation) energies and optimized geometries.

Energy

The accuracy by which FMO-LC-DFTB reproduces full LC-DFTB energies was examined for a polyalanine (COMe–$(\mathrm{Ala})_n$–NHMe, $n = 10, 20, \ldots, 200$) α-helix, and extended structure with two fragmentations of $nres$ residues per fragment ($nres$=1, 2). Figure 5.1 shows that the FMO-LC-DFTB errors in the total energies linearly increase with the number of atoms and decrease with the fragment size for the α-helix polyalanine and the extended polyalanine as usual in FMO.[41,44] In FMO, the LC-DFTB energy accuracy is comparable to that of DFTB; for example, for the largest extended polyalanine containing 2012 atoms, the FMO2-DFTB error with the $nres$=1 fragmentation is 9.4 and 10.6 kcal/mol with and without LC, respectively, while it reduces to only 0.76 and 0.72 kcal/mol, respectively, with the $nres$=2 fragmentation.

Because the FMO error is related to many-body charge transfer, which is large in α-helices due to multiple hydrogen bonding, the deviations of the total energy for the α-helix form are larger than for the extended form. Adding trimer corrections improves the accuracy. For instance, the largest error of 15.94 and 7.07 kcal/mol was found for the largest α-helix polyalanine for FMO2 and FMO3, respectively. The errors are much reduced when two residues are combined into one fragment.

Gradient

In order to evaluate the accuracy of the FMO-LC-DFTB analytic gradients, optimized geometries for polyalanines are compared to those obtained with full LC-DFTB. As previously observed in similar comparisons between FMO2-DFTB and full DFTB,[41] the presence of many local minima on the potential energy surfaces complicates the geometry comparison, as the numerical geometry optimization procedure may converge to physically

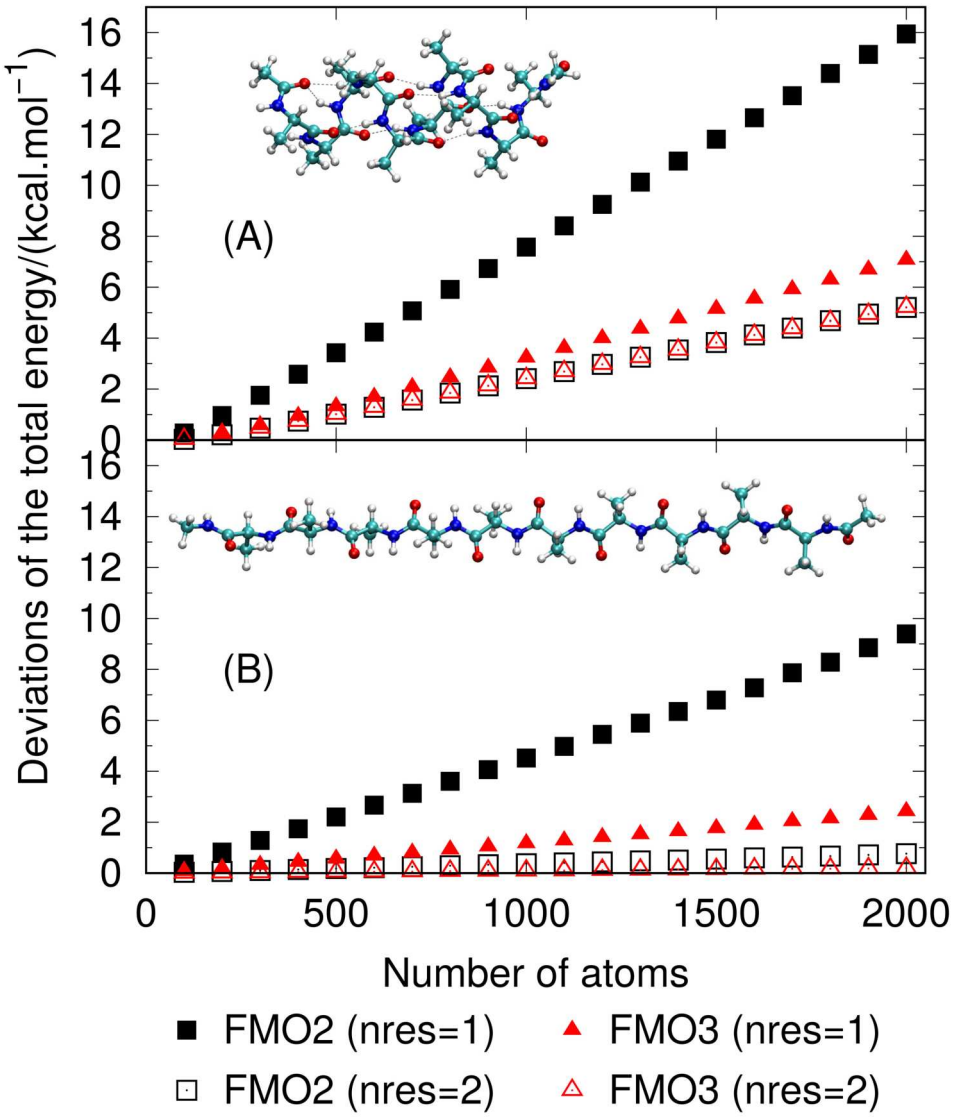

Figure 5.1: Deviations of FMO energies from the values in full unfragmented LC-DFTB for (A) α-helix and (B) extended polyalanine (COMe$-$(Ala)$_n-$NHMe, n = 10, 20,..., 200), *nres* stands for residues per fragment. As illustration, the structures of α-helix and extended COMe$-$(Ala)$_{20}-$NHMe are shown.

distinct minima in FMO-based and full LC-DFTB surfaces even though the difference between the gradients for identical geometries is small. To mitigate such purely numerical effects of the 'minimum search', the FMO geometry optimizations were started from the full LC-DFTB optimized structures. Table 5.1 shows the difference in total energy ΔE between FMO and full LC-DFTB total energies, as well as the root mean square deviation (RMSD) for optimized structures of the α-helix and extended form of a 20-residue polyalanine; two fragmentations of $nres = 1$ and 2 are compared.

FMO2 geometry optimization of the α-helix with the $nres$=1 fragmentation has the largest RMSD of 0.048 Å. Remarkably, the error of FMO3 for the same system and same fragmentations is significantly decreased, resulting in only 0.011 Å. Furthermore, FMO2 perfectly reproduces bond lengths and angles, reported in Table C1 of the Supporting Information. The maximum of absolute deviation (MAX) for bond lengths is less than 0.003Å for the α-helix structure and less than 0.001Å for for the extended structure. For angles, MAX is less than 0.43° for the α-helix structure and less than 0.26° for the extended structure. FMO2 is also accurate in dihedral angle with a mean absolute deviation (MAD) of less than 0.69°, although the MAX is 10.41° for the α-helix structure with the $nres$=1 fragmentation. The dihedral MAX reduces to 8.38° when the size of fragment is doubled. On the other hand, FMO3 remarkably improves the dihedral angle, the errors reduce to only 3.30° with the $nres$=1 fragmentation. The results emphasize the significant improvement in computed dihedral angles due to the FMO3 three-body expansion.

The precision of the implemented fully analytic FMO-LC-DFTB analytic gradient was evaluated by comparing the difference between the analytic and numerical gradients for a $(H_2O)_{64}$ cluster. The maximum deviations (MAX) are only 1.5x10^{-6} and 9.8x10^{-6} hartree/bohr for FMO2-LC-DFTB and FMO3-LC-DFTB, respectively. The numerical gradient was calculated using the three-point formula with a step size of 1.0x10^{-3} bohr. Finally, the precision of the implemented FMO-LC-DFTB analytic gradients was verified by analyzing the energy conservation in NVE molecular dynamics simulations for a $(H_2O)_{64}$ cluster with varying time integration intervals. For the slope of the energy fluctuations versus the time step, ideally, the fully analytic gradient would yield a slope of 2 when plotted on a double-logarithmic scale due to our use of a second-order velocity Verlet time integration

Table 5.1: Comparison for energies and geometries of α-helix and extended (ext.) forms of COMe$-$(Ala)$_{20}-$NHMe optimized by FMO and full LC-DFTB (in FMO, $nres$ residues are assigned to a fragment)

Methods	ΔE (kcal/mol)		RMSD (Å)	
	α-helix	ext.	α-helix	ext.
FMO2				
$nres = 1$	-0.031	0.769	0.048	0.095
$nres = 2$	0.095	0.027	0.045	0.059
FMO3				
$nres = 1$	0.420	0.121	0.011	0.059
$nres = 2$	0.289	0.011	0.011	0.000

algorithm. Figure C. 1 shows that the obtained slopes are very close to the theoretical slope: 1.99 for FMO2 and 1.98 for FMO3. With a time step of 1 fs, the root mean square error (RMSE) in total energy conservation is 0.42 kcal/mol for the $(H_2O)_{64}$. It is worth noting that the fluctuation of the FMO-LC-DFTB total energy is two orders of magnitude smaller than the fluctuations in kinetic and potential energies for a time step smaller than 1 fs (Figure C1 of the Supporting Information). Especially when employing the RATTLE constraint, the ratio of fluctuations in total energy and potential energy is lower and slowly increases with the step size. This result suggests that it is possible to accelerate FMO-LC-DFTB/MD simulations by using time steps equal or even greater than 1 fs.

Energies and Gradients in Implicit Solvent

The accuracy of FMO-LC-DFTB/PCM compared to full calculations without fragmentation was examined for the Chignolin and Trp-cage proteins in terms of single point energy and optimized geometry. The FMO/PCM$\langle 1 \rangle$ level of theory is employed throughout, and $\langle 1 \rangle$ is omitted for brevity. Note that FMO-LC-DFTB/PCM gives the identical non-electrostatic (cavitation, dispersion, and repulsion) energies and gradients to the full LC-DFTB/PCM. Table 5.2 shows that FMO is very accurate in reproducing the PCM solvation energy; the error in solvation energy is less than 0.3 kcal/mol for the Trp-cage and less than 0.1 kcal/mol for the Chignolin protein. The PCM solvation energy is defined as the difference in total energy with and without PCM. Furthermore, the FMO gradient is also very accurate; RMSD of FMO structures at all levels is less than 0.033 and 0.024 Å for the one and two residue fragmentation, respectively, see Table C2 in the Supporting Information.

5.4.2 Scaling of FMO-LC-DFTB

To evaluate the scaling of FMO computing time (wall-clock) with system size, single point energy and gradient calculations were performed for a series of water, ethanol, and glucose clusters using a single CPU core. In these calculations, one fragment consists of a single isolated molecule. The scaling of FMO-LC-DFTB computing time as a function of cluster size is near-linear, $\sim O(N^{1.15})$ for energies and $\sim O(N^{1.25})$ for gradients, Figure 5.3.

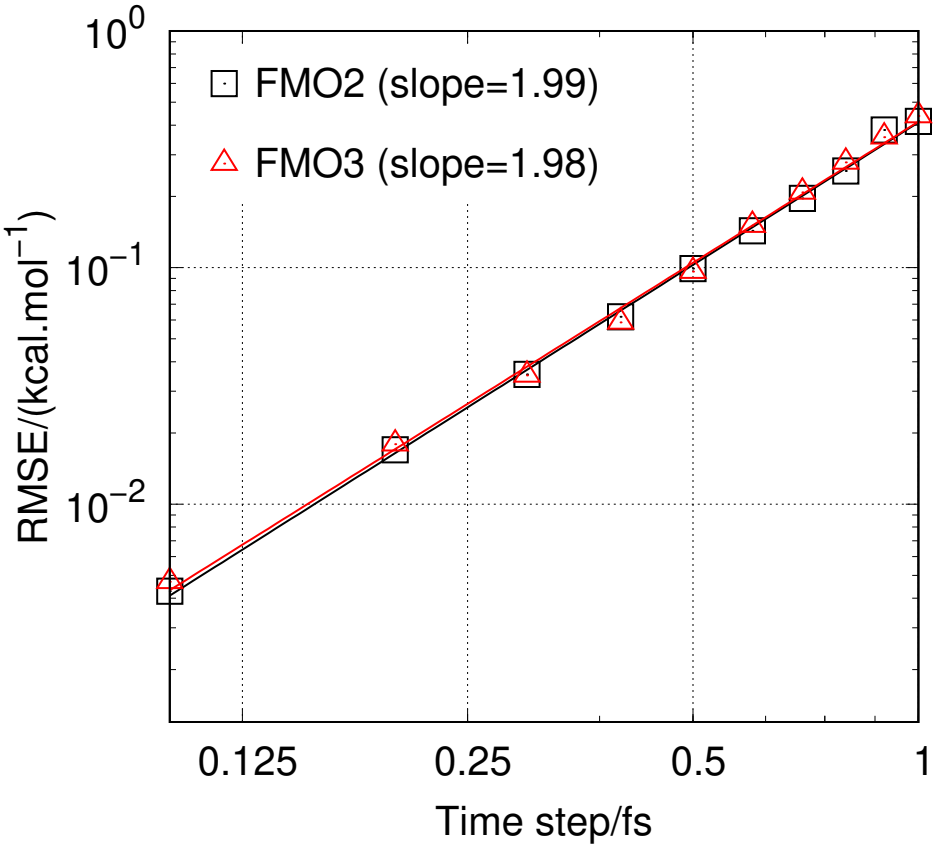

Figure 5.2: The root mean square error (RMSE) of FMO2-LC-DFTB total energy versus time step from the simulations of a 64 water cluster.

Table 5.2: Deviations in total energy (ΔE_{tot}) and PCM solvation energy (ΔE_{solv}) contribution (kcal/mol) of Chignolin and Trp-cage calculated by FMO-LC-DFTB/PCM and compared to LC-DFTB/PCM (in FMO, *nres* residues are assigned to a fragment)

Methods	Trp-cage		Chignolin	
	ΔE_{tot}	ΔE_{solv}	ΔE_{tot}	ΔE_{solv}
FMO2				
$nres = 1$	1.162	0.294	0.562	0.091
$nres = 2$	0.432	0.228	0.277	0.064
FMO3				
$nres = 1$	0.553	0.298	0.120	0.099
$nres = 2$	0.336	0.226	0.061	0.055

As shown earlier,[242] the numbers of SCC dimers and trimers are linear because of the approximations (this is why both FMO2 and FMO3 have a nearly linear scaling); deviations from linearity arise from bookkeeping, embedding potential and separated dimers. It is interesting that in two cases (water and ethanol) FMO3 has in fact a lower scaling than FMO2; this is because the linear-scaling trimer calculation has a large weight in the total timing and the observed total scaling is a combined effect of several steps each having a different scaling; for glucose, however, the embedding potential for large fragments may have increased the scaling.

In order to demonstrate the practical computer time requirements for the methods discussed in this work, we list a few representative timings obtained on a single CPU core: The single point energy calculation for $(H_2O)_{3191}$ (9573 atoms), $(C_2H_5OH)_{1044}$ (9396 atoms) and $(C_6H_{12}O_6)_{416}$ (9984 atoms) clusters were carried out in 32, 21 and 66 seconds with the FMO2-DFTB method, and in 38, 28, and 94 seconds with the FMO2-LC-DFTB method. FMO-LC-DFTB is only slightly slower than the standard FMO-DFTB, even though LC-DFTB by itself is about one order of magnitude slower than standard DFTB.[90] This favorable performance can be attributed to the relatively small fragment size and the near-linear scaling behavior of FMO. To illustrate the speed-up due to fragmentation, a cluster of 220 EMIM-nitrate ion pairs (5060 atoms) was computed. A single point energy+gradient calculation on a single CPU core took 84,735 seconds (23.5 hours) with LC-DFTB and only 38 seconds with FMO2-LC-DFTB, giving a speed-up factor of 2229.

5.4.3 Fragment HOMO-LUMO Gaps and PIEs of Chignolin and Trp-cage Proteins in the Gas Phase

To demonstrate the ability of FMO-LC-DFTB to accurately describe zwitterionic structures in the gas phase, the electronic structure of the Trp-cage and Chignolin proteins were computed *in vacuo*. Zwitterionic systems are indeed found experimentally in the gas phase, such as proteins in ion mobility spectroscopy.[243] As mentioned in the Introduction, standard FMO-DFTB calculations for such zwitterionic species in the gas phase often fail due to convergence problems in dimer calculations containing fragments with opposite charges.

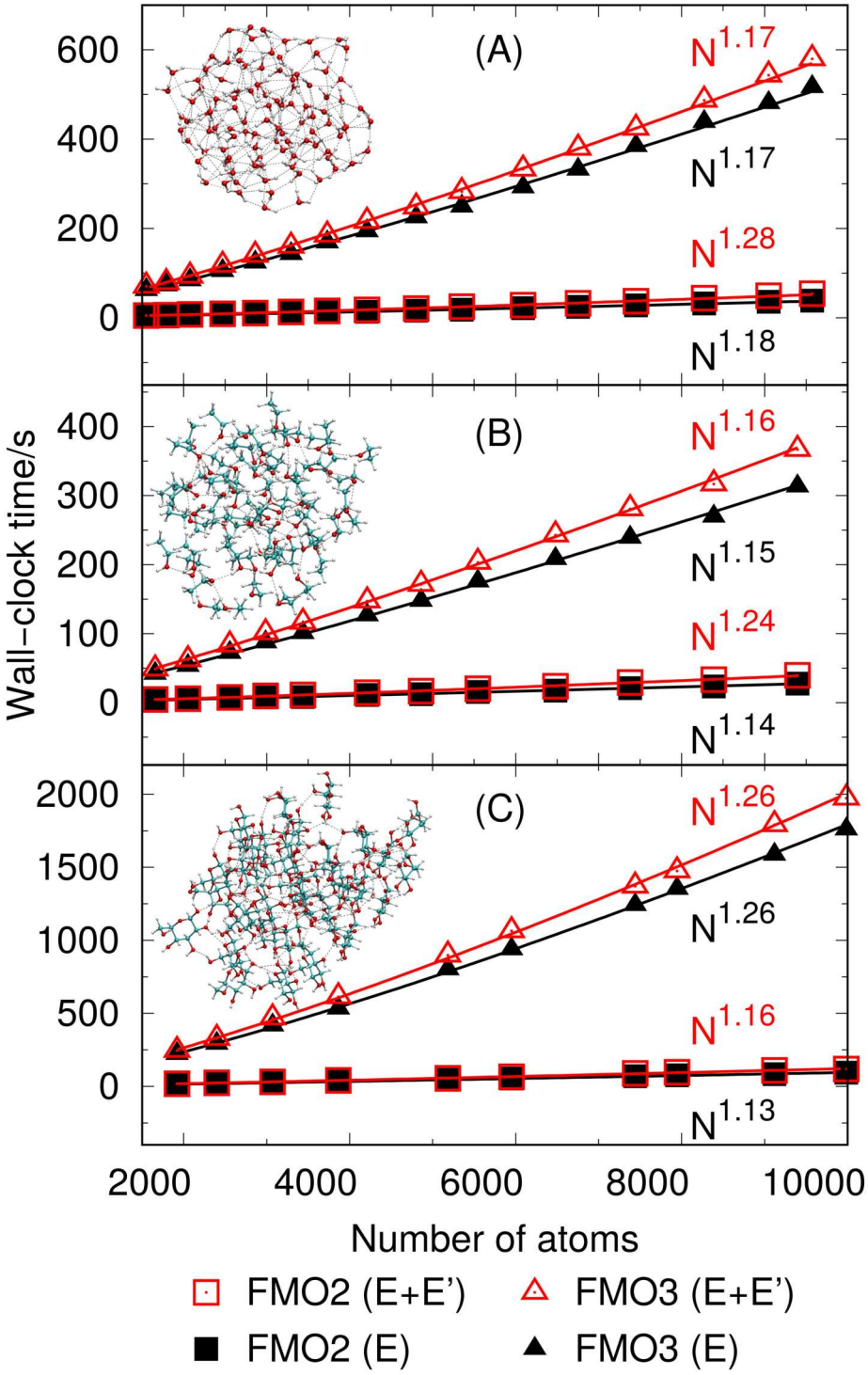

Figure 5.3: Wall-clock time of the single point energy (E) and gradient (E′) calculations by FMO-LC-DFTB for (A) water clusters, (B) ethanol clusters and (C) glucose clusters.

The HOMO and LUMO of each fragment ($nres$=1 fragmentation) were computed for NMR-derived molecular structures at the FMO1 level with both DFTB and LC-DFTB, following the approach described earlier..[80] In FMO, DFTB underestimates the HOMO-LUMO gap of the residues, compared to LC-BLYP, as DFTB destabilizes the HOMO and overstabilizes the LUMO energy levels, see Figure 5.4. The destabilization of the HOMO and the stabilization of the LUMO are particularly pronounced for anionic and cationic fragments, respectively. The FMO1-DFTB LUMOs of the cationic fragments are lower than the HOMOs of the anionic fragments, causing artificial two-electron charge transfer from anionic to cationic fragments and hence never-ending orbital occupation oscillations in the SCC calculations of the zwitterionic dimers.[80] This artificial violation of the Aufbau principle was discussed previously by Nishimoto et al.[80]

On the other hand, the long-range correction in LC-DFTB stabilizes the HOMO and raises the LUMO relative to DFTB orbital energies in the gas phase, thereby solving fundamentally the issue of artificial two-electron charge transfer from anionic to cationic fragment. Figure 5.4 shows that the LC-DFTB HOMO-LUMO gap for each residue is comparative to the LC-BLYP gap for the Chignolin and Trp-cage proteins, and that the LC-DFTB orbital energies of the highest HOMO among all fragments of the protein remains lower than the lowest LUMO level ('total' HOMO-LUMO gap indicated by a grey bar). As a consequence, convergence issues due to the SIE in dimer calculations for fragments with opposite charges are no longer encountered, and FMO2-LC-DFTB calculations of energies and gradients for the entire zwitterionic system in the gas phase or non-polar solvents become possible.

The pair interaction energy (PIE) analysis between proteins and ligands is very useful for the purpose of virtual ligand screening and in silico design of new drugs.[231,244,245] Here, PIEs computed with FMO-based LC-DFTB are compared to the values obtained with long-range corrected BLYP (LC-BLYP) and CAM-B3LYP. The LC-DFTB PIEs for the Trp-cage and Chignolin proteins in the gas phase show a strong correlation to both LC-DFT functionals with R^2 values greater than 0.96, see Figure 5.5. This implies that FMO-LC-DFTB is a reliable, computationally much more economical alternative to FMO-DFT for predicting molecular recognition in large aggregates. The results also suggest that FMO-LC-DFTB is

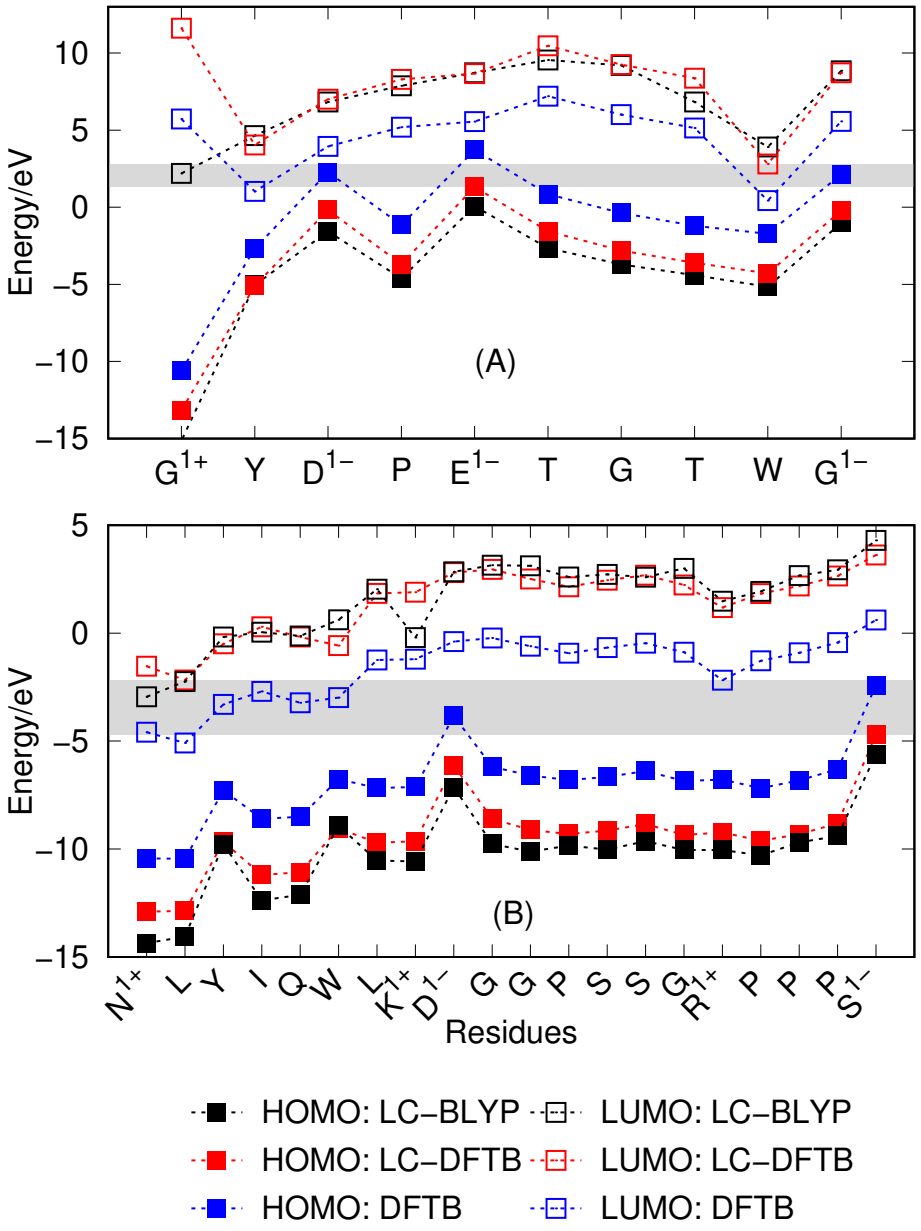

Figure 5.4: HOMOs and LUMOs of residues for (A) Trp-cage and (B) Chignolin in the gas phase. One letter abbreviation was used for residue names with the superscript indicating total non-zero charge.

a promising method in drug discovery to screen and analyze drug candidates.[246] The slope of PIE values for DFTB vs DFT is close to 1 (1.02-1.08), on the same order the slope of one DFT functional vs another (0.96-1.02), showing that not only the correlation is high, but also the absolute values are very similar (high precision and high accuracy).

5.4.4 Molecular Dynamics Simulations of the Trp-Cage Protein in the Gas Phase

UV photodissociation[247] and electron transfer dissociation[248] experiments have shown that the zwitterionic structure of the Trp-cage exists in vacuum.[249,250] However, to the best of our knowledge, no experimental structure of the protein in the gas phase has been determined. FMO2-LC-DFTB based molecular dynamics (MD) simulations were performed for the Trp-cage in four possible protonation states[236] (RCK, RDK, RCQ and RDQ, see Supporting Information) in vacuo. The details for these MD simulations are given in Section 5.3.4. The potential energy and geometrical RMSD variation as a function of simulation time are shown in Figure C2 and C3 of the Supporting Information, respectively. The lowest energy conformation collected during the MD simulation of each protonation state was reoptimized by FMO2-LC-DFTB. After reoptimization, only RCK and RDK, which were also predicted as the two most stable protonation states by a force-field based study,[236] are able to preserve their protonation states, see Figure 5.6. The other two structures (RCQ and RDQ) underwent proton transfer and charge neutralization.

The difference in energy between the two stable protonation states is relatively small, RCK is ∼0.25 kcal/mol more stable than RDK. This difference appears to be in better agreement with the OPLS-AA force-field prediction[236] (1.9 kcal/mol) and vastly different from the PM3 method, which predicted that RDK is 35.9 kcal/mol more stable than RCK.[236] Because the ultra-violet photodissociation experiment suggested the coexistence of these protonation states in the gas phase,[247] the small differences in potential energy in this FMO-LC-DFTB and the force field-based studies confirm the experimental observation. FMO simulation reveals that RCK stabilizes the zwitterionic structure by a network of hydrogen bonds, and that RDK stabilizes the zwitterionic structure by a salt-bridge in between residues

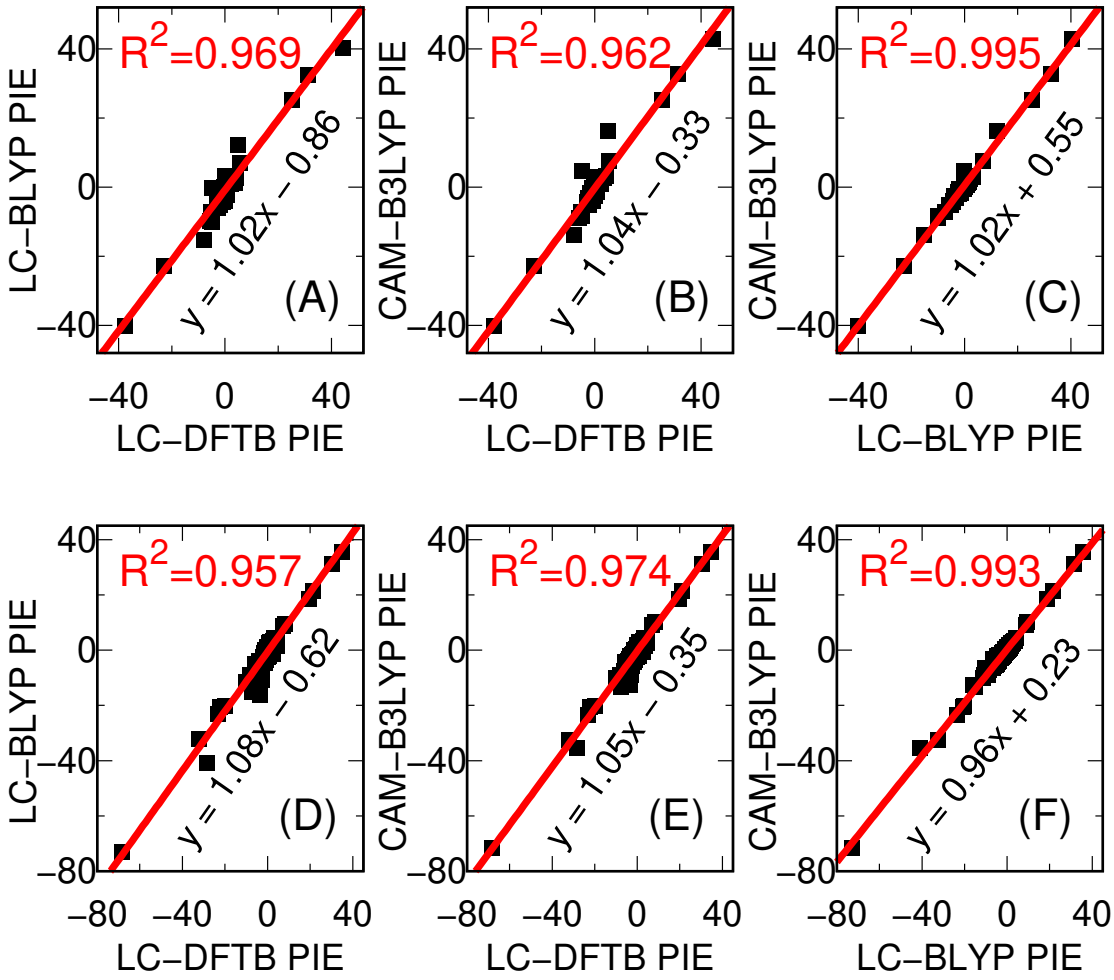

Figure 5.5: Correlation between the LC-DFTB and LC-DFT pair interaction energies (PIE, in kcal/mol) in FMO at several levels of theory for (A–C) Chignolin and (D–F) Trp-cage proteins.

Lys8, Asp9 and Arg16 see Figure 5.6. In the case of RDK, the formation of the salt-bridge from two nearby residues does not require significant changes in the secondary structure of the protein from solution; therefore, the structure change is small, consistent with other computational studies.[236,251]

5.4.5 Global Minimum Structures and Energetics of Ionic Liquid Clusters

The faithful simulation of solvent structure is a necessary prerequisite for understanding diverse fields of technological interest, such as ionic solutions, mineral growth mechanisms, supercapacitor and battery development, etc. In particular the prediction of physicochemical properties of ionic liquids is an active field of theory development due to the many short-comings of classical force field methods on one hand, and the large computer time requirements for traditional quantum- chemical approaches.[252]

The DFTB method is filling this gap as a quantum-chemical method with low-cost requirement.[239] Because simulations of solvent structure require large-scale model systems, the linear-scaling FMO-DFTB method promises great potential for these types of applications. Unfortunately, FMO-DFTB often fails in simulatons of ionic liquids that consist of cations having low-lying LUMO levels, e.g. imidazolium derivatives, or anions with high HOMO, e.g. acetate, due to the aforementioned artificial two-electron charge transfer between ion pairs. Therefore, the combination of stochastic sampling or replica-exchange umbrella sampling[253,254] methods with FMO-DFTB to study these systems is severely limited. Here, the applicability of FMO2-LC-DFTB is demonstrated to stochastically search for the global minimum structure of a model ionic liquid cluster system, namely clusters of 1-ethyl-3-methylimidazolium (EMIM) nitrate with varying from 2 up to 100 ion pairs.

Before carrying out the stochastic search, the accuracy of the FMO2-LC-DFTB isomer energy compared to the full LC-DFTB was evaluated for cluster of 2, 3, 4, and 5 ion pairs. The isomer energy of a structure for a cluster size is defined as the difference in total energy of that structure and the energy of the minimum structure. Figure 5.7 shows a good correlation between FMO2-based and full isomer energy ΔE with $R^2 = 0.999$ for all the test sets without

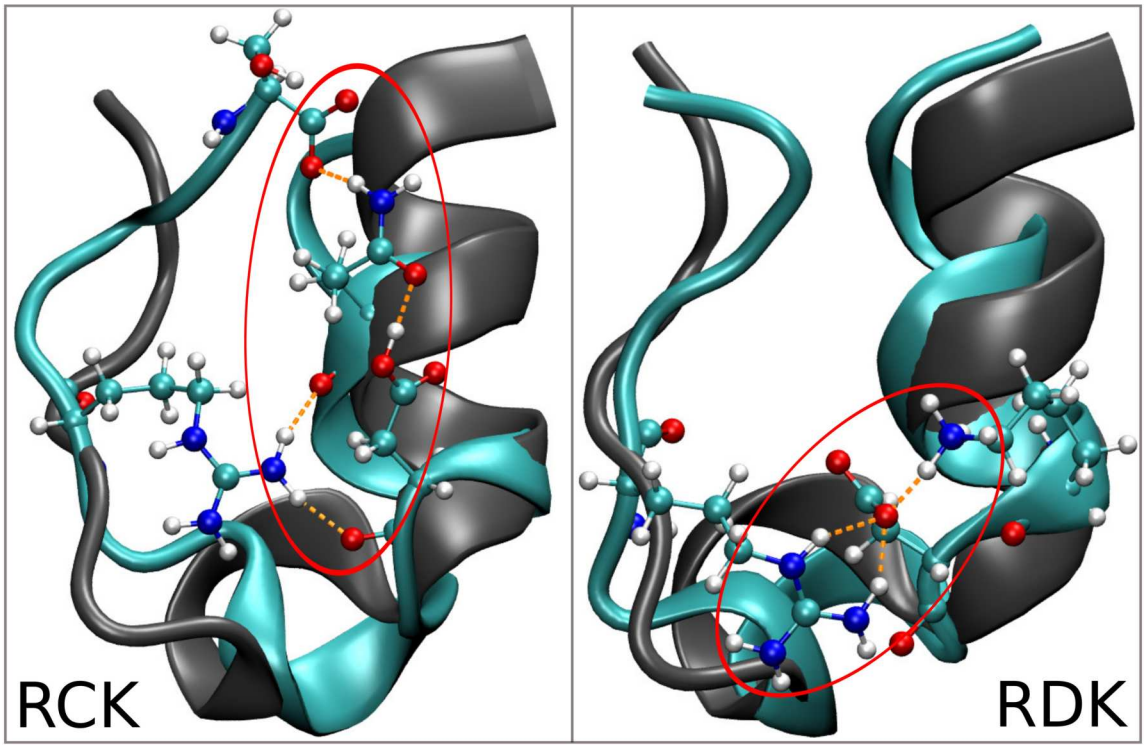

Figure 5.6: The optimal secondary structure of two stable protonation states RCK and RDK of the Trp-cage protein in the gas phase compared to the experimental solvated NMR-structure. The NMR structure is in grey, that of the RCK and RDK is in cyan. Atomistic models show only selected residues involved in the stabilization of the zwitterionic residues.

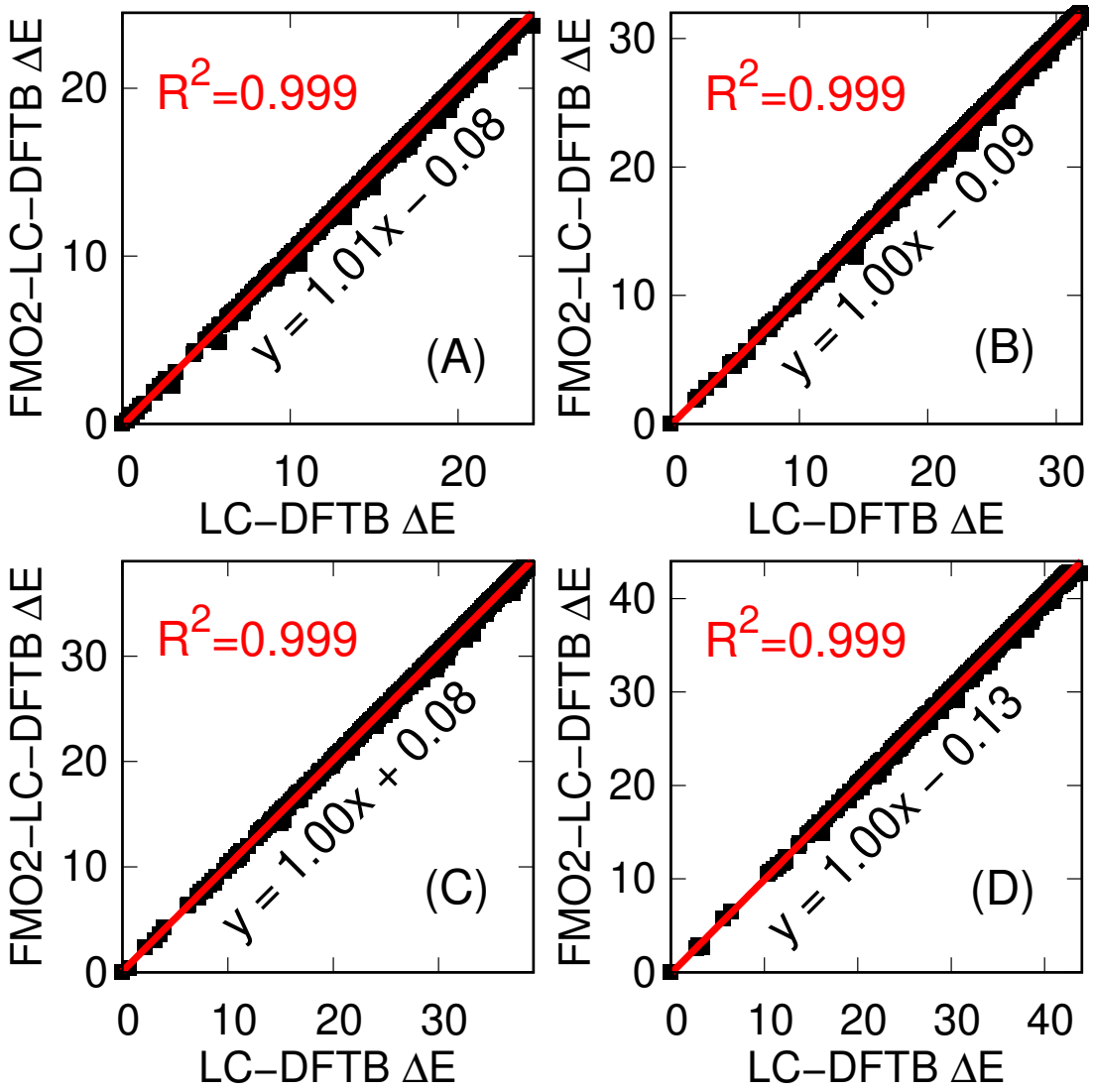

Figure 5.7: Correlation between FMO2-LC-DFTB isomer energy and the full LC-DFTB isomer energy (ΔE in kcal/mol) of EMIM nitrate clusters for (A) 2 ion pairs, (B) 3 ion pairs, (C) 4 ion pairs, (D) 5 ion pairs.

loss of accuracy for isomer energy predictions. The slope is 1.00-1.01, indiating the agreement of absolute values.

Finally, a stochastic search for the optimal structure of EMIM nitrate clusters was performed for 1, 2, 3, 4, 5, 10, 20, 30, 50 and 100 ion pairs. For each cluster size, 10,000 structures were sampled in total (see Section 5.3.4). The 100 lowest potential energy structures were further refined in geometry optimizations. The optimal structure of these clusters are provided in the Supporting Information. The cluster binding energy per ion pair is shown in Figure 5.8; energy of the single anion, cation and 1 ion pair structures was calculated by the full LC-DFTB. The absolute binding energy per ion pair shows the expected trend of a rapid decrease for the first ten ion pairs and slowly decays further to a bulk-like limit. The difference in binding energy per ion pair between 50 and 100 ion pairs is only 0.2 kcal/mol,indicating converence.

5.5 Conclusions

The long-range correction (LC) by Della Sala and Niehaus[89] has been integrated into the fragment molecular orbital method combined with density-functional tight-binding in order to allow simulations of zwitterionic systems. The LC approach was designed to mitigate the DFTB self-interaction error, thereby improving HOMO-LUMO gaps and the DFTB charge convergence in zwitterionic species.[90] The FMO-LC-DFTB energy and analytic first-order geometrical energy derivatives have been implemented and validated within the GAMESS-US package for both two- and three-body expansions in gas phase and solution. The computer time requirements for FMO-based DFTB and LC-DFTB are comparable.

A satisfactory accuracy of FMO-LC-DFTB in reproducing the full LC-DFTB energies and geometries has been demonstrated. When a polypeptide system is partitioned with fragment sizes of two residues, the total energy of an extended (linear) structure with 200 residues (100 fragments) was reproduced by FMO-LC-DFTB within 1 kcal/mol, and within 5 kcal/mol for an α-helix conformation. For a polyalanine containing of 20 residues, structures optimized with FMO-LC-DFTB had RMSD values of 0.1 Å or less, compared to the minima obtained with full LC-DFTB. For FMO-LC-DFTB combined with the polarizable continuum model

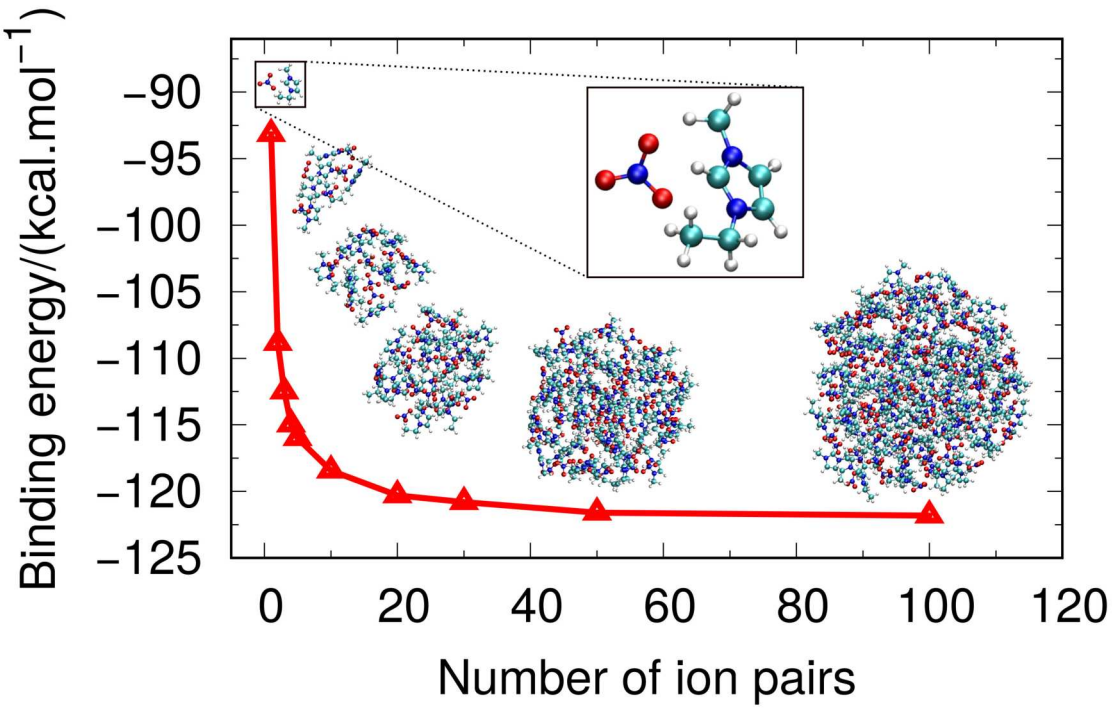

Figure 5.8: Binding energy per ion pair of EMIM nitrate clusters with respect to the number of ion pairs. The most stable structures of 1, 5, 10, 20, 50 and 100 ion pairs are shown.

(PCM), the solvation energy of full LC-DFTB/PCM calculations are reproduced within 0.45 kcal/mol for two proteins. The scaling of FMO-LC-DFTB with respect to the number of atoms N measured for realistic globular systems is almost linear, $\sim O(N^{1.13-1.28})$ for both energy and gradients.

The addition of LC corrects the underestimated DFTB HOMO-LUMO gap in zwitterionic systems, thereby eliminating the artificial two-electron charge transfer occurring in FMO dimer calculations for fragments containing opposite charges. This artifact causes instability of SCC in the FMO-DFTB zwitterionic dimer calculations, and results in orbital occupation oscillations and convergence failure. Although this problem is somewhat alleviated with the inclusion of solvent, it is not completely eradicated, and the presented LC approach profoundly corrects the problem with zwitterionic species. The FMO-LC-DFTB methods allow for the first time the application of the combination of DFTB with near-linear scaling FMO for the large-scale simulation of zwitterionic species in the gas phase or in solutions with weakly polar solvents, or in systems where charges are buried deep inside their center, away from surfaces accessible to the solvent.

It has been demonstrated in this work that FMO-LC-DFTB is not affected by the aforementioned convergence problems and offers a natural approach to treat zwitterionic systems, such as almost all biomolecular systems and ionic liquids or solutions. Taking advantage of this capability, FMO2-LC-DFTB has been used to carry out MD simulations of four charge states of the Trp-cage protein in the gas phase for 1 ns, and performed stochastic searches for the global minimum structure of an EMIM nitrate ionic liquid cluster containing up to 2300 atoms. The new methods offer advanced capabilities for approximate first principles-based modeling of artificial protein folding and peptide-ligand or peptide-peptide interactions, enzymatic chemical reactions, as well as ion transport in solution or ionic liquids.

Chapter 6

Summary and Outlook

The density-functional tight-binding (DFTB) method has been successfully employed in the simulation of complex chemical processes such as fullerene formation[255,256] and host-guest encapsulation,[257] the design of photoactive covalent frameworks,[258] drug design,[259] and charge transport in porous materials.[260] It has gained considerable visibility despite the rise of massively parallel computer platforms, due to its capability in sustaining long-timescale reactive MD simulations with explicit consideration of the electronic structure. Furthermore, its inexpensive computational requirements allow for the effective sampling of amorphous or disordered materials as they require large model systems in excess of thousands of atoms. These capabilities are desperately required for predictive simulations of nanomaterials synthesis or degradation processes. Unfortunately, the potentially compelling DFTB method suffers from the lack of available accurate parameters, in particular involving transition metal elements, ever since its conception more than 30 years ago. Such parameters are extremely important in chemical energy sciences, most notably catalysis and chemical energy storage. In this dissertation, my previously developed DFTBparaopt semi-automatic parameterization was therefore employed for the development of two sets of urgently needed DFTB parameters involving prominent transition metals, (1) for phosphine-stabilized nanoscale gold clusters, and (2) for platinum nanoparticles in the vacuum and on TiO_2 support. In addition to these parameterizations, I have focused on the development of an accurate DFTB-based linear-scaling method capable of describing zwitterionic systems for the simulation of electrolytes. To realize this method, the combination of the

fragment molecular orbital (FMO) approach with the recently developed long-range corrected DFTB (LC-DFTB) method had been selected and implemented. Initial benchmarks and demonstration applications were presented.

In chapter 3, the parameterization of the DFTB method for the quantum chemical simulation of phosphine-ligated nanoscale gold clusters, metalloids, and gold surfaces was discussed. As a major new insight, it was found that the Au 6p and P 3d virtual atomic orbital energy levels strongly influence the overall performance of the combined parameter set. The Au-P repulsive potential was consistently optimized to a near-global minimum in the scoring function, for different choices of the atomic orbital energies. The new parameters were validated extensively against DFT geometries, ligand binding and cluster isomerization energies, ligand dissociation potential energy curves, molecular orbital energies, and chemisorption for various phosphine-ligated gold clusters and surfaces. Overall, the new parameters are accurate and decently transferable, showing a very good agreement between DFTB and DFT methods for a wide range of systems or, in other words, a wide range of chemical environments. Nevertheless, in a few cases, DFTB exhibits a notable underestimation in binding energy for Au-P interactions in the moderate-range distance (1-3 Å longer than the covalent bond distance), indicating shortcomings in terms of transferability of the electronic parameters. The new parameters were used to the predict properties of a large gold metalloid $Au_{108}S_{24}(PPh_3)_{16}$ cluster containing ~700 atoms in total. These simulations suggest that with the new parameters, DFTB can be used to investigate phosphine-stabilized nanoscale gold clusters and assist in the predictive modeling of Au-cluster catalysis in the future.

In chapter 4, the parameterization of the DFTB method for platinum nanoparticles in the vacuum and on TiO_2 support was reported. Performance of the new DFTB parameters was validated for geometries, energetic properties, and electronic structure of a wide range of Pt_n clusters, and the chemisorption of Pt_n clusters on the TiO_2 surfaces. In general, the developed parameters reproduce DFT-computed geometries and energies for Pt_n clusters accurately. DFTB-computed band structures match DFT-computed bands well near the Fermi level. The parameters are also accurate for geometries and energies of Pt clusters on the TiO_2 surfaces. Good transferability between rutile and anatase phase simulations

was observed. However, similar as in the case of the Au-P interaction, DFTB shows a notable underestimation of binding energies for Pt-X (X = Pt, Ti, O) interactions in the moderate-range distance, (1-3 Å longer than the corresponding typical covalent bond distance). Since our goal was to leave the existing electronic parameters of the well-established tiorg parameter set intact, we did not attempt to reoptimize the Ti and O electronic parameters. Nevertheless, the accuracy of the resulting pt-tiorg parameter set was found to be sufficient for the qualitative description of potential energy surfaces related to platinum clusters adsorbed on titania surfaces, and we decided to employ the new parameters in the simulation of atom Pt_1 diffusion and the nucleation of Pt_6 from Pt_5 and Pt_1 on a rutile (110) surface using the steered molecular dynamics (SMD) method. Increasing temperatures were found to significantly reduce the energy barrier of the Pt atom migration on the TiO_2 surface at the transition state of the Pt_6 cluster merger, while only a minor effect was observed for the total nucleation energy. The simulations represent possibly the first-ever quantum chemical simulations of the free energy profile for these processes, and provide a sound atomistic description for the temperature-dependent sintering of nanoparticles on a metal oxide support. With the new parameters, it is hoped that DFTB can be used to simulate Pt clusters on TiO_2 surfaces, and with the ongoing development of parameters for Pt-X (X=C, H, N, O) interactions pave the way for the future simulations of Pt-based catalytic systems stabilized by metal oxide and perovskite support.

In chapter 5, an extension of the FMO-DFTB is presented in which the FMO linear scaling formalism was connected with the LC-DFTB method. The resulting FMO-LC-DFTB method is designed to mitigate the DFTB self-interaction error in the simulation of zwitterionic, large-scale systems on long timescales. Both energy and analytic gradient were developed for the gas phase and the polarizable continuum model of solvation. The FMO-LC-DFTB energy and analytic first-order geometrical energy derivatives were implemented and validated within the GAMESS-US program. A satisfactory level of accuracy of FMO-LC-DFTB in terms of reproducing full LC-DFTB energies and geometries was demonstrated. The near-linear scaling behavior of FMO-LC-DFTB with respect to the number of atoms N was determined for realistic globular systems, for both energy and gradients, with $\sim O(N^{1.13-1.28})$. The FMO-LC-DFTB method was used in demonstration studies to (1)

simulate four charge states of the Trp-cage protein in the gas phase to probe the existence of salt bridges in the gas phase and (2) to determine the global minimum structure of 1-ethyl-3-methylimidazolium nitrate (EMIN) ionic liquid clusters containing up to 2300 atoms, which would be impossible to achieve with standard DFT methods due to the vast structural search space involved. The new method offers advance capabilities for first principles-based modeling of large-size ionic liquids, ions interaction with electrodes, and other chemical energy storage systems.

From the work on parameterization and benchmark of DFTB for two transition metals, I found that besides optimizing the pairwise repulsive potentials and traditional orbital and electron density compression radii for the electronic parameters, the tuning of virtual atomic orbital energy levels present in the valence shell could similarly influence the method's overall performance. These virtual atomic orbital levels, such as Au and Pt 6p, and P 3d, tend to participate heavily in covalent bonding. While the developed DFTB parameters are reasonably transferable, I found that creating a single DFTB parameter set with the same level of accuracy DFT method for different chemical environments remains challenging. To establish a "proper" (=transferable) parameter set for DFTB, one always needs to validate the parameters for a wide range of test sets with various chemical environments. The DFTB performance is generally less satisfactory for high-energy systems, including moderate-range interactions in a range of 1-3 Å longer than covalent bond distances. This is attributed to drawbacks of the current DFTB methodology, which uses a minimal basis set and monopole approximation. While my preliminary work extending DFTB with multipole expansion[261] improves the moderate-range electrostatic interactions, the expansion of the minimum basis set by including polarization functions (e.g. 2p orbital for H, 3d orbital for C, N, and O) is more complicated. As such, attempts to do so can increase errors of the two-center approximation as neglected three-center integrals become more significant and affect the Mulliken point charges in an unreasonable/unphysical way. Prospectively, these research directions will be worth investigations to fundamentally improve the DFTB method and will be my primary research target in the future. Besides fundamentally correcting for the electronic interactions, quick corrections to DFTB with recently developed Δ-machine learning[262] or many-body repulsive potentials could also be worth exploring. While such

readily accessible corrections will have low transferability, they have the potential to increase the accuracy of DFTB for specific applications. With these future developments, it is expected that the applicability of the DFTB method for chemical energy sciences in routine investigations of complex dynamic phenomena will become an invaluable tool to sample free energy surfaces and structural diversity several orders of magnitude faster than traditional DFT, and far more reliable than reactive force fields.

Bibliography

(1) Winter, M.; Barnett, B.; Xu, K. *Chem. Rev.* **2018**, *118*, 11433–11456.

(2) Hosaka, T.; Kubota, K.; Hameed, A. S.; Komaba, S. *Chem. Rev.* **2020**, *120*, 6358–6466.

(3) Arroyo-de Dompablo, M. E.; Ponrouch, A.; Johansson, P.; Palacín, M. R. *Chem. Rev.* **2020**, *120*, 6331–6357.

(4) Fleischmann, S.; Mitchell, J. B.; Wang, R.; Zhan, C.; Jiang, D.-e.; Presser, V.; Augustyn, V. *Chem. Rev.* **2020**, *120*, 6738–6782.

(5) Tian, Y.; Zeng, G.; Rutt, A.; Shi, T.; Kim, H.; Wang, J.; Koettgen, J.; Sun, Y.; Ouyang, B.; Chen, T.; Lun, Z.; Rong, Z.; Persson, K.; Ceder, G. *Chem. Rev.* **2021**, *121*, 1623–1669.

(6) Winter, M.; Brodd, R. J. *Chem. Rev.* **2004**, *104*, 4245–4270.

(7) Franco, A. A.; Rucci, A.; Brandell, D.; Frayret, C.; Gaberscek, M.; Jankowski, P.; Johansson, P. *Chem. Rev.* **2019**, *119*, 4569–4627.

(8) Zhan, C.; Sun, W.; Xie, Y.; Jiang, D.-e.; Kent, P. R. C. *ACS Appl. Mater. Interfaces* **2019**, *11*, 24885–24905.

(9) Van der Ven, A.; Deng, Z.; Banerjee, S.; Ong, S. P. *Chem. Rev.* **2020**, *120*, 6977–7019.

(10) Chen, B. W. J.; Xu, L.; Mavrikakis, M. *Chem. Rev.* **2021**, *121*, 1007–1048.

(11) Abidi, N.; Lim, K. R. G.; Seh, Z. W.; Steinmann, S. N. *WIREs Comput. Mol. Sci.* **2020**, *10*, 1–27.

(12) Cornell, W. D.; Cieplak, P.; Bayly, C. I.; Gould, I. R.; Merz, K. M.; Ferguson, D. M.; Spellmeyer, D. C.; Fox, T.; Caldwell, J. W.; Kollman, P. A. *J. Am. Chem. Soc.* **1995**, *117*, 5179–5197.

(13) Jorgensen, W. L.; Maxwell, D. S.; Tirado-Rives, J. *J. Am. Chem. Soc.* **1996**, *118*, 11225–11236.

(14) MacKerell, A. D. et al. *J. Phys. Chem. B* **1998**, *102*, 3586–3616.

(15) Jorgensen, W. L.; Tirado-Rives, J. *J. Am. Chem. Soc.* **1988**, *110*, 1657–1666.

(16) Wang, J.; Wolf, R. M.; Caldwell, J. W.; Kollman, P. A.; Case, D. A. *J. Comput. Chem.* **2004**, *25*, 1157–1174.

(17) Senftle, T. P.; Hong, S.; Islam, M. M.; Kylasa, S. B.; Zheng, Y.; Shin, Y. K.; Junkermeier, C.; Engel-Herbert, R.; Janik, M. J.; Aktulga, H. M.; Verstraelen, T.; Grama, A.; van Duin, A. C. T. *npj Comput. Mater.* **2016**, *2*, 15011.

(18) Moerman, E.; Furman, D.; Wales, D. J. *J. Chem. Theory Comput.* **2021**, *17*, 497–514.

(19) Akimov, A. V.; Prezhdo, O. V. *Chem. Rev.* **2015**, *115*, 5797–5890.

(20) Ratcliff, L. E.; Mohr, S.; Huhs, G.; Deutsch, T.; Masella, M.; Genovese, L. *Wiley Interdiscip. Rev. Comput. Mol. Sci.* **2017**, *7*, e1290.

(21) Pople, J. A.; Santry, D. P.; Segal, G. A. *J. Chem. Phys.* **1965**, *43*, S129–S135.

(22) Pople, J. A.; Beveridge, D. L.; Dobosh, P. A. *J. Chem. Phys.* **1967**, *47*, 2026–2033.

(23) Dewar, M. J. S.; Thiel, W. *J. Am. Chem. Soc.* **1977**, *99*, 4899–4907.

(24) Dewar, M. J. S.; Zoebisch, E. G.; Healy, E. F.; Stewart, J. J. P. *J. Am. Chem. Soc.* **1985**, *107*, 3902–3909.

(25) Stewart, J. J. P. *J. Comput. Chem.* **1989**, *10*, 221–264.

(26) Stewart, J. J. P. *J. Comput. Chem.* **1989**, *10*, 209–220.

(27) Stewart, J. J. P. *J. Mol. Model.* **2007**, *13*, 1173–1213.

(28) Stewart, J. J. P. *J. Mol. Model.* **2013**, *19*, 1–32.

(29) Kolb, M.; Thiel, W. *J. Comput. Chem.* **1993**, *14*, 775–789.

(30) Weber, W.; Thiel, W. *Theor. Chem. Accounts Theory, Comput. Model. (Theoretica Chim. Acta)* **2000**, *103*, 495–506.

(31) Dral, P. O.; Wu, X.; Spörkel, L.; Koslowski, A.; Thiel, W. *J. Chem. Theory Comput.* **2016**, *12*, 1097–1120.

(32) Thiel, W. *Wiley Interdiscip. Rev. Comput. Mol. Sci.* **2014**, *4*, 145–157.

(33) Christensen, A. S.; Kubař, T.; Cui, Q.; Elstner, M. *Chem. Rev.* **2016**, *116*, 5301–5337.

(34) Husch, T.; Vaucher, A. C.; Reiher, M. *Int. J. Quantum Chem.* **2018**, *118*, e25799.

(35) Miriyala, V. M.; Řezáč, J. *J. Comput. Chem.* **2017**, *38*, 688–697.

(36) Řezáč, J.; Bím, D.; Gutten, O.; Rulíšek, L. *J. Chem. Theory Comput.* **2018**, *14*, 1254–1266.

(37) Kromann, J. C.; Steinmann, C.; Jensen, J. H. *J. Chem. Phys.* **2018**, *149*, 104102.

(38) Elstner, M.; Seifert, G. *Philos. Trans. R. Soc. A Math. Phys. Eng. Sci.* **2014**, *372*, 20120483.

(39) Domínguez-Gutiérrez, F. J.; Bedoya, F.; Krstić, P. S.; Allain, J. P.; Irle, S.; Skinner, C. H.; Kaita, R.; Koel, B. *Nucl. Fusion* **2017**, *57*, 086050.

(40) Fedorov, D. G. *WIREs Comput. Mol. Sci.* **2017**, *7*, 1–17.

(41) Nishimoto, Y.; Fedorov, D. G.; Irle, S. *J. Chem. Theory Comput.* **2014**, *10*, 4801–4812.

(42) Nishimoto, Y. *J. Chem. Phys.* **2015**, *143*, 094108.

(43) Nishimoto, Y.; Nakata, H.; Fedorov, D. G.; Irle, S. *J. Phys. Chem. Lett.* **2015**, *6*, 5034–5039.

(44) Nishimoto, Y.; Fedorov, D. G. *J. Comput. Chem.* **2017**, *38*, 406–418.

(45) Nishimoto, Y.; Fedorov, D. G. *J. Chem. Phys.* **2018**, *148*, 064115.

(46) Hu, H.; Lu, Z.; Elstner, M.; Hermans, J.; Yang, W. *J. Phys. Chem. A* **2007**, *111*, 5685–5691.

(47) Nishizawa, H.; Nishimura, Y.; Kobayashi, M.; Irle, S.; Nakai, H. *J. Comput. Chem.* **2016**, *37*, 1983–1992.

(48) Nishimura, Y.; Nakai, H. *J. Comput. Chem.* **2018**, *39*, 105–116.

(49) Giese, T. J.; Chen, H.; Dissanayake, T.; Giambaşu, G. M.; Heldenbrand, H.; Huang, M.; Kuechler, E. R.; Lee, T.-S.; Panteva, M. T.; Radak, B. K.; York, D. M. *J. Chem. Theory Comput.* **2013**, *9*, 1417–1427.

(50) Foulkes, W. M. C.; Haydock, R. *Phys. Rev. B* **1989**, *39*, 12520–12536.

(51) Hohenberg, P.; Kohn, W. *Phys. Rev.* **1964**, *136*, B864–B871.

(52) Kohn, W.; Sham, L. J. *Phys. Rev.* **1965**, *140*, A1133–A1138.

(53) Porezag, D.; Frauenheim, T.; Köhler, T.; Seifert, G.; Kaschner, R. *Phys. Rev. B* **1995**, *51*, 12947–12957.

(54) Seifert, G.; Porezag, D.; Frauenheim, T. *Int. J. Quantum Chem.* **1996**, *58*, 185–192.

(55) Gaus, M.; Cui, Q.; Elstner, M. *J. Chem. Theory Comput.* **2011**, *7*, 931–948.

(56) Grimme, S.; Bannwarth, C.; Caldeweyher, E.; Pisarek, J.; Hansen, A. *J. Chem. Phys.* **2017**, *147*, 161708.

(57) Seifert, G.; Joswig, J.-O. *Wiley Interdiscip. Rev. Comput. Mol. Sci.* **2012**, *2*, 456–465.

(58) Elstner, M.; Porezag, D.; Jungnickel, G.; Elsner, J.; Haugk, M.; Frauenheim, T.; Suhai, S.; Seifert, G. *Phys. Rev. B* **1998**, *58*, 7260–7268.

(59) Gaus, M.; Cui, Q.; Elstner, M. *Wiley Interdiscip. Rev. Comput. Mol. Sci.* **2014**, *4*, 49–61.

(60) Zheng, G.; Witek, H. A.; Bobadova-Parvanova, P.; Irle, S.; Musaev, D. G.; Prabhakar, R.; Morokuma, K.; Lundberg, M.; Elstner, M.; Köhler, C.; Frauenheim, T. *J. Chem. Theory Comput.* **2007**, *3*, 1349–1367.

(61) Fihey, A.; Hettich, C.; Touzeau, J.; Maurel, F.; Perrier, A.; Köhler, C.; Aradi, B.; Frauenheim, T. *J. Comput. Chem.* **2015**, *36*, 2075–2087.

(62) Dolgonos, G.; Aradi, B.; Moreira, N. H.; Frauenheim, T. *J. Chem. Theory Comput.* **2010**, *6*, 266–278.

(63) Kilmartin, J.; Sarip, R.; Grau-Crespo, R.; Di Tommaso, D.; Hogarth, G.; Prestipino, C.; Sankar, G. *ACS Catal.* **2012**, *2*, 957–963.

(64) Haruta, M. *Gold Bull.* **2004**, *37*, 27–36.

(65) Choudhary, V. R.; Dumbre, D. K. *Top. Catal.* **2009**, *52*, 1677–1687.

(66) Du, Y.; Sheng, H.; Astruc, D.; Zhu, M. *Chem. Rev.* **2020**, *120*, 526–622.

(67) Weerawardene, K. D. M.; Häkkinen, H.; Aikens, C. M. *Annu. Rev. Phys. Chem.* **2018**, *69*, 205–229.

(68) Parrish, K. A.; King, M.; Ligare, M. R.; Johnson, G. E.; Hernández, H. *Phys. Chem. Chem. Phys.* **2019**, *21*, 1689–1699.

(69) Oliveira, L. F. L.; Tarrat, N.; Cuny, J.; Morillo, J.; Lemoine, D.; Spiegelman, F.; Rapacioli, M. *J. Phys. Chem. A* **2016**, *120*, 8469–8483.

(70) Shi, H.; Koskinen, P.; Ramasubramaniam, A. *J. Phys. Chem. A* **2017**, *121*, 2497–2502.

(71) Lee, K. H.; Vuong, V. Q.; Fung, V.; Jiang, D.-e.; Irle, S. *MRS Adv.* **2019**, *4*, 1821–1832.

(72) Van den Bossche, M. *J. Phys. Chem. A* **2019**, *123*, 3038–3045.

(73) Knaup, J. M.; Hourahine, B.; Frauenheim, T. *J. Phys. Chem. A* **2007**, *111*, 5637–5641.

(74) Doemer, M.; Liberatore, E.; Knaup, J. M.; Tavernelli, I.; Rothlisberger, U. *Mol. Phys.* **2013**, *111*, 3595–3607.

(75) Chou, C.-P.; Nishimura, Y.; Fan, C.-C.; Mazur, G.; Irle, S.; Witek, H. A. *J. Chem. Theory Comput.* **2016**, *12*, 53–64.

(76) Huran, A. W.; Steigemann, C.; Frauenheim, T.; Aradi, B.; Marques, M. A. L. *J. Chem. Theory Comput.* **2018**, *14*, 2947–2954.

(77) Vuong, V. Q.; Akkarapattiakal Kuriappan, J.; Kubillus, M.; Kranz, J. J.; Mast, T.; Niehaus, T. A.; Irle, S.; Elstner, M. *J. Chem. Theory Comput.* **2018**, *14*, 115–125.

(78) Gaus, M.; Chou, C.-P.; Witek, H.; Elstner, M. *J. Phys. Chem. A* **2009**, *113*, 11866–11881.

(79) Lundberg, M.; Nishimoto, Y.; Irle, S. *Int. J. Quantum Chem.* **2012**, *112*, 1701–1711.

(80) Nishimoto, Y.; Fedorov, D. G. *Phys. Chem. Chem. Phys.* **2016**, *18*, 22047–22061.

(81) Polo, V.; Gräfenstein, J.; Kraka, E.; Cremer, D. *Chem. Phys. Lett.* **2002**, *352*, 469–478.

(82) Gräfenstein, J.; Kraka, E.; Cremer, D. *Phys. Chem. Chem. Phys.* **2004**, *6*, 1096–1112.

(83) Gräfenstein, J.; Kraka, E.; Cremer, D. *J. Chem. Phys.* **2004**, *120*, 524–539.

(84) Cohen, A. J.; Mori-Sanchez, P.; Yang, W. *Science (80-.).* **2008**, *321*, 792–794.

(85) Körzdörfer, T.; Parrish, R. M.; Sears, J. S.; Sherrill, C. D.; Brédas, J.-L. *J. Chem. Phys.* **2012**, *137*, 124305.

(86) Cohen, A. J.; Mori-Sánchez, P.; Yang, W. *Chem. Rev.* **2012**, *112*, 289–320.

(87) Becke, A. D. *J. Chem. Phys.* **2014**, *140*, 18A301.

(88) Bao, J. L.; Gagliardi, L.; Truhlar, D. G. *J. Phys. Chem. Lett.* **2018**, *9*, 2353–2358.

(89) Niehaus, T. A.; Della Sala, F. *Phys. status solidi* **2012**, *249*, 237–244.

(90) Lutsker, V.; Aradi, B.; Niehaus, T. A. *J. Chem. Phys.* **2015**, *143*, 184107.

(91) Savin, A.; Flad, H.-J. *Int. J. Quantum Chem.* **1995**, *56*, 327–332.

(92) Leininger, T.; Stoll, H.; Werner, H.-J.; Savin, A. *Chem. Phys. Lett.* **1997**, *275*, 151–160.

(93) Livshits, E.; Baer, R. *Phys. Chem. Chem. Phys.* **2007**, *9*, 2932.

(94) Seth, M.; Ziegler, T. *J. Chem. Theory Comput.* **2012**, *8*, 901–907.

(95) Schmidt, M. W.; Baldridge, K. K.; Boatz, J. A.; Elbert, S. T.; Gordon, M. S.; Jensen, J. H.; Koseki, S.; Matsunaga, N.; Nguyen, K. A.; Su, S.; Windus, T. L.; Dupuis, M.; Montgomery, J. A. *J. Comput. Chem.* **1993**, *14*, 1347–1363.

(96) Barca, G. M. J. et al. *J. Chem. Phys.* **2020**, *152*, 154102.

(97) Schrödinger, E. *Phys. Rev.* **1926**, *28*, 1049–1070.

(98) Szabo, A.; Ostlund, N. S., *Modern Quantum Chemistry: Introduction to Advanced Electronic Structure Theory*; Dover Books on Chemistry; Dover Publications: 1996.

(99) David Sherrill, C.; Schaefer, H. F. In Löwdin, P.-O., Sabin, J. R., Zerner, M. C., Brändas, E., Eds.; Advances in Quantum Chemistry, Vol. 34; Academic Press: 1999, pp 143–269.

(100) Møller, C.; Plesset, M. S. *Phys. Rev.* **1934**, *46*, 618–622.

(101) Binkley, J. S.; Pople, J. A. *Int. J. Quantum Chem.* **1975**, *9*, 229–236.

(102) Dirac, P. A. M. *Math. Proc. Cambridge Philos. Soc.* **1930**, *26*, 376–385.

(103) Ceperley, D. M.; Alder, B. J. *Phys. Rev. Lett.* **1980**, *45*, 566–569.

(104) Tao, J.; Perdew, J. P.; Staroverov, V. N.; Scuseria, G. E. *Phys. Rev. Lett.* **2003**, *91*, 146401.

(105) Yu, H. S.; He, X.; Truhlar, D. G. *J. Chem. Theory Comput.* **2016**, *12*, 1280–1293.

(106) Becke, A. D. *J. Chem. Phys.* **1993**, *98*, 5648–5652.

(107) Yanai, T.; Tew, D. P.; Handy, N. C. *Chem. Phys. Lett.* **2004**, *393*, 51–57.

(108) Vydrov, O. A.; Heyd, J.; Krukau, A. V.; Scuseria, G. E. *J. Chem. Phys.* **2006**, *125*, 074106.

(109) Vydrov, O. A.; Scuseria, G. E. *J. Chem. Phys.* **2006**, *125*, 234109.

(110) Henderson, T. M.; Janesko, B. G.; Scuseria, G. E. *J. Phys. Chem. A* **2008**, *112*, 12530–12542.

(111) Chai, J.-D.; Head-Gordon, M. *Phys. Chem. Chem. Phys.* **2008**, *10*, 6615.

(112) Slater, J. C.; Koster, G. F. *Phys. Rev.* **1954**, *94*, 1498–1524.

(113) Gaus, M. Extension and Parametrization of an Approximate Density Functional Method for Organic and Biomolecules, Ph.D. Thesis, Karlsruhe Institute of Technology, 2011.

(114) Seifert, G. *J. Phys. Chem. A* **2007**, *111*, 5609–5613.

(115) Hourahine, B.; Sanna, S.; Aradi, B.; Köhler, C.; Niehaus, T.; Frauenheim, T. *J. Phys. Chem. A* **2007**, *111*, 5671–5677.

(116) Carbó, R.; Martin, M. *Int. J. Quantum Chem.* **1975**, *9*, 193–214.

(117) Ayed, O.; Bernard, E.; Silvi, B. *J. Mol. Struct. THEOCHEM* **1986**, *135*, 159–168.

(118) Kranz, J. J.; Elstner, M.; Aradi, B.; Frauenheim, T.; Lutsker, V.; Garcia, A. D.; Niehaus, T. A. *J. Chem. Theory Comput.* **2017**, *13*, 1737–1747.

(119) Fedorov, D.; Kitaura, K., *The Fragment Molecular Orbital Method: Practical Applications to Large Molecular Systems*; CRC Press: 2009.

(120) Steinmann, C.; Fedorov, D. G.; Jensen, J. H. *J. Phys. Chem. A* **2010**, *114*, 8705–8712.

(121) Nakano, T.; Kaminuma, T.; Sato, T.; Fukuzawa, K.; Akiyama, Y.; Uebayasi, M.; Kitaura, K. *Chem. Phys. Lett.* **2002**, *351*, 475–480.

(122) Fedorov, D. G.; Kitaura, K. *Chem. Phys. Lett.* **2004**, *389*, 129–134.

(123) Fedorov, D. G.; Kitaura, K. *Chem. Phys. Lett.* **2006**, *433*, 182–187.

(124) Fedorov, D. G.; Kitaura, K. *J. Chem. Phys.* **2004**, *120*, 6832–6840.

(125) Leven, I.; Hao, H.; Tan, S.; Guan, X.; Penrod, K. A.; Akbarian, D.; Evangelisti, B.; Hossain, M. J.; Islam, M. M.; Koski, J. P.; Moore, S.; Aktulga, H. M.; van Duin, A. C. T.; Head-Gordon, T. *J. Chem. Theory Comput.* **2021**, *17*, 3237–3251.

(126) Jahn, W. *J. Struct. Biol.* **1999**, *127*, 106–112.

(127) Meyer, R.; Lemire, C.; Shaikhutdinov, S. K.; Freund, H. .-. *Gold Bull.* **2004**, *37*, 72–124.

(128) Schaaff, T. G.; Shafigullin, M. N.; Khoury, J. T.; Vezmar, I.; Whetten, R. L.; Cullen, W. G.; First, P. N.; Gutiérrez-Wing, C.; Ascensio, J.; Jose-Yacamán, M. J. *J. Phys. Chem. B* **1997**, *101*, 7885–7891.

(129) Heuer-Jungemann, A. et al. *Chem. Rev.* **2019**, *119*, 4819–4880.

(130) Johnson, G. E.; Priest, T.; Laskin, J. *Chem. Sci.* **2014**, *5*, 3275.

(131) Anderson, D. P.; Alvino, J. F.; Gentleman, A.; Qahtani, H. A.; Thomsen, L.; Polson, M. I. J.; Metha, G. F.; Golovko, V. B.; Andersson, G. G. *Phys. Chem. Chem. Phys.* **2013**, *15*, 3917.

(132) Anderson, D. P.; Adnan, R. H.; Alvino, J. F.; Shipper, O.; Donoeva, B.; Ruzicka, J.-Y.; Al Qahtani, H.; Harris, H. H.; Cowie, B.; Aitken, J. B.; Golovko, V. B.; Metha, G. F.; Andersson, G. G. *Phys. Chem. Chem. Phys.* **2013**, *15*, 14806.

(133) Vajda, S.; White, M. G. *ACS Catal.* **2015**, *5*, 7152–7176.

(134) Tesana, S.; Metha, G. F.; Andersson, G. G.; Ridings, C.; Golovko, V. *Int. J. Nanotechnol.* **2018**, *15*, 669.

(135) Krishnan, G.; Eom, N.; Kirk, R. M.; Golovko, V. B.; Metha, G. F.; Andersson, G. G. *J. Phys. Chem. C* **2019**, *123*, 6642–6649.

(136) Zhu, M.; Aikens, C. M.; Hollander, F. J.; Schatz, G. C.; Jin, R. *J. Am. Chem. Soc.* **2008**, *130*, 5883–5885.

(137) Goel, S.; Velizhanin, K. A.; Piryatinski, A.; Tretiak, S.; Ivanov, S. A. *J. Phys. Chem. Lett.* **2010**, *1*, 927–931.

(138) Alvino, J. F.; Bennett, T.; Anderson, D.; Donoeva, B.; Ovoshchnikov, D.; Adnan, R. H.; Appadoo, D.; Golovko, V.; Andersson, G.; Metha, G. F. *RSC Adv.* **2013**, *3*, 22140.

(139) Varnholt, B.; Oulevey, P.; Luber, S.; Kumara, C.; Dass, A.; Bürgi, T. *J. Phys. Chem. C* **2014**, *118*, 9604–9611.

(140) Fernando, A.; Weerawardene, K. L. D. M.; Karimova, N. V.; Aikens, C. M. *Chem. Rev.* **2015**, *115*, 6112–6216.

(141) Muniz-Miranda, F.; Presti, D.; Menziani, M. C.; Pedone, A. *Theor. Chem. Acc.* **2016**, *135*, 5.

(142) Tlahuice-Flores, A. *Prog. Nat. Sci. Mater. Int.* **2016**, *26*, 510–515.

(143) Yamazoe, S.; Matsuo, S.; Muramatsu, S.; Takano, S.; Nitta, K.; Tsukuda, T. *Inorg. Chem.* **2017**, *56*, 8319–8325.

(144) Kenzler, S.; Schrenk, C.; Schnepf, A. *Angew. Chemie Int. Ed.* **2017**, *56*, 393–396.

(145) Kenzler, S.; Schrenk, C.; Frojd, A. R.; Häkkinen, H.; Clayborne, A. Z.; Schnepf, A. *Chem. Commun.* **2018**, *54*, 248–251.

(146) Zhang, S.-S.; Feng, L.; Senanayake, R. D.; Aikens, C. M.; Wang, X.-P.; Zhao, Q.-Q.; Tung, C.-H.; Sun, D. *Chem. Sci.* **2018**, *9*, 1251–1258.

(147) Burgos, J. C.; Mejía, S. M.; Metha, G. F. *ACS Omega* **2019**, *4*, 9169–9180.

(148) Tian, Z.; Xu, Y.; Cheng, L. *Nanomaterials* **2019**, *9*, 1132.

(149) Tlahuice-Flores, A.; Whetten, R. L.; Jose-Yacaman, M. *J. Phys. Chem. C* **2013**, *117*, 20867–20875.

(150) Tlahuice-Flores, A. *Mol. Simul.* **2013**, *39*, 428–431.

(151) Tlahuice-Flores, A.; Whetten, R. L.; Jose-Yacaman, M. *J. Phys. Chem. C* **2013**, *117*, 12191–12198.

(152) Palacios-Álvarez, O.; Tlahuice-Flores, A. *J. Raman Spectrosc.* **2019**, *50*, 52–62.

(153) Wing-Bocanegra, A.; Tlahuice-Flores, A. *Phys. Chem. Chem. Phys.* **2019**, *21*, 23855–23864.

(154) Haeberlen, O. D.; Roesch, N. *J. Phys. Chem.* **1993**, *97*, 4970–4973.

(155) Schwerdtfeger, P.; Boyd, P. D. W. *Inorg. Chem.* **1992**, *31*, 327–329.

(156) DeKock, R. L.; Baerends, E. J.; Boerrigter, P. M.; Hengelmolen, R. *J. Am. Chem. Soc.* **1984**, *106*, 3387–3396.

(157) Mingos, D. M. P.; Slee, T.; Zhenyang, L. *Chem. Rev.* **1990**, *90*, 383–402.

(158) Chung, L. W.; Sameera, W. M. C.; Ramozzi, R.; Page, A. J.; Hatanaka, M.; Petrova, G. P.; Harris, T. V.; Li, X.; Ke, Z.; Liu, F.; Li, H.-B.; Ding, L.; Morokuma, K. *Chem. Rev.* **2015**, *115*, 5678–5796.

(159) Vreven, T.; Morokuma, K. *J. Comput. Chem.* **2000**, *21*, 1419–1432.

(160) Donoeva, B. G.; Ovoshchnikov, D. S.; Golovko, V. B. *ACS Catal.* **2013**, *3*, 2986–2991.

(161) Cui, Q.; Elstner, M. *Phys. Chem. Chem. Phys.* **2014**, *16*, 14368–14377.

(162) Grimme, S.; Bannwarth, C.; Shushkov, P. *J. Chem. Theory Comput.* **2017**, *13*, 1989–2009.

(163) Bannwarth, C.; Ehlert, S.; Grimme, S. *J. Chem. Theory Comput.* **2019**, *15*, 1652–1671.

(164) Elstner, M. *J. Phys. Chem. A* **2007**, *111*, 5614–5621.

(165) Niehaus, T.; Elstner, M.; Frauenheim, T.; Suhai, S. *J. Mol. Struct. THEOCHEM* **2001**, *541*, 185–194.

(166) Mulliken, R. S. *J. Chem. Phys.* **1955**, *23*, 1833–1840.

(167) Perdew, J. P.; Burke, K.; Ernzerhof, M. *Phys. Rev. Lett.* **1996**, *77*, 3865–3868.

(168) Gaus, M.; Lu, X.; Elstner, M.; Cui, Q. *J. Chem. Theory Comput.* **2014**, *10*, 1518–1537.

(169) Kepp, K. P. *J. Phys. Chem. A* **2017**, *121*, 2022–2034.

(170) Weigend, F.; Ahlrichs, R. *Phys. Chem. Chem. Phys.* **2005**, *7*, 3297.

(171) Grimme, S.; Antony, J.; Ehrlich, S.; Krieg, H. *J. Chem. Phys.* **2010**, *132*, 154104.

(172) Grimme, S.; Ehrlich, S.; Goerigk, L. *J. Comput. Chem.* **2011**, *32*, 1456–1465.

(173) Řezáč, J.; Hobza, P. *J. Chem. Theory Comput.* **2012**, *8*, 141–151.

(174) Andrae, D.; Haubermann, U.; Dolg, M.; Stoll, H.; Preub, H. *Theor. Chim. Acta* **1990**, *77*, 123–141.

(175) Weigend, F. *Phys. Chem. Chem. Phys.* **2006**, *8*, 1057.

(176) Neese, F. *WIREs Comput. Mol. Sci.* **2018**, *8*, 4–9.

(177) Hourahine, B. et al. *J. Chem. Phys.* **2020**, *152*, 124101.

(178) Nishimoto, Y.; Kondo, H.; Yamaguchi, K.; Yokogawa, D.; Yamaguchi, J.; Itami, K.; Irle, S. *J. Org. Chem.* **2017**, *82*, 4900–4906.

(179) Van der Velden, J. W. A.; Bour, J. J.; Steggerda, J. J.; Beurskens, P. T.; Roseboom, M.; Noordik, J. H. *Inorg. Chem.* **1982**, *21*, 4321–4324.

(180) Briant, C. E.; Hall, K. P.; Mingos, D. M. P.; Wheeler, A. C. *J. Chem. Soc. Dalt. Trans.* **1986**, *37*, 687.

(181) Schulz-Dobrick, M.; Jansen, M. *Angew. Chemie Int. Ed.* **2008**, *47*, 2256–2259.

(182) Van der Velden, J. W. A.; Bour, J. J.; Bosman, W. P.; Noordik, J. H. *Inorg. Chem.* **1983**, *22*, 1913–1918.

(183) Wen, F.; Englert, U.; Gutrath, B.; Simon, U. *Eur. J. Inorg. Chem.* **2008**, *2008*, 106–111.

(184) Copley, R. C. B.; Mingos, D. M. P. *J. Chem. Soc., Dalt. Trans.* **1996**, 479–489.

(185) Wan, X.-K.; Yuan, S.-F.; Lin, Z.-W.; Wang, Q.-M. *Angew. Chemie Int. Ed.* **2014**, *53*, 2923–2926.

(186) Chen, J.; Zhang, Q.-F.; Bonaccorso, T. A.; Williard, P. G.; Wang, L.-S. *J. Am. Chem. Soc.* **2014**, *136*, 92–95.

(187) Wan, X.-K.; Wang, J.-Q.; Nan, Z.-A.; Wang, Q.-M. *Sci. Adv.* **2017**, *3*, e1701823.

(188) Blöchl, P. E. *Phys. Rev. B* **1994**, *50*, 17953–17979.

(189) Kresse, G.; Furthmüller, J. *Comput. Mater. Sci.* **1996**, *6*, 15–50.

(190) Kresse, G.; Furthmüller, J. *Phys. Rev. B* **1996**, *54*, 11169–11186.

(191) Spivey, K.; Williams, J. I.; Wang, L. *Chem. Phys. Lett.* **2006**, *432*, 163–166.

(192) Shafai, G.; Hong, S.; Bertino, M.; Rahman, T. S. *J. Phys. Chem. C* **2009**, *113*, 12072–12078.

(193) Walker, M. W.; Shao, L.; Volz, R. A. *CVGIP Image Underst.* **1991**, *54*, 358–367.

(194) Haberer, D. et al. *Adv. Mater.* **2011**, *23*, 4497–4503.

(195) Petroski, J.; Chou, M.; Creutz, C. *J. Organomet. Chem.* **2009**, *694*, 1138–1143.

(196) Stellwagen, D.; Weber, A.; Bovenkamp, G. L.; Jin, R.; Bitter, J. H.; Kumar, C. S. S. R. *RSC Adv.* **2012**, *2*, 2276.

(197) Vuong, V. Q.; Madridejos, J. M. L.; Aradi, B.; Sumpter, B. G.; Metha, G. F.; Irle, S. *Chem. Sci.* **2020**, *11*, 13113–13128.

(198) Pattabiraman, V. R.; Bode, J. W. *Nature* **2011**, *480*, 471–479.

(199) Horcajada, P.; Gref, R.; Baati, T.; Allan, P. K.; Maurin, G.; Couvreur, P.; Férey, G.; Morris, R. E.; Serre, C. *Chem. Rev.* **2012**, *112*, 1232–1268.

(200) Brunk, E.; Rothlisberger, U. *Chem. Rev.* **2015**, *115*, 6217–6263.

(201) Jiang, J.; Yaghi, O. M. *Chem. Rev.* **2015**, *115*, 6966–6997.

(202) Amarasekara, A. S. *Chem. Rev.* **2016**, *116*, 6133–6183.

(203) Panchenko, V. N.; Timofeeva, M. N.; Jhung, S. H. *Catal. Rev.* **2016**, *58*, 209–307.

(204) Dong, K.; Liu, X.; Dong, H.; Zhang, X.; Zhang, S. *Chem. Rev.* **2017**, *117*, 6636–6695.

(205) De Izarra, A.; Park, S.; Lee, J.; Lansac, Y.; Jang, Y. H. *J. Am. Chem. Soc.* **2018**, *140*, 5375–5384.

(206) Dral, P. O.; Wu, X.; Spörkel, L.; Koslowski, A.; Weber, W.; Steiger, R.; Scholten, M.; Thiel, W. *J. Chem. Theory Comput.* **2016**, *12*, 1082–1096.

(207) Kromann, J. C.; Welford, A.; Christensen, A. S.; Jensen, J. H. *ACS Omega* **2018**, *3*, 4372–4377.

(208) Oliveira, A. F.; Philipsen, P.; Heine, T. *J. Chem. Theory Comput.* **2015**, *11*, 5209–5218.

(209) Aradi, B.; Hourahine, B.; Frauenheim, T. *J. Phys. Chem. A* **2007**, *111*, 5678–5684.

(210) Nishimoto, Y.; Fedorov, D. G.; Irle, S. *Chem. Phys. Lett.* **2015**, *636*, 90–96.

(211) Rabuck, A. D.; Scuseria, G. E. *J. Chem. Phys.* **1999**, *110*, 695–700.

(212) Isom, D. G.; Castaneda, C. A.; Cannon, B. R.; Velu, P. D.; Garcia-Moreno E., B. *Proc. Natl. Acad. Sci.* **2010**, *107*, 16096–16100.

(213) Niehaus, T. A.; Suhai, S.; Della Sala, F.; Lugli, P.; Elstner, M.; Seifert, G.; Frauenheim, T. *Phys. Rev. B* **2001**, *63*, 085108.

(214) Humeniuk, A.; Mitrić, R. *J. Chem. Phys.* **2015**, *143*, 134120.

(215) Humeniuk, A.; Mitrić, R. *Comput. Phys. Commun.* **2017**, *221*, 174–202.

(216) Gordon, M. S.; Schmidt, M. W. In *Theory Appl. Comput. Chem.* Dykstra, C. E., Frenking, G., Kim, K. S., Scuseria, G. E., Eds.; Elsevier: Amsterdam, 2005, pp 1167–1189.

(217) Kitaura, K.; Ikeo, E.; Asada, T.; Nakano, T.; Uebayasi, M. *Chem. Phys. Lett.* **1999**, *313*, 701–706.

(218) Gordon, M. S.; Fedorov, D. G.; Pruitt, S. R.; Slipchenko, L. V. *Chem. Rev.* **2012**, *112*, 632–672.

(219) Otto, P.; Ladik, J. *Chem. Phys.* **1975**, *8*, 192–200.

(220) Gao, J. *J. Phys. Chem. B* **1997**, *101*, 657–663.

(221) Friedrich, J.; Yu, H.; Leverentz, H. R.; Bai, P.; Siepmann, J. I.; Truhlar, D. G. *J. Phys. Chem. Lett.* **2014**, *5*, 666–670.

(222) Thapa, B.; Beckett, D.; Erickson, J.; Raghavachari, K. *J. Chem. Theory Comput.* **2018**, *14*, 5143–5155.

(223) Kobayashi, M.; Fujimori, T.; Taketsugu, T. *J. Comput. Chem.* **2018**, *39*, 909–916.

(224) Li, Y.; Yuan, D.; Wang, Q.; Li, W.; Li, S. *Phys. Chem. Chem. Phys.* **2018**, *20*, 13547–13557.

(225) Fedorov, D. G.; Kitaura, K. *J. Phys. Chem. A* **2007**, *111*, 6904–6914.

(226) Fedorov, D. G.; Nagata, T.; Kitaura, K. *Phys. Chem. Chem. Phys.* **2012**, *14*, 7562.

(227) Tanaka, S.; Mochizuki, Y.; Komeiji, Y.; Okiyama, Y.; Fukuzawa, K. *Phys. Chem. Chem. Phys.* **2014**, *16*, 10310–10344.

(228) Nakano, T.; Kaminuma, T.; Sato, T.; Akiyama, Y.; Uebayasi, M.; Kitaura, K. *Chem. Phys. Lett.* **2000**, *318*, 614–618.

(229) Fedorov, D. G.; Ishida, T.; Uebayasi, M.; Kitaura, K. *J. Phys. Chem. A* **2007**, *111*, 2722–2732.

(230) Nagata, T.; Brorsen, K.; Fedorov, D. G.; Kitaura, K.; Gordon, M. S. *J. Chem. Phys.* **2011**, *134*, 124115.

(231) Fedorov, D. G.; Kitaura, K. *J. Phys. Chem. A* **2016**, *120*, 2218–2231.

(232) Honda, S.; Yamasaki, K.; Sawada, Y.; Morii, H. *Structure* **2004**, *12*, 1507–1518.

(233) Neidigh, J. W.; Fesinmeyer, R. M.; Andersen, N. H. *Nat. Struct. Biol.* **2002**, *9*, 425–430.

(234) Nagata, T.; Fedorov, D. G.; Li, H.; Kitaura, K. *J. Chem. Phys.* **2012**, *136*, 204112.

(235) Iikura, H.; Tsuneda, T.; Yanai, T.; Hirao, K. *J. Chem. Phys.* **2001**, *115*, 3540–3544.

(236) Patriksson, A.; Adams, C. M.; Kjeldsen, F.; Zubarev, R. a.; van der Spoel, D. *J. Phys. Chem. B* **2007**, *111*, 13147–13150.

(237) Andersen, H. C. *J. Comput. Phys.* **1983**, *52*, 24–34.

(238) Addicoat, M. A.; Metha, G. F. *J. Comput. Chem.* **2009**, *30*, 57–64.

(239) Addicoat, M. A.; Fukuoka, S.; Page, A. J.; Irle, S. *J. Comput. Chem.* **2013**, *34*, 2591–2600.

(240) Pipek, J.; Mezey, P. G. *J. Chem. Phys.* **1989**, *90*, 4916–4926.

(241) Rackers, J. A.; Wang, Z.; Lu, C.; Laury, M. L.; Lagardère, L.; Schnieders, M. J.; Piquemal, J.-P.; Ren, P.; Ponder, J. W. *J. Chem. Theory Comput.* **2018**, *14*, 5273–5289.

(242) Nagata, T.; Fedorov, D. G.; Kitaura, K. In *Challenges Adv. Comput. Chem. Phys.* 2011; Vol. 13, pp 17–64.

(243) Alexeev, Y.; Fedorov, D. G.; Shvartsburg, A. A. *J. Phys. Chem. A* **2014**, *118*, 6763–6772.

(244) Morao, I.; Fedorov, D. G.; Robinson, R.; Southey, M.; Townsend-Nicholson, A.; Bodkin, M. J.; Heifetz, A. *J. Comput. Chem.* **2017**, *38*, 1987–1990.

(245) Fedorov, D. G.; Kitaura, K. *J. Phys. Chem. A* **2018**, *122*, 1781–1795.

(246) Alexeev, Y.; Mazanetz, M. P.; Ichihara, O.; Fedorov, D. G. *Curr. Top. Med. Chem.* **2013**, *12*, 2013–2033.

(247) Kjeldsen, F.; Silivra, O. A.; Zubarev, R. A. *Chem. - A Eur. J.* **2006**, *12*, 7920–7928.

(248) Zhang, Z.; Vachet, R. W. *Int. J. Mass Spectrom.* **2017**, *420*, 51–56.

(249) Fung, Y. M. E.; Besson, T.; Lemaire, J.; Maitre, P.; Zubarev, R. A. *Angew. Chemie Int. Ed.* **2009**, *48*, 8340–8342.

(250) Meyer, T.; Gabelica, V.; Grubmüller, H.; Orozco, M. *Wiley Interdiscip. Rev. Comput. Mol. Sci.* **2013**, *3*, 408–425.

(251) Marchese, R.; Grandori, R.; Carloni, P.; Raugei, S. *PLoS Comput. Biol.* **2010**, *6*, ed. by Briggs, J. M., e1000775.

(252) Izgorodina, E. I.; Seeger, Z. L.; Scarborough, D. L. A.; Tan, S. Y. S. *Chem. Rev.* **2017**, *117*, 6696–6754.

(253) Sugita, Y.; Okamoto, Y. *Chem. Phys. Lett.* **1999**, *314*, 141–151.

(254) Ito, S.; Fedorov, D. G.; Okamoto, Y.; Irle, S. *Comput. Phys. Commun.* **2018**, *228*, 152–162.

(255) Irle, S.; Zheng, G.; Wang, Z.; Morokuma, K. *J. Phys. Chem. B* **2006**, *110*, 14531–14545.

(256) Qian, H.-J.; Wang, Y.; Morokuma, K. *Carbon N. Y.* **2017**, *114*, 635–641.

(257) Ousaka, N.; Yamamoto, S.; Iida, H.; Iwata, T.; Ito, S.; Hijikata, Y.; Irle, S.; Yashima, E. *Nat. Commun.* **2019**, *10*, 1457.

(258) Li, Z.; Huang, N.; Lee, K. H.; Feng, Y.; Tao, S.; Jiang, Q.; Nagao, Y.; Irle, S.; Jiang, D. *J. Am. Chem. Soc.* **2018**, *140*, 12374–12377.

(259) Acharya, A. et al. *J. Chem. Inf. Model.* **2020**, *60*, 5832–5852.

(260) Kitoh-Nishioka, H.; Welke, K.; Nishimoto, Y.; Fedorov, D. G.; Irle, S. *J. Phys. Chem. C* **2017**, *121*, 17712–17726.

(261) Bodrog, Z.; Aradi, B. *Phys. status solidi* **2012**, *249*, 259–269.

(262) Zhu, J.; Vuong, V. Q.; Sumpter, B. G.; Irle, S. *MRS Commun.* **2019**, *9*, 867–873.

(263) Lin, Y.-S.; Li, G.-D.; Mao, S.-P.; Chai, J.-D. *J. Chem. Theory Comput.* **2013**, *9*, 263–272.

(264) Yamaguchi, Y.; Goddard, J. D.; Osamura, Y.; Schaefer III, H. F., *A New Dimension to Quantum Chemistry: Analytic Derivative Methods in Ab Initio Molecular Electronic Structure Theory*; Oxford University Press: New York, 1994.

Appendices

A Supporting Information for "Density-Functional Tight-Binding for Phosphine-Stabilized Nanoscale Gold Clusters"

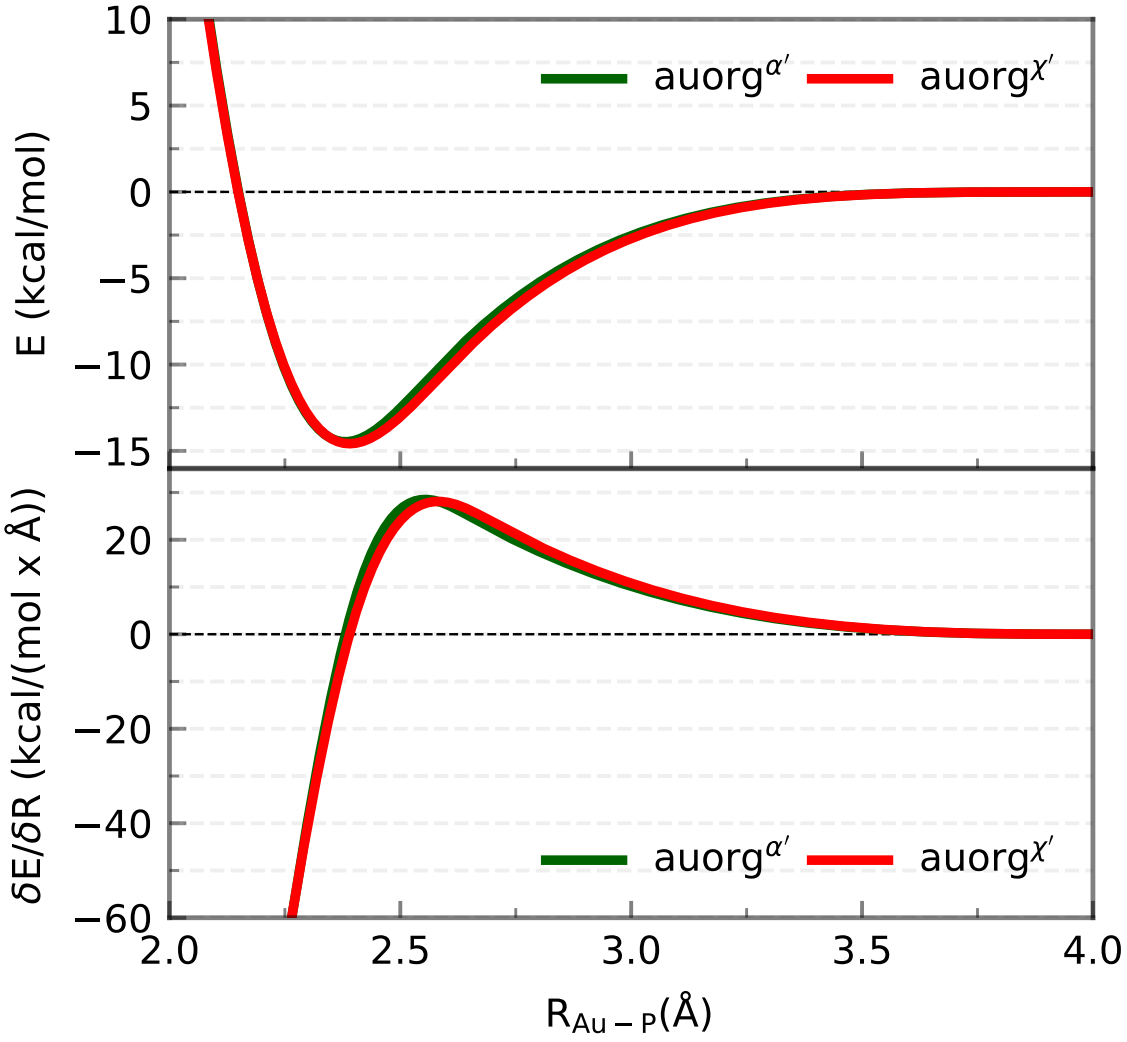

Figure A.1: The DFTB2 auorg$^{\alpha'}$ and auorg$^{\chi'}$ Au-P repulsive potentials. Ideally, the DFTB repulsive potentials are positive, however, in the case if Au-P potential the repulsive potential is negative in the bonding range of ≈2.4 Å. The attractive interaction was made to compensate the under-binding of Au-P electronic interaction, which ca be attributed to the effect of the minimum basis set in DFTB method. It is worth mentioning that Au-Au repulsive potential is also attractive ≈16 kcal/mol.[61]

Table A.1: Test results for selected chemical reactions involving H, C, N, O, P, and S containing compounds for DFTB2/mio with various values of the P 3d orbital energy. The DFTB chemical reaction energies are compared to that of wB97X-D3BJ/def2-TZVP method.[263] The chemical reaction energies and deviations are in kcal/mol, P 3d orbital energies are in Hartree.

Reactions					$\Delta E^{react.}$	DFTB2 Deivations						
					wB97XD3BJ	ϵ_P^{3d}=0.02	ϵ_P^{3d}=0.07	ϵ_P^{3d}=0.12	ϵ_P^{3d}=0.22	ϵ_P^{3d}=0.32	ϵ_P^{3d}=0.42	ϵ_P^{3d}=0.52
P_2	+ P_2	= P_4		⇒	-77.34	23.36	27.24	29.78	32.86	34.63	35.78	36.58
P_2	+ 2 H_2	= H_2PPH_2		⇒	-47.03	39.31	40.00	40.34	40.56	40.55	40.46	40.35
P_2	+ 2 H_3CCH_3	= $H_6C_2PPC_2H_6$		⇒	-40.35	4.71	6.86	8.34	10.27	11.48	12.32	12.93
P_2	+ 3 H_2	= 2 PH_3		⇒	-49.43	65.97	64.82	63.89	62.46	61.42	60.63	60.00
H_2PCH_3	+ H_2	= PH_3	+ CH_4	⇒	-12.93	10.04	9.72	9.48	9.10	8.84	8.64	8.48
$HP(CH_3)_2$	+ 2 H_2	= PH_3	+ 2 CH_4	⇒	-23.99	20.34	19.55	18.94	18.02	17.38	16.90	16.53
$P(CH_3)_3$	+ 3 H_2	= PH_3	+ 3 CH_4	⇒	-33.29	30.81	29.42	28.33	26.74	25.63	24.82	24.19
$OP(CH_3)_3$	+ 3 H_2	= H_3PO	+ 3 CH_4	⇒	-10.23	23.11	21.42	19.91	17.30	15.15	13.37	11.87
$HPCH_2$	+ H_2	= H_2PCH_3		⇒	-43.45	12.20	11.47	10.92	10.15	9.63	9.26	8.98
PCH	+ H_2	= $HPCH_2$		⇒	-34.93	16.99	16.37	15.89	15.20	14.72	14.37	14.10
PN	+ H_2	= HPNH		⇒	-19.42	10.01	12.18	13.69	15.55	16.58	17.20	17.59
HPNH	+ H_2	= H_2PNH_2		⇒	-45.32	28.84	25.86	23.76	20.96	19.11	17.79	16.79
H_2PNH_2	+ H_2	= PH_3	+ NH_3	⇒	-10.13	15.91	11.86	8.61	3.82	0.60	-1.70	-3.41
$P(NH_2)_3$	+ 3 H_2	= PH_3	+ 3 NH_3	⇒	-14.26	48.16	35.37	25.31	10.56	0.32	-7.09	-12.65
$P(NC_2H_6)_3$	+ 3 H_2	= PH_3	+ 3 $HN(CH_3)_2$	⇒	-4.26	43.49	30.27	19.72	4.16	-6.52	-14.16	-19.83
P_4	+ 3 O_2	= P_4O_6		⇒	-507.00	-450.11	-407.74	-372.00	-315.47	-273.00	-240.04	-213.77
P_4	+ 5 O_2	= P_4O_0		⇒	-865.78	-769.47	-692.40	-625.74	-516.83	-431.99	-364.24	-309.00
$P(OCH_3)_3$	+ 3 H_2	= PH_3	+ 3 $HOCH_3$	⇒	13.91	156.57	138.93	124.73	103.30	88.09	76.75	68.03
H_3PO_4	+ 3 H_2	= H_3PO	+ 3 H_2O	⇒	43.97	151.91	140.53	130.46	113.57	100.08	89.13	80.12
$OP(OCH_3)_3$	+ 3 H_2	= H_3PO	+ 3 $HOCH_3$	⇒	50.04	134.34	123.72	114.43	98.99	86.76	76.91	68.82
H_3PO_3	+ 2 H_2	= H_3PO	+ 2 H_2O	⇒	31.14	101.01	92.12	84.47	71.98	62.26	54.51	48.22
$OP(OH)_2CH_3$	+ H_2O	= H_3PO_4	+ CH_4	⇒	-15.38	-42.39	-40.38	-38.44	-34.90	-31.86	-29.28	-27.07
H_2PSH	+ H_2	= PH_3	+ H_2S	⇒	-1.51	14.96	12.98	11.51	9.49	8.17	7.25	6.57
H_2PSCH_3	+ H_2	= PH_3	+ $HSCH_3$	⇒	-0.25	15.19	13.18	11.71	9.71	8.43	7.53	6.87
H_3PS_4	+ 4 H_2	= PH_3	+ 4 H_2S	⇒	6.56	43.96	34.01	26.18	14.75	6.87	1.16	-3.17

Table A.2: Averaged and normalized ligand binding ernergies in kcal/mol for small-sized clusters.

Complexes	TPSS/def2-SVP	DFTB2/auorg$^{\alpha}$	DFTB2/auorg$^{\alpha'}$	DFTB2/auorg$^{\chi'}$
$Au_2(PH_3)_2$	-27.8	-39.1	-48.1	-45.9
$[Au_3(PH_3)_3]^+$	-47.8	-60.9	-67.3	-65.4
$Au_4(PH_3)_2$	-33.9	-40.3	-49.5	-47.6
$Au_2(PMe_3)_2$	-36.8	-41.8	-49.9	-47.7
$[Au_3(PMe_3)_3]^+$	-64.5	-66.8	-73.2	-71.4
$Au_4(PMe_3)_2$	-46.4	-44.2	-52.6	-50.8
$Au_2(PPh_3)_2$	-37.9	-41.8	-49.7	-47.6
$[Au_3(PPh_3)_3]^+$	-70.0	-70.0	-77.0	-74.8
$Au_4(PPh_3)_2$	-48.7	-45.0	-53.1	-51.4

Table A.3: Averaged and normalized ligand binding ernergies in kcal/mol for moderate-sized clusters.

Complexes	TPSS/def2-SVP	DFTB2/auorg$^{\alpha}$	DFTB2/auorg$^{\alpha'}$	DFTB2/auorg$^{\chi'}$
$[Au_6(PH_3)_6]^{2+}$	-52.1	-63.1	-69.4	-67.6
$[Au_7(PH_3)_7]^{+}$	-31.6	-34.5	-43.4	-42.4
$[Au_8(PH_3)_8]^{2+}$	-43.6	-47.9	-55.4	-54.1
$[Au_9(PH_3)_8]^{3+}$	-57.3	-69.2	-75.3	-73.4
$[Au_{11}(PH_3)_{10}]^{3+}$	-51.8	-56.7	-63.5	-62.3
$[Au_{13}(PH_3)_{12}]^{5+}$	-72.2	-84.8	-90.3	-88.5
$[Au_{20}(PH_3)_{16}]^{4+}$	-46.2	-48.6	-56.0	-54.4
$Au_{22}(PH_3)_{12}$	-25.5	-19.4	-30.0	-28.6
$[Au_6(PMe_3)_6]^{2+}$	-71.1	-70.7	-77.3	-75.4
$[Au_7(PMe_3)_7]^{+}$	-46.5	-39.4	-48.2	-46.9
$[Au_8(PMe_3)_8]^{2+}$	-60.8	-54.9	-62.4	-61.0
$[Au_9(PMe_3)_8]^{3+}$	-79.0	-78.5	-85.0	-83.1
$[Au_{11}(PMe_3)_{10}]^{3+}$	-71.2	-65.2	-72.6	-71.0
$[Au_{13}(PMe_3)_{12}]^{5+}$	-98.2	-97.8	-104.1	-102.3
$[Au_{20}(PMe_3)_{16}]^{4+}$	-65.9	-57.2	-64.6	-62.9
$Au_{22}(PMe_3)_{12}$	-41.8	-24.0	-34.1	-32.9

Table A.4: Averaged and normalized ligand binding ernergies in kcal/mol for large-sized clusters, TPSS denotes TPSS/def2-SVP, α denotes DFTB2/auorg$^{\alpha}$, TPSS//α denotes TPSS/def2-SVP//DFTB2/auorg$^{\alpha}$, $\alpha\prime$ denotes DFTB2/auorg$^{\alpha\prime}$, TPSS//$\alpha\prime$ denotes TPSS/def2-SVP//DFTB2/auorg$^{\alpha\prime}$, $\chi\prime$ denotes DFTB2/auorg$^{\chi\prime}$, TPSS//$\chi\prime$ denotes TPSS/def2-SVP//DFTB2/auorg$^{\chi\prime}$.

Complexes	TPSS	α	TPSS//α	$\alpha\prime$	TPSS//$\alpha\prime$	$\chi\prime$	TPSS//$\chi\prime$
$[Au_6(dppp)_4]^{2+}$	-67.6	-58.1	-64.9	-64.9	-64.2	-62.8	-64.5
$[Au_6(PPh_3)_6]^{2+}$	-87.2	-82.2	-86.2	-89.4	-85.9	-87.4	-85.8
$[Au_7(PPh_3)_7]^{+}$	-63.9	-49.9	-64.6	-58.6	-64.7	-57.6	-63.8
$[Au_8(PPh_3)_7]^{2+}$	-80.6	-73.0	-78.6	-80.2	-79.0	-78.3	-79.0
$[Au_8(PPh_3)_8]^{2+}$	-79.6	-69.7	-79.3	-77.3	-79.3	-75.8	-78.8
$[Au_8S_2(dppm)_4]^{2+}$	-70.0	-61.5	-71.9	-68.8	-72.1	-68.1	-70.4
$[Au_9(PPh_3)_8]^{3+}(C_4)$	-98.9	-92.3	-99.8	-99.4	-100.0	-96.4	-99.3
$[Au_9(PPh_3)_8]^{3+}(D_{2h})$	-99.3	-94.2	-99.4	-101.4	-99.8	-99.4	-99.5
$[Au_{11}(PMePh_2)_{10}]^{3+}$ (C_{3v})	-85.8	-76.4	-87.7	-83.8	-87.6	-82.6	-87.0
$[Au_{11}(PMePh_2)_{10}]^{3+}$ (D_{4d})	-85.6	-76.5	-87.0	-84.0	-87.1	-84.9	-86.6
$[Au_{13}(dppm)_6]^{5+}$	-108.6	-104.9	-109.0	-111.7	-109.2	-109.8	-108.6
$[Au_{20}(PP_3)_4]^{4+}$	-78.4	-57.2	-69.4	-62.6	-70.2	-60.8	-69.5
$Au_{22}(dppo)_6$	-49.5	-30.1	-51.5	-39.1	-50.7	-39.0	-49.5
$[Au_{38}(m\text{-}MBT)_{20}(PPh_3)_4]^{2+}$	-77.8	-58.9	-86.4	-65.5	-86.4	-65.1	-88.1
$Au_{70}S_{20}(PPh_3)_{12}$	-70.5	-47.3	-72.9	-54.8	-72.7	-53.4	-72.8

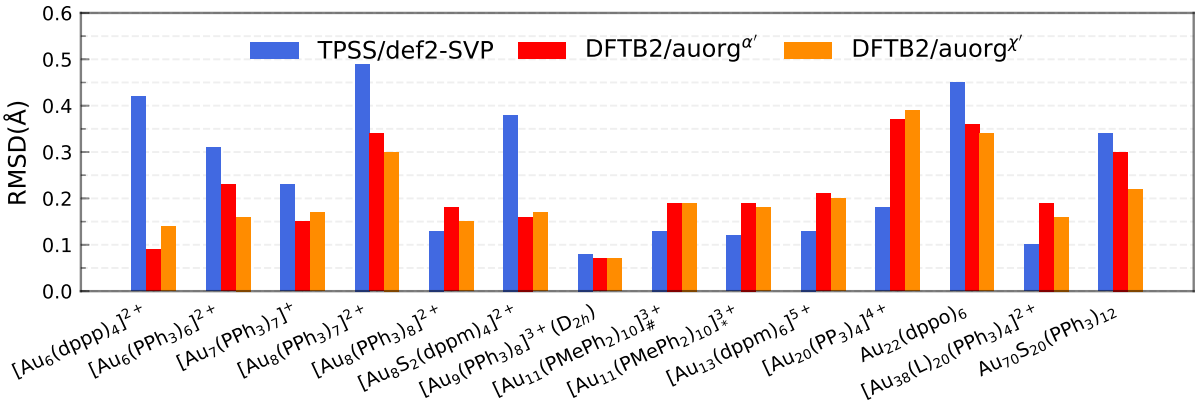

Figure A.2: RMSD over atomic positions for the large-sized phosphine-stabilized gold clusters. The RMSD of atomic positions considers Au, and P atoms for all large-sized phosphine-based gold clusters, $[Au_{11}(PMePh_2)_{10}]^{3+}_{\#}$ denotes $[Au_{11}(PMePh_2)_{10}]^{3+}$ (C_{3v}), $[Au_{11}(PMePh_2)_{10}]^{3+}_{*}$ denotes $[Au_{11}(PMePh_2)_{10}]^{3+}$ (D_{4d}), $[Au_{38}(L)_{20}(PPh_3)_4]^{2+}$ denotes $[Au_{38}(m\text{-}MBT)_{20}(PPh_3)_4]^{2+}$.

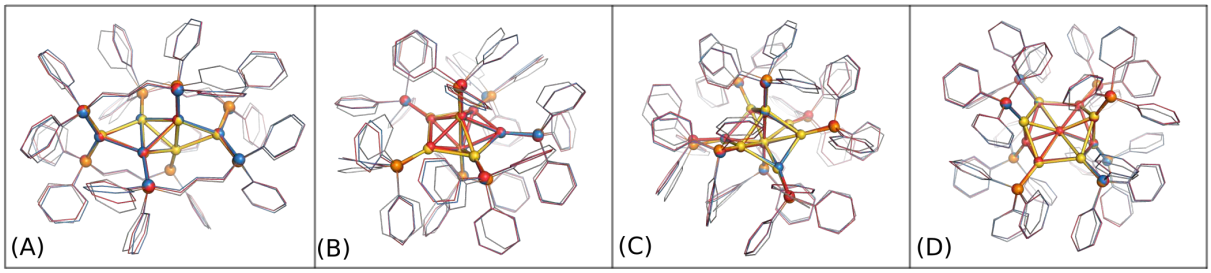

Figure A.3: Overlap of experimental crystal structure (Au in gold, P in orange and C in grey) and optimized DFTB/auorg$^{\alpha}$ and DFTB/auorg$^{\chi\prime}$ structures. auorg$^{\alpha}$ and auorg$^{\chi\prime}$ structures are represented by light red and sky blue, respectively. The gold nanoclusters considered in this figure are (A) $[Au_6(dppp)_4]^{2+}$ (BOTSOS), (B) $[Au_7(PPh_3)_7]^{+}$ (BIXZAK), (C) $[Au_8(PPh_3)_8]^{2+}$ (OPAUPF), and (D) $[Au_9(PPh_3)_8]^{3+}$ (MIVPOX-D_{2h}).

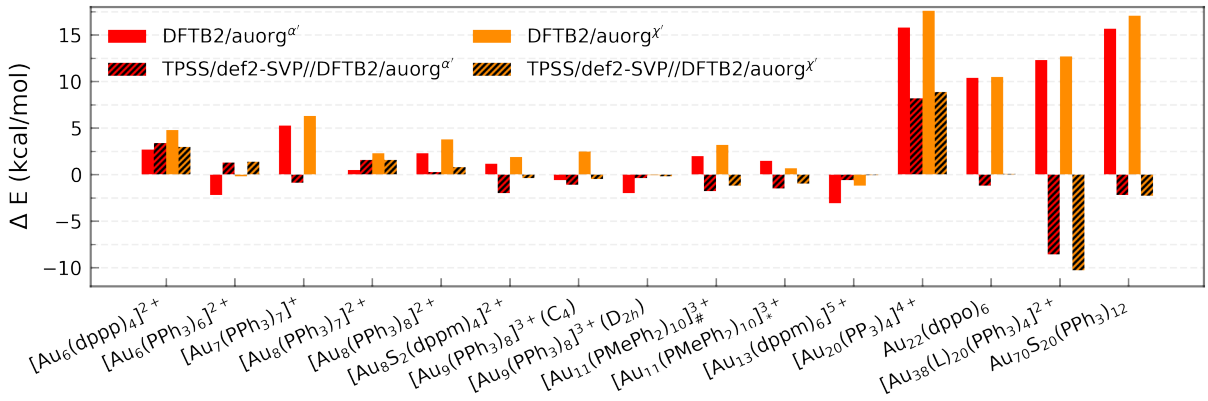

Figure A.4: Deviation in averaged and normalized ligand binding energies for the large-sized phosphine-stabilized gold clusters in reference to the TPSS/def2-SVP binding energies, $[Au_{11}(PMePh_2)_{10}]^{3+}_{\#}$ denotes $[Au_{11}(PMePh_2)_{10}]^{3+}$ (C_{3v}), $[Au_{11}(PMePh_2)_{10}]^{3+}_{*}$ denotes $[Au_{11}(PMePh_2)_{10}]^{3+}$ (D_{4d}), $[Au_{38}(L)_{20}(PPh_3)_4]^{2+}$ denotes $[Au_{38}(m\text{-}MBT)_{20}(PPh_3)_4]^{2+}$.

Table A.5: Comparison of relative energies with respect to the D_n isomers in kcal/mol as calculated by the following methods for $[Au_9(PPh_3)_8]^{3+}$ and $[Au_{11}(PMePh_2)_{10}]^{3+}$.

Methods	**Au_9**	**Au_{11}**
TPSS/def2-SVP	4.98	-3.20
DFTB2/auorg$^{\alpha\prime}$	11.81	1.78
DFTB2/auorg$^{\alpha}$	11.76	1.38
DFTB2/auorg$^{\chi\prime}$	10.13	1.82
TPSS/def2-SVP // DFTB2/auorg$^{\alpha\prime}$	6.29	-5.90
TPSS/def2-SVP // DFTB2/auorg$^{\alpha}$	5.19	-7.63
TPSS/def2-SVP // DFTB2/auorg$^{\chi\prime}$	6.31	-5.92

Isomerization energy of $[Au_9(PPh_3)_8]^{3+}$ and $[Au_{11}(PMePh_2)_{10}]^{3+}$ clusters

In practice, when studying chemical reactions, absolute cluster binding energies are not as important as relative binding energies, since a ligand is often replaced by another in the same reaction pathway. Therefore, to test the performance of DFTB for the prediction of isomerization energies, two particular examples, namely $[Au_9(PPh_3)_8]^{3+}$ and $[Au_{11}(PMePh_2)_{10}]^{3+}$ were investigated. In the solid phase, $[Au_9(PPh_3)_8]^{3+}$ is reported to have a Au_9 core with D_{2h} symmetry, as the full cluster takes a "butterfly" shape.[183] In a CH_2Cl_2 or methanol solution, this cluster isomerizes to a C_4 core with a crown-like structure.[143] The Au_{11} clusters have idealized C_{3v} and D_{4d} symmetric metal frameworks that differ around three adjacent peripheral sites.[184] The change in the skeletal geometries of Au_{11} clusters is proposed to be caused by the small variations in ligand packing and the presence of anionic ligands coordinated to the C_{3v} Au_{11} gold core. It has been previously predicted that C_4 Au_9 has a 5.7 kcal/mol lower energy than D_{2h} Au_9 in solution,[143] while so far no theoretical predictions were made yet for Au_{11} relative energy isomers. Here, we optimized the isomer structures of Au_9 (D_{2h} and C_4) and Au_{11} (C_{3v} and D_{4d}) with both DFTB and TPSS methods. Their relative structural energies are compared in Figure A.5.

The relative energies of the isomers presented in Figure A.5 were calculated with respect to the D_n isomers (on the left side) as the reference energy. For the $[Au_9(PPh_3)_8]^{3+}$ cluster, all methods predict that the higher symmetry D_{2h} structure is more stable than the less symmetric C_4 structure, with auorg$^{\alpha\prime}$ overstabilizing the high symmetry by about 5 kcal/mol. In the case of $[Au_{11}(PMePh_2)_{10}]^{3+}$ isomers, the TPSS/def2-SVP calculated C_{3V} isomer is lower in energy than the D_{4d} isomer, while DFTB methods still predict a slightly more stable high symmetry structure. We note that both the isomer relative energies and their DFTB deviations are very small, around 5 kcal/mol, and that it is difficult to achieve perfect agreement even between different density functionals for this energy range. TPSS/def2-SVP single point energy calculations using the DFTB2/auorg$^{\alpha\prime}$ optimized structures reduce the differences between the relative energies to only 1.33 and 2.72 kcal/mol for Au_9 and Au_{11} isomers, respectively, recovering the isomer energy ordering of the full TPSS calculations. The complete comparison of the isomer relative energies as calculated by DFTB with all parameter sets is shown in Table A.5 in the Supporting Information. The presented comparison demonstrates that, if one wishes to map the potential energy of a certain cluster with many isomers that are only a few kcal/mol apart in relative energies, performing geometry optimizations and pre-optimize structures with the DFTB method is a viable option to save computer time.

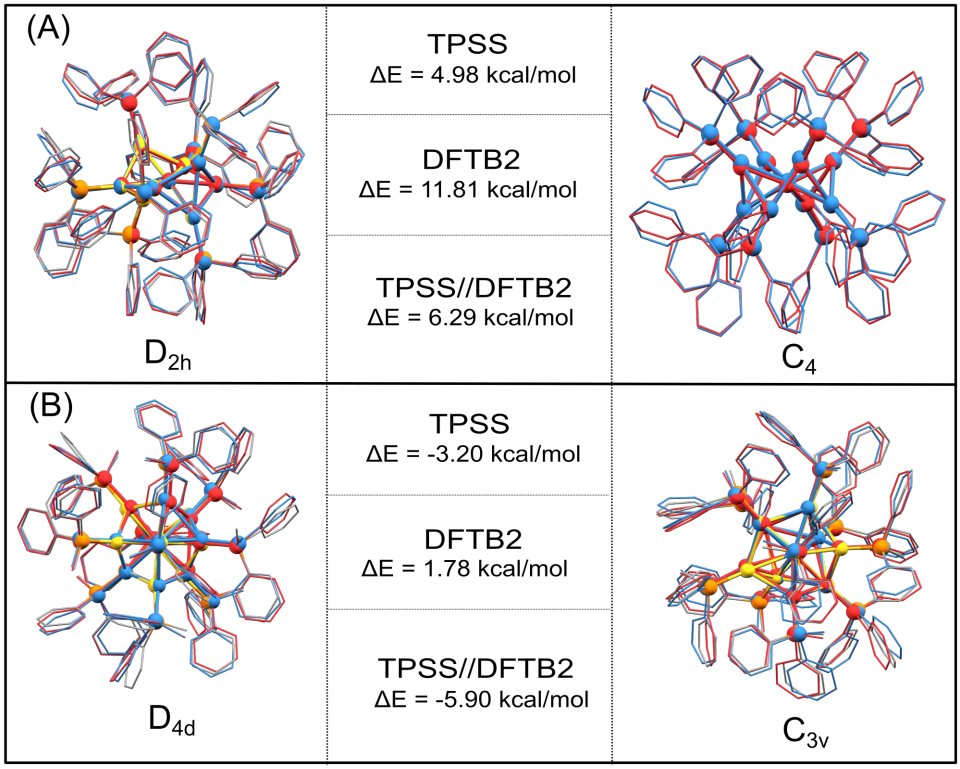

Figure A.5: Overlap of experimental X-ray (Au in gold, P in orange and C in grey) and optimized structures of (A) $[Au_9(PPh_3)_8]^{3+}$ D_{2h} and C_4 isomers and (B) $[Au_{11}(PMePh_2)_{10}]^{3+}$ D_{4d} and C_{3v} isomers. auorg$^{\alpha\prime}$ and DFT structures are represented by light red and sky blue, respectively. The relative energies in kcal/mol with respect to the D_n isomers are also shown as calculated by TPSS/def-SVP, DFTB2/auorg$^{\alpha\prime}$ and TPSS/def2-SVP//DFTB2/auorg$^{\alpha\prime}$. Note that the $[Au_9(PPh_3)_8]^{3+}$ C_4 isomer does not have an available experimental crystal structure.

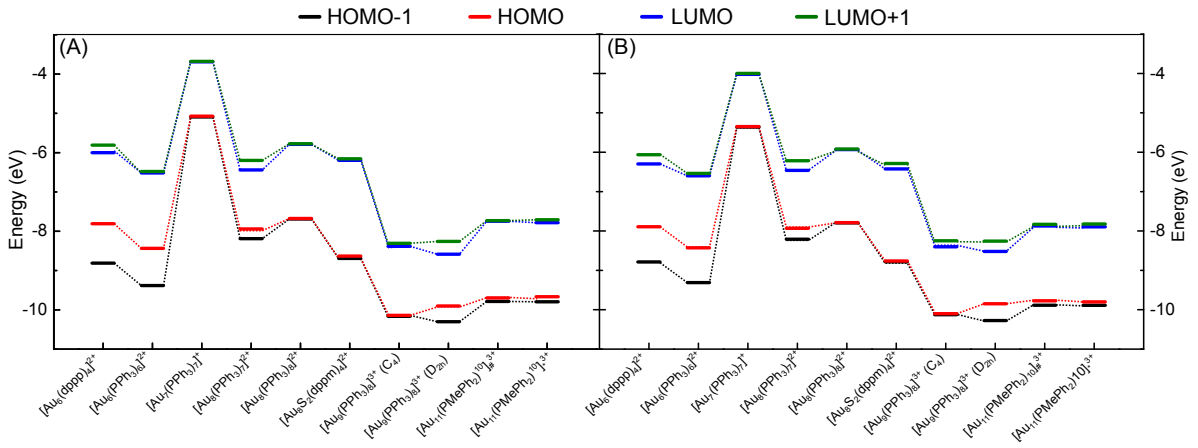

Figure A.6: Energy level diagram for the frontier orbitals of various clusters as calculated by (A) DFTB/auorg$^{\alpha}$ and (B) DFTB2/auorg$^{\chi\prime}$, $[Au_{11}(PMePh_2)_{10}]^{3+}_{\#}$ denotes $[Au_{11}(PMePh_2)_{10}]^{3+}$ (C_{3v}), $[Au_{11}(PMePh_2)_{10}]^{3+}_{*}$ denotes $[Au_{11}(PMePh_2)_{10}]^{3+}$ (D_{4d}). Dashed lines are included to guide the eye.

Table A.6: Comparison of HOMO and LUMO in eV as calculated by DFTB/auorg$^{\alpha\prime}$, DFTB/auorg$^{\alpha}$, DFTB/auorg$^{\chi\prime}$, and DFT for small gold clusters.

Complexes	TPSS/def2-SVP	DFTB2/auorg$^{\alpha\prime}$	DFTB2/auorg$^{\alpha}$	DFTB2/auorg$^{\chi\prime}$
$[Au_6(dppp)_4]^{2+}$ (BOTSOS)	-7.40 / -5.66	-8.00 / -6.45	-7.81 / -6.00	-7.89 / -6.30
$[Au_6(PPh_3)_6]^{2+}$ (CATPAO10)	-8.15 / -6.22	-8.51 / -6.82	-8.44 / -6.52	-8.43 / -6.60
$[Au_7(PPh_3)_7]^{+}$ (BIXZAK)	-5.10 / -3.47	-5.38 / -4.10	-5.07 / -3.69	-5.35 / -4.02
$[Au_8(PPh_3)_7]^{2+}$ (BASWUN)	-7.70 / -5.99	-8.01 / -6.68	-7.94 / -6.44	-7.93 / -6.47
$[Au_8(PPh_3)_8]^{2+}$ (OPAUPF)	-7.51 / -5.29	-7.83 / -6.18	-7.68 / -5.79	-7.79 / -5.93
$[Au_8S_2(dppm)_4]^{2+}$ (LEVKIJ)	-7.97 / -5.67	-8.86 / -6.52	-8.63 / -6.20	-8.76 / -6.42
$[Au_9(PPh_3)_8]^{3+}$ (MIVPOX-C_4)	-9.84 / -7.94	-10.17 / -8.58	-10.14 / -8.38	-10.10 / -8.40
$[Au_9(PPh_3)_8]^{3+}$ (MIVPOX-D_{2h})	-9.63 / -8.01	-9.92 / -8.74	-9.91 / -8.59	-9.85 / -8.52
$[Au_{11}(PMePh_2)_{10}]^{3+}$ (ZUCMAL)	-9.34 / -7.23	-9.86 / -8.13	-9.70 / -7.75	-9.78 / -7.87
$[Au_{11}(PMePh_2)_{10}]^{3+}$ (ZUCMEP)	-9.43 / -7.23	-9.83 / -8.15	-9.67 / -7.78	-9.8 0 / -7.90
$[Au_{13}(dppm)_6]^{5+}$ (LEVKAB)	-13.34 / -12.28	-13.73 / -12.48	-13.77 / -12.39	-13.69 / -12.40
$[Au_{20}(PP_3)_4]^{4+}$ (POFPUX)	-9.73 / -8.53	-10.28 / -9.346	-10.06 / -9.00	-10.21 / -9.16
$Au_{22}(dppo)_6$ (TOCFIC)	-2.11 / -1.67	-2.75 / -2.00	-2.30 / -1.73	-2.64 / -1.98
$[Au_{38}(m\text{-}MBT)_{20}(PPh_3)_4]^{2+}$ (CEMZIG)	-7.19 / -6.07	-7.55 / -6.50	-7.52 / -6.50	-7.52 / -6.40
$Au_{70}S_{20}(PPh_3)_{12}$ (TELMUV)	-3.45 / -2.90	-3.59 / -3.13	-3.47 / -2.99	-3.65 / -3.13

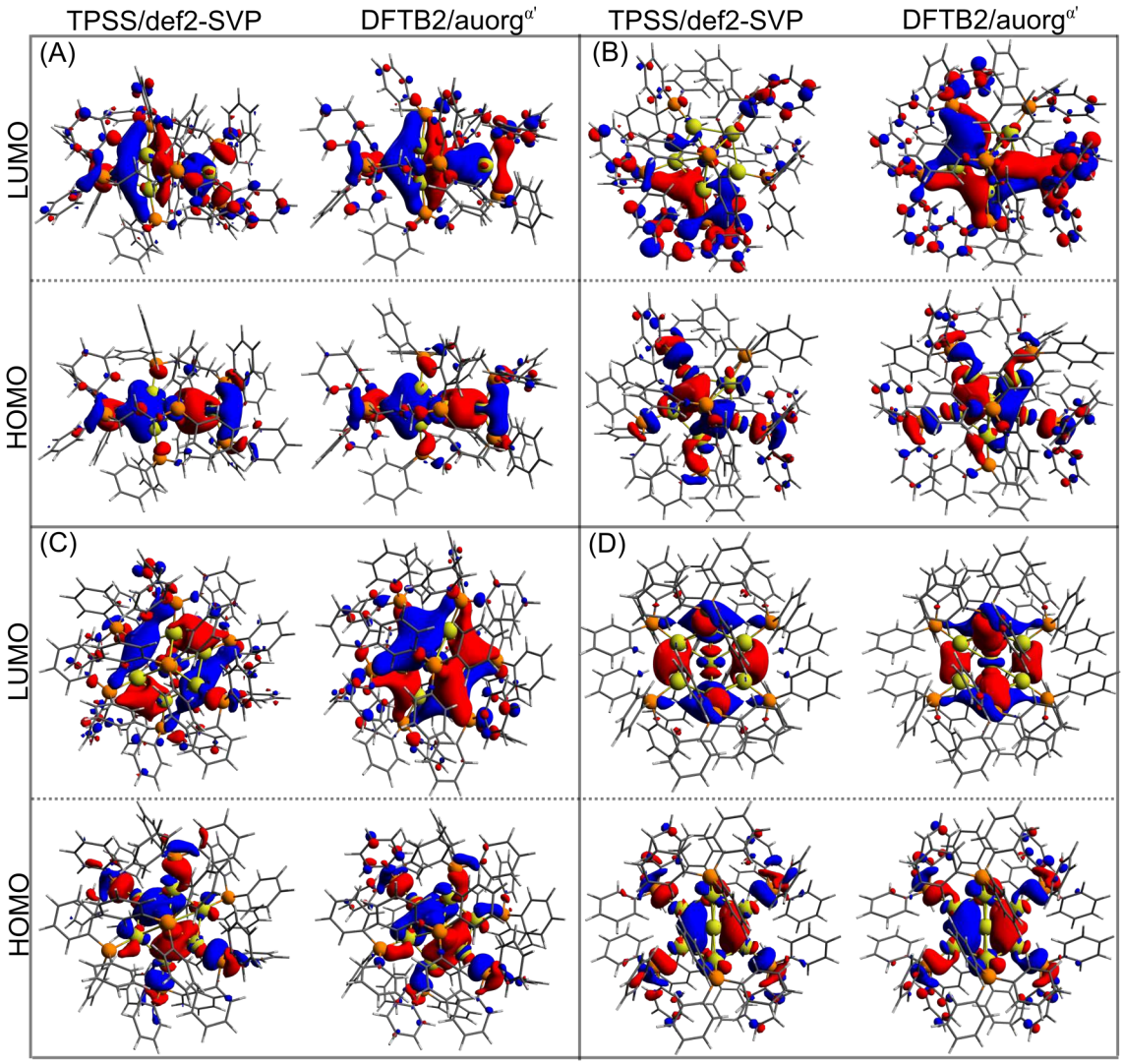

Figure A.7: HOMO and LUMO of (A) $[Au_6(dppp)_4]^{2+}$, (B) $[Au_7(PPh_3)_7]^{+}$ (BIXZAK), (C)$[Au_8(PPh_3)_8]^{2+}$ (OPAUPF) and (D) $[Au_9(PPh_3)_8]^{3+}$ (MIVPOX-D_{2h}) clusters as calculated by TPSS/def2-SVP and DFTB2/auorg$^{\alpha\prime}$; isosurface value = 0.02 a.u.

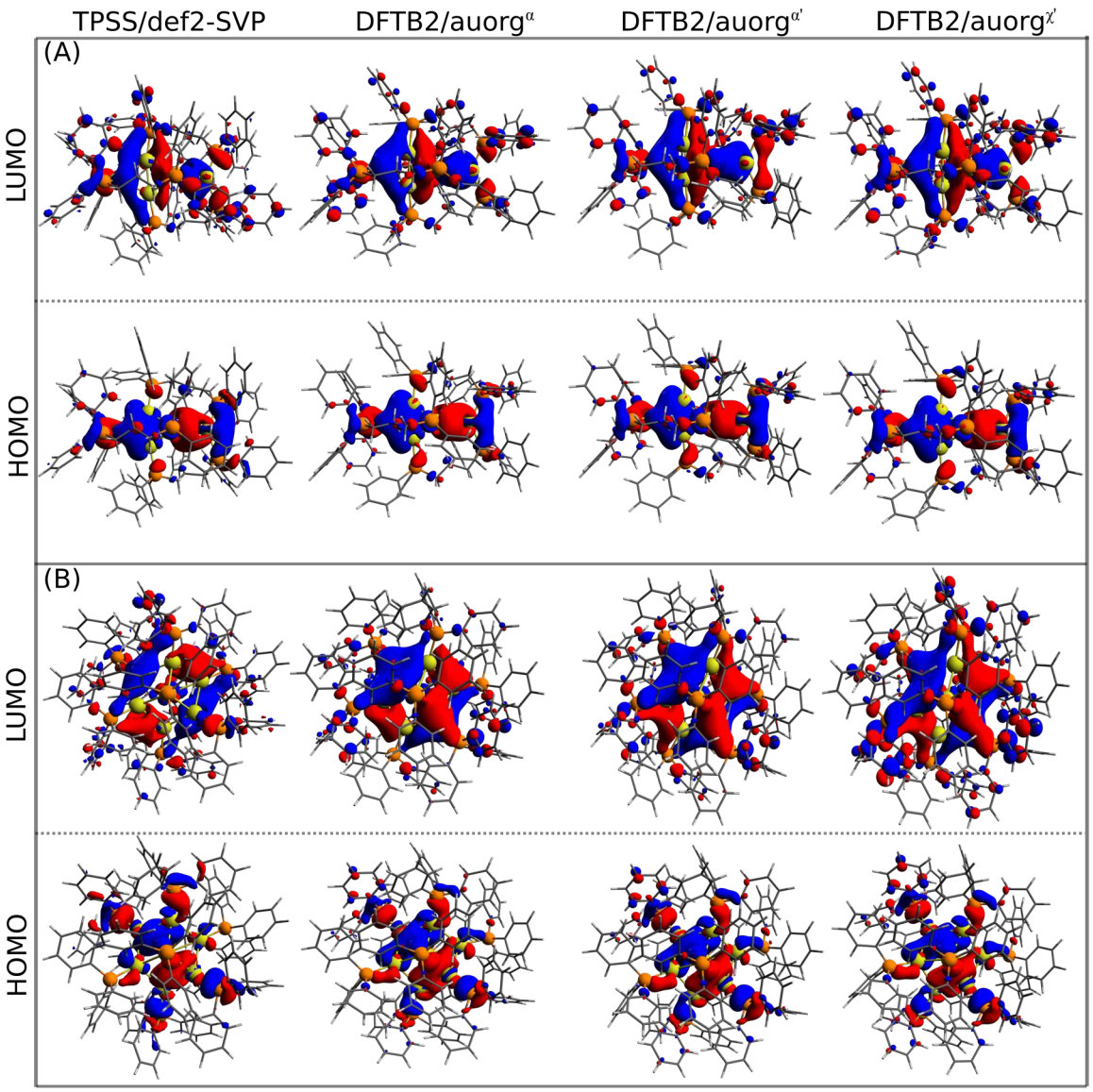

Figure A.8: HOMO and LUMO of (A) $[Au_6(dppp)_4]^{2+}$ and (B) $[Au_8(PPh_3)_8]^{2+}$ (OPAUPF) clusters as calculated by TPSS/def2-SVP, DFTB2/auorg$^{\alpha\prime}$, DFTB2/auorg$^{\alpha}$, and DFTB2/auorg$^{\chi\prime}$; isosurface value = 0.02 a.u.

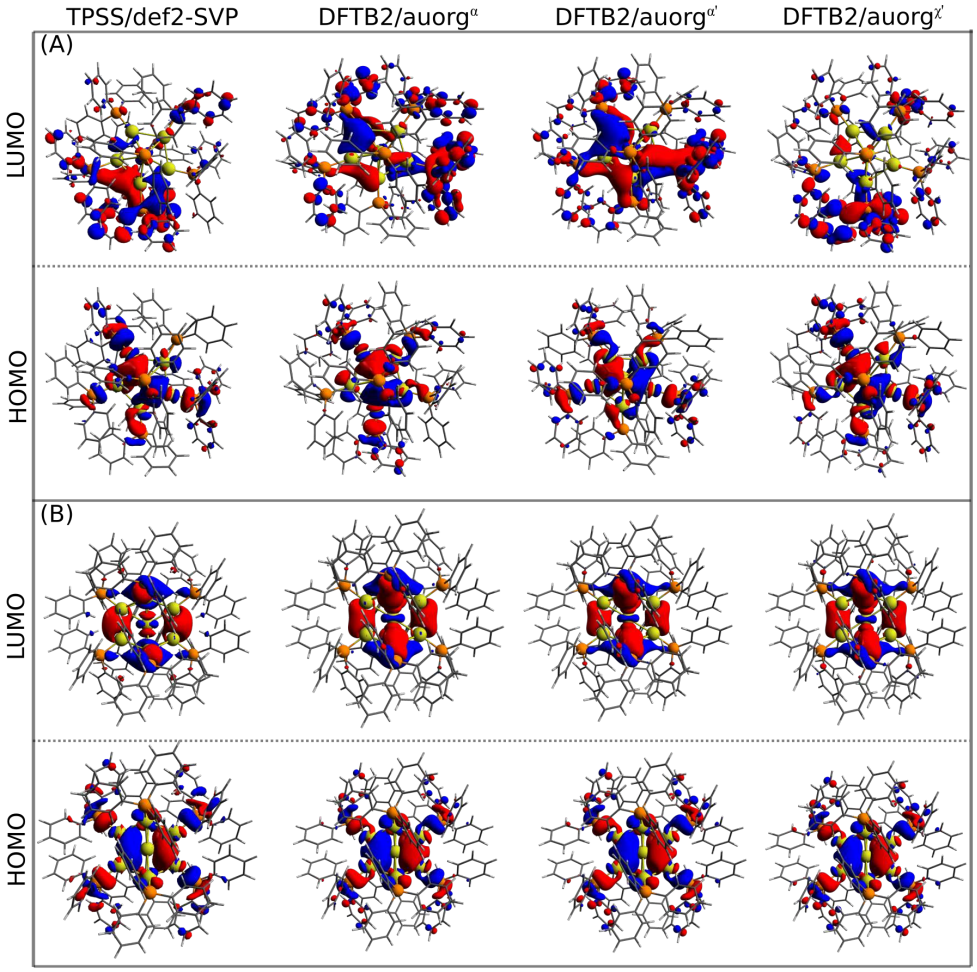

Figure A.9: HOMO and LUMO of (A) $[Au_7(PPh_3)_7]^+$ (BIXZAK) and (B) $[Au_9(PPh_3)_8]^{3+}$ (MIVPOX-D_{2h}) clusters as calculated by TPSS/def2-SVP, DFTB2/auorg$^{\alpha\prime}$, DFTB2/auorg$^{\alpha}$, and DFTB2/auorg$^{\chi\prime}$; isosurface value = 0.02 a.u.

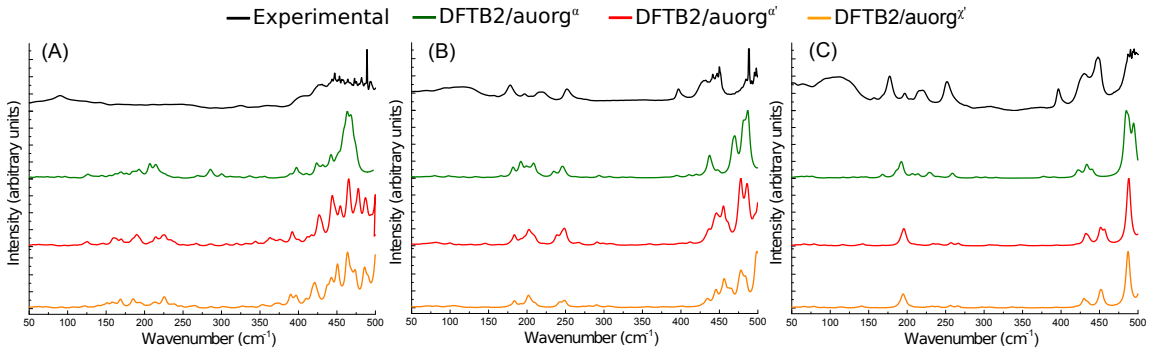

Figure A.10: Experimental (in black), computed auorg$^{\alpha}$ (in green) DFTB2/auorg$^{\alpha\prime}$ (in red), and auorg$^{\chi\prime}$ (in orange) far-IR spectra for (A) $[Au_6(dppp)_4]^{2+}$, (B) $[Au_8(PPh_3)_8]^{2+}$, and (C) $[Au_9(PPh_3)_8]^{3+}$ clusters.

Table A.7: Summary of contributing transitions as calculated by PBE/def2-SVP, DFTB2/auorg$^{\alpha\prime}$, DFTB2/auorg$^{\alpha}$ and DFTB2/auorg$^{\chi\prime}$ for the $[Au_6(dppp)_4]^{2+}$ cluster and their assignment to the experimental spectral peaks, as well as a brief description of the assigned transition modes

Experimental (cm-1)	PBE/def2-SVP (cm^{-1})	Intensity (km/mol)	DFTB2/auorg$^{\alpha\prime}$ (cm^{-1})	Intensity (km/mol)	DFTB2/auorg$^{\alpha}$ (cm^{-1})	Intensity (km/mol)	DFTB2/auorg$^{\chi\prime}$ (cm^{-1})	Intensity (km/mol)	Mode description
	85.52	2.6113	80.85	0.008	74.09	0.0142	70.44	0.0102	
90	87.06	3.0854			87.25	87.25	72.85	0.0119	
	89.74	1.7775			96.42	96.42	89.73	0.0102	
	119.65	1.9408	115.45	0.0101	126.85	0.0326	137.82	0.0151	Au core distortion
130	125.79	0.6063	121.47	0.0197	130.42	0.0114	140.15	0.0276	
			125.57	0.053	136.98	0.0149	145.69	0.0247	
					145.9	0.0135			
325	322.41	1.0008	331.99	0.0207	323.49	0.0139	327.67	0.0297	P_2Ph_4–$(CH_3)_3$ wag
	324.42	1.5474	336.12	0.011	336.48	0.0245			
	343.09	2.7216	344.08	0.0424	356.02	0.0225	339.77	0.0165	
	343.54	2.5989	351.05	0.015			351.16	0.0218	
358	346.55	2.2757	358.08	0.0242			353.92	0.0392	P–$(CH_2)_3$–P distortion
	348.18	2.8006	362.86	0.0826			358.28	0.0142	
			367.31	0.0253					
			367.66	0.0208					
	404.31	4.7347	391.89	0.1727	397.37	0.0977	389.66	0.2028	
	404.79	4.6453	395.32	0.0152	397.63	0.0307	394.54	0.0397	
	413.31	0.8692	399.06	0.0149	402.98	0.0236	397.03	0.0523	
410	414.48	13.2331	400.7	0.0301	410.2	0.036	397.37	0.1089	P–C–C–C–P bend
	416.7	9.3675	411.36	0.0713			409.68	0.0942	
	417.66	4.9216	416.86	0.076					
	419.21	6.3026							
	425.22	6.1159	424.99	0.0588	423.33	0.0516	417.41	0.1034	
	427.51	5.486	426.34	0.1706	423.53	0.1058	419.09	0.1037	
431	431.4	3.7808	426.51	0.0396	427.4	0.0423	421.43	0.2731	Au–P stretch and P–Ph stretch
	434.64	7.2679	428.16	0.1126	431.58	0.0984	424.72	0.1076	
	437.65	0.9142	430.5	0.122	436.3	0.0258			
					437.08	0.0141			
	441.92	33.2022	441.98	0.0892	441.62	0.0948	436.94	0.0762	
	442.69	8.5664	443.44	0.0586	442.55	0.1481	437.2	0.164	
			443.85	0.4207			437.2	0.22	
			447.01	0.1263			441.82	0.1873	
447							443.69	0.0253	$P(CH_2)_3Ph_2$ distortion
							447.98	0.5041	
							450.68	0.1313	
							451.31	0.0172	
475	457.58-485.52	Avg. 16.1239	448.67-477.85	Avg. 0.2416	448.97-475.05	Avg. 0.1546	453.31-473.89	Avg. 0.2414	

Table A.8: Summary of contributing transitions as calculated by PBE/def2-SVP, DFTB2/auorg$^{\alpha\prime}$, DFTB2/auorg$^{\alpha}$ and DFTB2/auorg$^{\chi\prime}$ for the $[Au_8(PPh_3)_8]^{2+}$ cluster and their assignment to the experimental spectral peaks, as well as a brief description of the assigned transition modes

Experimental (cm-1)	PBE/def2-SVP (cm^{-1})	Intensity (km/mol)	DFTB2/auorg$^{\alpha\prime}$ (cm^{-1})	Intensity (km/mol)	DFTB2/auorg$^{\alpha}$ (cm^{-1})	Intensity (km/mol)	DFTB2/auorg$^{\chi\prime}$ (cm^{-1})	Intensity (km/mol)	Mode description
182	173.46 176.12 176.23	1.4183 11.457 11.3283	146.17	0.0229	166.17	0.0347	176.69	0.0247	Au core distortion
218	185.35-223.02	Avg. 1.0292	178.65 183.44 183.68 191.34 191.9 196.17 199 201.5 202.39 204.11 206.59 206.82 208.4 210.53	0.0165 0.0782 0.091 0.028 0.0272 0.0607 0.0264 0.0867 0.0949 0.0638 0.0143 0.0448 0.0366 0.0729	181.34 182 191.17 192.78 193.37 198.77 199.03 202.03 202.42 205.02 206.4 207.82 208.45 208.72 209.04 209.86 210.49 216.17 217.81	0.0913 0.1359 0.23 0.0954 0.0533 0.0785 0.0718 0.0457 0.0446 0.035 0.0268 0.0365 0.0712 0.0708 0.0494 0.0415 0.0333 0.0181 0.0101	183.25 183.88 191.53 191.8 197.43 200.69 201.22 201.79 202.94 204.76 205.26 207.56 210.66	0.0941 0.089 0.0338 0.0251 0.0213 0.0749 0.0879 0.0822 0.0779 0.0173 0.0602 0.0173 0.0802	Ph rock
259	247.43-265.45	Avg. 1.3214	221.81 238.05 238.66 239.42 241.87 242.98 245 245.74 248.31 248.74 248.92 250.29 250.41	0.0131 0.0642 0.0594 0.017 0.0138 0.0168 0.061 0.0506 0.1025 0.0422 0.028 0.0241 0.0641	234.58 238 244 244.28 244.87 245.58 246.01 247.41 247.45 247.59 247.83 250.49 256.04 262.06	0.1216 0.0263 0.0378 0.0176 0.069 0.0131 0.0521 0.0436 0.0321 0.026 0.0218 0.0373 0.0008 0.0116	240.69 242.16 242.47 243.07 246.36 248.32 248.45 249.57 249.72 249.88	0.0348 0.0414 0.0303 0.0242 0.0409 0.0459 0.0297 0.0189 0.0118 0.0692	Ph rock
398	390.38- 406.89	Avg. 0.1938	351.07- 402.89	Avg. 0.0035	375.66- 396.94	Avg. 0.0033	350.18- 402.90	Avg. 0.0038	Ph twist
436	426.97-441.72	Avg. 2.6561	431.28-455.63	Avg. 0.0873	410.22-448.34	Avg. 0.0423	427.38-457.86	Avg. 0.0885	PPh_3 distortion
480	498.85-507.62	Avg. 21.2375	460.98-487.34	Avg. 0.2324	466.34-487.27	Avg. 0.2316	462.09-484.41	Avg. 0.2373	

Table A.9: Summary of contributing transitions as calculated by PBE/def2-SVP, DFTB2/auorg$^{\alpha\prime}$, DFTB2/auorg$^{\alpha}$ and DFTB2/auorg$^{\chi\prime}$ for the $[Au_9(PPh_3)_8]^{3+}$ cluster and their assignment to the experimental spectral peaks, as well as a brief description of the assigned transition modes

Experimental (cm-1)	PBE/def2-SVP (cm^{-1})	Intensity (km/mol)	DFTB2/auorg$^{\alpha\prime}$ (cm^{-1})	Intensity (km/mol)	DFTB2/auorg$^{\alpha}$ (cm^{-1})	Intensity (km/mol)	DFTB2/auorg$^{\chi\prime}$ (cm^{-1})	Intensity (km/mol)	Mode description
			136.28	0.0161	129.37	0.0176	141.33	0.0351	
			142.19	0.0637	131.6	0.0153	147.08	0.017	
157	148.81	2.2532	142.82	0.021	139.97	0.0291	158.37	0.0141	
			150.77	0.0136					
	163.28	2.6164							
177	169.95	9.6724	168.16	0.0136	168.01	0.1323	188	0.0321	
	174.7	17.3597							
	186.07	1.5613	190.19	0.0189	190.87	0.0694	194.67	0.2618	Au core distortion
	195	2.025	192.12	0.0159	191.15	0.1564	195.37	0.2421	
	198.75	4.7331	192.73	0.1244	191.84	0.1133	198.78	0.0721	
197	204.53	3.7443	193.1	0.0149	193.45	0.1528	205.06	0.0328	
			195.64	0.2757	193.51	0.1877			
			196.09	0.2851					
			208.95	0.0403					
	214.56	0.6717	215.13	0.0134	206.25	0.0615	213.7	0.0159	
	214.91	0.6573	217.12	0.015	207.4	0.0581	215.86	0.012	
	217.12	2.4079			214.06	0.1124	226.53	0.0412	
220*	217.77	0.1111			214.39	0.0153			Ph rock
	218.61	0.0122							
	218.69	1.4505							
	219.36	1.3855							
	238.93-251.52	Avg. 1.4416	231.09	0.0153	227.83	0.1353	232.29	0.0227	
			233.76	0.0244	229.86	0.0213	232.47	0.0258	
			233.97	0.0239	231.21	0.1022	232.84	0.0239	
			234.03	0.0215	240.05	0.0349	239.67	0.0522	
252			239.78	0.0499	244.58	0.0159	241.13	0.0175	PPh_3 distortion
			243.36	0.029	258.28	0.1192	256.19	0.1159	
			256.9	0.1193	259.19	0.0141	256.39	0.0101	
					259.32	0.0138			
					260.15	0.0371			
397	390.16-401.64	Avg. 0.2980	394.25	0.0091	389.87	0.0188	394.01	0.0114	
			420.43	0.0133			420.46	0.0146	
			431.79	0.401			429.48	0.397	
			432.69	0.0108			430.32	0.0537	
430	424.59-431.16	Avg. 2.4632	432.7	0.0339	412.30-435.88	Avg. 0.074	433.86	0.03	Ph twist
			434.9	0.0315			434.53	0.1603	
			435.54	0.1803			435.16	0.0201	
			435.91	0.0288					
			437.89	0.0106					
448	438.55-444.13	Avg. 5.2400	451.01-456.88	Avg. 0.2211	440.57	0.2226	450.55-453.26	Avg. 0.2197	PPh_3 distortion
480	489.33-492.65	Avg. 18.8798	486.37-488.36	Avg. 0.5519	483.27-496.16	0.5163	485.92-487.96	0.562	

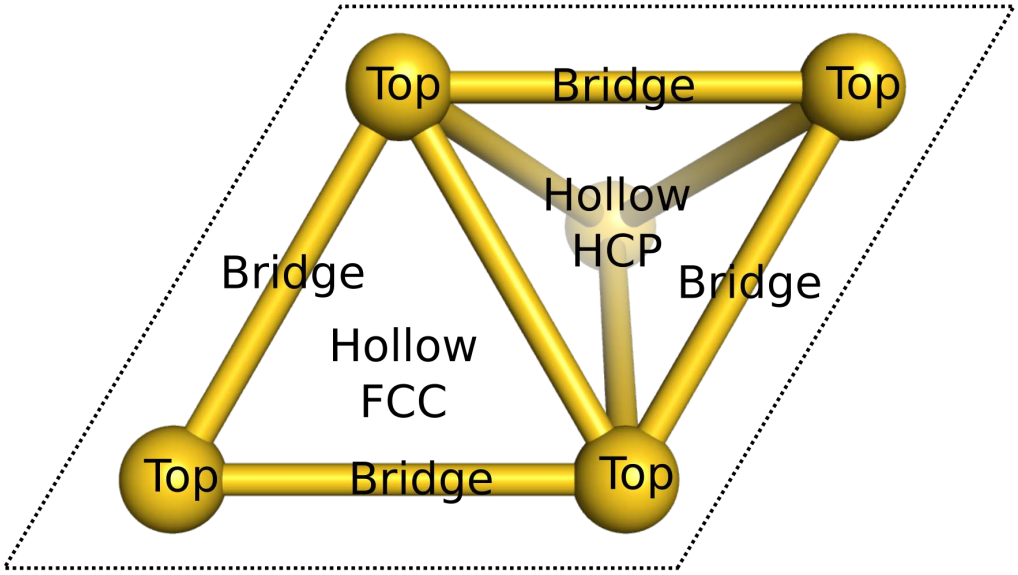

Figure A.11: Different adsorption binding sites on Au (111) surface, only the Au atoms of the top two layers are shown.

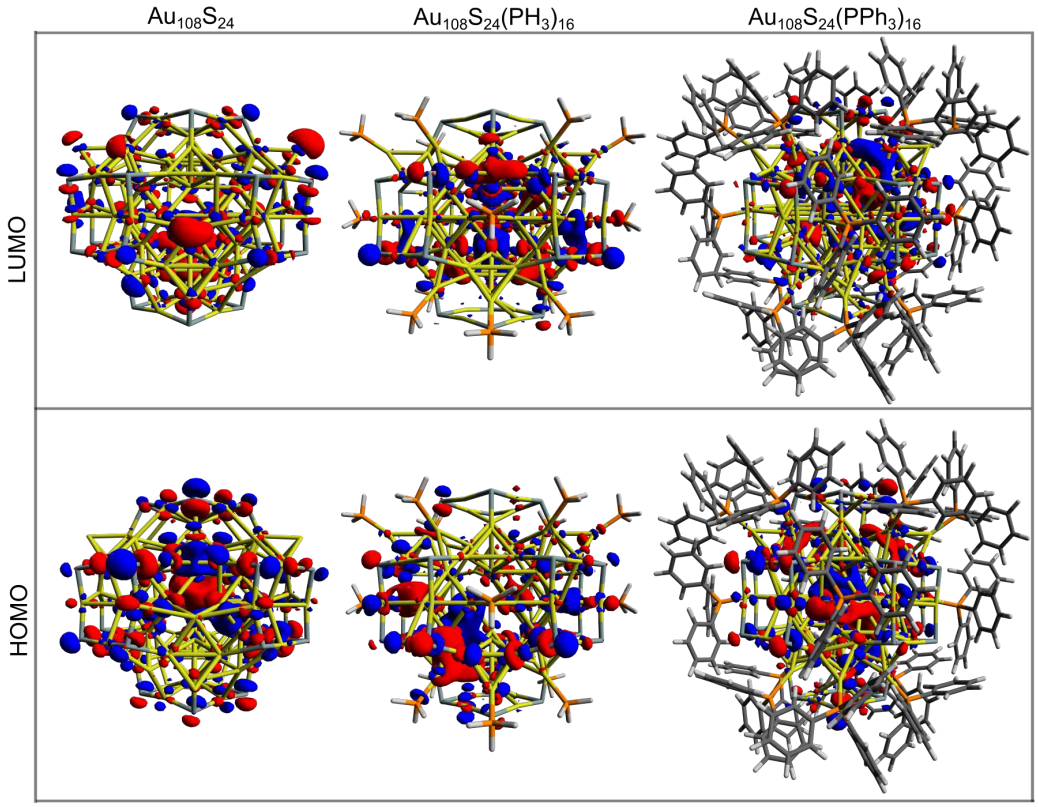

Figure A.12: HOMO and LUMO plots of $Au_{108}S_{24}$, $Au_{108}S_{24}(PH_3)_{16}$, and $Au_{108}S_{24}(PPh_3)_{16}$ clusters as calculated by TPSS/def2-SVP//DFTB2/auorg$^{\alpha\prime}$; isosurface value = 0.015 $e^{0.5/a_0^3}$.

Table A.10: Summary of contributing transitions determined by DFTB2/auorg$^{\alpha\prime}$ for the $[Au_{108}S_{24}(PPh_3)_{16}]$ cluster and brief description of the assigned transition modes, part 1.

DFTB2/auorg$^{\alpha\prime}$ (cm-1)	Intensity (km/mol)	Mode description
26.387	0.01195	Au core distortion
54.087	0.01243	
54.116	0.01255	
56.459	0.01452	
73.484	0.01721	
76.592	0.0112	
91.121	0.01114	Au core distortion
91.466	0.01238	
93.606	0.01015	asymmetric stretching Au-S-Au (planar rings) and PPh_3 twisting
93.638	0.01133	
102.984	0.01016	Au core distortion
103.05	0.0104	
110.089	0.01135	
113.072	0.01073	
114.583	0.01228	
118.282	0.02662	
118.435	0.02339	
118.772	0.01639	Au-Au-Au rocking (connected to planar rings)
119.34	0.01649	Au-Au-Au scissoring (connected to planar rings)
120.403	0.01194	Au-P asymmetric stretch and Au core distortion
120.684	0.01922	
124.009	0.01762	Au core distortion
124.278	0.01728	
124.451	0.01	
125.952	0.01163	
133.768	0.01069	
141.793	0.01276	
164.734	0.01712	Au-P stretch
165.461	0.01824	
165.477	0.01777	
167.11	0.01346	
167.291	0.01307	Au-Au symmetric stretching (connected to PPh_3)
180.925	0.02166	
181.058	0.01548	Au-P stretch
182.297	0.02001	
182.471	0.03368	
182.914	0.02397	
185.318	0.03596	
185.487	0.02547	
185.676	0.01155	
185.741	0.01826	
185.76-192.27	Avg. 0.0346	Ph rocking
198.523	0.14019	symmetric stretching S-Au-S (planar rings)
200.25	0.10294	
202.781	0.14811	
204.909	0.04854	Ph twist
204.915	0.0242	
205.337	0.04331	
207.877	0.08301	
208.089	0.05917	

Table A.11: Summary of contributing transitions determined by DFTB2/auorg$^{\alpha\prime}$ for the $[Au_{108}S_{24}(PPh_3)_{16}]$ cluster and brief description of the assigned transition modes, part 2.

DFTB2/auorg$^{\alpha\prime}$ (cm-1)	Intensity (km/mol)	Mode description
208.161	0.1301	Ph rock
208.402	0.05661	
208.717	0.09316	
209.314	0.05062	
210.34	0.06436	
211.184	0.04972	
218.041	0.01951	S-Au-S rocking (planar rings)
218.41	0.01103	
218.467	0.02623	
218.943	0.11707	Ph rocking
219.181	0.02061	
219.363	0.02627	
219.491	0.04727	
219.741	0.06469	
220.336	0.0208	S-Au-S rocking (planar rings)
222.196	0.04751	
222.776	0.03097	
222.996	0.00298	
223.114	0.04095	
223.41	0.03931	
226.198	0.11918	
234.336	0.00303	
234.5	0.00321	
237.519	0.02785	Ph rock and Au-S stretch
237.597	0.00845	
237.735	0.01358	
237.761	0.02369	
238.013	0.01369	
238.173	0.05096	
238.236	0.05156	
238.412	0.02354	
238.818	0.01568	
238.993	0.02562	
239.258	0.07917	
241.089	0.69303	Au-S stretch
241.192	0.64982	
241.595	0.25861	
241.738	0.01983	
242.066	0.10407	
242.172	0.02482	
243.156	0.05566	
243.74	0.05345	
243.962	0.01056	
247.977	0.06949	
248.71-252.17	Avg. 0.0379	Ph twist
255.09-262.74	Avg. 0.1307	PPh3 distortion and Au-S stretch
265.03-272.86	Avg. 0.0391	Au_4S_4 planar ring rock
274.386	0.05491	Au_4S_4 symmetric stretch
276.211	0.15656	
276.568	0.19116	
277.186	0.11359	Au_4S_4 asymmetric stretch
279.671	0.03883	
279.781	0.08326	

Table A.12: Summary of contributing transitions determined by DFTB2/auorg$^{\alpha\prime}$ for the $[Au_{108}S_{24}(PPh_3)_{16}]$ cluster and brief description of the assigned transition modes, part 3.

DFTB2/auorg$^{\alpha\prime}$ (cm-1)	Intensity (km/mol)	Mode description
280.284	0.0261	Au_4S_4 twist
285.686	0.06474	
287.051	0.06944	Au_4S_4 symmetric stretch
287.412	0.40739	
291.177	0.03524	PPh_3 distortion
291.437	0.01303	
292.643	0.02394	
294.434	0.02065	
297.485	0.01415	
302.74	0.02364	
334.01-372.66	Avg. 0.0205	Ph twist
431.06-459.86	Avg. 0.06291	PPh_3 distortion
471.809-495.78	Avg. 0.1485	
506.28-520.33	Avg. 0.4313	PPh_3 distortion and Au-S stretch
521.401	0.12228	Au-S stretch
522.278	0.02622	
522.656	0.00953	
525.037	0.11265	
525.403	0.24905	
525.648	0.18726	
532.85-554.38	Avg. 1.6027	Ph twist and Au-S stretch
559.916	9.29723	Au-P stretch and PPh_3 distortion
570.926	7.77941	
571.017	7.52268	
571.603	1.64805	
613.44-648.58	Avg. 0.1124	PPh_3 distortion

Validation of the DFTB Method in Predicting Infrared Spectra of Gold–Thiolates Clusters

To validate the reliability of the DFTB2 method in simulating IR spectra for gold–thiolates nanoclusters, we compare the DFTB predicted IR spectra to published DFT theoretical IR spectra for $Au_4(SCH_3)_4$, $Au_{18}(SCH_3)_{14}$, and $[Au_{25}(SCH_3)_{18}]^-$ clusters.[142,150,151] In addition, we evaluate the capability of the DFTB2 method in describing ligand-ligand interactions and the effects of ligands on the structure and vibrational properties of the gold–thiolates clusters. We compare DFTB2 calculated IR to DFT calculated and experimental IR spectra for Au_{18} core cluster with six different types of ligand; $-SCH_3$, $-S-c\text{-}C_6H_{11}$, $-SPh$, $-p\text{-}MBA$, $-SPhNO_2$, and $-TBBT$.[142] The effects of different ligands on the geometry of the Au_{18} core are compared as well. Figure A.13 shows that the DFTB calculated IR spectra are comparable to the corresponding DFT spectra predicted by Tlahuice-Flores in his previous work.[142] Similar to the IR spectra of the phosphine-stabilized $[Au_6(dppp)_4]^{2+}$, $[Au_8(PPh_3)_8]^{2+}$, and $[Au_9(PPh_3)_8]^{3+}$ clusters, the DFTB calculated intensities are significantly lower but the normalized spectral shapes agree with their DFT calculated counterparts.

Figure A.14 shows DFTB calculated IR spectra of a Au_{18} core cluster with six different types of ligands. Generally, DFTB calculated IR spectra resemble closely the DFT calculated spectra, but with smaller intensities than the reported ones by ≈20-40 km/mol.[142] DFTB reproduces the change in IR spectra with the change of ligands well in comparison to the DFT calculated IR spectra. In particular, the case of $Au_{18}(-S-c\text{-}C_6H_{11})_{14}$ clearly shows that the DFTB IR spectrum agrees extremely well with the experimental spectrum (using the same methodology as for the phosphine-stabilized clusters).[138] Small deviations between DFTB and DFT IR spectra might be caused by different initial geometries for the previously published DFT- and our own DFTB-optimized geometries,[142] and because the geometry optimization of these large and complicated clusters can converge to different local minima. Among these Au_{18} clusters, $Au_{18}(p\text{-}MBA)_{14}$ and $Au_{18}(SPhNO_2)_{14}$ clusters have highest intensity in their IR signals particularly for the Au-Au and Au-S stretches in $Au_{18}S_{14}$ core clusters when compared to the rest of the clusters. The increase in these IR intensities can be attributed to the large structural distortions caused by p-MBA and $SPhNO_2$ ligands. Figure A.15 shows the distortions of the Au_{18} core cluster caused by these ligands. This is consistent with the previous DFT-based study.[142] These results are very encouraging and suggests that the DFTB method is reliable in predicting the IR spectra for thiolate-protected gold clusters and confirms that it is able to describe the ligand-ligand interactions as well as ligands effects on gold clusters congruent with DFT predictions.

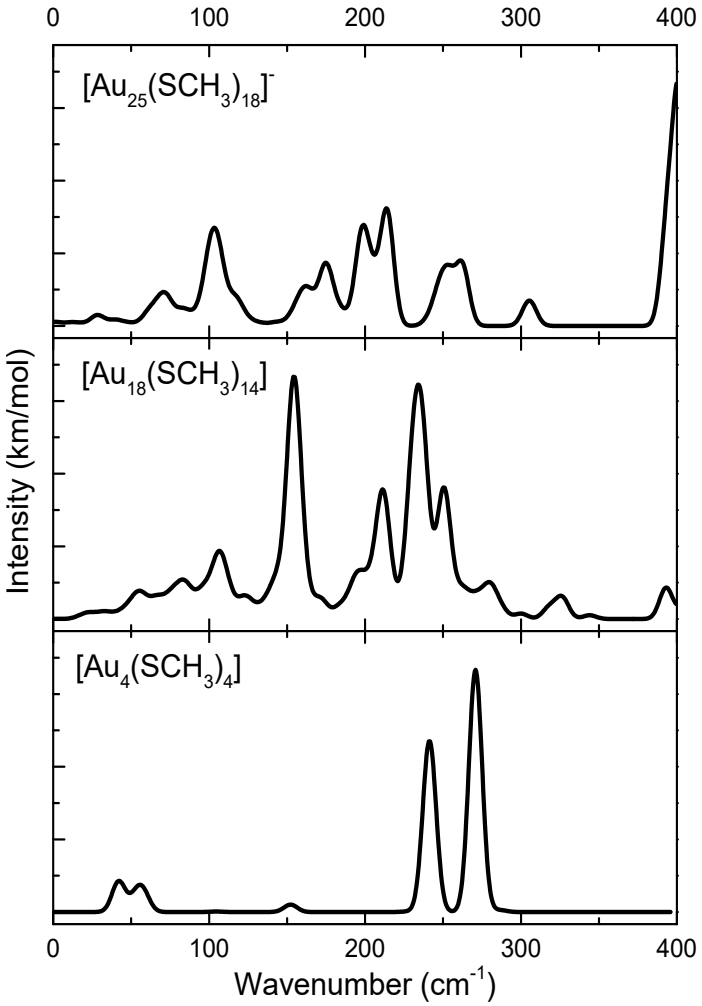

Figure A.13: DFTB calculated IR spectra of $Au_4(SCH_3)_4$, $Au_{18}(SCH_3)_{14}$, and $[Au_{25}(SCH_3)_{18}]^-$.

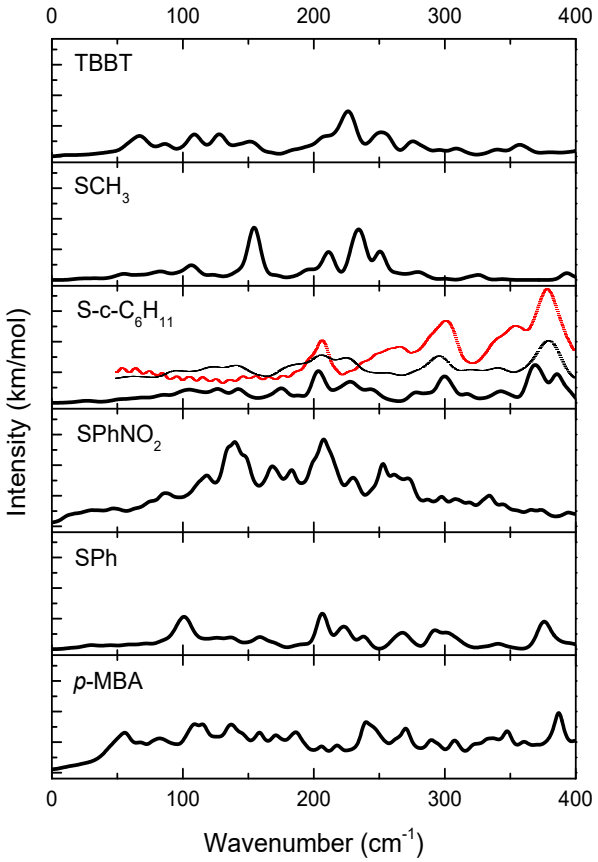

Figure A.14: Calculated IR spectra of $Au_{18}(SCH_3)_{14}$, $Au_{18}(S-c\text{-}C_6H_{11})_{14}$, $Au_{18}(SPh)_{14}$, $Au_{18}(p\text{-}MBA)_{14}$, $Au_{18}(SPhNO_2)_{14}$, and $Au_{18}(TBBT)_{14}$ clusters using a FWHM of 5 cm^{-1} Gaussian broadening. More intense IR spectra are observed on p-MBA- and $SPhNO_2$-protected clusters. The additional plots in $S-c\text{-}C_6H_{11}$-ligated Au_{18} are the experimental far-IR spectrum (dotted red) and the DFTB-simulated with a wider FWHM of 8 cm^{-1} Gaussian broadening.

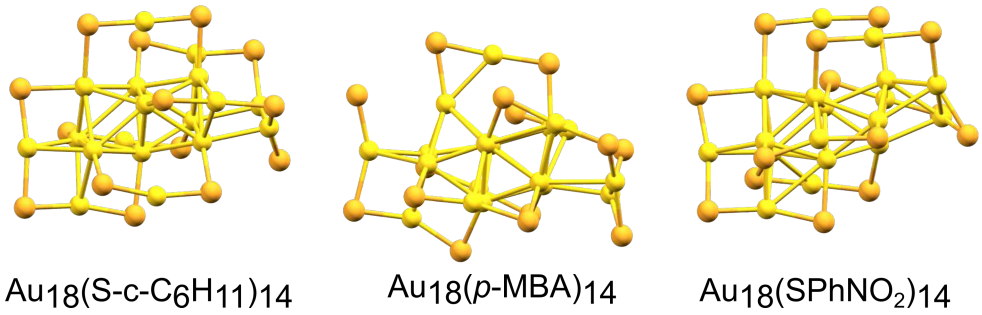

Figure A.15: $Au_{18}S_{14}$ core structures of $Au_{18}(S-c\text{-}C_6H_{11})_{14}$, $Au_{18}(p\text{-}MBA)_{14}$, and $Au_{18}(SPhNO_2)_{14}$ clusters with four different ligands (ligand structures are omitted for clarity). Au and S atoms are yellow and orange. The clusters are optimized by means of DFTB/auorg$^{\alpha\prime}$ with the D3 dispersion corrections.

B Supporting Information for "Density-Functional Tight-Binding for Platinum Nanoparticles in Vacuum and on TiO_2 Support"

Table B.1: Pt_2 to Pt_{116} clusters, their corresponding atomization energies ΔE^{at}, weight factors W^{at} and W^{force} used in the fitting of Pt-Pt repulsive potential.

Clusters	ΔE^{at} (kcal/mol)	W^{at}	W^{force}	Clusters	ΔE^{at} (kcal/mol)	W^{at}	W^{force}
pt2	93.23	5.00	1.0	pt24	2499.73	0.46	1.0
pt3	191.94	3.00	1.0	pt25	2613.09	0.45	1.0
pt4	276.56	2.00	1.0	pt26	2638.09	0.43	1.0
pt5	370.52	1.50	1.0	pt27	2867.45	0.42	1.0
pt6	468.94	1.30	1.0	pt28	2975.17	0.41	1.0
pt7	558.71	1.16	1.0	pt29	3089.80	0.40	1.0
pt8	687.04	1.05	1.0	pt30	3206.25	0.39	1.0
pt9	783.21	0.96	1.0	pt35	3763.68	0.35	1.0
pt10	896.13	0.89	1.0	pt40	4263.81	0.31	1.0
pt11	1031.75	0.83	1.0	pt45	5013.69	0.29	1.0
pt12	1136.74	0.78	1.0	pt50	5642.17	0.27	1.0
pt13	1188.11	0.73	1.0	pt55	6226.31	0.25	1.0
pt14	1312.78	0.69	1.0	pt60	6754.25	0.23	1.0
pt15	1434.30	0.66	1.0	pt65	7387.20	0.22	1.0
pt16	1551.90	0.62	1.0	pt70	8030.22	0.21	1.0
pt17	1657.96	0.60	1.0	pt75	8558.29	0.20	1.0
pt18	1776.94	0.57	1.0	pt80	9279.25	0.19	1.0
pt19	1836.88	0.55	1.0	pt85	9951.22	0.18	1.0
pt20	2048.27	0.53	1.0	pt90	10551.42	0.17	1.0
pt21	2140.13	0.51	1.0	pt95	11153.83	0.16	1.0
pt22	2278.23	0.49	1.0	pt100	11767.93	0.16	1.0
pt23	2389.94	0.48	1.0	pt116	13714.01	0.14	1.0
pt3-iso1	174.70	2.19	1.0	pt7-iso5	577.52	1.16	1.0
pt4-iso1	278.11	1.77	1.0	pt9-iso1	792.82	0.96	1.0
pt4-iso2	278.55	1.77	1.0	pt9-iso2	793.13	0.96	1.0
pt7-iso1	582.79	1.16	1.0	pt9-iso3	808.93	0.96	1.0
pt7-iso2	571.97	1.16	1.0	pt9-iso4	800.84	0.96	1.0
pt7-iso3	581.73	1.16	1.0	pt9-iso5	812.81	0.96	1.0
pt7-iso4	574.63	1.16	1.0	pt9-iso6	796.73	0.96	1.0

Table B.2: Twenty isomers of Pt_{10}, Pt_{11}, Pt_{12}, Pt_{13} clusters, their corresponding atomization energies ΔE^{at}, weight factors W^{at} and W^{force} used in the fitting of Pt-Pt repulsive potential.

Clusters	ΔE^{at} (kcal/mol)	W^{at}	W^{force}	Clusters	ΔE^{at} (kcal/mol)	W^{at}	W^{force}
pt10-iso1	913.19	0.89	1.0	pt12-iso1	1138.23	0.78	1.0
pt10-iso2	910.68	0.89	1.0	pt12-iso2	1143.92	0.78	1.0
pt10-iso3	932.64	0.89	1.0	pt12-iso3	1149.30	0.78	1.0
pt10-iso4	918.28	0.89	1.0	pt12-iso4	1148.58	0.78	1.0
pt10-iso5	910.39	0.89	1.0	pt12-iso5	1144.21	0.78	1.0
pt10-iso6	914.10	0.89	1.0	pt12-iso6	1140.75	0.78	1.0
pt10-iso7	911.10	0.89	1.0	pt12-iso7	1139.49	0.78	1.0
pt10-iso8	907.09	0.89	1.0	pt12-iso8	1131.65	0.78	1.0
pt10-iso9	908.01	0.89	1.0	pt12-iso9	1129.28	0.78	1.0
pt10-iso10	909.85	0.89	1.0	pt12-iso10	1119.02	0.78	1.0
pt10-iso11	900.81	0.89	1.0	pt12-iso11	1116.84	0.78	1.0
pt10-iso12	899.96	0.89	1.0	pt12-iso12	1116.48	0.78	1.0
pt10-iso13	902.20	0.89	1.0	pt12-iso13	1126.98	0.78	1.0
pt10-iso14	910.09	0.89	1.0	pt12-iso14	1108.72	0.78	1.0
pt10-iso15	899.57	0.89	1.0	pt12-iso15	1112.27	0.78	1.0
pt10-iso16	898.82	0.89	1.0	pt12-iso16	1105.44	0.78	1.0
pt10-iso17	903.46	0.89	1.0	pt12-iso17	1115.11	0.78	1.0
pt10-iso18	893.06	0.89	1.0	pt12-iso18	1098.91	0.78	1.0
pt10-iso19	902.08	0.89	1.0	pt12-iso19	1099.34	0.78	1.0
pt10-iso20	869.66	0.89	1.0	pt12-iso20	1083.88	0.78	1.0
pt11-iso1	1032.96	0.83	1.0	pt13-iso1	1188.30	0.73	1.0
pt11-iso2	1038.44	0.83	1.0	pt13-iso2	1251.04	0.73	1.0
pt11-iso3	1036.63	0.83	1.0	pt13-iso3	1258.14	0.73	1.0
pt11-iso4	1039.64	0.83	1.0	pt13-iso4	1264.10	0.73	1.0
pt11-iso5	1034.99	0.83	1.0	pt13-iso5	1256.96	0.73	1.0
pt11-iso6	1029.12	0.83	1.0	pt13-iso6	1250.67	0.73	1.0
pt11-iso7	1017.50	0.83	1.0	pt13-iso7	1256.38	0.73	1.0
pt11-iso8	1013.02	0.83	1.0	pt13-iso8	1250.97	0.73	1.0
pt11-iso9	1021.96	0.83	1.0	pt13-iso9	1244.40	0.73	1.0
pt11-iso10	1014.19	0.83	1.0	pt13-iso10	1233.89	0.73	1.0
pt11-iso11	1009.03	0.83	1.0	pt13-iso11	1241.34	0.73	1.0
pt11-iso12	1003.15	0.83	1.0	pt13-iso12	1228.49	0.73	1.0
pt11-iso13	1001.54	0.83	1.0	pt13-iso13	1227.87	0.73	1.0
pt11-iso14	1002.75	0.83	1.0	pt13-iso14	1228.23	0.73	1.0
pt11-iso15	996.96	0.83	1.0	pt13-iso15	1226.07	0.73	1.0
pt11-iso16	1007.23	0.83	1.0	pt13-iso16	1205.82	0.73	1.0
pt11-iso17	999.57	0.83	1.0	pt13-iso17	1214.67	0.73	1.0
pt11-iso18	986.67	0.83	1.0	pt13-iso18	1213.00	0.73	1.0
pt11-iso19	1005.08	0.83	1.0	pt13-iso19	1209.36	0.73	1.0
pt11-iso20	1004.85	0.83	1.0	pt13-iso20	1205.12	0.73	1.0

Table B.3: Clusters, their corresponding atomization energies ΔE^{at} in kcal/mol, weight factors W^{at} and W^{force} used in the fitting of Pt-Ti and Pt-O repulsive potentials.

Clusters	ΔE^{at}	W^{at}	W^{force}	Clusters	ΔE^{at}	W^{at}	W^{force}
pt1-ti1	147.22	2.97	1.0	pt4-o1-iso3	-	0.00	15.0
pt1-ti2	265.17	2.19	1.0	pt4-oh	-	0.00	1.0
pt2-ti1	298.68	2.19	1.0	pt4-oh_2	-	0.00	1.0
pt2-ti2	421.45	1.77	1.0	pt4-oh2	-	0.00	15.0
pt3-ti1-iso1	398.35	1.77	1.0	pt4-och3	-	0.00	1.0
pt3-ti1-iso2	396.64	1.77	1.0	pt4-och3_2	-	0.00	1.0
pt3-ti2	575.26	1.50	1.0	pt10-o1-iso1	-	0.00	1.0
pt4-ti1-iso1	408.69	1.50	1.0	pt10-o1-iso2	-	0.00	1.0
pt4-ti1-iso2	447.15	1.50	1.0	pt10-o1-iso3	-	0.00	1.0
pt4-ti1-iso3	489.19	1.50	1.0	pt10-o1-iso4	-	0.00	1.0
pt4-ti1-iso4	500.19	1.50	1.0	pt10-oh-iso1	-	0.00	1.0
pt4-ti2	691.43	1.30	1.0	pt10-oh-iso2	-	0.00	1.0
pt5-ti1-iso1	603.59	1.30	1.0	pt10-oh_2-iso1	-	0.00	1.0
pt5-ti1-iso2	601.21	1.30	1.0	pt10-oh_2-iso2	-	0.00	1.0
pt10-ti1-iso1	1109.98	0.83	1.0	pt10-oh2-iso1	-	0.00	15.0
pt10-ti1-iso2	1157.57	0.83	1.0	pt10-oh2-iso2	-	0.00	15.0
pt10-ti1-iso3	1154.16	0.83	1.0	pt10-oh2_2	-	0.00	15.0
pt1-o1	-	0.00	1.0	pt10-och3-iso1	-	0.00	1.0
pt1-o2	-	0.00	1.0	pt10-och3-iso2	-	0.00	1.0
pt1-oh	-	0.00	1.0	pt1-tio2	-	0.00	1.0
pt1-oh_2	-	0.00	1.0	pt1-tio2h2	-	0.00	1.0
pt1-oh2	-	0.00	15.0	pt1-otioh_3	-	0.00	15.0
pt1-och3	-	0.00	1.0	pt1-tio2_3-iso1	-	0.00	15.0
pt1-och3_2	-	0.00	1.0	pt1-tio2_3-iso2	-	0.00	15.0
pt1-co3	-	0.00	1.0	pt1-tio2_4-iso1	-	0.00	15.0
pt1-acac_2	-	0.00	1.0	pt1-tio2_4-iso2	-	0.00	15.0
pt3-o1-iso1	-	0.00	15.0	pt1-tio2_4-iso3	-	0.00	15.0
pt3-o1-iso2	-	0.00	1.0	pt2-tio2_3	-	0.00	1.0
pt3-o2-iso1	-	0.00	1.0	pt2-tio2_4-iso1	-	0.00	1.0
pt3-o2-iso2	-	0.00	15.0	pt2-tio2_4-iso2	-	0.00	1.0
pt3-o2-iso3	-	0.00	15.0	pt4-otioh_3	-	0.00	1.0
pt4-o1-iso1	-	0.00	1.0	pt4-tio2_3	-	0.00	1.0
pt4-o1-iso2	-	0.00	15.0	pt4-tio2_4	-	0.00	1.0

Table B.4: Distorted geometries of Pt_2 cluster, corresponding reaction energies $\Delta E^{\text{react.}}$ (energy of the change in geometry), and weight factors $W^{\text{react.}}$ used in the fitting of Pt-Pt repulsive potential.

Reactions			$\Delta E^{react.}$ (kcal/mol)	$W^{react.}$
pt1-pt1	⇒	pt1-pt1-dm0.5	127.34	1.0
pt1-pt1	⇒	pt1-pt1-dm0.4	70.21	2.0
pt1-pt1	⇒	pt1-pt1-dm0.3	33.76	3.0
pt1-pt1	⇒	pt1-pt1-dm0.2	12.76	4.0
pt1-pt1	⇒	pt1-pt1-dm0.1	2.71	5.0

Table B.5: Distorted geometries, corresponding reaction energies $\Delta E^{\text{react.}}$ (energy of the change in geometry), and weight factors $W^{\text{react.}}$ used in the fitting of Pt-Ti, and Pt-O repulsive potentials.

Reactions			$\Delta E^{react.}$ (kcal/mol)	$W^{react.}$
pt1-ti1	⇒	pt1-ti1-dm0.5	136.92	1.0
pt1-ti1	⇒	pt1-ti1-dm0.4	77.94	2.0
pt1-ti1	⇒	pt1-ti1-dm0.3	38.01	3.0
pt1-ti1	⇒	pt1-ti1-dm0.2	14.46	4.0
pt1-ti1	⇒	pt1-ti1-dm0.1	2.88	5.0
pt10-ti1	⇒	pt10-ti1-dm0.3	13.55	1.0
pt10-ti1	⇒	pt10-ti1-dm0.2	6.07	3.0
pt10-ti1	⇒	pt10-ti1-dm0.1	1.51	5.0
pt10-ti1	⇒	pt10-ti1-dp0.1	1.48	5.0
pt10-ti1	⇒	pt10-ti1-dp0.2	5.76	3.0
pt10-ti1	⇒	pt10-ti1-dp0.3	12.55	1.0
pt1-o1	⇒	pt1-o1-dm0.5	342.03	1.0
pt1-o1	⇒	pt1-o1-dm0.4	175.87	2.0
pt1-o1	⇒	pt1-o1-dm0.3	79.50	3.0
pt1-o1	⇒	pt1-o1-dm0.2	28.38	4.0
pt1-o1	⇒	pt1-o1-dm0.1	5.71	5.0

Table B.6: Reactions, corresponding reaction energies $\Delta E^{\text{react.}}$ in kcal/mol, and weight factors $W^{\text{react.}}$ used in the fitting of Pt-Ti, and Pt-O repulsive potentials. Empirically reaction energy of two reactions were shifted by -11 kcal/mol, the PBE-calculated values are listed in parentheses.

Reactions					$\Delta E^{react.}$	$W^{react.}$
pt1	+	tio5h5	⇒	pt1-vertex-tio5h5-dm0.1	-47.76	10.0
pt1	+	tio5h5	⇒	pt1-vertex-tio5h5	-49.04	30.0
pt1	+	tio5h5	⇒	pt1-vertex-tio5h5-dp0.1	-48.69	1.0
pt1	+	ti2o10h8	⇒	pt1-vertex-ti2o10h8-dm0.1	-66.21	10.0
pt1	+	ti2o10h8	⇒	pt1-vertex-ti2o10h8	-68.52	30.0
pt1	+	ti2o10h8	⇒	pt1-vertex-ti2o10h8-dp0.1	-66.69	1.0
pt1	+	ti2o10h8	⇒	pt1-middle-ti2o10h8-dm0.1	-75.80	10.0
pt1	+	ti2o10h8	⇒	pt1-middle-ti2o10h8	-77.52	30.0
pt1	+	ti2o10h8	⇒	pt1-middle-ti2o10h8-dp0.1	-76.30	1.0
pt4pyramid	+	tio5h5	⇒	pt4-vertex-tio5h5-dm0.1	-48.08	10.0
pt4pyramid	+	tio5h5	⇒	pt4-vertex-tio5h5	-48.77	30.0
pt4pyramid	+	tio5h5	⇒	pt4-vertex-tio5h5-dp0.1	-48.17	1.0
pt4pyramid	+	tio5h5	⇒	pt4-face-tio5h5-dm0.1	-90.95	10.0
pt4pyramid	+	tio5h5	⇒	pt4-face-tio5h5	-92.72	30.0
pt4pyramid	+	tio5h5	⇒	pt4-face-tio5h5-dp0.1	-91.46	1.0
pt4pyramid	+	ti2o10h8	⇒	pt4-vertex-ti2o10h8-dm0.1	-77.99	10.0
pt4pyramid	+	ti2o10h8	⇒	pt4-vertex-ti2o10h8	-80.22	30.0
pt4pyramid	+	ti2o10h8	⇒	pt4-vertex-ti2o10h8-dp0.1	-78.61	1.0
pt4pyramid	+	ti2o10h8	⇒	pt4-middle-ti2o10h8-dm0.1	-86.82	10.0
pt4pyramid	+	ti2o10h8	⇒	pt4-middle-ti2o10h8	-88.39	30.0
pt4pyramid	+	ti2o10h8	⇒	pt4-middle-ti2o10h8-dp0.1	-87.30	1.0
pt4pyramid	+	ti2o10h8	⇒	pt4-face-ti2o10h8-dm0.1	-65.58	10.0
pt4pyramid	+	ti2o10h8	⇒	pt4-face-ti2o10h8	-66.09	30.0
pt4pyramid	+	ti2o10h8	⇒	pt4-face-ti2o10h8-dp0.1	-65.52	1.0
pt1-vertex-ti2o10h8			⇒	pt1-middle-ti2o10h8	-18.00(-9.00)	100.0
pt4-vertex-ti2o10h8			⇒	pt4-middle-ti2o10h8	-17.17(-8.17)	100.0
pt4-face-tio5h5			⇒	pt4-vertex-tio5h5	43.95	1.0
pt4-face-ti2o10h8			⇒	pt4-vertex-ti2o10h8	-14.13	1.0

Table B.7: Additional constrains, and corresponding weight factors used in the fitting of Pt-Ti, and Pt-O repulsive potentials.

Potentials	Distances (Bohr)	Energy (a.u.)	Weights
Pt-Ti	5.102	-0.010358	150.0
Pt-Ti	5.480	-0.011554	150.0
Pt-Ti	5.858	-0.011155	150.0

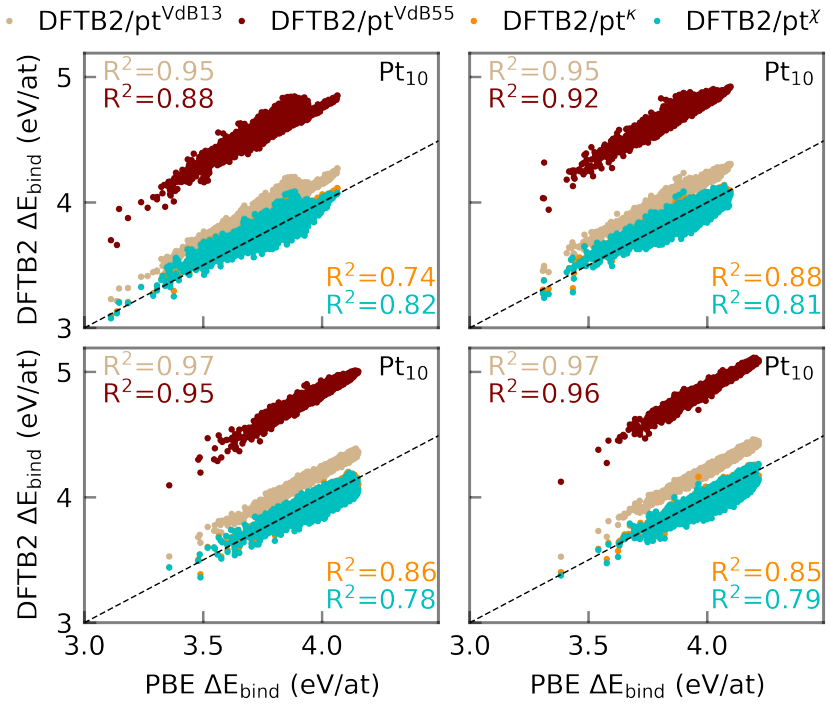

Figure B.1: DFTB2 normalized binding energies ΔE_{bind} comparing to PBE normalized binding energies ΔE_{bind} for $\approx$ 20,000 conformations of Pt_{10}, Pt_{11}, Pt_{12}, and Pt_{13}, clusters; pt^{VdB13} and pt^{VdB55} stands for the parameter sets previously developed by Van den Bossche et al.[72]

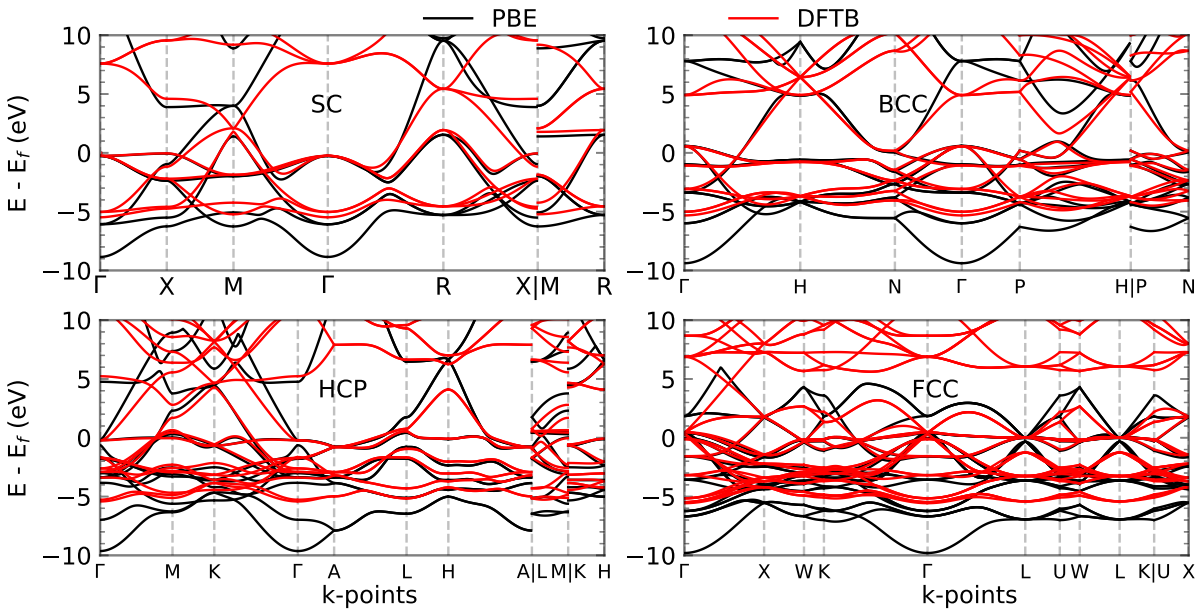

Figure B.2: Band structures computed by DFTB2/pt$^{\text{VdB13}}$ in comparison to the band structures computed by PBE for Pt simple cubic (SC), body-centered cubic (BCC), hexagonal closest packed (HCP), and face-centered cubic (FCC) unit cells.

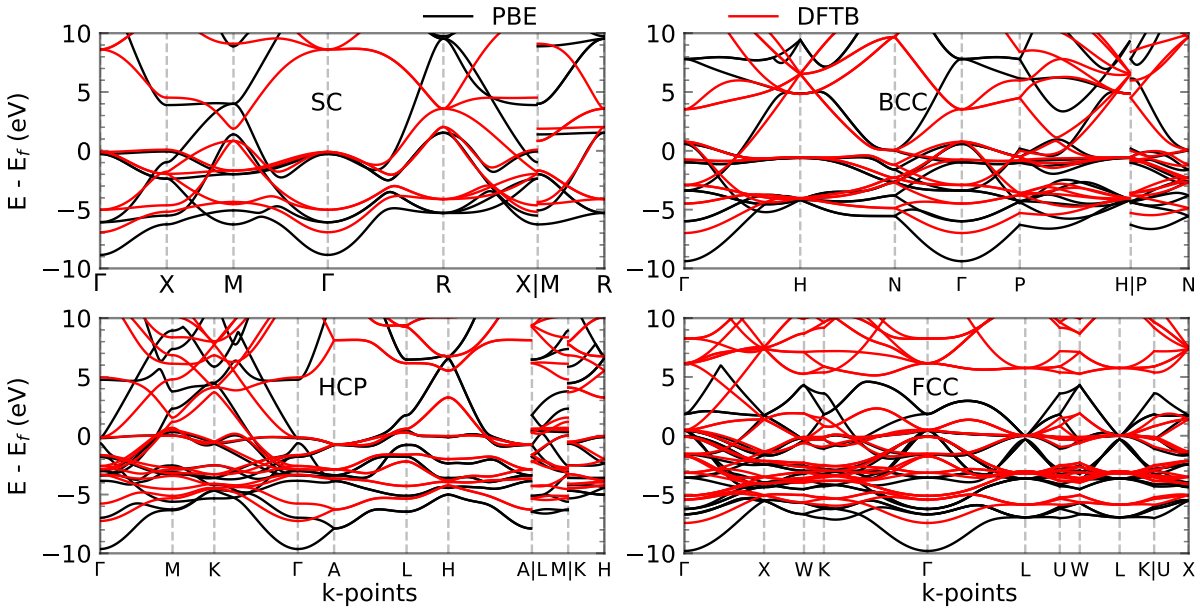

Figure B.3: Band structures computed by DFTB2/pt$^{\text{VdB55}}$ in comparison to the band structures computed by PBE for Pt simple cubic (SC), body-centered cubic (BCC), hexagonal closest packed (HCP), and face-centered cubic (FCC) unit cells.

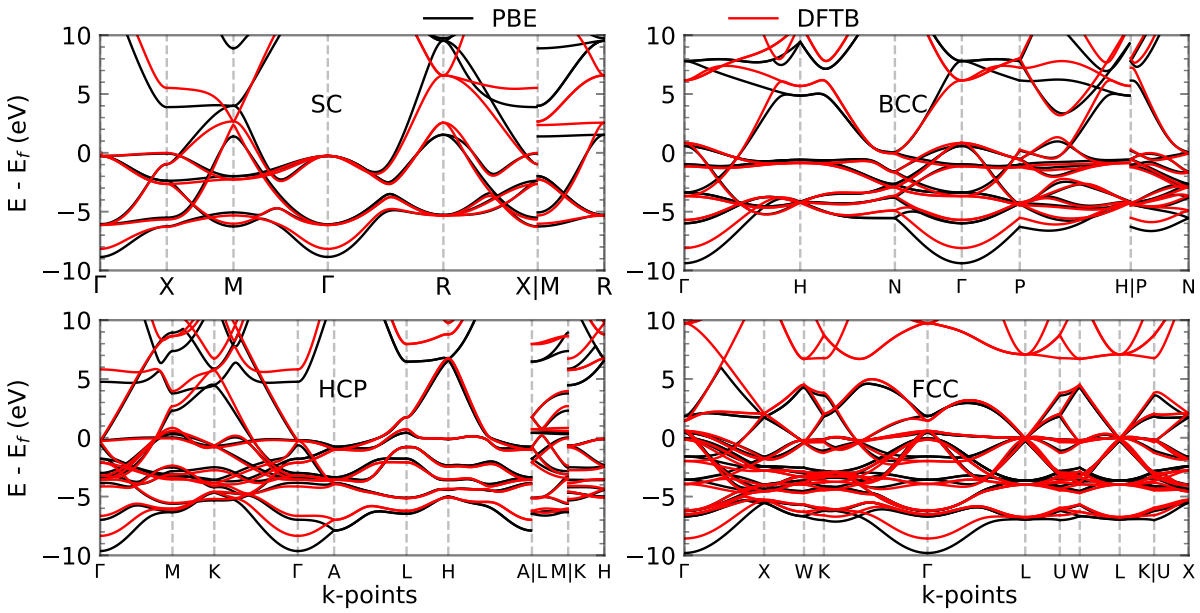

Figure B.4: Band structures computed by DFTB2/pt$^{\text{Shi}}$ in comparison to the band structures computed by PBE for Pt simple cubic (SC), body-centered cubic (BCC), hexagonal closest packed (HCP), and face-centered cubic (FCC) unit cells.

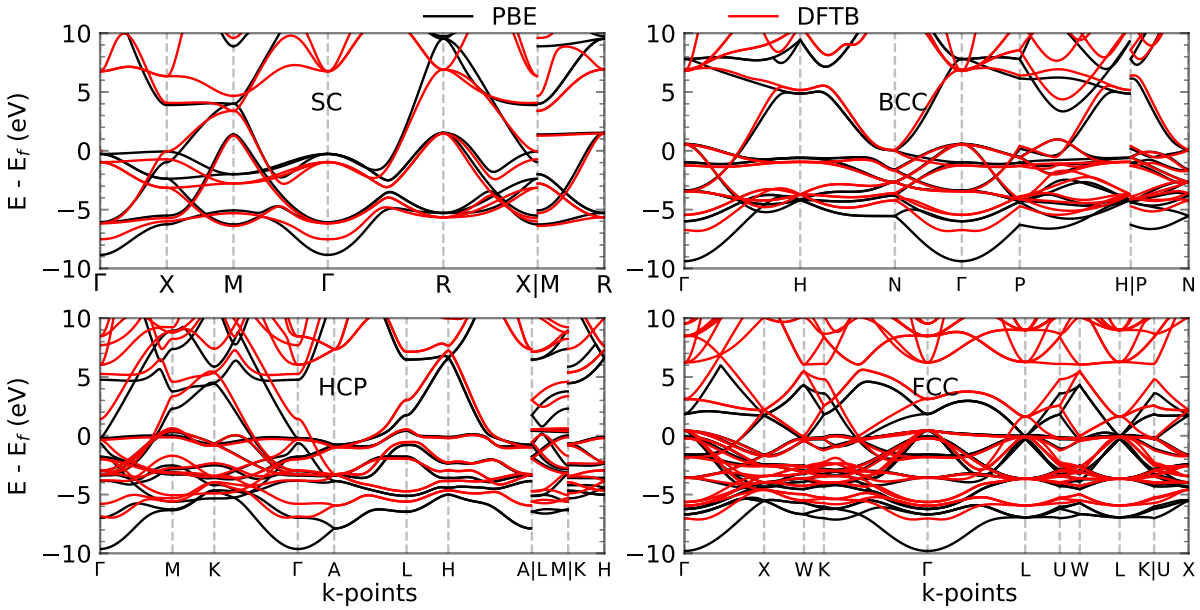

Figure B.5: Band structures computed by DFTB2/pt$^{\text{Lee}}$ in comparison to the band structures computed by PBE for Pt simple cubic (SC), body-centered cubic (BCC), hexagonal closest packed (HCP), and face-centered cubic (FCC) unit cells.

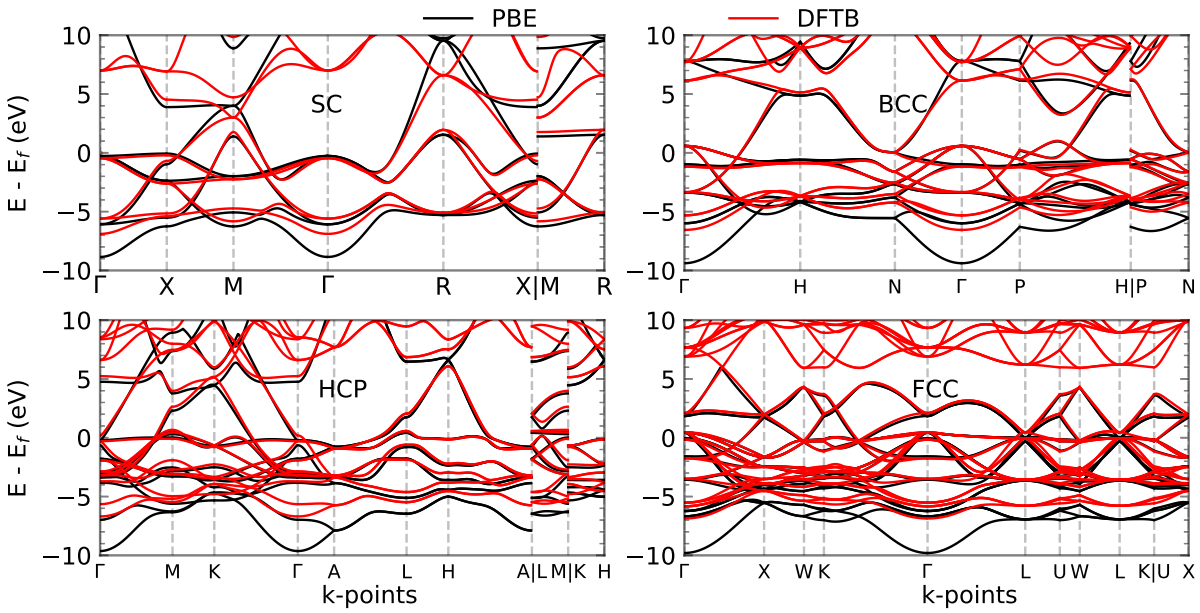

Figure B.6: Band structures computed by DFTB2/pt$^{\alpha}$ in comparison to the band structures computed by PBE for Pt simple cubic (SC), body-centered cubic (BCC), hexagonal closest packed (HCP), and face-centered cubic (FCC) unit cells.

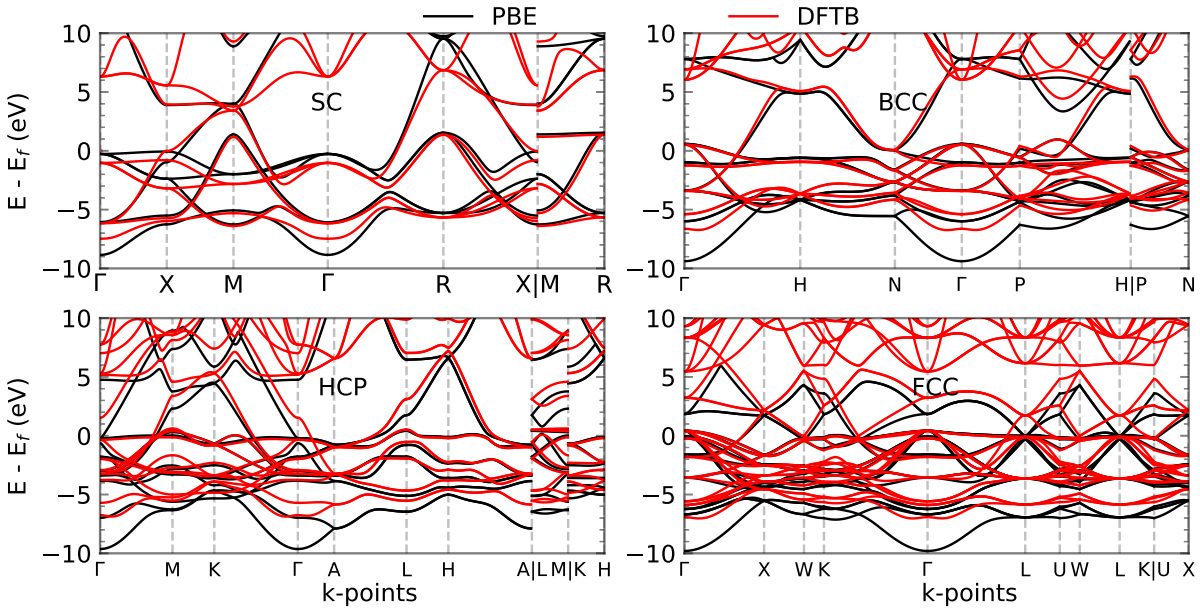

Figure B.7: Band structures computed by DFTB2/pt$^{\kappa}$ in comparison to the band structures computed by PBE for Pt simple cubic (SC), body-centered cubic (BCC), hexagonal closest packed (HCP), and face-centered cubic (FCC) unit cells.

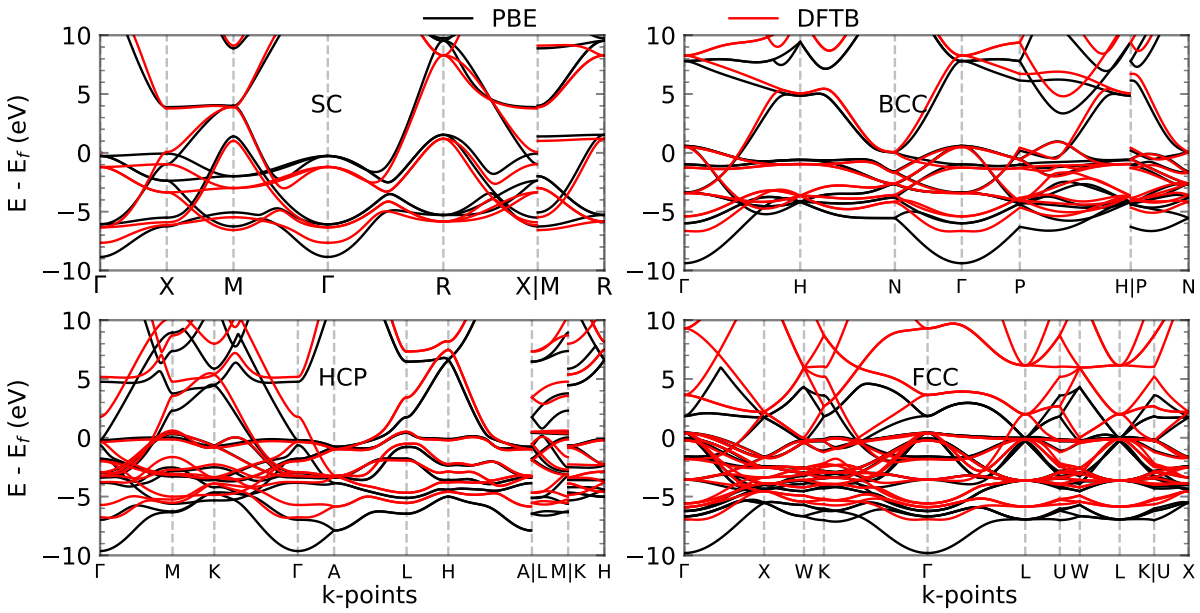

Figure B.8: Band structures computed by DFTB2/pt$^{\chi}$ in comparison to the band structures computed by PBE for Pt simple cubic (SC), body-centered cubic (BCC), hexagonal closest packed (HCP), and face-centered cubic (FCC) unit cells.

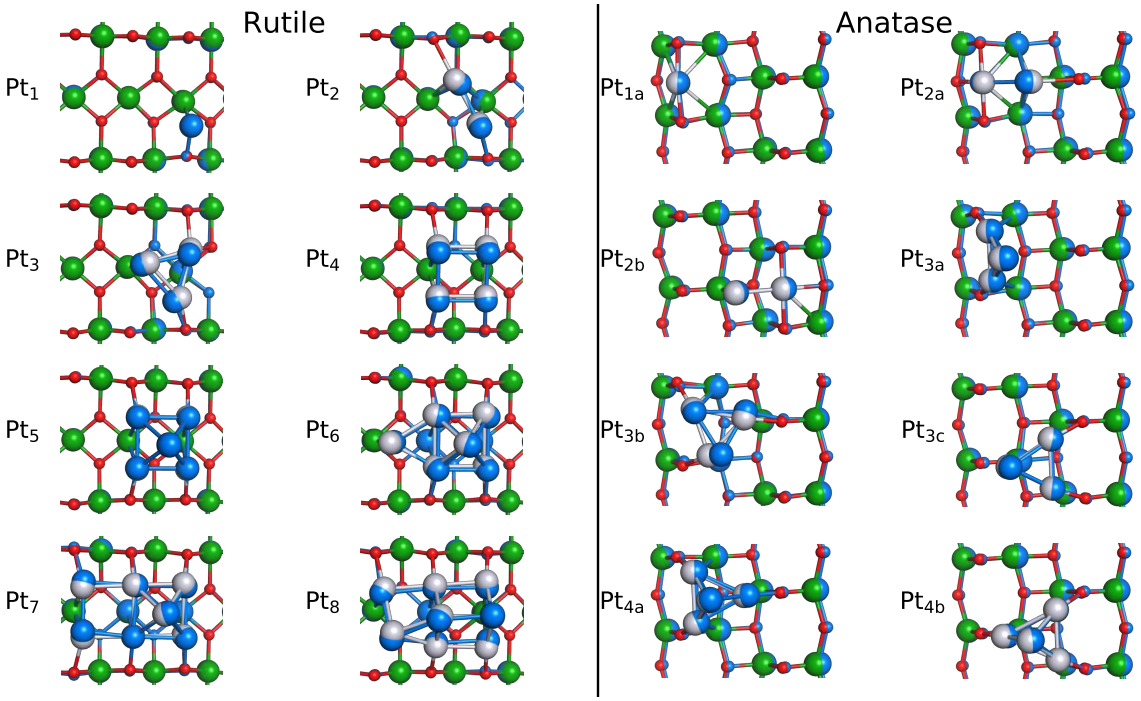

Figure B.9: Overlap of PBE-optimized structures (Pt in grey, Ti in green and O in red) and DFTB/pt$^{\kappa}$-tiorg optimized structures (in sky blue) for Pt_1 to Pt_8 clusters on the TiO_2 rutile (110) surface, and Pt_1 to Pt_4 clusters on the TiO_2 anatase (101) surface.

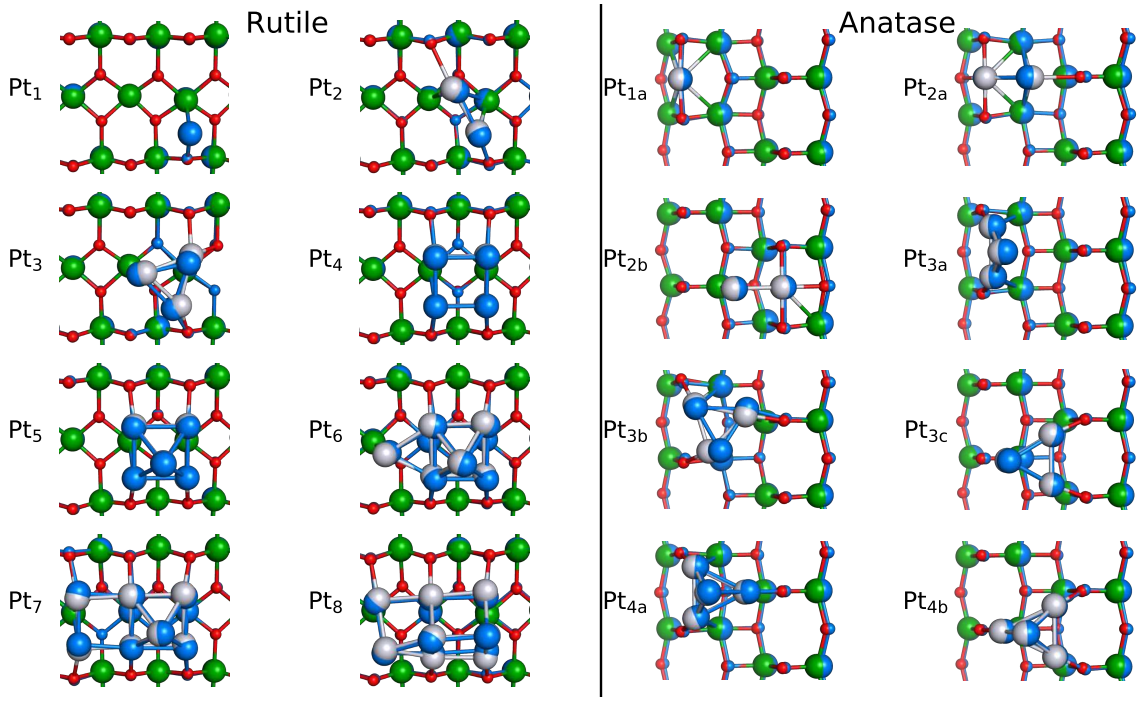

Figure B.10: Overlap of PBE-optimized structures (Pt in grey, Ti in green and O in red) and DFTB/pt$^{\chi}$-tiorg optimized structures (in sky blue) for Pt_1 to Pt_8 clusters on the TiO_2 rutile (110) surface, and Pt_1 to Pt_4 clusters on the TiO_2 anatase (101) surface.

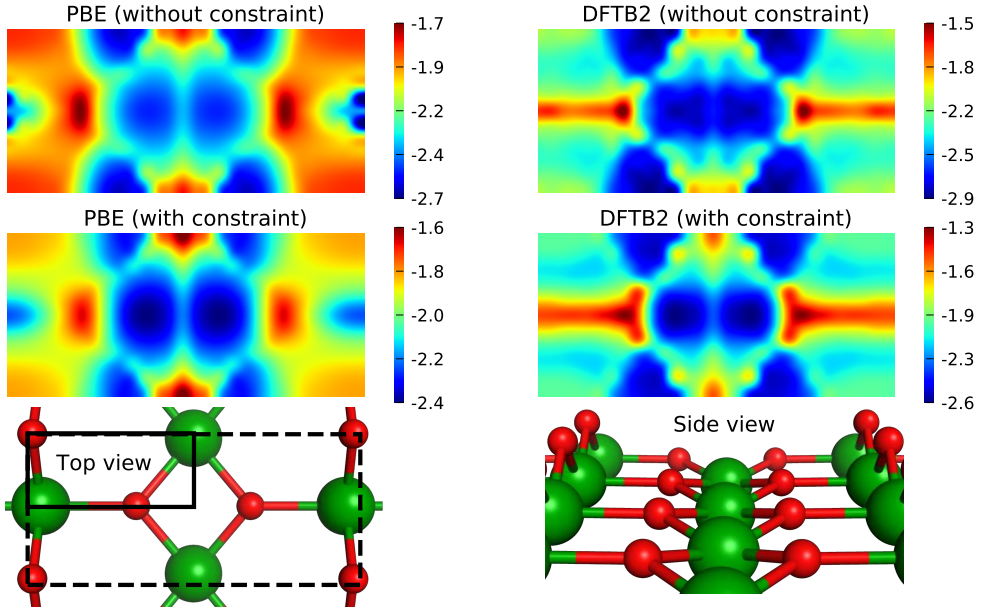

Figure B.11: Energy landscape in eV of Pt atom adsorption on the TiO_2 rutile (110) surface obtained at PBE and DFTB2/pt$^{\kappa}$-tiorg methods. "Without constraint" refers to the geometry optimization with the top two layers of TiO_2 surface were fully optimized, "with constrant" refers to the geometry optimization with only few selected Ti and O atoms nearby the Pt single atom were optimized.

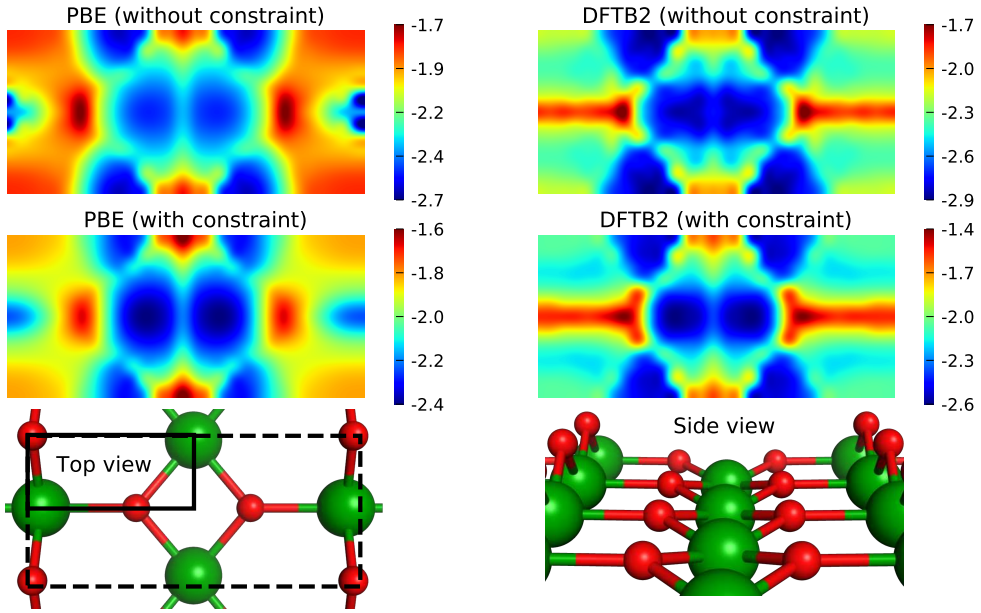

Figure B.12: Energy landscape in eV of Pt atom adsorption on the TiO_2 rutile (110) surface obtained at PBE and DFTB2/pt$^{\chi}$-tiorg methods. "Without constraint" refers to the geometry optimization with the top two layers of TiO_2 surface were fully optimized, "with constrant" refers to the geometry optimization with only few selected Ti and O atoms nearby the Pt single atom were optimized.

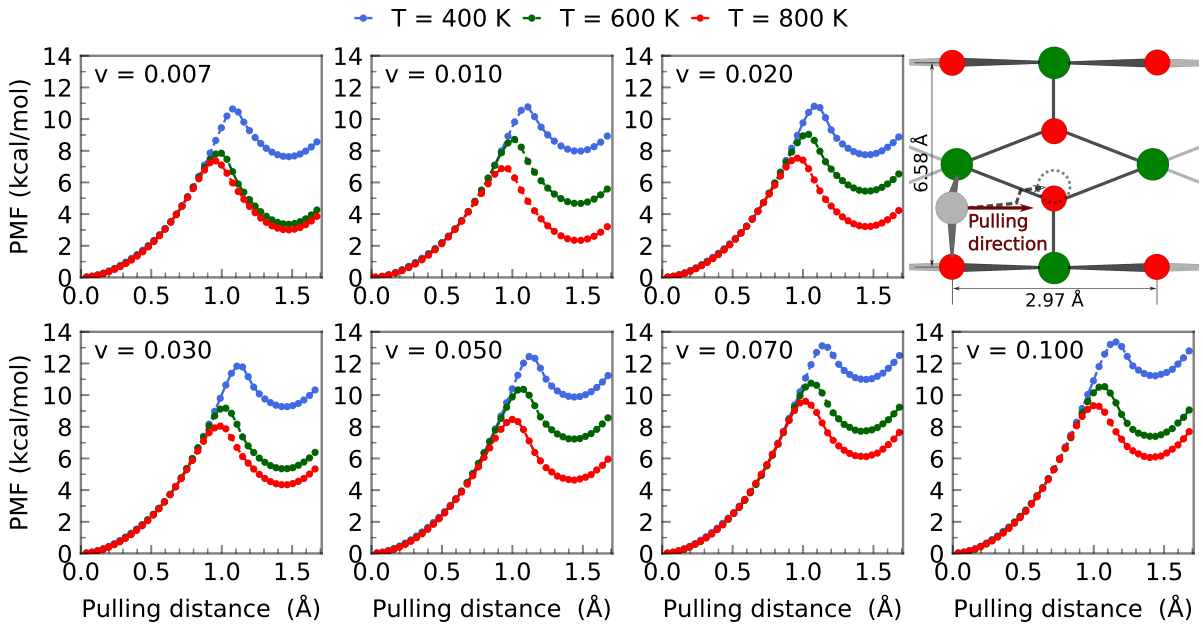

Figure B.13: Potential of mean force (PMF) of single Pt atom transport on the TiO_2 rutile (110) surface at three different temperatures computed by the steered molecular dynamics (SMD) method with various pulling speed.

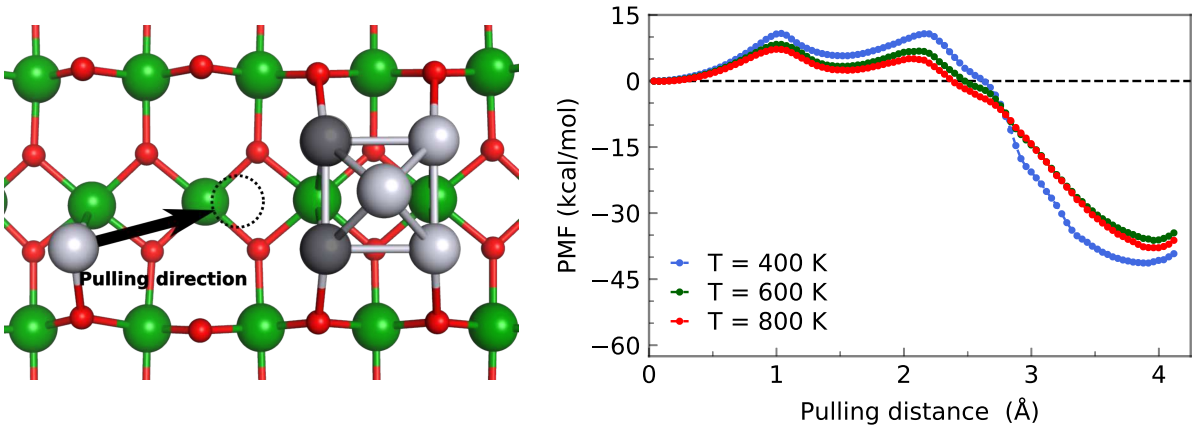

Figure B.14: Potential of mean force (PMF) of a nucleation of Pt_6 from Pt_5 and nearby single Pt atom on the TiO_2 rutile (110) surface at three different temperatures computed by the steered molecular dynamics (SMD) method. An additional restraint was applied on the Pt_5 cluster to reduce its dynamic along the reaction coordinate, pulling speed $v = 0.10$ Å/ns.

C Supporting Information for "The Fragment Molecular Orbital Method Based on Long-Range Corrected Density-Functional Tight-Binding"

Electrostatic Dimer Approximation within FMO-LC-DFTB

The coupling of the charge transfer to the embedding potential ΔE_{IJ}^{V} in FMO-LC-DFTB is defined as

$$\Delta E_{IJ}^{V} = \sum_{a \in IJ} \sum_{K \neq I,J} \sum_{c \in K} \gamma_{ac} \Delta\Delta q_a^{IJ} \Delta q_c^{K} \quad . \tag{1}$$

The $\Delta\Delta q_a^{IJ}$ is the difference between the Mulliken charge of atom 'a' in monomer and dimer calculations

$$\Delta\Delta q_a^{IJ} = \Delta q_a^{IJ} - \Delta q_a^{I} \delta_{a \in I} - \Delta q_a^{J} \delta_{a \in J}, \tag{2}$$

where $\delta_{a \in I} = 1$ when atom a belongs to fragment I, and otherwise it is zero. The inter-fragment charge transfer is short-ranged, so it is negligible if the inter-fragment distance of two fragments is larger than a certain threshold. In these cases, the electrostatic dimer (ES-DIM) approximation[41,121] is used for saving computational time. The energy of the separated dimer is given by

$$\begin{aligned}
E_{IJ}^{'} \approx & E_{I}^{'} + E_{J}^{'} + \sum_{a \in I} \sum_{b \in J} (E_{ab}^{\mathrm{rep}} + \gamma_{ab} \Delta q_a^{I} \Delta q_b^{J}) \\
& - \frac{1}{16} \sum_{(\mu \odot \alpha) \oslash (\nu \odot \beta)} \Delta D_{\mu\nu}^{IJ} \Delta D_{\alpha\beta}^{IJ} S_{\mu\alpha}^{I} S_{\beta\nu}^{J} (\gamma_{\mu\beta}^{\mathrm{lr}} + \gamma_{\mu\nu}^{\mathrm{lr}} + \gamma_{\alpha\beta}^{\mathrm{lr}} + \gamma_{\alpha\nu}^{\mathrm{lr}}) \\
& - \frac{1}{16} \sum_{\mu \odot \alpha, \nu \oslash \beta} \Delta D_{\mu\nu}^{IJ} \Delta D_{\alpha\beta}^{IJ} S_{\mu\alpha}^{I} S_{\beta\nu}^{IJ} (\gamma_{\mu\beta}^{\mathrm{lr}} + \gamma_{\mu\nu}^{\mathrm{lr}} + \gamma_{\alpha\beta}^{\mathrm{lr}} + \gamma_{\alpha\nu}^{\mathrm{lr}}) \\
& - \frac{1}{16} \sum_{\mu \oslash \alpha, \nu \odot \beta} \Delta D_{\mu\nu}^{IJ} \Delta D_{\alpha\beta}^{IJ} S_{\mu\alpha}^{IJ} S_{\beta\nu}^{J} (\gamma_{\mu\beta}^{\mathrm{lr}} + \gamma_{\mu\nu}^{\mathrm{lr}} + \gamma_{\alpha\beta}^{\mathrm{lr}} + \gamma_{\alpha\nu}^{\mathrm{lr}}) \\
& - \frac{1}{16} \sum_{\mu \oslash \alpha, \nu \oslash \beta} \Delta D_{\mu\nu}^{IJ} \Delta D_{\alpha\beta}^{IJ} S_{\mu\alpha}^{IJ} S_{\beta\nu}^{IJ} (\gamma_{\mu\beta}^{\mathrm{lr}} + \gamma_{\mu\nu}^{\mathrm{lr}} + \gamma_{\alpha\beta}^{\mathrm{lr}} + \gamma_{\alpha\nu}^{\mathrm{lr}}),
\end{aligned} \tag{3}$$

where $\mu, \alpha, \nu, \beta \in IJ$, $\mu \odot \nu$ means μ and ν are in the same monomers (I or J), and $\mu \oslash \nu$ means μ and ν are in different monomers. The orbital overlap $S_{\mu\nu}$ is short-ranged, so $S_{\mu\nu} \approx 0$ if μ and ν belongs to two far separated fragments. On the other hand, assuming that molecular orbitals are only localized on a fragment when the inter-fragment distance of two separated fragments is large, $\Delta D^{IJ}_{\mu\nu} \approx 0$ if μ and ν belongs to two different fragments. Consequently, the contributions of the last four terms of Equation 3 can be neglected. The total energy of the dimer is approximately rewritten as

$$E'_{IJ} \approx E'_I + E'_J + \sum_{a \in I} \sum_{b \in J} (E^{\mathrm{rep}}_{ab} + \gamma_{ab} \Delta q^I_a \Delta q^J_b). \tag{4}$$

The repulsion energy E^{rep}_{ab} is also short-ranged, so it can also be neglected,[41]

$$E'_{IJ} \approx E'_I + E'_J + \sum_{a \in I} \sum_{b \in J} \gamma_{ab} \Delta q^I_a \Delta q^J_b. \tag{5}$$

This expression is identical to that of the ES-DIM energy of the original FMO-DFTB.[41]

Coupled-Perturbed LC-DFTB Equation

In FMO-LC-DFTB, the Hamiltonian matrix of fragment X is defined as

$$\begin{aligned}
H^X_{\mu\nu} &= H^{0,X}_{\mu\nu} + \frac{1}{2} S^X_{\mu\nu} \sum_{c \in X} (\gamma_{ac} + \gamma_{bc}) \Delta q_c \\
&\quad - \frac{1}{8} \sum_{\rho\sigma \in X} S^X_{\mu\rho} \Delta D^X_{\rho\sigma} S^X_{\sigma\nu} \left(\gamma^{\mathrm{lr}}_{ad} + \gamma^{\mathrm{lr}}_{ab} + \gamma^{\mathrm{lr}}_{cd} + \gamma^{\mathrm{lr}}_{bc} \right) + V^X_{\mu\nu} \\
&= H^{0,X}_{\mu\nu} + \frac{1}{4} S^X_{\mu\nu} \sum_{\rho\sigma \in X} (\gamma_{\mu\rho} + \gamma_{\nu\rho} + \gamma_{\mu\sigma} + \gamma_{\nu\sigma}) S^X_{\rho\sigma} \Delta D^X_{\rho\sigma} \\
&\quad - \frac{1}{8} \sum_{\rho\sigma \in X} S^X_{\mu\rho} \Delta D^X_{\rho\sigma} S^X_{\sigma\nu} \left(\gamma^{\mathrm{lr}}_{\mu\sigma} + \gamma^{\mathrm{lr}}_{\mu\nu} + \gamma^{\mathrm{lr}}_{\rho\sigma} + \gamma^{\mathrm{lr}}_{\rho\nu} \right) + V^X_{\mu\nu} \\
&= H^{0,X}_{\mu\nu} + \sum_{\rho\sigma \in X} (\mu\nu|\rho\sigma)^{X,X} \Delta D^X_{\rho\sigma} - \frac{1}{2} \sum_{\rho\sigma \in X} (\mu\rho|\sigma\nu)^{\mathrm{lr},X} \Delta D^X_{\rho\sigma} + V^X_{\mu\nu} \\
&= H^{0,X}_{\mu\nu} + \sum_{\rho\sigma \in X} \left\{ (\mu\nu|\rho\sigma)^{X,X} - \frac{1}{2} (\mu\rho|\sigma\nu)^{\mathrm{lr},X} \right\} \Delta D^X_{\rho\sigma} + V^X_{\mu\nu} \ ,
\end{aligned} \tag{6}$$

for $\mu \in a$, $\nu \in b$, $\rho \in c$, and $\sigma \in d$, where $(\mu\nu|\rho\sigma)^{X,Y}$ and $(\mu\nu|\rho\sigma)^{\mathrm{lr},X}$ are the Coulombic and exchange-type integrals, respectively:

$$(\mu\nu|\rho\sigma)^{X,Y} = \frac{1}{4} S^X_{\mu\nu} S^Y_{\rho\sigma} \left(\gamma_{\mu\rho} + \gamma_{\nu\rho} + \gamma_{\mu\sigma} + \gamma_{\nu\sigma}\right) \tag{7}$$

and

$$(\mu\nu|\rho\sigma)^{\mathrm{lr},X} = \frac{1}{4} S^X_{\mu\nu} S^X_{\rho\sigma} \left(\gamma^{\mathrm{lr}}_{\mu\rho} + \gamma^{\mathrm{lr}}_{\nu\rho} + \gamma^{\mathrm{lr}}_{\mu\sigma} + \gamma^{\mathrm{lr}}_{\nu\sigma}\right) \quad . \tag{8}$$

$V^X_{\mu\nu}$ is the electrostatic potential exerted by the fragments other than fragment X:

$$V^X_{\mu\nu} = \sum_{K \neq X} V^{X(K)}_{\mu\nu} = \sum_{K \neq X} (\mu\nu|\rho\sigma)^{X,K} \Delta D^K_{\rho\sigma} \ , \tag{9}$$

where

$$V^{X(K)}_{\mu\nu} = \frac{1}{2} S^X_{\mu\nu} \sum_{c \in K} \left(\gamma_{ac} + \gamma_{bc}\right) \Delta q^K_c \quad . \tag{10}$$

The projection operator $P^X_{\mu\nu}$ is included in $H^{0,X}_{\mu\nu}$.

We derive the coupled-perturbed LC-DFTB equation from the diagonality condition of the Hamiltonian matrix:

$$\sum_{\mu\nu \in X} c^X_{\mu i} c^X_{\nu j} H^X_{\mu\nu} = 0 \quad (i \neq j) \quad . \tag{11}$$

The diagonal elements define the eigenvalue ε^X_i. Following the standard analytic derivative technique,[264] we arrive at the following condition for $i \neq j$:

$$\frac{\partial}{\partial r_a} \sum_{\mu\nu \in X} c^X_{\mu i} c^X_{\nu j} H^X_{\mu\nu} = U^{r_a,X}_{ij} \left(\varepsilon^X_i - \varepsilon^X_j\right) - \varepsilon^X_j S^{r_a,X}_{ij} + H^{r_a,X}_{ij} = 0, \tag{12}$$

where

$$\frac{\partial c^X_{\mu i}}{\partial r_a} = \sum_{m \in X}^{\text{all}} c^X_{\mu m} U^{r_a,X}_{mi} \tag{13}$$

and

$$H^{r_a,X}_{ij} = \sum_{\mu\nu \in X} c^X_{\mu i} c^X_{\nu j} \frac{\partial H^X_{\mu\nu}}{\partial r_a} \ . \tag{14}$$

Similarly, from the orthonormality of the overlap matrix, we obtain

$$U_{ij}^{r_a,X} + U_{ji}^{r_a,X} + S_{ij}^{r_a,X} = 0 \ , \tag{15}$$

where

$$S_{ij}^{r_a,X} = \sum_{\mu\nu\in X} c_{\mu i}^X c_{\nu j}^X \frac{\partial S_{\mu\nu}^X}{\partial r_a} \ . \tag{16}$$

Using the definition eq. 13, the derivative of the density atrix is written by

$$\begin{aligned} \frac{\partial D_{\mu\nu}^X}{\partial r_a} &= 2\frac{\partial}{\partial r_a}\sum_{i\in X}^{\text{occ.}} c_{\mu i}^X c_{\nu i}^X \\ &= 2\sum_{i\in X}^{\text{occ.}}\sum_{m\in X}^{\text{vir.}} \left(c_{\mu m}^X c_{\nu i}^X + c_{\mu i}^X c_{\nu m}^X\right) U_{mi}^{r_a,X} - \sum_{ij\in X}^{\text{occ.}} \left(c_{\mu i}^X c_{\nu j}^X + c_{\mu j}^X c_{\nu i}^X\right) S_{ij}^{r_a,X} \ . \end{aligned} \tag{17}$$

Now, by differentiating each term of eq 14 one by one, we obtain

$$\begin{aligned} H_{ij}^{r_a,X} &= \sum_{\mu\nu\in X} c_{\mu i}^X c_{\nu j}^X \left[\frac{\partial H_{\mu\nu}^{0,X}}{\partial r_a} + \sum_{\rho\sigma\in X} \left\{ \frac{\partial \left(\mu\nu|\rho\sigma\right)^{X,X}}{\partial r_a} - \frac{1}{2}\frac{\partial \left(\mu\rho|\sigma\nu\right)^{\text{lr},X}}{\partial r_a} \right\} \Delta D_{\rho\sigma}^X \right. \\ &\quad \left. + \sum_{\rho\sigma\in X} \left\{ \left(\mu\nu|\rho\sigma\right)^{X,X} - \frac{1}{2}\left(\mu\rho|\sigma\nu\right)^{\text{lr},X} \right\} \frac{\partial \Delta D_{\rho\sigma}^X}{\partial r_a} + \frac{\partial V_{\mu\nu}^X}{\partial r_a} \right] \\ &= H_{ij}^{0,r_a,X} + \sum_{\rho\sigma\in X} \left(\left(ij|\rho\sigma\right)^{X,X} - \frac{1}{2}\left(i\rho|\sigma j\right)^{\text{lr},X} \right) \Delta D_{\rho\sigma}^X \\ &\quad + 2\sum_{k\in X}^{\text{vir.}}\sum_{l\in X}^{\text{occ.}} U_{kl}^{r_a,X} \left\{ 2\left(ij|kl\right)^{X,X} - \frac{1}{2}\left(\left(ik|lj\right)^{\text{lr},X} + \left(il|kj\right)^{\text{lr},X} \right) \right\} \\ &\quad - \sum_{kl\in X}^{\text{occ.}} \left\{ 2\left(ij|kl\right)^{X,X} - \frac{1}{2}\left(\left(ik|lj\right)^{\text{lr},X} + \left(il|kj\right)^{\text{lr},X} \right) \right\} S_{kl}^{r_a,X} \\ &\quad + \sum_{K\neq X}\sum_{\rho\sigma\in K} \left(ij|\rho\sigma\right)^{r_a,X,K} \Delta D_{\rho\sigma}^K + 4\sum_{K\neq X}^{\text{vir.}}\sum_{k\in K}^{\text{occ.}}\sum_{l\in K} U_{kl}^{r_a,K} \left(ij|kl\right)^{X,K} \\ &\quad - 2\sum_{K\neq X}\sum_{kl\in X}^{\text{occ.}} \left(ij|kl\right)^{X,K} S_{kl}^{r_a,K} \quad . \end{aligned} \tag{18}$$

By combining eqs 12, 15, and 18 and collecting $\mathbf{U}^{r_a,X}$ terms, it is possible to write the coupled-perturbed LC-DFTB equation in the following form:

$$\sum_{K}^{N}\sum_{k\in K}^{\text{vir.}}\sum_{l\in K}^{\text{occ.}} A_{ij,kl}^{X,K} U_{kl}^{r_a,K} = B_{ij}^{r_a,X}, \tag{19}$$

where

$$A_{ij,kl}^{X,K} = \delta_{XK}\delta_{ik}\delta_{jl}\left(\varepsilon_j^X - \varepsilon_i^X\right) - 4\,(ij|kl)^{X,K} + \delta_{XK}\,(ik|lj)^{\text{lr},X} + \delta_{XK}\,(il|kj)^{\text{lr},X} \tag{20}$$

and

$$\begin{aligned} B_{ij}^{r_a,X} = H_{ij}^{0,r_a,X} - \varepsilon_j^X S_{ij}^{r_a,X} + \sum_{\rho\sigma\in X}\sum_{K}^{N}\left((ij|\rho\sigma)^{r_a,X,K} - \frac{\delta_{XK}}{2}\,(i\rho|\sigma j)^{\text{lr},r_a,X}\right)\Delta D_{\rho\sigma}^{K} \\ - \sum_{K}^{N}\sum_{kl\in K}^{\text{occ.}}\left\{2\,(ij|kl)^{X,K} - \frac{\delta_{XK}}{2}\left((ik|lj)^{\text{lr},X} + (il|kj)^{\text{lr},X}\right)\right\} S_{kl}^{r_a,K}\ . \end{aligned} \tag{21}$$

Self-Consistent Z-Vector Equation

As in the case of the standard FMO, it is possible to avoid explicitly solving coupled-perturbed equations by solving the following Z-vector equation instead:

$$\sum_{I}^{N}\sum_{i\in I}^{\text{vir.}}\sum_{j\in I}^{\text{occ.}} Z_{ij}^{I} A_{ij,kl}^{I,K} = \mathcal{L}_{kl}^{K}\ , \tag{22}$$

where

$$\begin{aligned} \mathcal{L}_{kl}^{K} &= \sum_{I>J}^{N}\sum_{K\neq I,J}^{N}\Delta L_{kl}^{IJ,K} \\ &= \sum_{I>J}^{N}\sum_{K\neq I,J}^{N}\Delta V_{kl}^{K(IJ)} \\ &= \sum_{I>J}^{N}\sum_{K\neq I,J}^{N}\left(V_{ij}^{K(IJ)} - V_{ij}^{K(I)} - V_{ij}^{K(J)}\right) \quad . \end{aligned} \tag{23}$$

Inspecting the orbital rotation Hessian for (FMO-)LC-DFTB,

$$A_{ij,kl}^{X,K} = \widetilde{A}_{ij,kl}^{X,K} + \delta_{XK}\,(ik|lj)^{\mathrm{lr},X} + \delta_{XK}\,(il|kj)^{\mathrm{lr},X} \quad , \tag{24}$$

where $\widetilde{A}_{ij,kl}^{X,K}$ is the orbital rotation Hessian of the standard DFTB, we notice that the difference between those of DFTB with and without long-range corrections is the two additional terms of the long-range part in the diagonal ($X = K$) contribution.

As described in the original self-consistent Z-vector paper,[230] the computation of this term is facilitated using symmetrized $Z_{\mu\nu}$. After solving the Z-vector equation, the response contribution is finally computed by

$$\begin{aligned} R^{r_a} &= \sum_{K}^{N} \sum_{k\in K}^{\text{vir.}} \sum_{l\in K}^{\text{occ.}} U_{kl}^{r_a,K} \mathcal{L}_{kl}^{K} \\ &= \sum_{K}^{N} \sum_{k\in K}^{\text{vir.}} \sum_{l\in K}^{\text{occ.}} U_{kl}^{r_a,K} \sum_{I}^{N} \sum_{i\in I}^{\text{vir.}} \sum_{j\in I}^{\text{occ}} Z_{ij}^{I} A_{ij,kl}^{I,K} \\ &= \sum_{I}^{N} \sum_{i\in I}^{\text{vir.}} \sum_{j\in I}^{\text{occ}} Z_{ij}^{I} \left(\sum_{K}^{N} \sum_{k\in K}^{\text{vir.}} \sum_{l\in K}^{\text{occ}} A_{ij,kl}^{I,K} U_{kl}^{r_a,K} \right) \\ &= \sum_{I}^{N} \sum_{i\in I}^{\text{vir.}} \sum_{j\in I}^{\text{occ.}} Z_{ij}^{I} B_{ij}^{r_a,I} \quad , \end{aligned} \tag{25}$$

and the response contribution can thus be computed without solving coupled-perturbed equations for each derivative parameter.

LC-DFTB Hybrid Orbitals used for sp^3 Carbon Atoms

LC-DFTB 4 4

1 0	0.52152787	0.00000000	0.00000000	0.85323425
0 1	0.52152784	0.40221915	0.69666272	-0.28441084
0 1	-0.52152808	0.80443699	0.00000000	0.28441097
0 1	-0.52152784	-0.40221915	0.69666272	0.28441084

Table C. 1: Comparisons of mean square error (RMSE), mean absolute deviation (MAD), maximum of absolute deviation (MAX) for bond lengths, angles and dihedral angles of α-helix and extended form of COMe–$(Ala)_{20}$–NHMe optimized by FMO(2,3)-LC-DFTB and LC-DFTB.

Structures	Methods	Properties	Bond length (Å)	Angle (∘)	Dihedral angle (∘)
α-helix					
	FMO2($nres$=1)	MSE	0.000	0.003	-0.043
		MAD	0.000	0.057	0.691
		MAX	0.003	0.425	10.413
	FMO2($nres$=2)	MSE	0.000	0.001	-0.014
		MAD	0.000	0.038	0.437
		MAX	0.001	0.322	8.384
	FMO3($nres$=1)	MSE	0.000	0.000	0.001
		MAD	0.000	0.013	0.139
		MAX	0.000	0.114	3.295
	FMO3($nres$=2)	MSE	0.000	0.000	0.004
		MAD	0.000	0.011	0.126
		MAX	0.000	0.102	3.130
extended form					
	FMO2($nres$=1)	MSE	0.000	-0.005	-0.014
		MAD	0.000	0.033	0.309
		MAX	0.001	0.255	7.431
	FMO2($nres$=2)	MSE	0.000	-0.002	-0.010
		MAD	0.000	0.014	0.190
		MAX	0.000	0.157	4.809
	FMO3($nres$=1)	MSE	0.000	-0.002	-0.008
		MAD	0.000	0.015	0.195
		MAX	0.000	0.172	5.215
	FMO3($nres$=2)	MSE	0.000	0.000	0.000
		MAD	0.000	0.000	0.000
		MAX	0.000	0.000	0.000

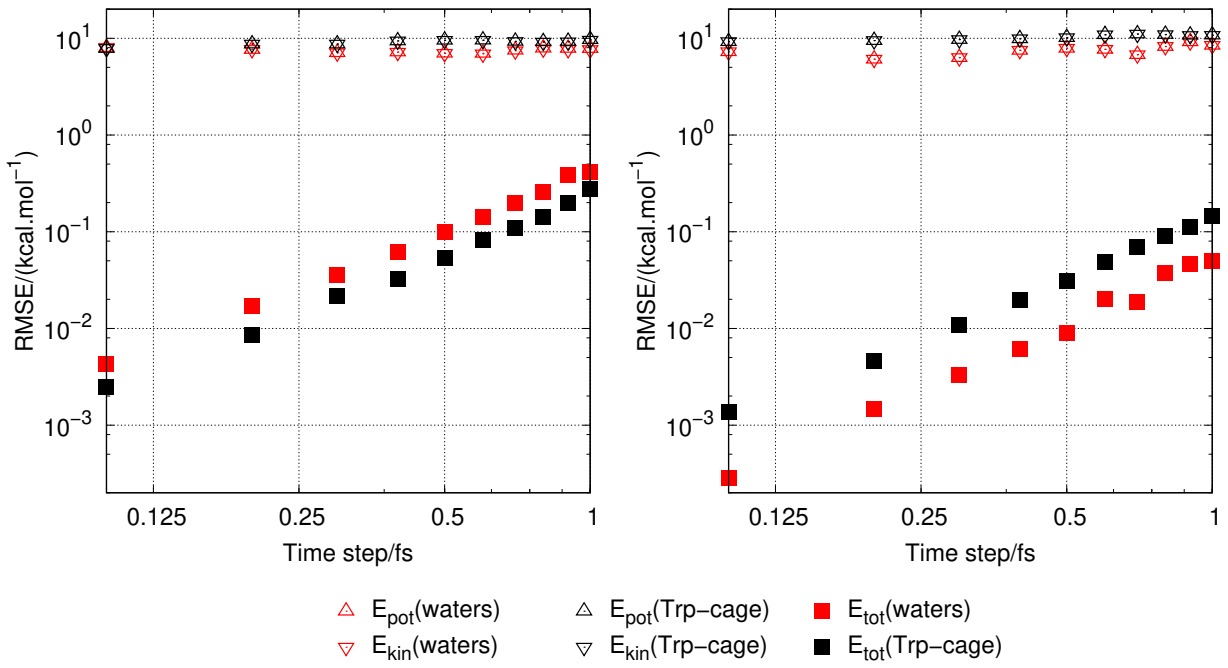

Figure C. 1: The root mean square error (RMSE) of FMO2-LC-DFTB total energy ΔE_{tot}, potential energy ΔE_{pot} and kinetic energy ΔE_{kin}, versus time step from the simulations of 64 water cluster and Trp-cage protein.

Table C. 2: Comparisons for energies and geometries of Trp-cage and Chignolin optimized by LC-DFTB and structures reoptimized by FMO2-LC-DFTB and FMO3-LC-DFTB.

Methods	ΔE(kcal/mol)		RMSD(Å)	
	Trp-cage	Chignolin	Trp-cage	Chignolin
FMO2($nres$=1)	1.140	0.699	0.033	0.026
FMO2($nres$=2)	-0.036	1.301	0.015	0.024
FMO3($nres$=1)	0.830	0.204	0.003	0.026
FMO3($nres$=2)	0.516	0.177	0.003	0.013

Protonation Preparation for MD Simulation of the Trp-cage Protein in the Gas Phase

For protonation state RCK: the N terminal was neutralized, residues Lys8, Aps9, and Arg16 were protonated, and residue Gln5 and C terminal were deprotonated. For protonation state RDK: the N and C terminals were neutralized, residues Lys8 and Arg16 were protonated, residues Gln5 and Asp9 was deprotonated. For protonation state RCQ: the N terminal was neutralized, residues Gln5, Aps9, and Arg16 were protonated, and residue Lys8 and C terminal were deprotonated. For protonation state RDQ: the N and C terminals were neutralized, residues Gln5 and Arg16 were protonated, residues Lys8 and Asp9 was deprotonated.

Cartesian Coordinates of 20-residue Polyalanine

α-helix

C -0.056 0.702 1.229	H 4.804 -2.759 3.589	H 6.275 -3.806 5.302	N 9.370 -4.226 11.203	C 13.604 -5.206 15.818
C 0.026 0.070 2.597	H 5.363 -0.680 2.413	H 5.610 -5.446 5.487	C 10.803 -3.938 11.164	O 14.424 -5.689 16.596
O 1.115 -0.093 3.137	H 3.648 -0.239 2.316	N 6.881 -2.159 7.774	C 11.238 -2.995 12.303	C 12.429 -6.671 14.096
H 0.948 0.960 0.893	H 4.255 -1.667 1.443	C 7.713 -1.133 8.403	O 12.263 -3.234 12.938	H 10.631 -5.015 14.607
H -0.659 1.607 1.285	N 3.178 -0.476 5.348	C 7.542 -1.103 9.934	C 11.149 -3.367 9.784	H 12.206 -6.770 16.223
H -0.506 0.002 0.527	C 3.153 0.160 6.666	O 8.532 -1.010 10.658	H 8.799 -3.921 10.422	H 13.287 -7.345 14.086
N -1.121 -0.320 3.152	C 3.246 -0.872 7.808	C 7.387 0.221 7.763	H 11.349 -4.874 11.292	H 12.556 -5.923 13.313
C -1.229 -0.818 4.529	O 4.006 -0.675 8.754	H 6.153 -1.856 7.136	H 12.224 -3.191 9.721	H 11.524 -7.247 13.898
C -0.302 -2.012 4.841	C 1.891 1.025 6.769	H 8.760 -1.363 8.198	H 10.624 -2.426 9.622	N 13.751 -3.975 15.315
O 0.260 -2.079 5.930	H 2.360 -0.399 4.755	H 8.032 0.990 8.189	H 10.860 -4.077 9.007	C 14.857 -3.088 15.676
C -2.697 -1.170 4.797	H 4.022 0.815 6.751	H 6.346 0.486 7.950	N 10.439 -1.970 12.619	C 14.812 -2.675 17.160
H -1.976 -0.142 2.649	H 1.891 1.553 7.723	H 7.557 0.172 6.686	C 10.682 -1.083 13.756	O 15.845 -2.674 17.827
H -0.946 -0.010 5.207	H 0.999 0.400 6.712	N 6.313 -1.253 10.440	C 10.578 -1.823 15.103	C 14.831 -1.872 14.742
H -2.809 -1.501 5.831	H 1.874 1.756 5.960	C 6.044 -1.364 11.873	O 11.422 -1.625 15.977	H 13.075 -3.644 14.635
H -3.023 -1.971 4.132	N 2.543 -2.005 7.695	C 6.660 -2.638 12.484	C 9.705 0.096 13.673	H 15.796 -3.620 15.516
H -3.326 -0.292 4.643	C 2.642 -3.114 8.644	O 7.254 -2.577 13.559	H 9.634 -1.783 12.031	H 15.677 -1.222 14.967
N -0.076 -2.916 3.880	C 4.039 -3.762 8.642	C 4.528 -1.299 12.092	H 11.697 -0.690 13.679	H 13.905 -1.312 14.878
C 0.855 -4.036 4.043	O 4.589 -4.028 9.709	H 5.524 -1.273 9.802	H 9.904 0.793 14.489	H 14.902 -2.201 13.704
C 2.324 -3.582 4.177	C 1.540 -4.131 8.322	H 6.498 -0.510 12.379	H 8.677 -0.259 13.752	N 13.623 -2.393 17.705
O 3.070 -4.145 4.975	H 1.884 -2.093 6.930	H 4.313 -1.332 13.161	H 9.833 0.617 12.723	C 13.440 -2.111 19.128
C 0.666 -4.995 2.862	H 2.465 -2.727 9.649	H 4.040 -2.143 11.605	N 9.604 -2.726 15.260	C 13.764 -3.332 20.010
H -0.562 -2.820 3.004	H 1.571 -4.943 9.050	H 4.134 -0.370 11.680	C 9.480 -3.578 16.443	O 14.423 -3.186 21.037
H 0.600 -4.572 4.960	H 1.686 -4.543 7.323	N 6.594 -3.774 11.781	C 10.663 -4.554 16.583	C 12.007 -1.610 19.346
H 1.325 -5.857 2.986	H 0.563 -3.648 8.373	C 7.246 -5.016 12.197	O 11.192 -4.723 17.681	H 12.809 -2.354 17.101
H 0.912 -4.495 1.924	N 4.654 -3.952 7.468	C 8.782 -4.893 12.203	C 8.135 -4.312 16.377	H 14.127 -1.313 19.415
H -0.366 -5.347 2.828	C 6.028 -4.444 7.358	O 9.428 -5.344 13.147	H 8.902 -2.813 14.532	H 11.869 -1.349 20.396
N 2.733 -2.532 3.455	C 7.049 -3.470 7.977	C 6.765 -6.150 11.284	H 9.478 -2.942 17.329	H 11.291 -2.386 19.075
C 4.070 -1.952 3.580	O 7.951 -3.901 8.693	H 6.050 -3.784 10.925	H 8.006 -4.916 17.276	H 11.827 -0.725 18.734
C 4.227 -1.174 4.898	C 6.330 -4.728 5.882	H 6.935 -5.246 13.218	H 8.104 -4.963 15.503	N 13.374 -4.541 19.591
O 5.268 -1.270 5.544	H 4.139 -3.777 6.613	H 7.205 -7.093 11.610	H 7.321 -3.589 16.315	C 13.733 -5.783 20.275
C 4.348 -1.074 2.353	H 6.104 -5.384 7.907	H 7.062 -5.956 10.253	N 11.135 -5.144 15.479	C 15.248 -6.058 20.227
H 2.059 -2.034 2.892	H 7.333 -5.146 5.790	H 5.678 -6.230 11.334	C 12.326 -5.993 15.467	O 15.834 -6.437 21.238

C 12.921 -6.930 19.662
H 12.785 -4.602 18.767
H 13.454 -5.693 21.327
H 13.142 -7.857 20.193
H 13.178 -7.053 18.610
H 11.855 -6.717 19.748
N 15.903 -5.804 19.088
C 17.356 -5.912 18.957
C 18.098 -4.888 19.837
O 19.099 -5.232 20.460
C 17.724 -5.767 17.476
H 15.367 -5.544 18.267
H 17.662 -6.905 19.291
H 18.801 -5.894 17.356
H 17.438 -4.781 17.112
H 17.210 -6.530 16.891
N 17.585 -3.658 19.953
C 18.123 -2.648 20.865
C 17.926 -3.032 22.345
O 18.838 -2.855 23.150
C 17.479 -1.297 20.532
H 16.795 -3.405 19.370
H 19.198 -2.566 20.696
H 17.906 -0.524 21.170
H 16.402 -1.343 20.698
H 17.671 -1.044 19.488
N 16.776 -3.615 22.702
C 16.508 -4.132 24.047
C 17.370 -5.360 24.413
O 17.614 -5.604 25.592
C 15.010 -4.443 24.152
H 16.038 -3.690 22.011
H 16.746 -3.351 24.771
H 14.777 -4.773 25.165
H 14.743 -5.235 23.451
H 14.428 -3.549 23.925
N 17.863 -6.104 23.417
C 18.831 -7.189 23.584
C 20.304 -6.715 23.635
O 21.201 -7.539 23.820
C 18.589 -8.212 22.466
H 17.549 -5.903 22.476
H 18.632 -7.684 24.536
H 19.241 -9.074 22.612
H 18.809 -7.761 21.497
H 17.550 -8.543 22.483
N 20.567 -5.410 23.475
C 21.905 -4.826 23.487
H 19.786 -4.785 23.322
H 21.830 -3.740 23.424
H 22.473 -5.202 22.634
H 22.419 -5.104 24.408

Extended form

C 0.324 1.847 -1.405
C 0.476 0.723 -0.407
O 1.133 -0.269 -0.694
H 0.867 1.587 -2.313
H 0.735 2.762 -0.983
H -0.731 1.984 -1.636
N -0.137 0.882 0.763
C -0.148 -0.109 1.840
C -1.471 -0.057 2.626
O -2.184 0.946 2.586
C 1.060 0.142 2.755
H -0.696 1.709 0.909
H -0.053 -1.107 1.407
H 1.088 -0.607 3.547
H 0.988 1.134 3.203
H 1.981 0.074 2.175
N -1.786 -1.129 3.356
C -2.967 -1.242 4.211
C -2.669 -2.109 5.449
O -1.704 -2.873 5.457
C -4.123 -1.821 3.383
H -1.136 -1.901 3.390
H -3.254 -0.248 4.560
H -5.024 -1.885 3.994
H -3.862 -2.818 3.025
H -4.325 -1.174 2.528
N -3.506 -2.001 6.483
C -3.418 -2.785 7.716
C -4.820 -3.052 8.295
O -5.780 -2.366 7.946
C -2.529 -2.032 8.717
H -4.309 -1.395 6.397
H -2.956 -3.749 7.497
H -2.426 -2.614 9.633
H -2.972 -1.064 8.955
H -1.538 -1.878 8.287
N -4.931 -4.036 9.190
C -6.164 -4.396 9.889
C -5.860 -4.907 11.310
O -4.728 -5.291 11.605
C -6.913 -5.450 9.060
H -4.098 -4.531 9.475
H -6.798 -3.511 9.980
H -7.852 -5.711 9.549
H -6.302 -6.348 8.958
H -7.134 -5.051 8.069
N -6.872 -4.926 12.179
C -6.789 -5.432 13.550
C -8.128 -6.060 13.983
O -9.164 -5.802 13.371
C -6.382 -4.279 14.478
H -7.790 -4.648 11.864
H -6.023 -6.208 13.601
H -6.284 -4.641 15.502
H -7.136 -3.491 14.448
H -5.422 -3.870 14.159
N -8.105 -6.867 15.045
C -9.282 -7.504 15.637
C -9.118 -7.648 17.162
O -8.003 -7.576 17.678
C -9.499 -8.866 14.963
H -7.234 -7.000 15.538
H -10.160 -6.881 15.452
H -10.391 -9.345 15.368
H -8.636 -9.511 15.137
H -9.634 -8.729 13.889
N -10.224 -7.868 17.875
C -10.259 -8.093 19.320
C -11.398 -9.058 19.696
O -12.324 -9.266 18.911
C -10.412 -6.738 20.027
H -11.104 -7.969 17.389
H -9.317 -8.546 19.637
H -10.409 -6.880 21.109
H -11.350 -6.266 19.731
H -9.580 -6.085 19.758
N -11.337 -9.633 20.899
C -12.354 -10.530 21.451
C -12.455 -10.369 22.979
O -11.540 -9.841 23.612
C -12.005 -11.973 21.058
H -10.581 -9.384 21.520
H -13.326 -10.278 21.023
H -12.768 -12.656 21.434
H -11.038 -12.251 21.478
H -11.963 -12.059 19.971
N -13.556 -10.838 23.568
C -13.804 -10.830 25.010
C -14.637 -12.056 25.430
O -15.277 -12.691 24.591
C -14.507 -9.517 25.383
H -14.248 -11.308 23.002
H -12.850 -10.876 25.539
H -14.674 -9.476 26.460
H -15.467 -9.448 24.870
H -13.883 -8.669 25.094
N -14.639 -12.376 26.725
C -15.411 -13.469 27.316
C -15.858 -13.112 28.747
O -15.303 -12.204 29.365
C -14.558 -14.745 27.294
H -14.137 -11.786 27.373
H -16.308 -13.640 26.718
H -15.127 -15.581 27.702
H -13.655 -14.602 27.890
H -14.277 -14.983 26.266
N -16.847 -13.837 29.273
C -17.365 -13.685 30.633
C -17.829 -15.041 31.197
O -18.048 -15.988 30.441
C -18.510 -12.661 30.613
H -17.227 -14.604 28.737
H -16.572 -13.306 31.280
H -18.891 -12.509 31.624
H -19.320 -13.019 29.976
H -18.145 -11.707 30.230
N -17.991 -15.127 32.518
C -18.479 -16.311 33.227
C -19.302 -15.907 34.465
O -19.207 -14.773 34.933
C -17.278 -17.188 33.609
H -17.847 -14.301 33.081
H -19.131 -16.884 32.564
H -17.622 -18.092 34.112
H -16.612 -16.639 34.276
H -16.730 -17.474 32.710
N -20.093 -16.839 35.000
C -20.902 -16.660 36.206
C -21.005 -17.978 36.996
O -20.744 -19.052 36.455
C -22.286 -16.136 35.798
H -20.087 -17.768 34.604
H -20.426 -15.919 36.851
H -22.897 -15.965 36.686
H -22.786 -16.862 35.155
H -22.180 -15.192 35.261
N -21.400 -17.895 38.269
C -21.607 -19.038 39.158
C -22.753 -18.761 40.149
O -23.138 -17.610 40.350
C -20.290 -19.340 39.888
H -21.653 -16.991 38.642
H -21.882 -19.911 38.563
H -20.413 -20.210 40.534
H -19.995 -18.483 40.495
H -19.505 -19.553 39.161
N -23.283 -19.814 40.775
C -24.336 -19.743 41.789
C -24.157 -20.851 42.844
O -23.449 -21.829 42.606
C -25.700 -19.843 41.091
H -22.888 -20.729 40.609
H -24.278 -18.780 42.301
H -26.502 -19.761 41.826
H -25.785 -20.801 40.575
H -25.805 -19.033 40.367
N -24.809 -20.702 43.998
C -24.805 -21.673 45.093
C -26.156 -21.670 45.833
O -26.931 -20.721 45.713
C -23.643 -21.343 46.041
H -25.417 -19.904 44.115
H -24.648 -22.674 44.687
H -23.602 -22.073 46.850
H -23.779 -20.347 46.466
H -22.700 -21.374 45.493
N -26.428 -22.723 46.607
C -27.631 -22.871 47.427
C -27.320 -23.650 48.719
O -26.299 -24.332 48.805
C -28.714 -23.571 46.592
H -25.730 -23.446 46.708
H -27.997 -21.883 47.711
H -29.631 -23.665 47.175
H -28.374 -24.566 46.299
H -28.926 -22.985 45.697
N -28.208 -23.561 49.711
C -28.112 -24.273 50.986
C -29.511 -24.637 51.517
O -30.510 -24.059 51.089
C -27.340 -23.396 51.984
H -29.053 -23.028 49.562
H -27.558 -25.201 50.839
H -27.230 -23.922 52.933
H -27.877 -22.462 52.153
H -26.348 -23.175 51.590
N -29.578 -25.581 52.458
C -30.807 -26.019 53.120
C -30.529 -26.424 54.580
O -29.382 -26.675 54.950
C -31.412 -27.180 52.318
H -28.719 -25.981 52.807
H -31.523 -25.194 53.132
H -32.348 -27.502 52.776
H -30.717 -28.020 52.295
H -31.618 -26.855 51.297
N -31.579 -26.503 55.400
C -31.517 -26.926 56.800
C -32.802 -27.674 57.203
O -33.828 -27.548 56.537
C -31.284 -25.689 57.678
H -32.503 -26.338 55.027
H -30.676 -27.609 56.931
H -31.204 -25.983 58.725
H -32.116 -24.991 57.566
H -30.358 -25.194 57.381
N -32.745 -28.441 58.300
C -33.876 -29.207 58.820
H -31.870 -28.489 58.798
H -33.586 -29.746 59.723
H -34.214 -29.922 58.067
H -34.703 -28.533 59.052

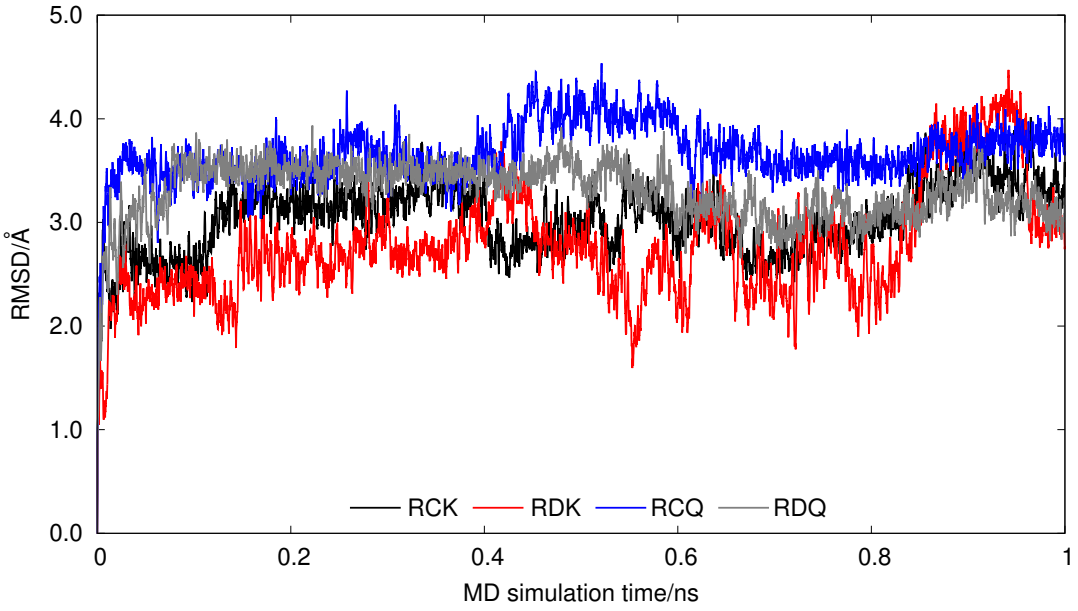

Figure C. 2: The root-mean-square deviations (RMSD) of backbone structure (consisting of C, Cα, N, O atoms) of the Trp-cage protonation states RCK, RDK, RCQ and RDQ compared to the NMR solvated structure as a function of MD simulation time.

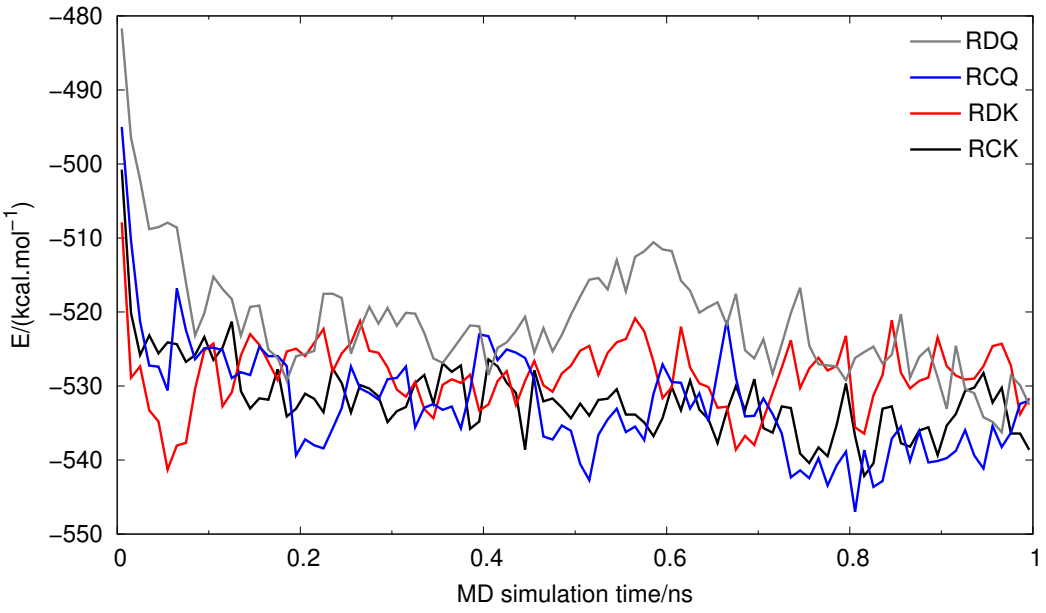

Figure C. 3: Averaged potential energy of the Trp-cage protonation states RCK, RDK, RCQ and RDQ as a function of MD simulation time.

Optimal Cartesian Coordinates of RCK and RDK Protonation States of the Trp-cage Protein

RCK

N -5.042 5.065 -2.397
C -5.125 3.865 -1.532
C -4.397 4.072 -0.214
O -4.712 3.412 0.805
C -4.506 2.586 -2.203
C -5.409 1.938 -3.226
N -5.856 2.690 -4.269
O -5.738 0.731 -3.101
H -6.188 3.669 -1.318
H -3.539 2.869 -2.705
H -4.273 1.840 -1.421
H -5.311 3.541 -4.538
H -6.374 2.230 -5.011
H -5.425 4.866 -3.328
H -4.060 5.343 -2.547
N -3.351 4.936 -0.192
C -2.353 4.942 0.910
C -2.136 3.513 1.390
O -1.724 2.647 0.590
C -2.643 5.989 2.017
C -1.340 6.733 2.425
C -0.224 5.738 2.811
C -0.868 7.645 1.273
H -3.059 5.429 -1.047
H -1.397 5.239 0.420
H -3.371 6.722 1.648
H -3.093 5.507 2.901
H -1.565 7.361 3.304
H -0.519 5.106 3.657
H 0.015 5.080 1.955
H 0.695 6.283 3.081
H -0.794 7.066 0.334
H -1.574 8.465 1.111
H 0.122 8.069 1.497
N -2.340 3.189 2.704
C -2.019 1.827 3.211
C -2.557 0.744 2.292
O -1.931 -0.337 2.163
C -2.564 1.670 4.651
C -2.230 0.353 5.350
C -1.228 -0.529 4.898
C -2.949 0.013 6.515
C -0.974 -1.736 5.566
C -2.688 -1.178 7.204
C -1.702 -2.058 6.725
O -1.448 -3.228 7.373
H -2.632 3.910 3.365
H -0.908 1.716 3.251
H -2.164 2.503 5.253
H -3.656 1.803 4.641
H -0.643 -0.288 3.996
H -3.723 0.687 6.880
H -0.196 -2.410 5.210
H -3.245 -1.433 8.105
H -2.010 -3.299 8.162
N -3.759 0.892 1.673
C -4.247 -0.254 0.862
C -3.230 -0.686 -0.180
O -3.174 -1.883 -0.560
C -5.604 0.025 0.146
C -6.587 0.788 1.070
C -6.186 -1.327 -0.317
C -6.946 -0.010 2.331
H -4.211 1.817 1.558
H -4.409 -1.105 1.559
H -5.400 0.660 -0.744
H -6.130 1.755 1.341
H -7.502 1.012 0.503
H -7.017 -1.194 -1.020
H -5.401 -1.936 -0.810
H -6.542 -1.894 0.560
H -7.416 -0.964 2.057
H -6.040 -0.249 2.918
H -7.636 0.549 2.969
N -2.491 0.278 -0.802
C -1.510 -0.076 -1.869
C -0.223 -0.708 -1.321
O 0.711 -1.018 -2.093
C -1.218 1.153 -2.768
C -1.030 0.759 -4.252
C -2.382 0.510 -4.895
N -3.153 1.595 -5.123
O -2.778 -0.654 -5.171
H -2.386 1.202 -0.345
H -1.993 -0.871 -2.480
H -2.051 1.886 -2.702
H -0.320 1.679 -2.396
H -0.527 1.579 -4.781
H -0.400 -0.139 -4.332
H -2.888 2.527 -4.708
H -4.103 1.494 -5.470
N -0.179 -0.917 0.020
C 0.793 -1.769 0.762
C 0.079 -3.079 1.112
O 0.329 -4.151 0.525
C 1.269 -1.043 2.048
C 2.024 0.251 1.802
C 2.956 0.534 0.815
C 1.924 1.439 2.618
C 2.811 2.397 2.057
C 1.190 1.770 3.784
N 3.420 1.823 0.968
C 2.966 3.686 2.614
C 1.337 3.045 4.329
C 2.214 3.998 3.746
H -1.005 -0.647 0.582
H 1.655 -1.974 0.102
H 0.378 -0.830 2.682
H 1.911 -1.742 2.623
H 3.342 -0.095 0.011
H 4.158 2.270 0.410
H 0.545 1.020 4.258
H 3.682 4.392 2.186
H 0.785 3.317 5.229
H 2.309 4.982 4.207
N -0.884 -3.003 2.077
C -1.521 -4.213 2.666
C -1.935 -5.237 1.609
O -1.667 -6.434 1.797
C -2.653 -3.803 3.644
C -3.715 -2.832 3.057
C -4.830 -3.526 2.245
C -4.351 -1.970 4.167
H -1.094 -2.086 2.500
H -0.744 -4.734 3.274
H -3.129 -4.705 4.049
H -2.166 -3.279 4.495
H -3.168 -2.142 2.380
H -4.408 -4.177 1.465
H -5.470 -4.133 2.894
H -5.459 -2.764 1.749
H -4.920 -2.586 4.870
H -3.582 -1.415 4.729
H -5.042 -1.235 3.716
N -2.628 -4.848 0.485
C -2.991 -5.889 -0.521
C -1.925 -6.038 -1.601
O -1.836 -7.064 -2.288
C -4.353 -5.598 -1.197
C -4.369 -4.198 -1.844
C -5.280 -4.073 -3.083
C -5.610 -2.599 -3.380
N -4.432 -1.699 -3.173
H -2.764 -3.861 0.236
H -3.057 -6.838 0.034
H -4.523 -6.370 -1.960
H -5.165 -5.686 -0.462
H -4.679 -3.444 -1.091
H -3.340 -3.922 -2.142
H -4.788 -4.535 -3.950
H -6.223 -4.614 -2.928
H -5.975 -2.463 -4.406
H -6.389 -2.240 -2.687
H -3.664 -1.794 -3.887
H -4.768 -0.695 -3.181
H -3.990 -1.883 -2.233
N -1.108 -4.952 -1.819
C 0.029 -5.066 -2.769
C 1.251 -5.664 -2.070
O 2.395 -5.207 -2.228
C 0.349 -3.721 -3.458
C -0.835 -2.950 -3.985
O -1.913 -2.821 -3.386
O -0.635 -2.329 -5.141
H -1.015 -4.260 -1.069
H -0.299 -5.796 -3.532
H 0.847 -3.042 -2.735
H 1.071 -3.892 -4.265
H -1.439 -1.743 -5.320
N 1.004 -6.749 -1.270
C 2.095 -7.519 -0.649
C 2.153 -7.461 0.863
O 3.073 -8.063 1.472
H 0.051 -7.124 -1.242
H 2.033 -8.572 -0.962
H 3.045 -7.123 -1.046
N 1.211 -6.763 1.544
C 1.246 -6.654 3.021
C 2.598 -6.147 3.497
O 2.966 -4.975 3.265
H 0.521 -6.185 1.049
H 0.451 -5.945 3.318
H 1.022 -7.633 3.476
N 3.410 -6.993 4.188
C 4.785 -6.571 4.588
C 5.557 -5.952 3.425
O 6.309 -4.977 3.591
C 5.450 -7.874 5.099
C 4.284 -8.828 5.434
C 3.150 -8.421 4.479
H 4.711 -5.828 5.399
H 6.078 -8.309 4.308
H 6.097 -7.689 5.964
H 4.567 -9.880 5.318
H 3.969 -8.685 6.476
H 3.180 -8.997 3.537
H 2.150 -8.548 4.920
N 5.464 -6.580 2.204
C 6.202 -6.055 1.020
C 5.638 -4.740 0.478
O 6.048 -4.272 -0.602
C 6.342 -7.144 -0.062
O 5.079 -7.651 -0.486
H 4.686 -7.235 2.017
H 7.217 -5.800 1.375
H 6.837 -6.720 -0.947
H 6.965 -7.975 0.322
H 4.540 -7.916 0.303
N 4.755 -4.072 1.273
C 4.383 -2.640 1.146
C 5.353 -1.891 0.250
O 4.932 -1.252 -0.731
C 4.349 -2.032 2.571
O 5.601 -2.192 3.231
H 4.427 -4.523 2.145
H 3.368 -2.554 0.700
H 4.126 -0.952 2.513
H 3.543 -2.522 3.154
H 5.771 -3.153 3.393
N 6.681 -1.852 0.602
C 7.705 -1.586 -0.435
C 7.313 -0.479 -1.406
O 7.354 -0.667 -2.638
H 6.969 -2.455 1.374
H 8.641 -1.293 0.063
H 7.901 -2.513 -0.998
N 7.048 0.749 -0.862
C 6.822 1.996 -1.628
C 6.477 3.104 -0.643
O 6.093 2.840 0.511
C 5.720 1.862 -2.717
C 4.362 1.341 -2.182
C 3.676 0.375 -3.174
N 4.587 -0.754 -3.495
C 4.403 -2.025 -3.063
N 3.182 -2.486 -2.747
N 5.475 -2.857 -3.087
H 6.907 0.849 0.146
H 7.761 2.280 -2.148
H 5.601 2.846 -3.203
H 6.100 1.167 -3.483
H 4.526 0.792 -1.236
H 3.680 2.183 -1.944
H 2.750 -0.039 -2.739
H 3.405 0.900 -4.105
H 5.583 -0.473 -3.542
H 2.385 -1.842 -2.623
H 3.035 -3.469 -2.460
H 6.386 -2.378 -3.095
H 5.451 -3.692 -2.491
N 6.639 4.387 -1.078
C 6.134 5.552 -0.306
C 4.644 5.408 -0.008
O 3.956 4.521 -0.542
C 6.397 6.777 -1.225
C 7.375 6.286 -2.313
C 7.134 4.771 -2.413
H 6.692 5.646 0.644
H 5.456 7.109 -1.685
H 6.795 7.630 -0.660
H 7.216 6.796 -3.270
H 8.412 6.480 -2.006
H 6.379 4.521 -3.185
H 8.047 4.202 -2.656
N 4.103 6.336 0.837
C 2.623 6.512 0.993
C 1.975 6.601 -0.391
O 2.190 7.584 -1.116
C 2.474 7.805 1.823
C 3.855 8.068 2.459

C 4.868 7.405 1.512
H 2.224 5.630 1.553
H 2.189 8.636 1.161
H 1.678 7.694 2.581
H 4.051 9.139 2.590
H 3.910 7.602 3.453
H 5.264 8.119 0.766
H 5.733 6.973 2.042
N 1.169 5.575 -0.811
C 0.771 5.507 -2.249
C -0.612 6.083 -2.519
O -1.398 6.378 -1.602
C 0.784 3.992 -2.606
C 1.261 3.252 -1.337
C 1.057 4.243 -0.179
H 1.522 6.068 -2.831
H -0.234 3.662 -2.897
H 1.441 3.790 -3.462
H 0.707 2.310 -1.187
H 2.336 2.991 -1.426
H 0.050 4.130 0.281
H 1.806 4.126 0.631
N -0.950 6.227 -3.841
C -2.392 6.231 -4.234
C -2.894 4.775 -4.361
C -2.634 7.039 -5.523
O -2.348 6.251 -6.684
O -3.918 4.545 -5.081
O -2.252 3.866 -3.722
H -0.322 5.829 -4.535
H -2.936 6.692 -3.390
H -3.688 7.374 -5.562
H -1.990 7.930 -5.558
H -2.883 5.431 -6.582

RDK

N -8.590 4.987 0.060
C -7.756 4.792 1.276
C -6.325 4.482 0.866
O -6.017 3.348 0.446
C -8.250 3.622 2.172
C -7.315 3.438 3.353
N -7.506 2.330 4.153
O -6.407 4.246 3.586
H -7.778 5.728 1.858
H -9.277 3.794 2.521
H -8.247 2.688 1.580
H -8.025 1.520 3.811
H -6.792 2.156 4.870
H -9.574 5.099 0.302
H -8.496 4.195 -0.575
N -5.374 5.454 0.993
C -3.967 5.191 0.592
C -3.465 3.862 1.150
O -2.661 3.158 0.505
C -3.029 6.323 1.079
C -3.549 7.736 0.701
C -2.599 8.827 1.231
C -3.756 7.882 -0.821
H -5.609 6.405 1.281
H -3.912 5.163 -0.522
H -2.911 6.266 2.171
H -2.021 6.138 0.638
H -4.535 7.852 1.198
H -2.402 8.690 2.300
H -1.646 8.791 0.688
H -3.036 9.820 1.083
H -2.787 8.060 -1.321
H -4.190 6.961 -1.246
H -4.417 8.724 -1.048
N -3.831 3.537 2.427
C -3.315 2.303 3.082
C -3.492 1.071 2.206
O -2.736 0.084 2.312
C -4.046 2.057 4.424
C -3.907 3.195 5.428
C -2.701 3.900 5.583
C -5.001 3.528 6.251
C -2.586 4.916 6.542
C -4.900 4.539 7.212
C -3.686 5.233 7.358
O -3.587 6.216 8.293
H -4.617 4.024 2.883
H -2.232 2.444 3.294
H -5.120 1.879 4.236
H -3.647 1.130 4.865
H -1.846 3.648 4.941
H -5.942 2.983 6.120
H -1.651 5.463 6.665
H -5.750 4.793 7.842
H -2.693 6.596 8.285
N -4.582 1.031 1.381
C -4.846 -0.199 0.594
C -3.693 -0.526 -0.339
O -3.529 -1.695 -0.754
C -6.215 -0.135 -0.145
C -7.320 0.416 0.796
C -6.580 -1.540 -0.666
C -7.441 -0.399 2.093
H -5.109 1.892 1.154
H -4.912 -1.036 1.327
H -6.121 0.557 -0.999
H -7.099 1.477 1.031
H -8.281 0.407 0.262
H -6.976 -2.153 0.165
H -7.341 -1.490 -1.450
H -5.685 -2.047 -1.058
H -7.832 -1.407 1.880
H -6.450 -0.537 2.557
H -8.101 0.099 2.820
N -2.833 0.472 -0.692
C -1.545 0.145 -1.375
C -1.001 -1.169 -0.828
O -0.650 -2.114 -1.568
C -0.531 1.284 -1.111
C 0.797 1.122 -1.876
C 0.687 1.304 -3.375
N 1.681 2.019 -3.970
O -0.249 0.807 -4.044
H -2.903 1.396 -0.233
H -1.715 0.053 -2.463
H -1.000 2.256 -1.374
H -0.325 1.322 -0.030
H 1.538 1.848 -1.491
H 1.231 0.113 -1.703
H 2.431 2.425 -3.399
H 1.695 2.155 -4.975
N -0.840 -1.242 0.525
C -0.189 -2.421 1.152
C -1.075 -3.654 1.125
O -0.559 -4.797 1.056
C 0.314 -2.049 2.572
C 1.334 -0.928 2.495
C 2.619 -1.011 1.987
C 1.122 0.458 2.837
C 2.328 1.146 2.521
C 0.022 1.179 3.362
N 3.216 0.227 2.011
C 2.461 2.537 2.727
C 0.158 2.551 3.561
C 1.365 3.227 3.246
H -1.263 -0.537 1.144
H 0.700 -2.662 0.527
H -0.539 -1.737 3.190
H 0.755 -2.951 3.044
H 3.152 -1.878 1.600
H 4.138 0.446 1.617
H -0.923 0.673 3.577
H 3.384 3.067 2.475
H -0.688 3.124 3.969
H 1.437 4.307 3.412
N -2.426 -3.489 1.167
C -3.323 -4.650 0.865
C -2.905 -5.310 -0.454
O -2.903 -6.537 -0.593
C -4.803 -4.202 0.800
C -5.480 -4.105 2.196
C -4.911 -2.948 3.042
C -7.011 -3.981 2.051
H -2.804 -2.560 0.940
H -3.202 -5.390 1.673
H -4.868 -3.232 0.265
H -5.361 -4.934 0.199
H -5.264 -5.050 2.726
H -5.224 -1.970 2.629
H -5.272 -3.007 4.074
H -3.814 -2.977 3.051
H -7.414 -4.810 1.460
H -7.495 -3.988 3.033
H -7.281 -3.033 1.545
N -2.564 -4.462 -1.482
C -2.125 -4.994 -2.795
C -0.607 -4.955 -2.970
O -0.095 -5.013 -4.099
C -2.850 -4.301 -3.974
C -2.844 -2.751 -3.880
C -2.306 -2.083 -5.165
C -0.840 -2.467 -5.419
N 0.017 -1.948 -4.317
H -2.564 -3.441 -1.353
H -2.406 -6.063 -2.787
H -2.335 -4.612 -4.897
H -3.883 -4.668 -4.038
H -3.858 -2.381 -3.676
H -2.217 -2.432 -3.022
H -2.913 -2.388 -6.029
H -2.391 -0.990 -5.078
H -0.737 -3.568 -5.433
H -0.473 -2.061 -6.371
H 1.023 -2.352 -4.273
H 0.068 -0.898 -4.327
H -0.395 -2.182 -3.376
N 0.161 -4.910 -1.834
C 1.642 -4.927 -1.888
C 2.246 -6.079 -1.099
O 3.435 -6.397 -1.261
C 2.270 -3.598 -1.386
C 2.426 -2.502 -2.467
O 2.472 -2.888 -3.709
O 2.559 -1.315 -2.097
H -0.290 -4.850 -0.909
H 1.906 -5.043 -2.958
H 1.683 -3.199 -0.540
H 3.283 -3.797 -0.993
N 1.443 -6.712 -0.176
C 2.014 -7.697 0.764
C 2.340 -7.112 2.124
O 3.235 -7.605 2.838
H 0.540 -6.282 0.063
H 1.334 -8.555 0.874
H 2.957 -8.066 0.315
N 1.636 -6.014 2.540
C 2.086 -5.234 3.716
C 3.590 -5.014 3.644
O 4.080 -4.314 2.726
H 0.916 -5.598 1.931
H 1.569 -4.255 3.686
H 1.808 -5.746 4.654
N 4.390 -5.573 4.586
C 5.875 -5.418 4.539
C 6.456 -5.638 3.141
O 7.413 -4.956 2.740
C 6.397 -6.463 5.556
C 5.208 -6.746 6.496
C 3.958 -6.533 5.628
C 6.134 -4.398 4.870
H 6.690 -7.383 5.031
H 7.279 -6.100 6.096
H 5.251 -7.756 6.922
H 5.211 -6.036 7.335
H 3.630 -7.470 5.143
H 3.104 -6.130 6.195
N 5.929 -6.670 2.403
C 6.445 -7.048 1.056
C 6.400 -5.917 0.037
O 6.892 -6.069 -1.100
C 5.678 -8.284 0.528
O 6.249 -8.744 -0.687
H 5.030 -7.085 2.695
H 7.507 -7.330 1.169
H 5.729 -9.103 1.263
H 4.600 -8.031 0.374
H 6.510 -7.951 -1.211
N 5.804 -4.744 0.405
C 5.942 -3.507 -0.393
C 7.382 -3.001 -0.489
O 7.842 -2.598 -1.576
C 5.100 -2.382 0.259
O 5.498 -2.152 1.609
H 5.447 -4.635 1.368
H 5.556 -3.694 -1.418
H 5.251 -1.435 -0.294
H 4.021 -2.644 0.222
H 5.155 -2.896 2.161
N 8.087 -2.859 0.669
C 9.265 -1.965 0.696
C 9.024 -0.636 -0.024
O 9.970 0.037 -0.438
H 7.739 -3.273 1.540
H 9.518 -1.758 1.745
H 10.136 -2.462 0.243
N 7.720 -0.178 -0.118
C 7.383 0.943 -1.029
C 6.200 1.727 -0.477
O 5.464 1.269 0.418
C 7.183 0.454 -2.498
C 6.016 -0.543 -2.685
C 6.267 -1.518 -3.858
N 5.286 -2.631 -3.892
C 5.551 -3.919 -3.595
N 6.819 -4.372 -3.430
N 4.515 -4.790 -3.565
H 6.945 -0.811 0.102
H 8.258 1.620 -1.034
H 7.040 1.340 -3.144
H 8.120 -0.027 -2.814
H 5.911 -1.132 -1.755
H 5.065 -0.012 -2.828
H 6.231 -0.983 -4.820
H 7.269 -1.963 -3.758
H 4.273 -2.395 -3.942
H 7.518 -3.654 -3.181
H 6.933 -5.237 -2.879
H 3.560 -4.372 -3.630
H 4.600 -5.692 -3.092
N 6.015 2.990 -0.966
C 5.044 3.940 -0.355
C 3.610 3.706 -0.814
O 3.323 2.986 -1.786
C 5.560 5.336 -0.791
C 6.339 5.075 -2.096

C 6.901 3.651 -1.948
H 5.073 3.830 0.745
H 4.738 6.060 -0.923
H 6.233 5.742 -0.023
H 5.658 5.124 -2.956
H 7.129 5.818 -2.259
H 6.901 3.091 -2.902
H 7.941 3.648 -1.572
N 2.644 4.334 -0.075
C 1.219 4.388 -0.497
C 1.082 5.315 -1.700
O 2.073 5.918 -2.159
C 0.514 4.953 0.759
C 1.552 5.912 1.375
C 2.923 5.312 1.002
H 0.860 3.370 -0.759
H -0.458 5.444 0.533
H 0.320 4.129 1.472
H 1.449 6.925 0.941
H 1.426 5.993 2.464
H 3.624 6.088 0.636
H 3.399 4.789 1.856
N -0.155 5.497 -2.251
C -0.422 6.674 -3.148
C 0.023 7.931 -2.389
O -0.675 8.401 -1.478
C -1.947 6.643 -3.398
C -2.492 5.350 -2.747
C -1.405 4.882 -1.769
H 0.159 6.557 -4.078
H -2.401 7.521 -2.903
H -2.190 6.697 -4.466
H -3.441 5.541 -2.208
H -2.691 4.582 -3.507
H -1.621 5.237 -0.732
H -1.300 3.778 -1.719
N 1.230 8.480 -2.731
C 1.890 9.491 -1.865
C 3.048 10.107 -2.616
O 3.657 11.126 -1.980
C 2.367 8.868 -0.525
O 3.420 7.920 -0.721
O 3.425 9.736 -3.719
H 1.843 7.998 -3.389
H 1.151 10.276 -1.634
H 2.756 9.656 0.135
H 1.516 8.366 -0.014
H 3.078 7.183 -1.291
H 4.394 11.450 -2.528

Optimal Cartesian Coordinates of 1-Ethyl-3-MethylImidazolium Nitrate Ionic Liquid Clusters

1 ion pair

C -5.868 -2.601 7.057
N -7.193 -2.232 6.969
C -7.273 -0.893 7.034
N -6.028 -0.394 7.127
C -5.134 -1.446 7.158
C -5.679 1.033 7.272
C -6.901 1.858 7.674
C -8.343 -3.131 6.876
H -8.133 -4.057 7.417
H -8.560 -3.368 5.827
H -9.210 -2.611 7.327
H -8.184 -0.322 6.900
H -4.068 -1.297 7.259
H -5.553 -3.636 7.053
H -4.893 1.107 8.036
H -5.247 1.391 6.323
H -6.604 2.871 7.958
H -7.618 1.924 6.848
H -7.406 1.374 8.527
O -9.882 -0.928 8.126
N -9.332 -0.543 9.214
O -8.034 -0.507 9.239
O -9.984 -0.209 10.188

2 ion pairs

C -5.636 -3.224 5.990
N -4.764 -2.266 6.452
C -4.811 -1.208 5.632
N -5.694 -1.462 4.658
C -6.224 -2.714 4.857
C -6.102 -0.518 3.602
C -4.944 -0.144 2.672
C -3.904 -2.378 7.628
H -3.517 -3.398 7.709
H -4.469 -2.134 8.536
H -3.069 -1.662 7.505
H -4.237 -0.289 5.739
H -6.965 -3.140 4.194
H -5.768 -4.177 6.483
H -6.922 -0.988 3.043
H -6.491 0.381 4.111
H -5.324 0.400 1.802
H -4.230 0.514 3.199
H -4.411 -1.033 2.321
O -0.923 0.081 4.786
N -1.766 -0.587 5.427
O -2.126 -0.188 6.599
O -2.322 -1.600 4.934
C -2.285 4.490 4.445
N -2.224 3.119 4.406
C -2.334 2.648 5.656
N -2.446 3.684 6.495
C -2.425 4.849 5.766
C -2.650 3.557 7.951
C -1.814 2.413 8.528
C -2.178 2.274 3.217
H -1.958 2.878 2.334
H -3.157 1.772 3.100
H -1.415 1.491 3.357
H -2.275 1.599 5.967
H -2.513 5.824 6.226
H -2.230 5.099 3.553
H -2.398 4.519 8.417
H -3.728 3.369 8.108
H -2.085 2.231 9.572
H -1.984 1.486 7.954
H -0.745 2.646 8.487
O -5.336 2.820 6.846
N -5.433 1.840 6.083
O -4.603 1.710 5.103
O -6.299 0.941 6.254

3 ion pairs

C 3.085 -4.123 -3.539
N 1.719 -3.983 -3.475
C 1.367 -2.893 -4.172
N 2.469 -2.349 -4.703
C 3.559 -3.088 -4.311
C 2.497 -1.104 -5.493
C 3.021 0.066 -4.655
C 0.792 -4.866 -2.771
H 0.298 -5.540 -3.481
H 0.027 -4.247 -2.259
H 1.340 -5.458 -2.033
H 0.339 -2.572 -4.364
H 4.570 -2.831 -4.597
H 3.609 -4.926 -3.038
H 3.128 -1.268 -6.378
H 1.460 -0.912 -5.832
H 3.017 0.987 -5.245
H 2.380 0.212 -3.767
H 4.044 -0.124 -4.313
O -1.390 -2.631 -5.199
N -1.441 -1.384 -5.451
O -2.379 -0.689 -4.986
O -0.506 -0.848 -6.116
C -0.534 1.486 -4.267
N -1.650 2.259 -4.070
C -1.578 2.823 -2.858
N -0.444 2.417 -2.266
C 0.226 1.580 -3.125
C -0.050 2.708 -0.875
C -0.667 4.009 -0.368
C -2.768 2.383 -5.004
H -3.596 2.897 -4.492
H -3.071 1.374 -5.317
H -2.461 2.958 -5.886
H -2.351 3.450 -2.398
H 1.153 1.069 -2.865
H -0.392 0.877 -5.164
H -0.387 1.846 -0.263
H 1.047 2.734 -0.830
H -0.422 4.159 0.688
H -0.292 4.869 -0.932
H -1.767 3.977 -0.473
O -4.379 3.892 -2.910
N -4.625 3.434 -1.760
O -5.708 2.873 -1.497
O -3.693 3.474 -0.873
C -4.583 0.098 -1.609
N -3.413 -0.126 -0.928
C -2.886 -1.290 -1.342
N -3.689 -1.810 -2.280
C -4.755 -0.966 -2.466
C -3.443 -3.056 -3.025
C -2.643 -4.066 -2.201
C -2.838 0.759 0.084
H -3.121 0.419 1.087
H -3.216 1.788 -0.082
H -1.737 0.751 -0.007
H -1.935 -1.724 -1.022
H -5.536 -1.171 -3.185
H -5.177 1.010 -1.465
H -4.417 -3.468 -3.322
H -2.879 -2.800 -3.953
H -2.530 -4.998 -2.763
H -1.631 -3.676 -1.975
H -3.144 -4.295 -1.253
O -0.109 -0.259 -0.935
N 0.390 -1.259 -1.515
O 1.353 -1.118 -2.321
O -0.109 -2.413 -1.323

4 ion pairs

C -0.415 5.441 6.930
N -0.014 4.334 6.220
C -1.079 3.810 5.606
N -2.159 4.542 5.910
C -1.771 5.571 6.733
C -3.536 4.215 5.493
C -3.770 4.434 3.998
C 1.331 3.770 6.148
H 2.068 4.518 6.449
H 1.513 3.440 5.112
H 1.394 2.894 6.808
H -1.053 2.920 4.982
H -2.471 6.301 7.115
H 0.273 6.042 7.509
H -3.702 3.149 5.753
H -4.224 4.823 6.096
H -4.727 3.974 3.702
H -3.783 5.498 3.744
H -2.978 3.946 3.396
O -1.228 -0.341 0.817
N -0.509 -0.173 -0.250
O 0.689 -0.521 -0.236
O -1.028 0.389 -1.239
C -3.379 -0.630 2.867
N -3.071 0.554 3.493
C -3.862 0.691 4.568
N -4.669 -0.374 4.643
C -4.389 -1.215 3.590
C -5.697 -0.595 5.673
C -6.161 0.731 6.276
C -2.042 1.493 3.058
H -2.508 2.426 2.658
H -1.438 1.007 2.264
H -1.385 1.760 3.904
H -3.832 1.520 5.279
H -4.927 -2.139 3.430
H -2.869 -0.933 1.952
H -6.535 -1.127 5.202
H -5.279 -1.257 6.449
H -5.341 1.214 6.819
H -6.486 1.410 5.475
H -6.991 0.569 6.968
O -0.272 1.183 6.520
N -1.506 0.917 6.490
O -2.352 1.817 6.804
O -1.914 -0.197 6.068
C 3.482 0.637 2.549
N 2.398 0.959 1.773
C 1.294 0.464 2.350
N 1.648 -0.180 3.470
C 3.009 -0.083 3.623
C 0.725 -0.846 4.407
C -0.419 -1.548 3.673
C 2.430 1.735 0.537
H 1.996 1.131 -0.274
H 3.462 2.003 0.300
H 1.818 2.648 0.673
H 0.271 0.515 1.964
H 3.530 -0.525 4.461
H 4.488 0.934 2.288
H 1.310 -1.560 5.002
H 0.326 -0.082 5.114
H -1.201 -1.825 4.387
H -0.864 -0.879 2.911
H -0.069 -2.451 3.163
O 0.334 3.774 1.402
N 0.134 3.728 2.638
O -0.601 4.574 3.214
O 0.650 2.781 3.332
C -4.368 1.630 -1.916
N -3.864 0.960 -0.829
C -2.984 1.751 -0.207
N -2.905 2.913 -0.865
C -3.762 2.866 -1.940
C -2.089 4.062 -0.434
C -2.596 4.618 0.899
C -4.242 -0.363 -0.346
H -3.372 -0.802 0.173
H -4.553 -0.999 -1.178
H -5.070 -0.250 0.381
H -2.419 1.477 0.682
H -3.876 3.694 -2.626
H -5.100 1.194 -2.581
H -1.044 3.731 -0.323
H -2.126 4.822 -1.226
H -1.893 5.355 1.298
H -3.580 5.084 0.787
H -2.691 3.802 1.646
O -5.807 2.167 3.526
N -5.501 1.776 2.362
O -6.049 0.768 1.857
O -4.561 2.372 1.732

5 ion pairs

C -0.558 -1.374 -0.058
N -0.967 -2.164 0.988
C -1.440 -1.377 1.965
N -1.347 -0.102 1.566
C -0.799 -0.069 0.309
C -1.875 1.052 2.313
C -1.406 1.047 3.768
C -0.933 -3.624 1.023
H -0.779 -4.014 -0.003
H -1.905 -3.991 1.405
H -0.128 -3.973 1.680
H -1.843 -1.714 2.909
H -0.615 0.881 -0.214
H -0.168 -1.806 -0.990
H -1.574 1.978 1.784
H -2.982 0.993 2.261
H -1.865 1.872 4.319
H -1.683 0.106 4.259
H -0.318 1.159 3.831
O 0.088 -3.002 -2.514
N -0.749 -3.932 -2.736
O -1.103 -4.702 -1.789
O -1.267 -4.057 -3.871
C -5.032 1.737 1.278
N -5.559 1.311 0.084
C -5.385 2.275 -0.834
N -4.760 3.309 -0.251
C -4.532 3.002 1.066
C -4.357 4.575 -0.896
C -4.898 4.693 -2.318
C -6.267 0.049 -0.122
H -7.285 0.131 0.278
H -5.746 -0.772 0.407
H -6.322 -0.170 -1.204
H -5.635 2.199 -1.895
H -4.019 3.680 1.734
H -5.021 1.104 2.157
H -4.718 5.400 -0.266
H -3.243 4.621 -0.896
H -4.596 5.650 -2.754
H -4.502 3.882 -2.958
H -5.992 4.638 -2.335
O -0.216 2.763 -0.473
N -1.109 3.646 -0.321
O -1.851 3.622 0.708
O -1.317 4.503 -1.220
C -0.931 1.094 -2.887
N -1.618 1.759 -3.874
C -1.876 0.900 -4.871
N -1.358 -0.294 -4.552
C -0.767 -0.204 -3.316
C -1.402 -1.506 -5.388
C 0.001 -2.087 -5.573
C -2.025 3.163 -3.833
H -1.724 3.669 -4.755
H -1.562 3.658 -2.960
H -3.128 3.219 -3.730
H -2.392 1.136 -5.790
H -0.301 -1.077 -2.842
H -0.614 1.592 -1.959
H -2.053 -2.255 -4.888
H -1.865 -1.235 -6.345
H 0.671 -1.363 -6.048
H 0.410 -2.366 -4.588
H -0.040 -2.986 -6.193
O -5.421 -2.677 1.146
N -4.399 -2.281 1.773
O -4.127 -1.047 1.835
O -3.630 -3.128 2.322
C -4.106 -3.480 -3.581
N -4.289 -4.764 -3.134
C -5.376 -4.799 -2.349
N -5.894 -3.559 -2.290
C -5.120 -2.717 -3.048
C -7.057 -3.155 -1.478
C -7.885 -2.080 -2.183
C -3.411 -5.900 -3.408
H -3.984 -6.832 -3.282
H -2.564 -5.872 -2.688
H -3.016 -5.827 -4.424
H -5.796 -5.694 -1.866
H -5.355 -1.652 -3.159
H -3.256 -3.199 -4.208
H -7.653 -4.054 -1.273
H -6.674 -2.776 -0.511
H -8.723 -1.771 -1.552
H -7.256 -1.195 -2.392
H -8.286 -2.451 -3.132
O -4.779 1.966 -3.771
N -5.009 0.721 -3.809
O -5.965 0.247 -3.118
O -4.268 -0.043 -4.475
C -6.371 -6.378 3.013
N -6.183 -7.596 2.390
C -5.246 -7.453 1.441
N -4.830 -6.180 1.443
C -5.516 -5.488 2.409
C -3.892 -5.585 0.474
C -2.931 -6.618 -0.111
C -6.913 -8.828 2.677
H -6.473 -9.648 2.103
H -7.965 -8.718 2.391
H -6.860 -9.062 3.746
H -4.890 -8.244 0.771
H -5.337 -4.427 2.570
H -7.083 -6.241 3.814
H -4.499 -5.136 -0.342
H -3.355 -4.757 0.986
H -2.336 -6.158 -0.923
H -2.242 -6.997 0.652
H -3.492 -7.471 -0.525
O -5.048 -9.031 -0.983
N -5.648 -8.086 -1.563
O -5.583 -7.919 -2.792
O -6.288 -7.224 -0.841

10 ion pairs

C 3.085 -4.709 4.858
N 2.505 -3.897 5.809
C 1.329 -3.464 5.342
N 1.134 -3.985 4.121
C 2.219 -4.761 3.792
C -0.076 -3.779 3.302
C 0.034 -4.440 1.933
C 3.033 -3.612 7.139
H 4.124 -3.548 7.106
H 2.734 -4.407 7.834
H 2.607 -2.653 7.493
H 0.652 -2.815 5.876
H 2.281 -5.304 2.841
H 4.049 -5.175 5.004
H -0.939 -4.196 3.873
H -0.232 -2.691 3.196
H -0.883 -4.259 1.337
H 0.901 -4.047 1.371
H 0.171 -5.531 2.031
O -2.624 -3.933 0.429
N -2.537 -2.696 0.156
O -3.375 -2.171 -0.649
O -1.641 -1.992 0.675
C -4.123 -5.193 2.713
N -5.453 -5.412 2.972
C -5.678 -5.208 4.274
N -4.517 -4.881 4.861
C -3.530 -4.857 3.904
C -4.310 -4.497 6.265
C -4.302 -2.970 6.405
C -6.442 -5.783 1.967
H -7.351 -6.140 2.456
H -6.010 -6.576 1.327
H -6.678 -4.890 1.355
H -6.622 -5.342 4.780
H -2.488 -4.629 4.152
H -3.710 -5.265 1.709
H -5.104 -4.949 6.874
H -3.334 -4.917 6.580
H -3.983 -2.681 7.416
H -3.589 -2.538 5.695
H -5.293 -2.553 6.194
O 1.922 -1.017 4.678
N 1.963 -0.324 5.733
O 2.186 0.911 5.682
O 1.735 -0.883 6.857
C 3.399 1.772 2.515
N 2.172 2.069 3.051
C 1.333 1.059 2.792
N 1.990 0.125 2.093
C 3.280 0.539 1.911
C 1.407 -1.142 1.620
C 2.467 -2.030 0.976
C 1.812 3.263 3.808
H 1.524 2.962 4.832

H 0.947 3.760 3.317
H 2.665 3.944 3.849
H 0.286 1.046 3.084
H 3.999 -0.054 1.361
H 4.245 2.438 2.601
H 0.940 -1.645 2.488
H 0.589 -0.899 0.911
H 2.045 -3.011 0.688
H 2.870 -1.535 0.073
H 3.294 -2.211 1.670
O -4.851 2.092 -1.781
N -4.069 2.951 -1.301
O -2.824 2.644 -1.162
O -4.466 4.075 -0.930
C -1.805 0.274 6.939
N -0.694 1.009 7.275
C -0.021 0.350 8.230
N -0.680 -0.779 8.521
C -1.798 -0.856 7.726
C -0.266 -1.787 9.519
C 1.245 -1.769 9.738
C -0.302 2.283 6.669
H -0.356 3.090 7.408
H -0.972 2.497 5.822
H 0.731 2.204 6.273
H 0.895 0.677 8.703
H -2.470 -1.718 7.749
H -2.495 0.599 6.171
H -0.804 -1.581 10.458
H -0.606 -2.773 9.146
H 1.531 -2.534 10.465
H 1.770 -1.972 8.787
H 1.577 -0.792 10.109
O 2.656 -5.177 0.523
N 2.167 -6.333 0.533
O 1.890 -6.931 -0.547
O 1.896 -6.895 1.645
C -3.375 0.714 2.406
N -2.775 0.710 1.170
C -3.678 0.326 0.257
N -4.837 0.079 0.880
C -4.679 0.319 2.222
C -6.075 -0.401 0.245
C -7.033 0.748 -0.081
C -1.372 1.011 0.915
H -0.812 0.072 0.733
H -0.947 1.512 1.799
H -1.270 1.666 0.020
H -3.497 0.243 -0.813
H -5.498 0.157 2.921
H -2.830 1.021 3.295
H -5.778 -0.948 -0.680
H -6.542 -1.134 0.935
H -7.927 0.364 -0.582
H -7.346 1.257 0.836
H -6.542 1.479 -0.742
O -4.224 -8.035 2.977
N -3.827 -8.177 1.798
O -4.572 -7.840 0.824
O -2.652 -8.597 1.556
C -3.950 1.004 -4.225
N -3.945 -0.109 -3.426
C -2.761 -0.188 -2.801
N -2.013 0.859 -3.175
C -2.729 1.616 -4.066
C -0.680 1.183 -2.640
C 0.081 2.167 -3.525
C -5.049 -1.045 -3.259
H -4.787 -2.008 -3.735
H -5.951 -0.635 -3.719
H -5.236 -1.232 -2.177
H -2.485 -0.972 -2.100
H -2.324 2.523 -4.496
H -4.808 1.283 -4.822
H -0.814 1.615 -1.615
H -0.116 0.241 -2.543
H 1.016 2.462 -3.017
H 0.339 1.707 -4.487
H -0.519 3.065 -3.718
O 3.196 0.379 -0.930
N 2.328 1.304 -0.995
O 2.538 2.326 -1.687
O 1.232 1.181 -0.355
C 2.204 -3.521 -1.994
N 1.588 -4.085 -3.084
C 1.433 -3.146 -4.028
N 1.943 -1.995 -3.569
C 2.429 -2.200 -2.303
C 1.902 -0.699 -4.267
C 3.188 0.099 -4.054
C 1.137 -5.471 -3.180
H 1.630 -5.972 -4.020
H 0.049 -5.481 -3.346
H 1.382 -5.997 -2.239
H 0.974 -3.294 -4.995
H 2.859 -1.384 -1.706
H 2.415 -4.090 -1.078
H 1.718 -0.896 -5.332
H 1.028 -0.136 -3.878
H 3.107 1.085 -4.520
H 3.372 0.240 -2.973
H 4.050 -0.419 -4.488
O -1.237 -4.486 6.031
N -0.984 -4.244 7.261
O -1.904 -3.840 8.022
O 0.192 -4.367 7.690
C -4.334 -4.396 -2.729
N -4.925 -4.503 -1.490
C -4.296 -5.468 -0.805
N -3.334 -5.990 -1.577
C -3.328 -5.328 -2.780
C -2.367 -7.018 -1.150
C -1.055 -6.374 -0.692
C -6.007 -3.656 -0.991
H -5.716 -2.588 -1.099
H -6.197 -3.867 0.078
H -6.925 -3.834 -1.563
H -4.553 -5.817 0.197
H -2.596 -5.511 -3.560
H -4.617 -3.639 -3.458
H -2.831 -7.594 -0.325
H -2.194 -7.702 -1.993
H -0.378 -7.130 -0.255
H -0.530 -5.910 -1.541
H -1.245 -5.590 0.064
O -1.235 2.308 3.837
N -1.713 3.363 3.299
O -0.922 4.212 2.785
O -2.948 3.535 3.238
C -2.370 6.839 0.259
N -2.989 5.767 0.853
C -2.276 4.665 0.595
N -1.217 4.998 -0.150
C -1.246 6.355 -0.370
C -0.149 4.075 -0.573
C 1.053 4.160 0.373
C -4.251 5.781 1.586
H -5.044 5.383 0.940
H -4.495 6.804 1.885
H -4.151 5.137 2.472
H -2.530 3.667 0.925
H -0.487 6.866 -0.946
H -2.762 7.845 0.323
H -0.574 3.044 -0.594
H 0.147 4.328 -1.601
H 1.813 3.436 0.052
H 1.492 5.164 0.349
H 0.749 3.942 1.413
O -6.737 -2.938 4.173
N -6.873 -2.275 3.102
O -6.705 -2.862 1.973
O -7.135 -1.055 3.131
C 0.303 -9.964 2.993
N 0.116 -9.117 1.930
C -0.355 -7.952 2.388
N -0.461 -8.021 3.721
C -0.061 -9.275 4.125
C -0.928 -6.942 4.613
C -2.249 -7.293 5.302
C 0.367 -9.406 0.522
H 0.823 -8.509 0.047
H -0.578 -9.642 0.018
H 1.046 -10.258 0.436
H -0.576 -7.082 1.775
H -0.067 -9.577 5.164
H 0.676 -10.972 2.873
H -0.144 -6.748 5.359
H -1.046 -6.019 4.012
H -2.590 -6.420 5.886
H -3.020 -7.546 4.553
H -2.125 -8.145 5.978
O -2.920 -2.624 -4.598
N -1.703 -2.816 -4.352
O -0.955 -1.831 -4.040
O -1.210 -3.982 -4.395

20 ion pairs

C 1.124 -3.999 4.772
N 1.815 -3.086 5.529
C 2.085 -3.635 6.725
N 1.584 -4.875 6.747
C 0.979 -5.127 5.545
C 1.655 -5.814 7.877
C 0.359 -6.616 8.022
C 2.158 -1.729 5.115
H 1.394 -1.363 4.403
H 3.139 -1.712 4.622
H 2.195 -1.061 6.003
H 2.634 -3.154 7.539
H 0.496 -6.073 5.331
H 0.774 -3.777 3.756
H 2.522 -6.486 7.701
H 1.885 -5.230 8.782
H 0.287 -7.042 9.027
H -0.509 -5.961 7.853
H 0.318 -7.449 7.303
O 4.222 -5.573 3.889
N 4.359 -6.550 4.689
O 3.709 -6.581 5.768
O 5.136 -7.502 4.396
C 3.412 -3.176 -2.617
N 3.934 -4.413 -2.900
C 5.245 -4.404 -2.615
N 5.567 -3.194 -2.133
C 4.440 -2.406 -2.129
C 6.900 -2.746 -1.689
C 7.251 -3.270 -0.296
C 3.201 -5.530 -3.491
H 3.496 -5.650 -4.540
H 2.115 -5.333 -3.428
H 3.441 -6.462 -2.940
H 5.914 -5.264 -2.681
H 4.457 -1.370 -1.793
H 2.358 -2.939 -2.757
H 7.643 -3.088 -2.434
H 6.881 -1.636 -1.699
H 8.272 -2.947 -0.025
H 6.548 -2.876 0.461
H 7.204 -4.368 -0.271
O -1.284 -1.482 1.614
N -0.410 -2.251 2.094
O 0.737 -1.815 2.394
O -0.699 -3.469 2.320
C 7.026 -6.335 7.410
N 6.073 -7.310 7.575
C 6.324 -8.306 6.712
N 7.423 -8.000 6.014
C 7.881 -6.773 6.423
C 7.938 -8.812 4.900
C 9.461 -8.831 4.808
C 4.935 -7.243 8.487
H 4.021 -6.986 7.911
H 5.107 -6.455 9.235
H 4.782 -8.216 8.969
H 5.752 -9.228 6.600
H 8.731 -6.277 5.955
H 7.016 -5.416 8.001
H 7.519 -9.831 5.012
H 7.507 -8.389 3.967
H 9.757 -9.495 3.978
H 9.860 -7.825 4.596
H 9.913 -9.209 5.730
O 7.358 -1.152 3.223
N 6.593 -0.166 3.387
O 6.847 0.943 2.855
O 5.504 -0.312 4.043
C -0.071 3.286 2.372
N 0.188 2.351 1.393
C -0.035 1.129 1.897
N -0.441 1.261 3.170
C -0.475 2.591 3.488
C -0.809 0.144 4.065
C -0.897 0.548 5.534
C 0.685 2.649 0.050
H 1.765 2.911 0.092
H 0.132 3.493 -0.372
H 0.556 1.767 -0.591
H 0.078 0.186 1.355
H -0.763 2.934 4.474
H 0.044 4.348 2.204
H -1.773 -0.271 3.702
H -0.041 -0.648 3.929
H -1.290 -0.301 6.117
H 0.103 0.814 5.923
H -1.564 1.407 5.667
O 0.646 -0.610 -0.564
N 1.010 -0.136 -1.685
O 2.222 -0.235 -2.043
O 0.165 0.418 -2.433
C 0.706 -2.518 10.188
N 1.685 -1.628 9.822
C 2.716 -1.750 10.669
N 2.412 -2.678 11.583
C 1.166 -3.184 11.301
C 3.300 -3.092 12.684
C 2.507 -3.613 13.883
C 1.646 -0.712 8.687
H 2.154 -1.161 7.807
H 2.174 0.219 8.949
H 0.609 -0.499 8.416
H 3.603 -1.127 10.669
H 0.716 -3.962 11.904
H -0.209 -2.621 9.617
H 3.974 -3.873 12.297
H 3.907 -2.214 12.956
H 3.185 -3.996 14.651
H 1.901 -2.816 14.328

H 1.835 -4.423 13.576
O 4.146 -2.928 8.853
N 4.537 -4.024 9.393
O 3.705 -4.742 9.995
O 5.741 -4.377 9.290
C 8.812 -6.336 1.356
N 7.621 -6.254 2.035
C 7.078 -7.478 2.103
N 7.900 -8.341 1.486
C 8.988 -7.654 1.012
C 7.709 -9.796 1.338
C 9.025 -10.538 1.572
C 7.070 -5.028 2.599
H 6.090 -5.234 3.071
H 6.931 -4.283 1.796
H 7.779 -4.616 3.349
H 6.139 -7.711 2.600
H 9.801 -8.168 0.493
H 9.442 -5.470 1.167
H 6.930 -10.125 2.057
H 7.328 -9.990 0.324
H 8.880 -11.617 1.469
H 9.789 -10.205 0.845
H 9.403 -10.333 2.588
O 3.611 3.153 -0.688
N 4.824 3.559 -0.513
O 5.727 3.103 -1.272
O 5.079 4.354 0.405
C 3.778 -10.462 7.506
N 3.232 -10.694 6.267
C 2.869 -11.978 6.194
N 3.174 -12.581 7.351
C 3.742 -11.651 8.193
C 2.911 -13.991 7.677
C 1.733 -14.532 6.866
C 3.061 -9.723 5.195
H 2.015 -9.351 5.215
H 3.247 -10.209 4.220
H 3.758 -8.882 5.328
H 2.407 -12.459 5.345
H 4.070 -11.900 9.192
H 4.153 -9.487 7.809
H 3.824 -14.577 7.483
H 2.704 -14.054 8.755
H 1.469 -15.541 7.195
H 0.861 -13.874 6.985
H 1.985 -14.568 5.800
O 4.035 -0.073 12.607
N 4.125 0.966 11.902
O 4.720 1.986 12.300
O 3.602 0.961 10.720
C 4.613 4.703 3.154
N 4.245 3.380 3.136
C 5.040 2.697 3.973
N 5.923 3.549 4.509
C 5.674 4.809 4.020
C 7.068 3.171 5.351
C 7.495 4.303 6.286
C 3.174 2.811 2.327
H 3.320 1.723 2.248
H 3.193 3.236 1.303
H 2.194 3.009 2.794
H 5.011 1.619 4.146
H 6.268 5.664 4.319
H 4.118 5.450 2.550
H 6.798 2.269 5.932
H 7.909 2.879 4.670
H 8.461 4.073 6.744
H 7.590 5.245 5.730
H 6.762 4.457 7.099
O 9.324 -4.715 4.758
N 10.455 -5.154 4.374
O 10.504 -6.143 3.589
O 11.517 -4.586 4.744
C 4.530 0.339 -4.986
N 4.930 0.852 -3.778
C 3.979 1.678 -3.320
N 2.983 1.717 -4.213
C 3.297 0.884 -5.260
C 1.729 2.474 -4.059
C 1.952 3.783 -3.300
C 6.193 0.582 -3.096
H 6.143 -0.389 -2.559
H 6.366 1.378 -2.354
H 7.010 0.541 -3.821
H 4.007 2.233 -2.373
H 2.637 0.741 -6.104
H 5.109 -0.409 -5.536
H 1.318 2.657 -5.061
H 1.013 1.822 -3.513
H 0.996 4.278 -3.107
H 2.450 3.588 -2.333
H 2.583 4.469 -3.875
O -0.326 -2.616 7.462
N -1.373 -3.045 6.916
O -2.239 -2.240 6.465
O -1.561 -4.299 6.789
C -2.768 -4.443 -1.738
N -2.492 -3.519 -0.764
C -1.494 -2.725 -1.183
N -1.128 -3.127 -2.411
C -1.905 -4.195 -2.780
C -0.062 -2.532 -3.239
C 0.399 -3.496 -4.330
C -3.189 -3.460 0.518
H -2.451 -3.471 1.349
H -3.853 -4.338 0.596
H -3.782 -2.535 0.597
H -1.029 -1.914 -0.616
H -1.771 -4.696 -3.730
H -3.524 -5.210 -1.583
H -0.434 -1.586 -3.665
H 0.783 -2.279 -2.574
H 1.210 -3.052 -4.914
H 0.767 -4.434 -3.865
H -0.424 -3.750 -5.008
O 9.699 -0.287 -0.573
N 10.376 -1.324 -0.784
O 11.554 -1.429 -0.340
O 9.869 -2.295 -1.440
C 4.333 -3.288 1.949
N 3.089 -3.281 1.377
C 2.916 -2.124 0.725
N 4.032 -1.388 0.871
C 4.935 -2.095 1.625
C 4.237 -0.038 0.309
C 5.707 0.249 0.012
C 2.125 -4.365 1.499
H 1.774 -4.688 0.502
H 1.245 -4.028 2.089
H 2.608 -5.200 2.027
H 2.024 -1.797 0.183
H 5.905 -1.693 1.914
H 4.691 -4.131 2.545
H 3.621 0.026 -0.611
H 3.837 0.701 1.033
H 5.800 1.216 -0.522
H 6.307 0.320 0.939
H 6.136 -0.534 -0.645
O 3.578 2.562 6.121
N 2.473 2.002 5.849
O 2.085 1.013 6.540
O 1.778 2.411 4.882
C -0.381 -6.573 2.618
N 0.518 -7.408 3.244
C -0.157 -8.259 4.029
N -1.463 -7.981 3.936
C -1.632 -6.939 3.053
C -2.548 -8.741 4.584
C -3.289 -9.617 3.570
C 1.964 -7.421 3.061
H 2.375 -6.398 3.089
H 2.224 -7.884 2.094
H 2.423 -8.013 3.865
H 0.298 -8.999 4.699
H -2.619 -6.548 2.792
H -0.069 -5.792 1.928
H -2.107 -9.356 5.397
H -3.248 -8.016 5.047
H -4.145 -10.107 4.043
H -3.648 -9.009 2.718
H -2.621 -10.397 3.164
O -1.479 -10.583 6.778
N -0.232 -10.613 6.756
O 0.401 -11.703 6.869
O 0.426 -9.524 6.584
C 11.679 2.509 0.713
N 11.338 1.375 1.408
C 10.002 1.296 1.478
N 9.480 2.358 0.852
C 10.504 3.134 0.366
C 8.054 2.719 0.815
C 7.748 3.722 1.931
C 12.274 0.404 1.964
H 11.953 0.149 2.986
H 13.283 0.825 1.969
H 12.251 -0.517 1.343
H 9.443 0.509 1.969
H 10.328 4.051 -0.179
H 12.707 2.783 0.521
H 7.806 3.134 -0.172
H 7.463 1.796 0.958
H 6.690 4.022 1.889
H 7.959 3.265 2.917
H 8.366 4.620 1.826
O 6.371 -6.236 -0.611
N 5.530 -7.166 -0.788
O 5.031 -7.335 -1.937
O 5.179 -7.902 0.177
C 4.069 -11.495 -0.552
N 3.903 -10.788 0.613
C 3.229 -9.666 0.336
N 2.947 -9.640 -0.972
C 3.466 -10.770 -1.553
C 2.259 -8.546 -1.676
C 1.341 -9.051 -2.787
C 4.375 -11.197 1.933
H 5.403 -10.823 2.121
H 4.387 -12.287 2.003
H 3.699 -10.790 2.707
H 2.923 -8.917 1.063
H 3.362 -10.968 -2.612
H 4.586 -12.445 -0.584
H 1.686 -7.961 -0.937
H 3.042 -7.869 -2.094
H 0.919 -8.193 -3.324
H 1.892 -9.684 -3.492
H 0.500 -9.636 -2.377
O -4.418 -5.981 2.139
N -4.432 -6.680 1.081
O -4.242 -7.927 1.138
O -4.579 -6.120 -0.044
C -5.987 -4.811 4.264
N -5.018 -5.206 5.152
C -3.967 -4.376 5.045
N -4.246 -3.465 4.106
C -5.496 -3.708 3.604
C -3.315 -2.411 3.674
C -4.011 -1.254 2.962
C -5.093 -6.364 6.039
H -4.817 -6.080 7.059
H -4.393 -7.147 5.688
H -6.109 -6.766 6.031
H -3.047 -4.408 5.654
H -5.929 -3.102 2.819
H -2.775 -2.061 4.574
H -2.562 -2.875 2.994
H -3.275 -0.453 2.800
H -4.392 -1.572 1.979
H -4.840 -0.853 3.554
O 4.874 -12.407 4.589
N 5.864 -11.644 4.771
O 6.058 -11.127 5.920
O 6.630 -11.346 3.816
C 11.788 -5.707 -0.125
N 12.420 -6.153 1.012
C 12.314 -5.211 1.961
N 11.626 -4.176 1.459
C 11.278 -4.461 0.161
C 11.257 -2.951 2.195
C 9.740 -2.766 2.260
C 13.084 -7.448 1.145
H 14.090 -7.402 0.710
H 12.491 -8.217 0.603
H 13.160 -7.713 2.203
H 12.704 -5.262 2.971
H 10.724 -3.749 -0.463
H 11.723 -6.328 -1.030
H 11.685 -3.035 3.205
H 11.719 -2.085 1.673
H 9.493 -1.862 2.849
H 9.318 -2.657 1.246
H 9.253 -3.628 2.751
O 5.233 -2.276 -6.295
N 5.853 -2.763 -5.343
O 6.549 -2.015 -4.567
O 5.806 -4.012 -5.084
C 9.147 -2.754 7.717
N 9.708 -2.289 6.552
C 8.776 -2.297 5.592
N 7.629 -2.755 6.115
C 7.832 -3.049 7.442
C 6.391 -2.992 5.351
C 5.373 -3.795 6.153
C 11.113 -1.954 6.345
H 11.172 -1.120 5.628
H 11.626 -2.832 5.916
H 11.576 -1.678 7.296
H 8.924 -1.972 4.558
H 7.044 -3.468 8.080
H 9.710 -2.842 8.637
H 5.968 -2.005 5.044
H 6.674 -3.534 4.430
H 4.539 -4.108 5.509
H 5.839 -4.705 6.571
H 4.969 -3.203 7.001
O 10.222 -0.183 4.071
N 9.472 0.735 4.542
O 8.716 0.481 5.522
O 9.511 1.887 4.032
C 6.531 0.985 7.695
N 5.217 0.584 7.642
C 4.466 1.465 8.316
N 5.267 2.412 8.820
C 6.561 2.134 8.452
C 4.843 3.536 9.671
C 5.845 4.688 9.594
C 4.694 -0.595 6.966
H 5.163 -0.711 5.969
H 3.597 -0.475 6.845
H 4.876 -1.512 7.564
H 3.387 1.392 8.427
H 7.387 2.770 8.742
H 7.333 0.460 7.183
H 3.848 3.856 9.338
H 4.744 3.149 10.715
H 5.456 5.573 10.105
H 6.796 4.410 10.061
H 6.053 4.949 8.542
O 0.782 -11.000 0.743
N 0.626 -10.456 1.869
O 1.626 -10.168 2.586
O -0.539 -10.158 2.271
C -1.670 -10.148 -1.871

N -2.055 -9.204 -0.950
C -2.290 -9.816 0.220
N -2.074 -11.129 0.063
C -1.685 -11.365 -1.230
C -2.152 -12.143 1.128
C -3.060 -13.310 0.736
C -2.147 -7.769 -1.217
H -3.036 -7.342 -0.721
H -2.219 -7.613 -2.296
H -1.233 -7.259 -0.848
H -2.647 -9.337 1.132
H -1.445 -12.357 -1.589
H -1.435 -9.891 -2.895
H -1.128 -12.495 1.325
H -2.509 -11.634 2.041
H -3.051 -14.078 1.514
H -4.094 -12.976 0.594
H -2.715 -13.764 -0.201
O 9.716 -8.944 -1.919
N 10.870 -8.764 -1.463
O 11.680 -7.984 -2.059
O 11.212 -9.292 -0.360
C 10.236 -5.592 -3.152
N 8.893 -5.621 -3.426
C 8.523 -4.426 -3.916
N 9.605 -3.637 -3.968
C 10.685 -4.335 -3.493
C 9.613 -2.227 -4.392
C 10.655 -1.972 -5.483
C 8.000 -6.762 -3.220
H 8.571 -7.588 -2.758
H 7.589 -7.093 -4.180
H 7.162 -6.470 -2.554
H 7.513 -4.164 -4.263
H 11.670 -3.894 -3.429
H 10.774 -6.459 -2.731
H 8.592 -1.980 -4.728
H 9.829 -1.624 -3.493
H 10.689 -0.908 -5.736
H 11.650 -2.277 -5.140
H 10.419 -2.533 -6.394
O 0.235 -6.111 -2.569
N 0.623 -5.657 -1.458
O 0.479 -6.337 -0.401
O 1.167 -4.511 -1.405

30 ion pairs

C 4.395 -3.271 3.499
N 4.850 -2.696 2.335
C 5.886 -3.413 1.877
N 6.103 -4.434 2.719
C 5.185 -4.372 3.738
C 7.063 -5.539 2.525
C 8.491 -5.153 2.913
C 4.279 -1.498 1.718
H 4.092 -1.686 0.647
H 4.977 -0.636 1.838
H 3.335 -1.255 2.229
H 6.435 -3.217 0.953
H 5.141 -5.140 4.507
H 3.539 -2.880 4.053
H 6.714 -6.389 3.137
H 7.023 -5.835 1.455
H 9.157 -6.013 2.804
H 8.879 -4.346 2.270
H 8.552 -4.806 3.965
O 8.259 0.801 1.181
N 7.283 0.210 1.725
O 7.317 -1.024 1.928
O 6.252 0.887 2.058
C 0.942 4.706 -0.923
N -0.069 3.907 -0.450
C 0.428 3.085 0.485
N 1.739 3.331 0.612
C 2.089 4.338 -0.254
C 2.668 2.632 1.522
C 3.700 1.821 0.736
C -1.474 4.008 -0.828
H -2.019 4.535 -0.035
H -1.906 2.997 -0.948
H -1.555 4.565 -1.777
H -0.126 2.323 1.027
H 3.127 4.680 -0.353
H 0.783 5.466 -1.706
H 3.165 3.390 2.159
H 2.060 1.989 2.183
H 4.357 1.246 1.413
H 3.208 1.103 0.057
H 4.345 2.485 0.130
O 12.161 -2.426 3.193
N 12.264 -3.374 2.357
O 13.336 -3.507 1.682
O 11.300 -4.150 2.153
C 8.917 3.760 -0.749
N 7.705 3.202 -0.412
C 7.585 3.217 0.921
N 8.690 3.758 1.453
C 9.535 4.118 0.427
C 8.921 3.944 2.894
C 10.113 4.853 3.176
C 6.730 2.580 -1.303
H 5.797 2.411 -0.745
H 7.117 1.613 -1.675
H 6.514 3.216 -2.186
H 6.743 2.815 1.475
H 10.506 4.557 0.613
H 9.264 3.846 -1.786
H 7.997 4.374 3.319
H 9.067 2.950 3.379
H 10.069 5.236 4.219
H 11.075 4.316 3.039
H 10.112 5.730 2.508
O 5.089 4.644 -0.241
N 5.306 5.559 0.608
O 6.296 5.469 1.387
O 4.532 6.555 0.667
C -3.558 2.911 4.737
N -3.630 2.282 5.955
C -2.579 1.458 6.073
N -1.824 1.566 4.970
C -2.420 2.456 4.115
C -0.571 0.821 4.747
C 0.205 1.290 3.516
C -4.701 2.431 6.935
H -4.333 2.955 7.825
H -5.052 1.423 7.222
H -5.521 3.003 6.493
H -2.343 0.835 6.935
H -1.992 2.720 3.151
H -4.303 3.622 4.408
H 0.048 0.937 5.660
H -0.819 -0.258 4.651
H 1.060 0.604 3.351
H -0.419 1.300 2.609
H 0.603 2.315 3.665
O 6.010 0.485 -3.528
N 6.468 1.308 -4.361
O 7.210 0.917 -5.302
O 6.160 2.541 -4.275
C 7.725 -6.415 8.532
N 6.453 -6.757 8.145
C 5.968 -5.795 7.356
N 6.901 -4.836 7.223
C 8.012 -5.202 7.947
C 6.745 -3.567 6.478
C 8.075 -3.034 5.945
C 5.733 -7.971 8.516
H 5.919 -8.741 7.752
H 4.658 -7.734 8.557
H 6.082 -8.325 9.489
H 4.962 -5.772 6.956
H 8.894 -4.555 8.017
H 8.329 -7.048 9.168
H 6.038 -3.753 5.643
H 6.275 -2.831 7.163
H 7.931 -2.046 5.462
H 8.821 -2.917 6.753
H 8.497 -3.737 5.197
O 11.899 -2.603 9.464
N 10.675 -2.819 9.571
O 9.969 -3.003 8.504
O 10.103 -2.862 10.686
C 14.358 -4.867 7.773
N 14.343 -3.504 7.947
C 13.288 -2.999 7.296
N 12.625 -4.008 6.708
C 13.274 -5.184 6.988
C 11.394 -3.855 5.907
C 10.595 -5.152 5.811
C 15.297 -2.717 8.721
H 14.795 -2.272 9.588
H 15.694 -1.914 8.078
H 16.112 -3.361 9.061
H 13.047 -1.936 7.222
H 12.945 -6.153 6.597
H 15.119 -5.499 8.208
H 10.774 -3.076 6.405
H 11.671 -3.478 4.901
H 9.766 -5.016 5.090
H 11.229 -6.001 5.475
H 10.146 -5.403 6.784
O -1.186 4.411 2.110
N -0.506 4.616 3.154
O 0.744 4.333 3.145
O -1.037 5.069 4.190
C -4.701 6.795 -4.690
N -3.645 6.463 -5.507
C -3.199 5.246 -5.164
N -3.953 4.787 -4.156
C -4.892 5.734 -3.836
C -3.682 3.539 -3.425
C -4.848 3.087 -2.551
C -3.032 7.337 -6.504
H -2.205 7.888 -6.027
H -3.773 8.046 -6.882
H -2.637 6.738 -7.329
H -2.398 4.691 -5.672
H -5.607 5.584 -3.037
H -5.223 7.738 -4.772
H -3.419 2.761 -4.175
H -2.783 3.715 -2.801
H -4.540 2.184 -2.000
H -5.125 3.865 -1.830
H -5.731 2.846 -3.154
O 7.818 0.716 6.769
N 8.382 0.897 5.649
O 8.715 2.071 5.295
O 8.635 -0.082 4.895
C 1.872 7.497 5.954
N 2.728 7.316 7.016
C 2.549 6.079 7.505
N 1.600 5.467 6.786
C 1.162 6.326 5.811
C 1.116 4.082 6.945
C 1.686 3.153 5.870
C 3.718 8.287 7.480
H 4.684 7.771 7.657
H 3.382 8.763 8.408
H 3.852 9.054 6.697
H 3.093 5.631 8.327
H 0.375 6.027 5.108
H 1.821 8.428 5.381
H 1.399 3.708 7.952
H 0.020 4.098 6.887
H 1.253 2.147 6.004
H 1.421 3.512 4.854
H 2.788 3.082 5.942
O 3.844 -5.452 -1.467
N 4.048 -4.749 -0.423
O 4.610 -5.265 0.566
O 3.628 -3.557 -0.379
C -2.208 -2.399 4.015
N -2.709 -2.104 2.775
C -1.691 -1.851 1.942
N -0.544 -1.965 2.631
C -0.839 -2.308 3.927
C 0.811 -1.816 2.071
C 1.552 -3.158 2.069
C -4.129 -2.062 2.452
H -4.268 -1.636 1.455
H -4.636 -1.442 3.209
H -4.547 -3.075 2.478
H -1.774 -1.581 0.886
H -0.064 -2.469 4.675
H -2.859 -2.642 4.860
H 0.693 -1.436 1.040
H 1.372 -1.059 2.669
H 2.449 -3.105 1.430
H 1.870 -3.422 3.095
H 0.900 -3.960 1.685
O 8.352 8.842 -3.301
N 9.610 8.754 -3.106
O 10.362 8.369 -4.030
O 10.070 8.995 -1.951
C 11.776 3.604 6.788
N 10.461 3.890 7.077
C 9.869 2.777 7.529
N 10.778 1.792 7.553
C 11.975 2.275 7.085
C 10.522 0.400 7.977
C 10.984 -0.591 6.912
C 9.805 5.181 6.909
H 8.752 5.094 7.227
H 9.845 5.494 5.841
H 10.313 5.945 7.506
H 8.831 2.689 7.821
H 12.855 1.629 6.991
H 12.456 4.350 6.398
H 11.046 0.220 8.928
H 9.440 0.311 8.153
H 10.655 -1.615 7.188
H 10.550 -0.341 5.928
H 12.086 -0.578 6.828
O 14.992 0.571 5.040
N 14.884 -0.203 6.029
O 14.028 0.011 6.927
O 15.637 -1.231 6.107
C 5.420 -9.035 1.214
N 5.150 -8.102 0.249
C 3.839 -7.827 0.270
N 3.260 -8.558 1.235
C 4.228 -9.327 1.836
C 1.822 -8.555 1.576
C 1.604 -8.731 3.078
C 6.121 -7.419 -0.605
H 6.837 -8.138 -1.044
H 6.682 -6.667 -0.007

H 5.572 -6.888 -1.404
H 3.333 -7.119 -0.394
H 3.997 -9.991 2.659
H 6.420 -9.444 1.370
H 1.378 -7.603 1.227
H 1.337 -9.372 1.017
H 0.535 -8.799 3.297
H 2.098 -9.643 3.435
H 2.010 -7.878 3.630
O -2.831 2.233 -6.011
N -1.615 2.438 -6.314
O -0.756 1.533 -6.157
O -1.268 3.586 -6.727
C 0.949 10.445 -0.068
N 0.794 9.569 -1.118
C 1.059 8.329 -0.679
N 1.372 8.394 0.620
C 1.306 9.698 1.032
C 1.737 7.243 1.461
C 1.004 7.277 2.797
C 0.412 9.921 -2.487
H 0.047 9.020 -3.014
H 1.277 10.326 -3.025
H -0.377 10.679 -2.466
H 0.998 7.424 -1.289
H 1.513 9.975 2.075
H 0.783 11.509 -0.172
H 1.518 6.322 0.888
H 2.837 7.269 1.626
H 1.325 6.416 3.416
H 1.236 8.211 3.343
H -0.080 7.206 2.662
O 7.941 -4.955 -0.279
N 7.352 -4.309 -1.184
O 6.987 -3.115 -0.980
O 7.156 -4.840 -2.320
C 11.077 -7.444 -0.769
N 11.438 -6.128 -0.621
C 12.385 -6.040 0.326
N 12.635 -7.274 0.790
C 11.832 -8.166 0.123
C 13.571 -7.616 1.877
C 14.238 -8.973 1.652
C 10.842 -5.011 -1.346
H 11.331 -4.078 -1.044
H 9.767 -4.950 -1.090
H 10.947 -5.148 -2.440
H 12.848 -5.115 0.692
H 11.835 -9.231 0.336
H 10.298 -7.779 -1.468
H 14.311 -6.809 1.952
H 13.003 -7.629 2.847
H 14.691 -9.320 2.587
H 13.487 -9.711 1.341
H 15.009 -8.921 0.875
O 9.794 -10.203 -0.603
N 8.686 -9.742 -0.973
O 7.614 -10.105 -0.418
O 8.639 -8.863 -1.903
C 10.733 -9.131 3.395
N 9.964 -9.276 4.523
C 8.951 -10.110 4.252
N 9.052 -10.502 2.976
C 10.156 -9.906 2.415
C 8.094 -11.370 2.272
C 8.803 -12.381 1.373
C 10.192 -8.619 5.809
H 9.223 -8.478 6.306
H 10.687 -7.645 5.635
H 10.850 -9.232 6.438
H 8.177 -10.396 4.952
H 10.413 -10.054 1.363
H 11.626 -8.490 3.395
H 7.468 -11.861 3.030
H 7.440 -10.715 1.655
H 8.071 -13.030 0.882
H 9.365 -11.840 0.593
H 9.496 -13.007 1.946
O -4.554 -2.384 5.943
N -4.463 -1.137 6.036
O -4.678 -0.550 7.135
O -4.083 -0.452 5.026
C 8.285 6.430 -6.819
N 7.904 5.136 -7.102
C 7.604 4.518 -5.952
N 7.784 5.385 -4.944
C 8.209 6.586 -5.455
C 7.628 5.055 -3.518
C 7.006 6.187 -2.703
C 7.855 4.538 -8.435
H 8.861 4.509 -8.867
H 7.207 5.133 -9.086
H 7.452 3.506 -8.360
H 7.227 3.500 -5.840
H 8.425 7.450 -4.815
H 8.578 7.129 -7.589
H 6.984 4.146 -3.458
H 8.630 4.768 -3.125
H 6.981 5.913 -1.642
H 7.569 7.136 -2.816
H 5.968 6.364 -3.025
O 1.257 -1.213 5.736
N 2.432 -1.149 5.310
O 3.385 -1.650 5.992
O 2.680 -0.602 4.193
C 1.889 4.373 -4.122
N 3.219 4.020 -4.085
C 3.479 3.220 -5.132
N 2.349 3.051 -5.829
C 1.344 3.762 -5.226
C 2.195 2.257 -7.063
C 2.462 3.116 -8.303
C 4.182 4.464 -3.080
H 5.103 3.842 -3.135
H 3.752 4.393 -2.066
H 4.468 5.513 -3.261
H 4.458 2.808 -5.385
H 0.331 3.779 -5.638
H 1.428 5.044 -3.389
H 2.921 1.429 -7.025
H 1.168 1.852 -7.062
H 2.309 2.525 -9.211
H 1.792 3.981 -8.336
H 3.503 3.470 -8.291
O 9.562 8.422 3.483
N 10.590 7.789 3.854
O 11.545 7.608 3.043
O 10.622 7.278 5.011
C 8.022 -5.723 -5.375
N 8.394 -6.595 -4.384
C 7.295 -7.063 -3.781
N 6.220 -6.519 -4.368
C 6.644 -5.674 -5.363
C 4.824 -6.763 -3.971
C 4.320 -8.123 -4.462
C 9.764 -6.955 -4.030
H 10.371 -6.033 -3.892
H 10.212 -7.554 -4.830
H 9.748 -7.545 -3.095
H 7.300 -7.748 -2.929
H 5.944 -5.077 -5.949
H 8.763 -5.170 -5.958
H 4.777 -6.699 -2.864
H 4.198 -5.942 -4.376
H 3.281 -8.269 -4.154
H 4.359 -8.183 -5.555
H 4.922 -8.940 -4.050
O 5.012 5.463 6.833
N 6.119 5.648 7.467
O 6.858 4.675 7.728
O 6.434 6.821 7.796
C 10.932 -0.389 0.330
N 10.201 -1.281 1.078
C 10.175 -0.854 2.347
N 10.870 0.290 2.429
C 11.358 0.603 1.184
C 11.018 1.085 3.657
C 12.270 1.961 3.669
C 9.540 -2.471 0.559
H 10.202 -2.986 -0.154
H 8.594 -2.207 0.040
H 9.313 -3.162 1.386
H 9.654 -1.325 3.169
H 11.986 1.470 0.992
H 11.074 -0.511 -0.737
H 10.104 1.713 3.785
H 11.023 0.379 4.509
H 12.483 2.277 4.702
H 13.140 1.405 3.287
H 12.137 2.881 3.060
O 6.089 -6.968 5.100
N 6.679 -8.079 4.953
O 7.130 -8.692 5.967
O 6.842 -8.565 3.799
C 7.608 6.592 4.752
N 7.186 7.799 5.243
C 5.881 7.942 4.974
N 5.458 6.846 4.325
C 6.511 5.984 4.183
C 4.090 6.631 3.823
C 3.591 5.199 4.036
C 8.025 8.717 6.010
H 7.796 9.751 5.740
H 9.079 8.489 5.785
H 7.832 8.564 7.080
H 5.245 8.798 5.224
H 6.413 5.027 3.683
H 8.652 6.263 4.852
H 3.427 7.342 4.358
H 4.066 6.902 2.741
H 2.479 5.186 4.029
H 3.930 4.520 3.236
H 3.940 4.798 5.006
O -1.241 7.733 -4.066
N -0.680 6.731 -3.565
O -1.271 5.617 -3.508
O 0.496 6.840 -3.079
C 5.165 1.742 4.895
N 5.345 0.463 5.349
C 5.207 0.456 6.678
N 4.943 1.704 7.092
C 4.904 2.531 5.996
C 4.862 2.085 8.514
C 3.923 3.258 8.775
C 5.734 -0.690 4.550
H 6.764 -0.999 4.821
H 5.709 -0.412 3.481
H 5.032 -1.524 4.734
H 5.298 -0.409 7.328
H 4.754 3.616 6.093
H 5.252 1.978 3.841
H 4.539 1.181 9.065
H 5.882 2.335 8.846
H 4.027 3.592 9.811
H 4.175 4.105 8.109
H 2.862 2.981 8.616
O 0.749 -5.146 -4.094
N 1.650 -4.552 -4.750
O 2.562 -5.197 -5.325
O 1.651 -3.276 -4.785
C 5.232 -3.154 -7.730
N 5.950 -1.986 -7.614
C 5.783 -1.499 -6.375
N 4.963 -2.320 -5.705
C 4.611 -3.367 -6.520
C 4.459 -2.112 -4.334
C 4.647 -3.344 -3.450
C 6.766 -1.378 -8.661
H 6.797 -0.272 -8.514
H 6.344 -1.614 -9.642
H 7.796 -1.770 -8.605
H 6.233 -0.577 -5.986
H 3.905 -4.140 -6.182
H 5.205 -3.727 -8.647
H 4.966 -1.221 -3.918
H 3.374 -1.889 -4.413
H 4.151 -3.182 -2.473
H 4.192 -4.234 -3.926
H 5.715 -3.559 -3.247
O 13.794 2.344 0.218
N 14.522 2.047 -0.770
O 14.751 0.844 -1.059
O 15.014 2.975 -1.489
C 7.142 -2.784 9.630
N 6.818 -3.617 10.672
C 5.529 -3.432 10.994
N 5.019 -2.486 10.192
C 6.004 -2.070 9.326
C 3.615 -2.016 10.236
C 3.219 -1.233 8.991
C 7.720 -4.609 11.248
H 7.369 -4.905 12.240
H 8.734 -4.175 11.303
H 7.747 -5.493 10.584
H 5.001 -3.932 11.792
H 5.817 -1.313 8.566
H 8.153 -2.774 9.189
H 2.980 -2.916 10.345
H 3.489 -1.399 11.140
H 2.187 -0.838 9.104
H 3.900 -0.375 8.828
H 3.232 -1.866 8.081
O 3.208 -6.269 8.380
N 3.436 -5.517 9.361
O 4.633 -5.444 9.823
O 2.533 -4.800 9.851
C 16.534 0.166 1.409
N 15.520 -0.471 2.076
C 15.997 -0.965 3.224
N 17.299 -0.655 3.311
C 17.662 0.051 2.188
C 18.175 -1.004 4.445
C 19.237 0.069 4.684
C 14.136 -0.534 1.623
H 13.516 0.127 2.257
H 13.761 -1.572 1.694
H 14.095 -0.172 0.583
H 15.447 -1.541 3.959
H 18.671 0.416 2.044
H 16.360 0.634 0.443
H 17.515 -1.127 5.325
H 18.648 -1.976 4.236
H 19.924 -0.244 5.475
H 19.816 0.247 3.769
H 18.775 1.015 4.985
O -2.557 -0.928 -0.920
N -2.125 0.252 -0.733
O -1.067 0.424 -0.057
O -2.734 1.233 -1.235
C 12.293 7.321 -0.859
N 12.716 6.339 -1.717
C 13.455 5.452 -1.029
N 13.506 5.849 0.251
C 12.792 7.012 0.386
C 14.257 5.161 1.322
C 13.518 5.190 2.660
C 12.393 6.276 -3.140
H 13.313 6.364 -3.740
H 11.703 7.100 -3.402
H 11.916 5.304 -3.377
H 13.940 4.544 -1.419
H 12.645 7.495 1.352
H 11.632 8.130 -1.198
H 14.423 4.122 0.982
H 15.238 5.654 1.411

H 14.208 4.975 3.480
H 13.048 6.174 2.837
H 12.714 4.424 2.689
O 10.401 -4.010 -6.214
N 11.266 -3.697 -5.344
O 11.935 -2.622 -5.488
O 11.438 -4.414 -4.327
C 7.948 -2.334 -3.836
N 8.509 -1.157 -3.410
C 9.142 -0.582 -4.444
N 9.014 -1.374 -5.515
C 8.265 -2.471 -5.167
C 9.633 -1.138 -6.827
C 9.582 0.339 -7.225
C 8.430 -0.629 -2.051
H 7.972 -1.392 -1.396
H 7.809 0.286 -2.042
H 9.436 -0.386 -1.675
H 9.671 0.374 -4.430
H 8.072 -3.288 -5.854
H 7.368 -2.991 -3.174
H 10.685 -1.503 -6.759
H 9.113 -1.769 -7.568
H 10.281 0.529 -8.052
H 8.565 0.639 -7.540
H 9.880 0.971 -6.372
O -0.663 -5.323 3.826
N -0.735 -5.379 2.578
O -1.587 -4.674 1.948
O 0.073 -6.110 1.917
C 7.319 8.048 1.744
N 8.118 7.991 0.631
C 7.463 8.536 -0.404
N 6.260 8.949 0.034
C 6.145 8.655 1.369
C 5.187 9.522 -0.796
C 4.354 10.545 -0.019
C 9.452 7.404 0.595
H 10.003 7.801 -0.276
H 9.382 6.300 0.513
H 9.991 7.649 1.530
H 7.839 8.636 -1.434
H 5.248 8.902 1.940
H 7.649 7.670 2.710
H 5.645 9.969 -1.688
H 4.547 8.690 -1.133
H 3.455 10.820 -0.584
H 4.035 10.126 0.952
H 4.931 11.454 0.177
O 12.615 -7.247 4.721
N 13.173 -8.252 5.316
O 13.560 -9.219 4.622
O 13.265 -8.242 6.561
C -1.713 -0.943 -4.594
N -2.921 -0.885 -3.947
C -3.128 -2.044 -3.309
N -2.086 -2.853 -3.547
C -1.182 -2.190 -4.341
C -1.942 -4.222 -3.020
C -3.263 -4.989 -3.067
C -3.817 0.266 -3.905
H -3.773 0.729 -2.895
H -4.844 -0.048 -4.117
H -3.487 1.016 -4.654
H -3.994 -2.301 -2.715
H -0.226 -2.639 -4.640
H -1.331 -0.100 -5.185
H -1.146 -4.724 -3.600
H -1.573 -4.143 -1.974
H -3.149 -5.971 -2.598
H -4.045 -4.438 -2.531
H -3.595 -5.139 -4.100
O 1.833 10.004 4.045
N 3.086 9.881 3.980
O 3.614 9.482 2.890
O 3.807 10.086 4.991
C -0.127 -3.723 -0.477
N 0.820 -4.503 -1.102
C 1.582 -3.718 -1.875
N 1.153 -2.452 -1.759
C 0.090 -2.424 -0.884
C 1.775 -1.297 -2.434
C 3.072 -0.856 -1.739
C 0.936 -5.955 -0.974
H 0.321 -6.446 -1.738
H 0.602 -6.258 0.039
H 1.994 -6.243 -1.114
H 2.423 -4.043 -2.482
H -0.450 -1.507 -0.626
H -0.826 -4.134 0.267
H 1.993 -1.617 -3.475
H 1.040 -0.484 -2.473
H 3.743 -0.358 -2.450
H 2.874 -0.161 -0.905
H 3.603 -1.737 -1.332
O 10.740 2.070 -4.748
N 10.140 2.675 -3.808
O 10.521 3.845 -3.468
O 9.190 2.131 -3.206
C 13.616 -0.226 -4.867
N 13.182 0.326 -6.045
C 13.148 1.659 -5.906
N 13.554 1.971 -4.669
C 13.853 0.814 -3.996
C 13.580 3.342 -4.134
C 14.285 4.295 -5.102
C 12.835 -0.414 -7.255
H 12.424 -1.400 -6.952
H 13.722 -0.559 -7.884
H 12.067 0.137 -7.818
H 12.836 2.370 -6.658
H 14.207 0.812 -2.958
H 13.678 -1.301 -4.734
H 12.524 3.669 -3.960
H 14.089 3.319 -3.148
H 14.200 5.331 -4.740
H 15.348 4.050 -5.198
H 13.825 4.242 -6.097
O 5.476 3.049 -7.303
N 5.765 1.861 -7.632
O 6.836 1.633 -8.277
O 4.985 0.913 -7.339
C -1.847 -3.164 7.057
N -1.285 -2.199 7.857
C 0.040 -2.399 7.909
N 0.338 -3.468 7.158
C -0.819 -3.963 6.611
C 1.694 -3.993 6.917
C 1.881 -4.426 5.461
C -2.009 -1.106 8.506
H -1.573 -0.135 8.187
H -1.925 -1.189 9.595
H -3.069 -1.139 8.208
H 0.747 -1.761 8.444
H -0.818 -4.799 5.915
H -2.915 -3.171 6.820
H 2.410 -3.187 7.184
H 1.875 -4.845 7.601
H 2.769 -5.059 5.363
H 1.003 -4.985 5.098
H 2.019 -3.549 4.797
O 0.504 0.126 9.370
N 0.430 1.263 8.828
O -0.318 1.422 7.801
O 1.088 2.232 9.282

50 ion pairs

C 9.243 4.014 -3.669
N 8.185 3.865 -2.807
C 7.913 2.558 -2.678
N 8.773 1.871 -3.439
C 9.613 2.751 -4.073
C 8.815 0.407 -3.572
C 10.251 -0.111 -3.499
C 7.469 4.937 -2.122
H 7.869 5.075 -1.090
H 6.402 4.668 -2.066
H 7.586 5.882 -2.685
H 7.117 2.131 -2.053
H 10.413 2.405 -4.735
H 9.666 4.996 -3.905
H 8.189 -0.019 -2.777
H 8.348 0.133 -4.548
H 10.279 -1.173 -3.794
H 10.890 0.452 -4.207
H 10.668 -0.009 -2.492
O 12.439 -7.932 -5.703
N 12.158 -6.730 -5.973
O 13.105 -5.926 -6.291
O 10.979 -6.319 -5.944
C 14.061 -7.314 -2.424
N 14.036 -6.786 -1.155
C 13.838 -5.464 -1.242
N 13.734 -5.136 -2.536
C 13.872 -6.269 -3.297
C 13.347 -3.805 -3.033
C 13.922 -3.512 -4.416
C 14.208 -7.570 0.064
H 13.512 -7.228 0.835
H 15.245 -7.470 0.430
H 14.009 -8.630 -0.183
H 13.784 -4.772 -0.414
H 13.802 -6.241 -4.385
H 14.186 -8.382 -2.583
H 12.235 -3.777 -3.049
H 13.694 -3.059 -2.295
H 13.571 -2.526 -4.774
H 15.027 -3.490 -4.378
H 13.606 -4.282 -5.148
O 17.857 -0.907 -5.870
N 18.658 0.022 -6.115
O 19.298 0.573 -5.158
O 18.819 0.454 -7.295
C 9.618 -0.955 -6.488
N 8.808 -1.457 -7.472
C 8.391 -0.444 -8.242
N 8.914 0.698 -7.767
C 9.684 0.405 -6.674
C 8.707 2.040 -8.338
C 9.554 3.095 -7.631
C 8.472 -2.865 -7.642
H 7.855 -2.979 -8.554
H 7.918 -3.240 -6.759
H 9.404 -3.444 -7.739
H 7.727 -0.555 -9.103
H 10.237 1.158 -6.107
H 10.061 -1.574 -5.710
H 8.958 1.984 -9.410
H 7.628 2.297 -8.273
H 9.195 4.100 -7.903
H 9.486 2.987 -6.536
H 10.617 3.003 -7.916
O 11.060 -5.298 0.849
N 10.530 -4.971 -0.256
O 11.239 -4.872 -1.290
O 9.294 -4.710 -0.305
C 19.711 -0.755 -1.325
N 20.044 0.418 -0.688
C 20.813 1.147 -1.506
N 20.990 0.468 -2.647
C 20.310 -0.715 -2.566
C 21.806 0.942 -3.775
C 21.447 2.391 -4.110
C 19.635 0.829 0.648
H 20.459 1.376 1.143
H 19.398 -0.069 1.239
H 18.739 1.488 0.592
H 21.201 2.137 -1.295
H 20.340 -1.457 -3.372
H 19.107 -1.536 -0.846
H 22.865 0.852 -3.491
H 21.619 0.276 -4.626
H 22.139 2.807 -4.856
H 20.419 2.437 -4.529
H 21.478 3.022 -3.201
O 17.538 -2.719 -0.209
N 16.546 -3.456 -0.546
O 16.707 -4.675 -0.785
O 15.394 -2.936 -0.650
C 13.185 -1.649 2.898
N 12.715 -1.805 1.615
C 13.637 -1.350 0.757
N 14.683 -0.898 1.463
C 14.425 -1.066 2.802
C 15.898 -0.307 0.890
C 16.457 0.792 1.791
C 11.394 -2.311 1.271
H 11.315 -3.396 1.523
H 11.214 -2.176 0.202
H 10.627 -1.767 1.859
H 13.584 -1.381 -0.328
H 15.124 -0.755 3.581
H 12.600 -1.965 3.766
H 16.641 -1.122 0.722
H 15.629 0.108 -0.102
H 17.164 1.432 1.228
H 15.651 1.432 2.164
H 16.993 0.369 2.664
O 10.900 -0.712 -11.858
N 10.352 -0.289 -10.797
O 9.333 0.442 -10.847
O 10.858 -0.590 -9.670
C 21.338 -2.134 1.568
N 21.868 -1.949 2.822
C 20.865 -1.811 3.698
N 19.704 -1.896 3.033
C 19.969 -2.098 1.699
C 18.376 -1.635 3.607
C 17.297 -2.522 2.992
C 23.297 -1.896 3.122
H 23.443 -1.486 4.124
H 23.802 -1.256 2.375
H 23.728 -2.904 3.080
H 20.952 -1.695 4.774
H 19.182 -2.243 0.949
H 21.958 -2.209 0.669
H 18.443 -1.772 4.699
H 18.135 -0.555 3.441
H 16.305 -2.210 3.368
H 17.304 -2.438 1.887
H 17.447 -3.578 3.270
O 16.185 -1.400 7.162
N 15.935 -1.306 5.918
O 16.389 -0.341 5.247
O 15.259 -2.209 5.351
C 16.361 -4.563 6.908
N 17.034 -5.588 6.297

C 17.410 -6.470 7.232
N 16.997 -6.034 8.427
C 16.339 -4.843 8.256
C 17.106 -6.793 9.683
C 17.427 -5.893 10.874
C 17.263 -5.751 4.864
H 16.502 -6.422 4.448
H 18.271 -6.175 4.708
H 17.201 -4.775 4.358
H 17.961 -7.385 7.047
H 15.883 -4.299 9.090
H 15.933 -3.722 6.350
H 16.133 -7.305 9.839
H 17.875 -7.578 9.530
H 17.503 -6.485 11.791
H 18.378 -5.356 10.727
H 16.631 -5.140 11.007
O 5.768 -4.951 -3.805
N 6.306 -5.436 -4.854
O 6.613 -4.675 -5.817
O 6.547 -6.668 -4.915
C 5.318 -0.028 2.853
N 4.745 0.138 4.092
C 4.238 1.377 4.169
N 4.473 2.007 3.010
C 5.145 1.156 2.170
C 4.090 3.399 2.704
C 2.916 3.841 3.577
C 4.692 -0.863 5.156
H 4.293 -0.391 6.069
H 5.699 -1.272 5.344
H 4.033 -1.709 4.854
H 3.704 1.802 5.029
H 5.412 1.428 1.144
H 5.785 -0.968 2.551
H 4.980 4.050 2.861
H 3.838 3.442 1.632
H 2.577 4.840 3.288
H 2.082 3.130 3.460
H 3.198 3.857 4.644
O 12.346 2.879 0.566
N 12.546 1.646 0.765
O 12.609 1.198 1.936
O 12.719 0.864 -0.225
C 10.212 -8.998 4.174
N 9.852 -8.435 2.974
C 10.131 -7.125 3.010
N 10.680 -6.840 4.200
C 10.737 -7.987 4.949
C 11.008 -5.481 4.669
C 11.983 -4.744 3.751
C 9.260 -9.154 1.848
H 10.008 -9.268 1.042
H 8.397 -8.586 1.476
H 8.938 -10.155 2.189
H 9.992 -6.406 2.202
H 11.171 -7.998 5.951
H 10.080 -10.068 4.371
H 10.043 -4.925 4.732
H 11.423 -5.567 5.694
H 12.162 -3.725 4.149
H 12.941 -5.270 3.687
H 11.559 -4.641 2.728
O 13.347 -10.163 -1.366
N 12.127 -10.217 -0.962
O 11.371 -11.130 -1.418
O 11.711 -9.400 -0.124
C 5.195 5.201 -4.286
N 5.031 4.218 -5.228
C 5.925 4.401 -6.209
N 6.660 5.481 -5.915
C 6.224 6.004 -4.722
C 7.707 6.059 -6.774
C 8.825 6.690 -5.950
C 4.044 3.149 -5.146
H 3.056 3.523 -5.439
H 4.001 2.779 -4.097
H 4.341 2.318 -5.810
H 6.074 3.780 -7.089
H 6.701 6.868 -4.260
H 4.607 5.233 -3.378
H 8.089 5.249 -7.426
H 7.229 6.802 -7.432
H 9.612 7.095 -6.604
H 8.450 7.509 -5.318
H 9.292 5.952 -5.274
O 17.437 4.234 2.130
N 18.184 3.759 1.248
O 19.447 3.816 1.371
O 17.688 3.165 0.233
C 13.062 3.653 -3.415
N 13.996 4.364 -4.121
C 14.649 5.178 -3.283
N 14.158 4.997 -2.047
C 13.167 4.048 -2.100
C 14.610 5.696 -0.827
C 14.898 4.724 0.318
C 14.226 4.273 -5.557
H 13.521 4.940 -6.086
H 14.074 3.225 -5.898
H 15.259 4.582 -5.780
H 15.463 5.836 -3.567
H 12.645 3.710 -1.195
H 12.414 2.923 -3.904
H 15.508 6.269 -1.089
H 13.832 6.431 -0.523
H 15.226 5.285 1.200
H 13.992 4.147 0.591
H 15.703 4.019 0.040
O 21.408 -8.262 -2.186
N 21.507 -8.039 -0.915
O 20.694 -8.588 -0.140
O 22.381 -7.246 -0.502
C 12.202 -13.224 -3.749
N 11.992 -13.461 -5.086
C 12.626 -12.519 -5.800
N 13.236 -11.680 -4.946
C 12.991 -12.101 -3.662
C 14.065 -10.514 -5.303
C 15.296 -10.932 -6.107
C 11.123 -14.497 -5.639
H 11.290 -14.579 -6.717
H 10.070 -14.204 -5.458
H 11.321 -15.453 -5.127
H 12.636 -12.442 -6.887
H 13.361 -11.554 -2.783
H 11.780 -13.852 -2.951
H 13.442 -9.793 -5.877
H 14.365 -10.027 -4.363
H 15.875 -10.043 -6.423
H 15.961 -11.574 -5.502
H 14.996 -11.479 -7.015
O 3.563 0.778 7.503
N 3.505 2.034 7.609
O 3.146 2.737 6.618
O 3.878 2.598 8.679
C 20.126 3.692 -8.986
N 20.525 3.064 -7.824
C 19.461 2.943 -7.014
N 18.402 3.482 -7.628
C 18.785 3.956 -8.857
C 17.034 3.528 -7.084
C 16.217 2.307 -7.520
C 21.871 2.564 -7.564
H 22.131 2.724 -6.505
H 22.588 3.093 -8.198
H 21.924 1.490 -7.780
H 19.472 2.501 -6.008
H 18.071 4.435 -9.528
H 20.816 3.904 -9.792
H 17.116 3.601 -5.978
H 16.560 4.455 -7.441
H 15.292 2.227 -6.912
H 15.924 2.408 -8.582
H 16.804 1.386 -7.398
O 20.461 0.630 4.550
N 21.423 1.253 3.992
O 22.082 2.104 4.638
O 21.706 1.001 2.785
C 16.354 -9.641 -1.722
N 17.512 -9.263 -1.091
C 18.557 -9.722 -1.791
N 18.095 -10.393 -2.858
C 16.724 -10.348 -2.844
C 18.931 -11.018 -3.895
C 18.315 -12.313 -4.421
C 17.634 -8.509 0.154
H 18.641 -8.075 0.206
H 17.499 -9.197 1.019
H 16.865 -7.724 0.196
H 19.602 -9.561 -1.510
H 16.125 -10.794 -3.636
H 15.356 -9.402 -1.343
H 19.046 -10.276 -4.716
H 19.926 -11.195 -3.465
H 18.928 -12.730 -5.225
H 18.229 -13.061 -3.627
H 17.305 -12.116 -4.823
O 7.298 -2.370 -12.497
N 7.714 -2.610 -11.348
O 8.742 -3.320 -11.155
O 7.098 -2.121 -10.331
C 6.830 2.405 8.466
N 6.925 1.109 8.909
C 8.178 0.685 8.719
N 8.893 1.677 8.165
C 8.073 2.762 7.988
C 10.345 1.609 7.921
C 10.885 2.717 7.020
C 5.845 0.323 9.507
H 5.622 0.706 10.509
H 6.162 -0.729 9.576
H 4.936 0.407 8.880
H 8.539 -0.314 8.958
H 8.448 3.706 7.571
H 5.884 2.956 8.523
H 10.852 1.638 8.915
H 10.565 0.622 7.476
H 11.979 2.772 7.146
H 10.677 2.511 5.955
H 10.457 3.704 7.277
O 17.739 -9.652 8.971
N 16.734 -10.365 8.682
O 15.695 -10.337 9.380
O 16.777 -11.111 7.644
C 11.710 7.883 -0.531
N 10.883 6.834 -0.228
C 9.639 7.131 -0.620
N 9.647 8.359 -1.162
C 10.929 8.848 -1.123
C 8.489 9.048 -1.755
C 8.187 8.521 -3.162
C 11.298 5.602 0.431
H 10.403 5.050 0.753
H 11.930 5.850 1.308
H 11.883 4.971 -0.261
H 8.763 6.486 -0.481
H 11.185 9.824 -1.514
H 12.771 7.861 -0.252
H 7.624 8.908 -1.092
H 8.722 10.121 -1.788
H 7.404 9.121 -3.636
H 9.096 8.546 -3.792
H 7.838 7.471 -3.113
O 14.549 4.978 -8.926
N 15.691 4.986 -9.463
O 16.473 5.970 -9.269
O 16.085 4.003 -10.146
C 8.364 -7.600 -2.614
N 7.608 -6.661 -1.949
C 7.987 -5.442 -2.357
N 8.966 -5.574 -3.257
C 9.222 -6.911 -3.440
C 9.691 -4.460 -3.891
C 8.762 -3.278 -4.161
C 6.583 -6.900 -0.937
H 6.307 -7.972 -0.905
H 5.692 -6.298 -1.180
H 6.948 -6.593 0.064
O 7.532 -4.501 -2.057
H 9.960 -7.249 -4.161
H 8.204 -8.674 -2.486
H 10.528 -4.172 -3.213
H 10.145 -4.844 -4.820
H 9.351 -2.373 -4.394
H 8.090 -3.488 -5.019
H 8.126 -3.065 -3.283
O 0.393 -2.174 -1.928
N 0.084 -3.373 -1.640
O 0.663 -4.328 -2.250
O -0.770 -3.620 -0.756
C 14.083 5.889 5.476
N 15.314 5.317 5.680
C 15.326 4.720 6.885
N 14.126 4.910 7.455
C 13.335 5.634 6.603
C 13.692 4.391 8.767
C 13.960 2.890 8.871
C 16.403 5.347 4.706
H 16.198 6.153 3.981
H 16.471 4.387 4.163
H 17.362 5.522 5.209
H 16.159 4.159 7.322
H 12.310 5.892 6.882
H 13.849 6.430 4.548
H 14.229 4.941 9.554
H 12.619 4.619 8.862
H 13.603 2.497 9.835
H 13.405 2.355 8.080
H 15.033 2.661 8.777
O 6.826 5.123 2.378
N 7.363 5.441 1.270
O 6.972 6.441 0.620
O 8.343 4.762 0.829
C 19.129 -6.893 -3.208
N 19.800 -6.868 -4.405
C 19.679 -5.650 -4.938
N 18.966 -4.880 -4.103
C 18.603 -5.637 -3.010
C 18.763 -3.433 -4.298
C 17.509 -2.895 -3.616
C 20.488 -7.990 -5.033
H 20.784 -7.699 -6.052
H 19.797 -8.853 -5.086
H 21.368 -8.265 -4.436
H 20.065 -5.328 -5.908
H 17.968 -5.243 -2.211
H 19.068 -7.796 -2.599
H 19.671 -2.910 -3.901
H 18.737 -3.242 -5.387
H 17.430 -1.814 -3.817
H 16.595 -3.373 -4.012
H 17.540 -3.060 -2.529
O 0.610 1.704 1.390
N 0.642 0.924 2.376
O 1.484 1.080 3.296
O -0.162 -0.072 2.406
C 9.907 -6.037 10.483
N 10.727 -5.977 9.388
C 11.926 -6.483 9.709
N 11.888 -6.879 10.989
C 10.640 -6.605 11.499
C 13.001 -7.474 11.757
C 13.945 -8.297 10.882
C 10.308 -5.490 8.080

H 9.796 -4.511 8.189
H 9.581 -6.206 7.655
H 11.187 -5.397 7.412
H 12.784 -6.592 9.035
H 10.372 -6.836 12.521
H 8.886 -5.666 10.443
H 13.543 -6.645 12.249
H 12.557 -8.095 12.548
H 14.661 -8.844 11.502
H 13.388 -9.030 10.278
H 14.517 -7.661 10.182
O 23.197 1.138 -0.460
N 23.583 -0.021 -0.086
O 24.422 -0.146 0.833
O 23.090 -1.045 -0.647
C 3.477 -8.118 -0.887
N 3.208 -7.465 -2.064
C 2.013 -6.865 -1.957
N 1.512 -7.119 -0.738
C 2.403 -7.902 -0.053
C 0.198 -6.663 -0.236
C 0.085 -6.821 1.279
C 4.096 -7.423 -3.223
H 3.508 -7.345 -4.162
H 4.703 -8.331 -3.251
H 4.771 -6.544 -3.161
H 1.545 -6.239 -2.717
H 2.204 -8.274 0.958
H 4.406 -8.678 -0.723
H 0.056 -5.604 -0.538
H -0.580 -7.253 -0.745
H -0.934 -6.557 1.604
H 0.314 -7.852 1.601
H 0.783 -6.149 1.792
O 10.170 -12.110 3.973
N 9.008 -12.540 3.736
O 8.741 -13.763 3.843
O 8.091 -11.721 3.386
C 14.603 1.018 -12.059
N 13.880 -0.150 -12.074
C 13.423 -0.386 -10.839
N 13.819 0.614 -10.038
C 14.566 1.501 -10.771
C 13.498 0.741 -8.602
C 13.137 2.180 -8.221
C 13.642 -1.008 -13.230
H 14.349 -1.857 -13.193
H 13.801 -0.438 -14.149
H 12.610 -1.376 -13.189
H 12.804 -1.229 -10.532
H 15.015 2.404 -10.328
H 15.077 1.417 -12.945
H 12.675 0.031 -8.398
H 14.380 0.415 -8.026
H 13.323 2.336 -7.141
H 13.762 2.902 -8.773
H 12.076 2.408 -8.420
O 17.700 3.109 7.896
N 17.875 2.118 8.672
O 19.016 1.563 8.724
O 16.920 1.658 9.350
C 11.308 -5.686 -10.128
N 11.240 -4.730 -11.109
C 11.630 -3.552 -10.597
N 11.959 -3.743 -9.312
C 11.763 -5.061 -8.991
C 12.535 -2.749 -8.391
C 12.057 -2.992 -6.963
C 10.790 -4.982 -12.477
H 11.462 -4.491 -13.188
H 9.775 -4.578 -12.599
H 10.792 -6.069 -12.649
H 11.648 -2.589 -11.112
H 11.974 -5.440 -7.990
H 11.028 -6.734 -10.301
H 13.633 -2.825 -8.459
H 12.251 -1.739 -8.755
H 12.448 -2.217 -6.281
H 10.954 -2.969 -6.923
H 12.399 -3.982 -6.600
O 10.594 6.662 -3.302
N 11.352 7.240 -4.136
O 12.419 6.680 -4.518
O 11.034 8.379 -4.592
C 13.699 -12.945 1.592
N 13.641 -13.057 0.224
C 12.383 -13.350 -0.134
N 11.636 -13.437 0.972
C 12.427 -13.180 2.065
C 10.185 -13.683 0.967
C 9.424 -12.382 0.691
C 14.738 -12.837 -0.717
H 14.983 -13.768 -1.239
H 15.628 -12.467 -0.173
H 14.419 -12.074 -1.453
H 12.027 -13.547 -1.146
H 12.027 -13.149 3.079
H 14.639 -12.731 2.120
H 9.978 -14.420 0.161
H 9.892 -14.115 1.937
H 8.382 -12.605 0.368
H 9.372 -11.737 1.584
H 9.927 -11.814 -0.114
O 5.245 4.778 -10.448
N 5.758 4.905 -9.317
O 5.265 5.672 -8.447
O 6.799 4.214 -9.006
C 19.514 -2.771 8.568
N 18.947 -1.594 8.156
C 18.151 -1.129 9.130
N 18.213 -1.977 10.166
C 19.051 -3.017 9.840
C 17.518 -1.793 11.453
C 17.531 -0.319 11.866
C 19.187 -0.947 6.871
H 18.253 -0.926 6.281
H 19.958 -1.502 6.314
H 19.509 0.096 7.040
H 17.551 -0.213 9.119
H 19.228 -3.853 10.510
H 20.158 -3.358 7.909
H 16.474 -2.166 11.348
H 18.017 -2.426 12.199
H 16.875 -0.156 12.730
H 18.542 0.010 12.126
H 17.166 0.310 11.030
O 3.645 -3.533 4.088
N 4.376 -3.443 3.057
O 5.576 -3.038 3.178
O 3.915 -3.713 1.919
C 7.828 -5.572 -9.387
N 6.665 -5.454 -8.664
C 6.609 -6.452 -7.775
N 7.706 -7.207 -7.907
C 8.484 -6.682 -8.909
C 7.987 -8.415 -7.108
C 9.466 -8.782 -7.123
C 5.669 -4.396 -8.801
H 4.916 -4.677 -9.546
H 6.176 -3.467 -9.127
H 5.175 -4.249 -7.827
H 5.793 -6.625 -7.083
H 9.420 -7.148 -9.230
H 8.119 -4.846 -10.151
H 7.623 -8.218 -6.086
H 7.373 -9.236 -7.535
H 9.630 -9.743 -6.599
H 9.843 -8.886 -8.157
H 10.063 -8.005 -6.617
O 17.600 -8.764 -5.280
N 17.350 -8.029 -6.279
O 17.745 -6.816 -6.285
O 16.727 -8.481 -7.268
C 7.297 -10.370 5.487
N 6.923 -11.467 6.216
C 5.593 -11.444 6.382
N 5.105 -10.354 5.768
C 6.148 -9.671 5.196
C 3.678 -9.983 5.669
C 3.485 -8.475 5.501
C 7.837 -12.480 6.732
H 7.289 -13.179 7.368
H 8.619 -11.970 7.317
H 8.299 -13.022 5.893
H 5.014 -12.171 6.931
H 5.987 -8.740 4.634
H 8.334 -10.153 5.240
H 3.235 -10.521 4.799
H 3.168 -10.354 6.568
H 2.427 -8.247 5.268
H 3.766 -7.942 6.425
H 4.117 -8.097 4.678
O 14.334 -3.083 -10.896
N 15.497 -3.339 -11.327
O 16.196 -4.241 -10.775
O 15.974 -2.672 -12.286
C 14.289 -6.785 -9.985
N 14.749 -6.736 -8.694
C 14.194 -7.737 -8.001
N 13.374 -8.418 -8.814
C 13.417 -7.848 -10.065
C 12.521 -9.544 -8.380
C 13.056 -10.903 -8.839
C 15.611 -5.696 -8.144
H 15.837 -4.971 -8.940
H 16.556 -6.139 -7.759
H 15.089 -5.203 -7.315
H 14.343 -7.961 -6.953
H 12.786 -8.184 -10.893
H 14.610 -6.058 -10.723
H 12.478 -9.493 -7.274
H 11.500 -9.365 -8.777
H 12.346 -11.702 -8.547
H 13.176 -10.931 -9.927
H 14.030 -11.123 -8.373
O 7.152 -10.386 -2.142
N 6.584 -10.716 -1.078
O 6.677 -11.906 -0.643
O 5.929 -9.860 -0.404
C -1.901 0.764 -1.391
N -1.410 -0.138 -0.479
C -0.079 -0.021 -0.433
N 0.299 0.935 -1.291
C -0.819 1.445 -1.901
C 1.683 1.420 -1.418
C 1.909 2.250 -2.678
C -2.182 -1.077 0.329
H -1.893 -0.947 1.384
H -1.943 -2.112 0.017
H -3.249 -0.883 0.202
H 0.577 -0.603 0.197
H -0.761 2.243 -2.630
H -2.957 0.859 -1.603
H 1.924 2.005 -0.513
H 2.342 0.535 -1.427
H 2.982 2.539 -2.743
H 1.668 1.669 -3.581
H 1.298 3.159 -2.673
O 10.513 0.049 5.378
N 10.433 -0.919 4.577
O 10.915 -2.054 4.894
O 9.868 -0.765 3.459
C 10.823 4.738 3.356
N 11.632 3.640 3.510
C 10.865 2.566 3.746
N 9.580 2.954 3.728
C 9.525 4.303 3.489
C 8.419 2.062 3.898
C 7.327 2.703 4.760
C 13.083 3.670 3.355
H 13.520 2.759 3.770
H 13.485 4.560 3.872
H 13.328 3.736 2.274
H 11.204 1.548 3.911
H 8.571 4.836 3.415
H 11.249 5.717 3.147
H 8.020 1.829 2.898
H 8.795 1.120 4.335
H 6.418 2.081 4.751
H 7.658 2.819 5.809
H 7.055 3.699 4.368
O 4.286 -8.251 -7.664
N 3.639 -7.443 -6.921
O 3.761 -6.193 -7.108
O 2.913 -7.870 -5.989
C 15.210 1.260 -1.864
N 15.535 0.282 -2.768
C 16.575 0.695 -3.509
N 16.926 1.923 -3.090
C 16.091 2.296 -2.066
C 17.959 2.803 -3.668
C 18.793 3.497 -2.589
C 14.841 -0.994 -2.889
H 15.560 -1.778 -3.178
H 14.061 -0.932 -3.681
H 14.376 -1.259 -1.924
H 17.055 0.112 -4.302
H 16.209 3.231 -1.516
H 14.350 1.166 -1.189
H 18.611 2.208 -4.348
H 17.447 3.568 -4.302
H 19.231 4.416 -2.996
H 18.174 3.744 -1.711
H 19.623 2.849 -2.242
O 11.931 1.446 10.603
N 11.157 0.647 11.197
O 10.018 0.392 10.709
O 11.549 0.030 12.233
C 0.936 -3.232 2.752
N 0.501 -2.412 3.763
C -0.837 -2.389 3.754
N -1.271 -3.192 2.775
C -0.184 -3.729 2.129
C -2.680 -3.532 2.523
C -2.898 -5.046 2.615
C 1.353 -1.630 4.650
H 0.986 -1.697 5.687
H 1.355 -0.568 4.319
H 2.383 -2.029 4.602
H -1.482 -1.819 4.414
H -0.285 -4.397 1.277
H 1.997 -3.409 2.555
H -3.278 -3.005 3.286
H -2.956 -3.151 1.524
H -3.925 -5.307 2.346
H -2.206 -5.583 1.944
H -2.705 -5.395 3.647
O 10.764 -12.972 -8.423
N 9.944 -12.455 -7.625
O 10.363 -11.691 -6.700
O 8.706 -12.709 -7.711
C 12.404 -1.197 7.469
N 13.207 -2.308 7.578
C 14.107 -2.097 8.553
N 13.895 -0.875 9.070
C 12.846 -0.293 8.404
C 14.645 -0.179 10.135
C 14.435 -0.805 11.516
C 13.093 -3.498 6.734
H 12.445 -4.267 7.201
H 14.095 -3.923 6.569
H 12.647 -3.213 5.764
H 14.853 -2.813 8.899
H 12.494 0.708 8.669
H 11.621 -1.103 6.709

H 15.724 -0.166 9.869
H 14.291 0.867 10.132
H 15.087 -0.309 12.247
H 13.384 -0.689 11.861
H 14.698 -1.878 11.498
O 10.808 -15.097 -1.737
N 10.723 -15.955 -2.708
O 9.601 -16.379 -3.049
O 11.764 -16.271 -3.324
C 4.780 -5.078 6.927
N 5.625 -5.963 7.559
C 6.891 -5.617 7.287
N 6.872 -4.535 6.496
C 5.573 -4.179 6.255
C 8.068 -3.828 6.011
C 7.722 -2.469 5.414
C 5.201 -7.082 8.396
H 6.014 -7.830 8.467
H 4.320 -7.557 7.936
H 4.937 -6.729 9.400
H 7.776 -6.160 7.630
H 5.300 -3.346 5.604
H 3.697 -5.151 6.995
H 8.767 -3.740 6.865
H 8.555 -4.470 5.235
H 8.608 -2.035 4.931
H 6.928 -2.577 4.653
H 7.368 -1.784 6.196
O 1.222 -10.657 4.171
N 1.059 -9.568 3.558
O 0.618 -8.552 4.169
O 1.395 -9.478 2.338
C 18.672 -2.203 -8.718
N 18.626 -2.469 -10.064
C 18.733 -3.795 -10.246
N 18.862 -4.380 -9.047
C 18.821 -3.408 -8.077
C 19.071 -5.816 -8.790
C 20.468 -6.065 -8.204
C 18.476 -1.470 -11.121
H 19.376 -1.444 -11.746
H 18.324 -0.488 -10.667
H 17.603 -1.732 -11.749
H 18.731 -4.305 -11.198
H 18.923 -3.627 -7.014
H 18.609 -1.189 -8.308
H 18.284 -6.153 -8.072
H 18.925 -6.357 -9.733
H 20.508 -7.026 -7.668
H 21.236 -6.070 -8.984
H 20.721 -5.264 -7.479
O 14.683 -7.006 5.901
N 13.968 -6.934 6.913
O 12.704 -6.735 6.808
O 14.458 -7.055 8.075
C 15.022 9.287 -5.671
N 15.896 8.669 -6.534
C 15.214 7.788 -7.281
N 13.926 7.836 -6.915
C 13.775 8.759 -5.915
C 12.844 7.003 -7.469
C 11.568 7.818 -7.665
C 17.336 8.905 -6.602
H 17.699 8.662 -7.605
H 17.860 8.260 -5.864
H 17.550 9.954 -6.378
H 15.642 7.127 -8.054
H 12.801 8.934 -5.447
H 15.346 10.037 -4.962
H 13.211 6.551 -8.404
H 12.670 6.177 -6.749
H 10.763 7.182 -8.050
H 11.245 8.238 -6.695
H 11.725 8.641 -8.371
O 10.322 -8.620 -10.275
N 10.375 -8.726 -11.558
O 11.228 -8.046 -12.184
O 9.575 -9.485 -12.145
C 23.697 4.894 -0.012
N 22.512 4.200 0.028
C 22.608 3.233 0.958
N 23.824 3.305 1.518
C 24.523 4.326 0.929
C 24.356 2.388 2.544
C 25.675 2.890 3.128
C 21.359 4.485 -0.822
H 20.433 4.316 -0.240
H 21.354 3.816 -1.711
H 21.402 5.522 -1.163
H 21.824 2.527 1.247
H 25.540 4.562 1.216
H 23.859 5.723 -0.687
H 23.587 2.275 3.335
H 24.487 1.397 2.057
H 26.060 2.170 3.855
H 26.429 3.021 2.343
H 25.543 3.852 3.636
O 17.127 5.493 -4.852
N 18.367 5.820 -4.934
O 19.214 4.928 -5.245
O 18.719 6.992 -4.711
C 19.461 -8.362 5.550
N 19.667 -8.916 6.794
C 19.276 -10.200 6.765
N 18.832 -10.481 5.534
C 18.938 -9.357 4.756
C 18.270 -11.772 5.100
C 19.317 -12.887 5.120
C 20.126 -8.192 7.980
H 19.313 -8.193 8.734
H 20.354 -7.153 7.696
H 21.012 -8.675 8.405
H 19.311 -10.889 7.596
H 18.614 -9.359 3.718
H 19.698 -7.311 5.320
H 17.429 -12.013 5.783
H 17.852 -11.629 4.087
H 18.866 -13.831 4.800
H 20.146 -12.660 4.441
H 19.725 -13.024 6.128
O 13.050 -3.994 10.176
N 13.924 -4.116 11.093
O 13.588 -4.544 12.222
O 15.125 -3.767 10.860
C 11.888 -11.164 6.091
N 12.576 -10.601 7.134
C 13.766 -11.209 7.245
N 13.855 -12.147 6.287
C 12.694 -12.138 5.555
C 14.993 -13.072 6.101
C 14.946 -13.785 4.751
C 12.084 -9.500 7.956
H 11.014 -9.661 8.178
H 12.176 -8.542 7.397
H 12.673 -9.435 8.885
H 14.538 -10.971 7.993
H 12.522 -12.801 4.708
H 10.895 -10.838 5.788
H 15.931 -12.488 6.221
H 14.965 -13.804 6.923
H 15.683 -14.593 4.730
H 13.953 -14.218 4.577
H 15.179 -13.103 3.913
O 6.557 -2.796 10.340
N 7.263 -3.018 9.340
O 7.893 -4.133 9.228
O 7.414 -2.141 8.441
C 7.399 -10.086 -10.135
N 7.636 -11.434 -10.098
C 6.722 -12.016 -9.309
N 5.904 -11.063 -8.835
C 6.304 -9.848 -9.332
C 4.773 -11.258 -7.906
C 3.741 -12.238 -8.470
C 8.757 -12.098 -10.764
H 9.451 -12.502 -10.005
H 9.275 -11.349 -11.384
H 8.392 -12.918 -11.392
H 6.653 -13.071 -9.088
H 5.764 -8.937 -9.078
H 8.048 -9.429 -10.717
H 5.173 -11.630 -6.952
H 4.330 -10.259 -7.724
H 2.933 -12.391 -7.749
H 3.303 -11.855 -9.397
H 4.203 -13.209 -8.683
O 21.167 -3.560 -6.428
N 21.672 -3.544 -5.273
O 22.060 -4.644 -4.752
O 21.705 -2.484 -4.595
C 8.440 -12.931 -4.653
N 8.951 -12.022 -3.760
C 8.803 -12.508 -2.522
N 8.210 -13.705 -2.594
C 7.972 -13.996 -3.912
C 7.908 -14.546 -1.426
C 6.912 -15.659 -1.731
C 9.508 -10.699 -4.035
H 8.837 -9.934 -3.605
H 9.610 -10.552 -5.124
H 10.489 -10.615 -3.549
H 9.153 -12.024 -1.614
H 7.511 -14.927 -4.216
H 8.437 -12.757 -5.733
H 8.877 -14.967 -1.072
H 7.535 -13.865 -0.625
H 6.652 -16.180 -0.798
H 5.990 -15.258 -2.168
H 7.353 -16.379 -2.430
O 16.543 -12.463 2.487
N 16.991 -11.463 1.855
O 17.314 -10.415 2.492
O 17.099 -11.494 0.599
C 3.703 -11.594 2.763
N 4.650 -10.702 2.320
C 5.740 -11.385 1.940
N 5.508 -12.692 2.113
C 4.247 -12.851 2.632
C 6.437 -13.776 1.757
C 5.701 -15.088 1.484
C 4.461 -9.256 2.209
H 4.928 -8.911 1.275
H 4.917 -8.718 3.072
H 3.375 -9.044 2.176
H 6.653 -10.956 1.551
H 3.833 -13.827 2.847
H 2.716 -11.274 3.132
H 6.987 -13.438 0.845
H 7.189 -13.888 2.568
H 6.359 -15.792 0.955
H 5.360 -15.559 2.413
H 4.826 -14.914 0.849
O 7.860 -6.254 4.211
N 6.982 -6.690 3.397
O 7.275 -6.807 2.171
O 5.848 -7.032 3.821
C 7.346 2.276 -13.219
N 7.567 0.937 -13.005
C 6.943 0.575 -11.876
N 6.330 1.649 -11.364
C 6.563 2.727 -12.180
C 5.604 1.700 -10.082
C 5.198 0.311 -9.599
C 8.455 0.069 -13.776
H 8.003 -0.928 -13.864
H 9.413 -0.040 -13.231
H 8.632 0.501 -14.764
H 6.939 -0.424 -11.433
H 6.167 3.711 -11.925
H 7.757 2.801 -14.070
H 6.276 2.199 -9.344
H 4.737 2.363 -10.208
H 4.860 0.358 -8.552
H 4.392 -0.106 -10.212
H 6.058 -0.384 -9.650
O 4.025 2.777 -0.301
N 4.909 2.480 -1.115
O 5.756 1.564 -0.850
O 4.975 3.075 -2.250
C 9.210 -2.956 11.917
N 10.260 -2.546 11.128
C 11.358 -2.457 11.889
N 11.047 -2.816 13.141
C 9.708 -3.126 13.187
C 12.006 -2.875 14.259
C 12.628 -1.504 14.533
C 10.195 -2.287 9.694
H 9.436 -1.513 9.482
H 9.896 -3.210 9.159
H 11.173 -1.943 9.324
H 12.347 -2.168 11.551
H 9.217 -3.431 14.101
H 8.198 -3.069 11.523
H 11.473 -3.258 15.139
H 12.787 -3.605 13.983
H 13.438 -1.589 15.263
H 13.029 -1.080 13.597
H 11.880 -0.804 14.921
O -2.105 -4.020 5.424
N -2.819 -3.119 6.022
O -2.850 -3.119 7.279
O -3.418 -2.277 5.335
C 0.586 -6.383 6.190
N -0.783 -6.395 6.313
C -1.149 -5.428 7.167
N -0.049 -4.795 7.597
C 1.052 -5.376 7.002
C -0.058 -3.629 8.504
C 1.099 -2.677 8.209
C -1.708 -7.176 5.494
H -2.459 -7.665 6.123
H -1.136 -7.925 4.929
H -2.216 -6.488 4.790
H -2.155 -5.201 7.497
H 2.065 -5.020 7.178
H 1.110 -7.090 5.540
H -1.037 -3.133 8.366
H -0.006 -3.993 9.543
H 1.112 -1.853 8.928
H 2.059 -3.204 8.264
H 1.004 -2.246 7.197
O 7.068 -9.488 8.258
N 8.267 -9.123 8.115
O 8.609 -7.937 8.378
O 9.128 -9.951 7.677
C 3.908 -3.479 -5.632
N 2.802 -3.834 -4.901
C 2.449 -2.801 -4.123
N 3.309 -1.794 -4.338
C 4.233 -2.189 -5.276
C 3.169 -0.458 -3.731
C 4.503 0.204 -3.402
C 2.062 -5.093 -4.968
H 1.407 -5.093 -5.846
H 1.450 -5.189 -4.056
H 2.748 -5.959 -5.051
H 1.622 -2.786 -3.406
H 5.049 -1.532 -5.596
H 4.385 -4.162 -6.340
H 2.594 0.176 -4.430
H 2.553 -0.568 -2.822
H 4.347 1.283 -3.180
H 4.982 -0.267 -2.529
H 5.190 0.122 -4.256
C 12.006 -2.875 14.259
C 12.628 -1.504 14.533
C 10.195 -2.287 9.694
H 9.436 -1.513 9.482
H 9.896 -3.210 9.159
H 11.173 -1.943 9.324
H 12.347 -2.168 11.551
H 9.217 -3.431 14.101
H 8.198 -3.069 11.523
H 11.473 -3.258 15.139
H 12.787 -3.605 13.983
H 13.438 -1.589 15.263
H 13.029 -1.080 13.597
H 11.880 -0.804 14.921
O -2.105 -4.020 5.424
N -2.819 -3.119 6.022
O -2.850 -3.119 7.279
O -3.418 -2.277 5.335
C 0.586 -6.383 6.190
N -0.783 -6.395 6.313
C -1.149 -5.428 7.167
N -0.049 -4.795 7.597
C 1.052 -5.376 7.002
C -0.058 -3.629 8.504
C 1.099 -2.677 8.209
C -1.708 -7.176 5.494
H -2.459 -7.665 6.123
H -1.136 -7.925 4.929
H -2.216 -6.488 4.790
H -2.155 -5.201 7.497
H 2.065 -5.020 7.178
H 1.110 -7.090 5.540
H -1.037 -3.133 8.366
H -0.006 -3.993 9.543
H 1.112 -1.853 8.928
H 2.059 -3.204 8.264
H 1.004 -2.246 7.197
O 7.068 -9.488 8.258
N 8.267 -9.123 8.115
O 8.609 -7.937 8.378
O 9.128 -9.951 7.677
C 3.908 -3.479 -5.632
N 2.802 -3.834 -4.901
C 2.449 -2.801 -4.123
N 3.309 -1.794 -4.338
C 4.233 -2.189 -5.276
C 3.169 -0.458 -3.731
C 4.503 0.204 -3.402
C 2.062 -5.093 -4.968
H 1.407 -5.093 -5.846
H 1.450 -5.189 -4.056
H 2.748 -5.959 -5.051
H 1.622 -2.786 -3.406
H 5.049 -1.532 -5.596
H 4.385 -4.162 -6.340
H 2.594 0.176 -4.430
H 2.553 -0.568 -2.822
H 4.347 1.283 -3.180
H 4.982 -0.267 -2.529
H 5.190 0.122 -4.256

N 14.142 7.351 2.311
O 14.176 7.811 1.142
O 13.141 6.628 2.680
C 24.688 -4.868 -2.162
N 23.846 -5.887 -2.547
C 22.581 -5.487 -2.378
N 22.589 -4.241 -1.890
C 23.890 -3.827 -1.749
C 21.413 -3.399 -1.637
C 20.314 -4.120 -0.858
C 24.221 -7.215 -3.020
H 24.483 -7.183 -4.085
H 23.354 -7.882 -2.872
H 25.078 -7.589 -2.452
H 21.706 -6.090 -2.598
H 24.122 -2.835 -1.370
H 25.765 -4.958 -2.203
H 21.768 -2.514 -1.076
H 21.032 -3.037 -2.625
H 19.501 -3.411 -0.594
H 19.870 -4.931 -1.461
H 20.705 -4.553 0.069
O 20.653 -3.588 5.888
N 20.286 -4.800 5.903
O 20.264 -5.477 4.850
O 19.890 -5.325 6.997
C 19.264 4.147 4.534
N 18.788 2.932 4.968
C 19.462 2.575 6.068
N 20.349 3.530 6.358
C 20.251 4.526 5.414
C 21.285 3.471 7.491
C 21.599 4.864 8.036
C 17.722 2.156 4.344
H 18.129 1.234 3.880
H 17.239 2.781 3.574
H 16.986 1.850 5.096
H 19.333 1.656 6.639
H 20.881 5.405 5.444
H 18.879 4.606 3.624
H 20.819 2.832 8.259
H 22.205 2.973 7.146
H 22.362 4.808 8.817
H 21.970 5.513 7.233
H 20.704 5.328 8.463
O 12.151 1.562 -5.374
N 13.122 0.743 -5.286
O 14.306 1.185 -5.297
O 12.898 -0.493 -5.170
C 4.896 5.078 6.140
N 5.500 5.606 7.256
C 6.562 6.333 6.872
N 6.649 6.274 5.536
C 5.629 5.496 5.054
C 7.703 6.899 4.721
C 7.461 8.397 4.518
C 5.051 5.393 8.630
H 4.186 6.032 8.846
H 5.860 5.635 9.323
H 4.746 4.328 8.751
H 7.287 6.823 7.532
H 5.523 5.271 3.989
H 4.031 4.401 6.199
H 8.660 6.716 5.237
H 7.717 6.358 3.753
H 8.265 8.830 3.915
H 6.512 8.574 4.000
H 7.434 8.922 5.479
O 9.061 6.990 8.313
N 9.696 6.037 7.806
O 10.841 5.713 8.206
O 9.155 5.369 6.845
C 7.908 -1.932 1.530
N 8.052 -3.258 1.845
C 7.197 -3.976 1.105
N 6.512 -3.136 0.317
C 6.930 -1.851 0.567
C 5.493 -3.504 -0.680
C 5.691 -2.703 -1.966
C 9.038 -3.787 2.776
H 8.578 -4.522 3.470
H 9.469 -2.949 3.355
H 9.856 -4.302 2.211
H 7.087 -5.063 1.140
H 6.515 -0.998 0.042
H 8.512 -1.171 2.015
H 5.587 -4.589 -0.878
H 4.499 -3.331 -0.235
H 4.928 -2.959 -2.710
H 5.635 -1.619 -1.766
H 6.681 -2.923 -2.409
O 6.798 -0.426 -5.740
N 6.244 0.671 -6.053
O 5.080 0.669 -6.542
O 6.858 1.762 -5.863

100 ion pairs

C -1.534 2.981 2.475
N -1.252 2.611 3.772
C 0.071 2.411 3.880
N 0.633 2.626 2.686
C -0.344 2.994 1.792
C 2.045 2.373 2.355
C 2.674 3.574 1.654
C -2.234 2.430 4.832
H -1.837 1.735 5.586
H -3.183 2.028 4.427
H -2.446 3.398 5.337
H 0.622 2.171 4.784
H -0.131 3.254 0.748
H -2.543 3.201 2.136
H 2.567 2.118 3.294
H 2.067 1.468 1.695
H 3.668 3.330 1.252
H 2.038 3.885 0.814
H 2.785 4.430 2.350
O -4.873 0.876 4.626
N -5.132 -0.076 5.413
O -4.266 -0.488 6.239
O -6.280 -0.614 5.398
C 5.538 1.772 2.978
N 6.246 1.619 1.806
C 6.545 2.828 1.320
N 6.052 3.757 2.151
C 5.415 3.127 3.190
C 6.129 5.211 1.928
C 5.308 5.967 2.966
C 6.677 0.362 1.201
H 7.168 0.581 0.246
H 5.806 -0.290 1.028
H 7.384 -0.158 1.873
H 7.092 3.025 0.395
H 4.937 3.688 3.995
H 5.142 0.929 3.549
H 7.197 5.525 1.942
H 5.740 5.416 0.909
H 4.237 5.695 2.896
H 5.633 5.739 3.996
H 5.401 7.052 2.819
O 10.259 3.156 3.769
N 9.082 2.687 3.702
O 8.828 1.733 2.900
O 8.166 3.154 4.416
C 11.743 -4.153 0.326
N 12.664 -3.468 -0.426
C 12.286 -2.184 -0.510
N 11.142 -2.036 0.170
C 10.783 -3.244 0.705
C 10.435 -0.766 0.406
C 10.939 -0.108 1.694
C 13.852 -4.035 -1.050
H 13.692 -4.120 -2.150
H 14.058 -5.033 -0.629
H 14.722 -3.384 -0.880
H 12.814 -1.394 -1.051
H 9.890 -3.366 1.315
H 11.839 -5.204 0.575
H 10.612 -0.107 -0.466
H 9.357 -0.992 0.471
H 10.321 0.773 1.950
H 10.886 -0.815 2.530
H 11.982 0.208 1.587
O 4.692 5.898 -0.776
N 4.502 4.730 -1.251
O 4.694 3.717 -0.535
O 4.095 4.607 -2.443
C 7.057 4.828 8.064
N 7.308 5.496 6.892
C 8.414 4.987 6.334
N 8.876 4.003 7.118
C 8.047 3.883 8.203
C 10.115 3.247 6.862
C 10.044 1.811 7.381
C 6.470 6.551 6.327
H 5.697 6.101 5.671
H 7.090 7.245 5.725
H 5.988 7.098 7.148
H 8.846 5.329 5.401
H 8.193 3.125 8.976
H 6.218 5.086 8.716
H 10.285 3.258 5.769
H 10.957 3.798 7.337
H 10.951 1.252 7.091
H 9.954 1.785 8.480
H 9.168 1.277 6.965
O -0.328 4.542 -0.912
N -1.512 4.971 -0.771
O -2.298 4.410 0.056
O -1.920 5.949 -1.450
C 7.652 0.801 -4.384
N 9.000 0.559 -4.370
C 9.216 -0.684 -3.923
N 8.025 -1.249 -3.655
C 7.037 -0.339 -3.934
C 7.786 -2.623 -3.172
C 6.361 -2.792 -2.642
C 10.007 1.517 -4.801
H 9.676 2.526 -4.506
H 10.138 1.476 -5.893
H 10.981 1.297 -4.314
H 10.200 -1.135 -3.801
H 5.980 -0.570 -3.804
H 7.245 1.769 -4.672
H 7.971 -3.332 -4.002
H 8.508 -2.860 -2.374
H 6.204 -3.839 -2.327
H 6.200 -2.154 -1.766
H 5.605 -2.538 -3.399
O -4.647 -4.426 -2.991
N -3.517 -4.419 -2.470
O -2.723 -5.402 -2.635
O -3.132 -3.428 -1.765
C 2.180 6.658 0.623
N 1.671 7.200 -0.528
C 1.053 8.348 -0.225
N 1.161 8.557 1.096
C 1.861 7.513 1.651
C 0.575 9.698 1.818
C 1.554 10.327 2.811
C 1.739 6.606 -1.861
H 1.473 7.362 -2.604
H 1.024 5.758 -1.915
H 2.754 6.220 -2.048
H 0.595 9.030 -0.943
H 2.051 7.422 2.716
H 2.715 5.713 0.639
H 0.255 10.443 1.055
H -0.342 9.343 2.340
H 1.045 11.126 3.387
H 1.926 9.574 3.516
H 2.418 10.778 2.281
O 7.873 7.779 2.078
N 7.799 7.743 3.337
O 8.485 6.917 3.995
O 7.035 8.558 3.952
C 12.565 1.587 10.580
N 12.314 2.725 11.298
C 10.995 2.831 11.497
N 10.390 1.786 10.915
C 11.351 0.989 10.329
C 8.929 1.602 10.863
C 8.445 0.248 11.383
C 13.325 3.627 11.838
H 13.295 3.585 12.941
H 13.098 4.663 11.520
H 14.308 3.328 11.454
H 10.473 3.634 12.007
H 11.114 0.071 9.794
H 13.574 1.313 10.293
H 8.487 2.428 11.455
H 8.600 1.743 9.805
H 7.340 0.268 11.451
H 8.738 -0.574 10.710
H 8.843 0.027 12.389
O 6.456 -0.837 9.215
N 7.246 -0.231 8.434
O 7.215 1.020 8.347
O 8.080 -0.898 7.737
C 5.989 9.531 -0.202
N 5.797 9.615 1.153
C 6.841 10.250 1.699
N 7.710 10.562 0.729
C 7.203 10.123 -0.472
C 8.966 11.304 0.934
C 8.681 12.754 1.342
C 4.641 9.140 1.903
H 4.122 8.345 1.353
H 3.933 9.979 2.057
H 4.989 8.752 2.873
H 6.975 10.451 2.760
H 7.714 10.288 -1.412
H 5.276 9.055 -0.861
H 9.564 10.790 1.709
H 9.541 11.265 -0.010
H 9.587 13.259 1.736
H 8.323 13.337 0.480
H 7.894 12.775 2.118
O 12.087 -1.773 -4.410
N 11.580 -2.915 -4.280
O 12.051 -3.741 -3.450
O 10.591 -3.245 -5.016
C 1.723 3.858 -4.680
N 2.681 2.968 -5.098
C 2.995 2.168 -4.070
N 2.264 2.524 -3.009
C 1.460 3.579 -3.355
C 2.432 1.916 -1.680

C 1.130 1.767 -0.899
C 3.309 2.917 -6.415
H 4.241 3.514 -6.419
H 2.610 3.319 -7.176
H 3.560 1.875 -6.668
H 3.684 1.326 -4.097
H 0.793 4.062 -2.633
H 1.296 4.595 -5.347
H 2.885 0.918 -1.844
H 3.166 2.535 -1.118
H 1.350 1.303 0.084
H 0.644 2.746 -0.725
H 0.423 1.121 -1.430
O 4.803 13.286 -0.322
N 4.703 12.540 0.687
O 5.628 12.531 1.562
O 3.681 11.814 0.850
C 7.979 9.536 11.638
N 8.206 10.452 10.641
C 8.836 11.515 11.162
N 9.022 11.299 12.470
C 8.496 10.072 12.795
C 9.653 12.225 13.429
C 9.542 13.675 12.961
C 7.819 10.287 9.244
H 8.651 9.850 8.665
H 7.557 11.269 8.804
H 6.956 9.594 9.181
H 9.147 12.389 10.596
H 8.531 9.698 13.820
H 7.450 8.606 11.453
H 9.169 12.070 14.402
H 10.722 11.940 13.539
H 9.775 14.360 13.782
H 10.253 13.868 12.142
H 8.523 13.883 12.597
O 14.457 -3.095 3.758
N 14.086 -2.752 2.583
O 14.619 -3.286 1.581
O 13.231 -1.836 2.447
C 5.677 -4.918 9.640
N 6.017 -4.100 8.594
C 7.150 -3.452 8.907
N 7.531 -3.825 10.136
C 6.629 -4.740 10.616
C 8.709 -3.328 10.868
C 9.671 -2.591 9.941
C 5.272 -4.014 7.345
H 5.240 -2.969 6.971
H 4.241 -4.368 7.521
H 5.745 -4.657 6.579
H 7.664 -2.715 8.286
H 6.704 -5.192 11.605
H 4.785 -5.538 9.618
H 8.358 -2.678 11.696
H 9.215 -4.208 11.321
H 10.485 -2.134 10.513
H 10.113 -3.305 9.216
H 9.152 -1.798 9.370
O 8.243 -4.206 -0.649
N 7.512 -3.579 0.187
O 7.764 -2.378 0.470
O 6.538 -4.174 0.727
C 14.480 9.576 7.382
N 14.585 9.848 6.036
C 14.144 11.095 5.817
N 13.760 11.625 6.985
C 13.961 10.700 7.981
C 13.262 13.004 7.172
C 14.381 13.912 7.692
C 15.109 8.944 5.017
H 14.486 9.038 4.114
H 15.084 7.907 5.394
H 16.151 9.229 4.748
H 14.101 11.587 4.851
H 13.733 10.905 9.031
H 14.754 8.618 7.810
H 12.885 13.366 6.194
H 12.427 12.974 7.884
H 14.038 14.959 7.762
H 14.696 13.598 8.700
H 15.249 13.887 7.020
O 11.786 14.599 4.665
N 11.539 14.180 3.500
O 10.743 14.819 2.737
O 12.103 13.139 3.069
C -1.513 -1.774 -5.343
N -0.325 -1.849 -6.023
C 0.578 -2.473 -5.249
N -0.016 -2.804 -4.090
C -1.320 -2.383 -4.123
C 0.582 -3.612 -3.014
C 0.388 -5.105 -3.302
C -0.098 -1.347 -7.378
H 0.667 -1.953 -7.886
H 0.230 -0.283 -7.340
H -1.048 -1.418 -7.938
H 1.621 -2.668 -5.503
H -2.003 -2.562 -3.290
H -2.416 -1.344 -5.786
H 1.655 -3.335 -2.936
H 0.079 -3.336 -2.069
H 0.794 -5.377 -4.285
H 0.894 -5.729 -2.547
H -0.693 -5.348 -3.299
O 5.986 -5.253 -9.472
N 6.055 -4.841 -10.660
O 5.066 -4.207 -11.175
O 7.084 -5.037 -11.343
C 4.270 3.454 8.860
N 4.806 2.337 9.457
C 4.327 1.247 8.841
N 3.504 1.639 7.860
C 3.448 3.009 7.851
C 2.730 0.754 6.972
C 2.733 1.238 5.521
C 5.795 2.348 10.528
H 5.904 1.335 10.960
H 5.486 3.044 11.326
H 6.779 2.658 10.129
H 4.595 0.222 9.101
H 2.850 3.562 7.112
H 4.524 4.468 9.186
H 3.160 -0.255 7.045
H 1.695 0.707 7.368
H 1.948 0.707 4.955
H 2.516 2.321 5.475
H 3.699 1.037 5.029
O 6.986 2.922 13.167
N 7.667 4.000 13.189
O 8.437 4.276 12.256
O 7.562 4.771 14.204
C 7.394 -2.446 -12.195
N 8.586 -2.931 -12.676
C 9.582 -2.199 -12.172
N 9.063 -1.254 -11.376
C 7.692 -1.386 -11.372
C 9.835 -0.179 -10.730
C 9.946 -0.318 -9.212
C 8.760 -4.057 -13.585
H 9.830 -4.223 -13.740
H 8.257 -3.844 -14.543
H 8.310 -4.962 -13.136
H 10.641 -2.376 -12.351
H 7.045 -0.719 -10.795
H 6.434 -2.907 -12.438
H 10.840 -0.162 -11.213
H 9.333 0.783 -10.985
H 10.553 0.515 -8.818
H 8.950 -0.269 -8.755
H 10.435 -1.262 -8.923
O 3.188 17.533 -0.904
N 2.661 18.380 -1.699
O 2.811 19.602 -1.511
O 2.001 17.955 -2.704
C 2.380 6.416 9.100
N 1.588 7.290 9.805
C 0.328 7.189 9.351
N 0.299 6.274 8.375
C 1.564 5.778 8.192
C -0.900 5.828 7.643
C -0.776 4.356 7.254
C 2.032 8.187 10.870
H 1.893 7.727 11.866
H 1.443 9.121 10.827
H 3.110 8.428 10.752
H -0.530 7.745 9.724
H 1.790 5.024 7.426
H 3.445 6.281 9.314
H -1.772 5.983 8.301
H -1.037 6.463 6.748
H -1.647 4.060 6.641
H 0.137 4.192 6.657
H -0.742 3.713 8.139
O -3.465 8.553 -6.704
N -3.321 9.602 -6.002
O -2.774 9.558 -4.878
O -3.737 10.717 -6.461
C 4.652 -6.338 -1.535
N 4.193 -7.031 -2.629
C 5.156 -7.052 -3.561
N 6.219 -6.378 -3.094
C 5.932 -5.926 -1.827
C 7.466 -6.097 -3.834
C 8.708 -6.322 -2.972
C 2.896 -7.691 -2.732
H 2.731 -8.042 -3.768
H 2.090 -6.990 -2.456
H 2.857 -8.570 -2.051
H 5.085 -7.554 -4.525
H 6.667 -5.388 -1.215
H 4.036 -6.203 -0.646
H 7.497 -6.744 -4.726
H 7.431 -5.040 -4.171
H 9.617 -6.072 -3.544
H 8.672 -5.692 -2.063
H 8.771 -7.380 -2.665
O -2.466 -4.381 4.412
N -2.050 -5.576 4.545
O -1.002 -5.810 5.224
O -2.664 -6.514 3.986
C 9.254 6.606 -3.140
N 8.362 6.733 -2.104
C 7.162 6.286 -2.508
N 7.266 5.891 -3.781
C 8.556 6.080 -4.203
C 6.163 5.378 -4.609
C 6.599 4.186 -5.459
C 8.668 7.264 -0.781
H 8.310 6.582 0.008
H 8.183 8.249 -0.644
H 9.762 7.378 -0.684
H 6.259 6.238 -1.896
H 8.863 5.823 -5.214
H 10.306 6.876 -3.022
H 5.334 5.109 -3.928
H 5.823 6.213 -5.262
H 5.766 3.842 -6.092
H 7.438 4.471 -6.116
H 6.936 3.349 -4.823
O 0.715 3.501 -7.760
N 0.336 2.289 -7.694
O -0.583 1.877 -8.449
O 0.911 1.492 -6.897
C 11.222 5.633 17.200
N 9.888 5.756 17.496
C 9.745 6.648 18.488
N 10.959 7.087 18.847
C 11.899 6.472 18.053
C 11.233 8.141 19.838
C 10.211 8.133 20.975
C 8.797 5.079 16.802
H 8.256 5.795 16.160
H 8.082 4.657 17.529
H 9.211 4.264 16.182
H 8.817 6.937 18.960
H 12.956 6.678 18.148
H 11.590 4.964 16.407
H 12.252 7.996 20.219
H 11.206 9.104 19.296
H 10.387 8.974 21.651
H 9.194 8.219 20.574
H 10.272 7.207 21.556
O 7.468 2.963 -10.023
N 6.851 2.104 -9.310
O 7.168 0.889 -9.386
O 5.898 2.478 -8.568
C 8.165 15.885 4.637
N 7.266 15.904 5.670
C 6.630 14.726 5.717
N 7.109 13.947 4.734
C 8.072 14.648 4.048
C 6.694 12.570 4.412
C 7.651 11.520 4.984
C 7.040 17.028 6.570
H 6.171 17.616 6.213
H 7.937 17.665 6.563
H 6.838 16.636 7.578
H 5.859 14.467 6.431
H 8.632 14.221 3.216
H 8.795 16.745 4.398
H 5.679 12.421 4.800
H 6.656 12.484 3.307
H 7.354 10.515 4.634
H 8.680 11.705 4.653
H 7.633 11.551 6.083
O -6.247 11.609 7.210
N -6.349 11.168 8.382
O -5.587 11.570 9.304
O -7.213 10.257 8.643
C 2.688 -2.937 -0.410
N 2.988 -1.991 0.538
C 2.980 -2.570 1.747
N 2.679 -3.863 1.595
C 2.477 -4.121 0.261
C 2.437 -4.823 2.683
C 0.930 -5.061 2.836
C 3.260 -0.585 0.271
H 2.521 0.058 0.805
H 3.173 -0.406 -0.815
H 4.278 -0.328 0.610
H 3.241 -2.077 2.686
H 2.282 -5.132 -0.092
H 2.620 -2.691 -1.474
H 2.956 -5.762 2.440
H 2.870 -4.396 3.609
H 0.709 -5.700 3.706
H 0.406 -4.099 2.982
H 0.521 -5.541 1.937
O 4.046 2.036 -11.779
N 4.317 2.853 -12.697
O 4.488 2.471 -13.879
O 4.457 4.097 -12.413
C 12.153 -1.880 -7.425
N 12.677 -0.615 -7.498
C 13.344 -0.488 -8.653
N 13.273 -1.653 -9.316
C 12.534 -2.537 -8.573
C 13.893 -1.948 -10.624
C 12.960 -1.632 -11.799
C 12.494 0.436 -6.505
H 12.244 -0.012 -5.531
H 11.683 1.109 -6.829
H 13.422 1.026 -6.400
H 13.842 0.409 -8.993

H 12.359 -3.566 -8.917
H 11.572 -2.225 -6.566
H 14.821 -1.363 -10.689
H 14.148 -3.018 -10.631
H 13.531 -1.565 -12.728
H 12.217 -2.445 -11.922
H 12.413 -0.676 -11.661
O 12.054 1.992 -8.881
N 12.214 3.261 -8.796
O 12.985 3.834 -9.617
O 11.592 3.921 -7.931
C 7.456 2.604 -14.652
N 7.255 2.589 -13.300
C 7.063 3.844 -12.870
N 7.124 4.668 -13.927
C 7.364 3.917 -15.055
C 6.851 6.116 -13.908
C 7.542 6.850 -15.056
C 7.215 1.387 -12.475
H 7.969 1.474 -11.662
H 7.466 0.521 -13.105
H 6.215 1.267 -12.032
H 6.890 4.127 -11.833
H 7.454 4.384 -16.033
H 7.657 1.694 -15.205
H 5.751 6.257 -14.000
H 7.170 6.524 -12.931
H 7.183 7.889 -15.080
H 8.631 6.849 -14.940
H 7.287 6.375 -16.018
O 9.411 10.106 15.652
N 9.676 9.388 16.659
O 10.813 9.447 17.195
O 8.798 8.586 17.107
C 4.057 -2.901 11.105
N 4.232 -3.520 12.318
C 4.735 -2.636 13.188
N 4.893 -1.461 12.558
C 4.473 -1.599 11.258
C 5.386 -0.209 13.165
C 4.293 0.463 14.002
C 4.000 -4.939 12.566
H 3.756 -5.108 13.628
H 4.913 -5.517 12.307
H 3.165 -5.282 11.938
H 4.970 -2.855 14.225
H 4.530 -0.786 10.536
H 3.644 -3.440 10.250
H 6.268 -0.452 13.791
H 5.736 0.442 12.335
H 4.585 1.480 14.333
H 3.358 0.552 13.417
H 4.078 -0.130 14.899
O 0.947 9.993 -2.724
N 0.889 11.107 -2.152
O 1.295 12.158 -2.741
O 0.430 11.190 -0.971
C 5.794 10.503 14.292
N 4.846 9.770 13.623
C 4.934 8.491 14.010
N 5.921 8.389 14.915
C 6.474 9.629 15.109
C 6.314 7.182 15.668
C 5.227 6.782 16.671
C 3.883 10.314 12.671
H 3.880 9.698 11.745
H 4.154 11.356 12.423
H 2.871 10.302 13.128
H 4.314 7.674 13.653
H 7.331 9.779 15.768
H 5.902 11.583 14.139
H 6.504 6.349 14.956
H 7.264 7.419 16.181
H 5.551 5.913 17.262
H 4.995 7.604 17.356
H 4.304 6.483 16.147
O 0.611 -7.743 -0.051
N 1.648 -7.894 0.668
O 2.573 -7.041 0.618
O 1.761 -8.913 1.407
C 15.691 1.182 5.843
N 14.499 0.771 5.297
C 14.749 -0.182 4.380
N 16.073 -0.386 4.335
C 16.682 0.448 5.235
C 16.806 -1.340 3.474
C 18.057 -0.687 2.884
C 13.191 1.313 5.674
H 12.711 1.795 4.815
H 13.339 2.045 6.487
H 12.524 0.511 6.050
H 14.008 -0.704 3.760
H 17.767 0.423 5.385
H 15.746 1.968 6.602
H 17.092 -2.212 4.097
H 16.120 -1.694 2.692
H 18.625 -1.414 2.298
H 17.798 0.155 2.233
H 18.706 -0.316 3.702
O 4.203 -2.979 4.557
N 4.310 -1.741 4.816
O 4.251 -0.890 3.885
O 4.540 -1.366 6.003
C -5.822 6.904 10.747
N -6.693 7.965 10.716
C -5.988 9.104 10.760
N -4.684 8.794 10.792
C -4.552 7.428 10.797
C -3.585 9.779 10.802
C -2.311 9.230 10.156
C -8.142 7.861 10.558
H -8.447 8.455 9.678
H -8.654 8.242 11.448
H -8.397 6.798 10.402
H -6.381 10.113 10.710
H -3.571 6.944 10.796
H -6.178 5.867 10.721
H -3.956 10.676 10.275
H -3.383 10.069 11.853
H -1.437 9.843 10.454
H -2.129 8.187 10.471
H -2.387 9.244 9.064
O 10.137 8.389 -11.680
N 9.343 7.413 -11.656
O 9.784 6.227 -11.785
O 8.101 7.605 -11.493
C -1.635 5.424 -8.951
N -0.822 5.314 -10.050
C -0.626 6.534 -10.562
N -1.296 7.422 -9.822
C -1.938 6.759 -8.804
C -1.308 8.868 -10.079
C -1.266 9.665 -8.779
C -0.257 4.089 -10.601
H 0.812 4.261 -10.837
H -0.779 3.811 -11.545
H -0.349 3.271 -9.864
H -0.002 6.780 -11.417
H -2.551 7.293 -8.075
H -1.929 4.561 -8.369
H -0.443 9.095 -10.726
H -2.230 9.127 -10.662
H -1.337 10.743 -9.003
H -2.113 9.373 -8.127
H -0.322 9.478 -8.237
O 11.694 7.458 -1.489
N 12.752 7.030 -2.072
O 13.873 7.175 -1.514
O 12.652 6.465 -3.186
C -6.233 4.339 -0.987
N -6.894 4.813 -2.095
C -6.029 4.878 -3.116
N -4.830 4.469 -2.688
C -4.927 4.123 -1.362
C -3.604 4.372 -3.501
C -3.103 2.926 -3.555
C -8.297 5.208 -2.154
H -8.829 4.588 -2.896
H -8.356 6.269 -2.463
H -8.750 5.083 -1.155
H -6.265 5.261 -4.105
H -4.059 3.800 -0.788
H -6.743 4.215 -0.026
H -3.844 4.746 -4.505
H -2.844 5.039 -3.052
H -2.289 2.828 -4.279
H -2.734 2.614 -2.572
H -3.925 2.249 -3.842
O 10.375 7.318 9.888
N 10.684 6.083 9.860
O 11.244 5.549 10.851
O 10.499 5.425 8.796
C -7.927 3.565 5.797
N -8.770 4.319 5.013
C -8.324 4.293 3.749
N -7.221 3.536 3.704
C -6.944 3.073 4.969
C -6.414 3.250 2.505
C -4.923 3.435 2.790
C -9.892 5.108 5.524
H -10.841 4.592 5.341
H -9.900 6.096 5.025
H -9.746 5.252 6.608
H -8.765 4.782 2.885
H -6.108 2.395 5.151
H -8.082 3.444 6.878
H -6.609 2.203 2.199
H -6.776 3.905 1.686
H -4.321 3.306 1.880
H -4.725 4.451 3.188
H -4.577 2.697 3.538
O 12.379 4.022 14.897
N 11.574 3.058 14.877
O 11.634 2.189 13.966
O 10.670 2.960 15.774
C 8.385 -1.206 3.549
N 7.621 -0.955 4.662
C 7.108 -2.111 5.097
N 7.492 -3.095 4.269
C 8.303 -2.559 3.304
C 6.950 -4.469 4.333
C 7.681 -5.434 3.411
C 7.316 0.351 5.242
H 6.330 0.300 5.717
H 7.312 1.118 4.450
H 8.066 0.622 6.010
H 6.451 -2.227 5.958
H 8.763 -3.164 2.524
H 8.929 -0.414 3.029
H 6.986 -4.810 5.385
H 5.880 -4.400 4.068
H 7.334 -6.461 3.592
H 7.485 -5.180 2.352
H 8.770 -5.399 3.592
O 10.321 -5.295 8.398
N 10.682 -5.888 9.474
O 11.045 -5.223 10.463
O 10.619 -7.156 9.534
C 4.128 5.637 -8.025
N 4.168 4.860 -9.157
C 5.421 4.860 -9.629
N 6.186 5.620 -8.830
C 5.401 6.122 -7.820
C 7.635 5.838 -9.038
C 8.368 6.270 -7.770
C 3.048 4.102 -9.706
H 3.431 3.221 -10.251
H 2.469 4.719 -10.426
H 2.375 3.790 -8.881
H 5.757 4.348 -10.530
H 5.781 6.773 -7.019
H 3.216 5.791 -7.464
H 8.041 4.887 -9.424
H 7.757 6.595 -9.841
H 9.434 6.454 -7.986
H 7.943 7.188 -7.333
H 8.319 5.486 -6.992
O 1.555 0.117 9.551
N 1.587 -0.153 10.786
O 0.782 -0.995 11.269
O 2.433 0.431 11.533
C 11.264 8.802 13.629
N 12.416 9.496 13.915
C 13.405 9.023 13.146
N 12.914 8.031 12.386
C 11.580 7.878 12.662
C 13.648 7.306 11.335
C 13.400 7.951 9.967
C 12.499 10.624 14.837
H 13.537 10.777 15.143
H 11.865 10.423 15.719
H 12.135 11.529 14.312
H 14.430 9.359 13.161
H 10.982 7.132 12.136
H 10.320 9.043 14.123
H 14.716 7.316 11.592
H 13.293 6.253 11.336
H 13.965 7.433 9.177
H 12.325 7.889 9.719
H 13.687 9.016 9.981
O 1.806 4.212 5.536
N 2.716 4.920 4.964
O 2.424 5.622 3.968
O 3.891 4.876 5.408
C -5.017 1.090 8.725
N -6.328 0.850 9.074
C -6.637 1.611 10.134
N -5.562 2.339 10.460
C -4.537 2.035 9.601
C -5.479 3.329 11.546
C -6.135 2.805 12.824
C -7.223 -0.099 8.415
H -6.754 -0.471 7.487
H -8.170 0.393 8.173
H -7.415 -0.948 9.097
H -7.582 1.622 10.656
H -3.569 2.523 9.695
H -4.545 0.563 7.891
H -4.411 3.559 11.692
H -5.988 4.257 11.201
H -6.029 3.530 13.636
H -7.202 2.626 12.655
H -5.679 1.859 13.135
O 10.597 -4.501 3.425
N 11.291 -5.533 3.367
O 11.178 -6.345 2.383
O 12.093 -5.830 4.303
C -2.709 -6.654 1.054
N -2.119 -6.988 -0.138
C -1.344 -5.974 -0.543
N -1.431 -4.986 0.359
C -2.273 -5.388 1.369
C -0.754 -3.679 0.259
C -1.163 -2.727 1.378
C -2.283 -8.251 -0.843
H -1.285 -8.655 -1.093
H -2.853 -8.112 -1.781
H -2.803 -8.959 -0.181
H -0.726 -5.958 -1.436
H -2.477 -4.763 2.240
H -3.357 -7.344 1.600
H 0.347 -3.856 0.284
C 11.264 8.802 13.629
H -0.994 -3.254 -0.734
N 12.416 9.496 13.915
H -0.658 -1.757 1.258
C 13.405 9.023 13.146
H -2.253 -2.564 1.381

H -0.862 -3.133 2.358
O -0.031 8.491 14.400
N 1.188 8.779 14.331
O 2.028 7.919 13.920
O 1.584 9.953 14.618
C -0.881 13.015 14.260
N -0.518 11.937 13.492
C 0.800 11.995 13.266
N 1.293 13.086 13.869
C 0.264 13.741 14.499
C 2.723 13.439 13.953
C 3.436 12.574 14.998
C -1.394 10.851 13.066
H -1.202 10.626 11.997
H -2.442 11.134 13.207
H -1.159 9.944 13.659
H 1.372 11.292 12.671
H 0.416 14.653 15.060
H -1.901 13.185 14.575
H 3.198 13.278 12.962
H 2.798 14.506 14.197
H 4.526 12.659 14.855
H 3.179 12.877 16.018
H 3.147 11.520 14.862
O 8.263 3.292 -3.085
N 7.960 3.097 -1.866
O 7.948 4.096 -1.067
O 7.704 1.951 -1.444
C 8.210 -7.471 -9.931
N 8.712 -7.848 -11.151
C 9.824 -8.563 -10.957
N 10.046 -8.665 -9.637
C 9.055 -7.987 -8.972
C 11.189 -9.368 -9.027
C 10.837 -9.969 -7.667
C 8.137 -7.543 -12.455
H 8.738 -8.016 -13.234
H 8.124 -6.448 -12.608
H 7.092 -7.910 -12.505
H 10.444 -8.985 -11.733
H 9.034 -7.907 -7.877
H 7.328 -6.837 -9.829
H 11.511 -10.147 -9.732
H 12.021 -8.654 -8.927
H 11.659 -10.594 -7.307
H 10.660 -9.178 -6.921
H 9.927 -10.591 -7.719
O 7.907 -3.234 15.298
N 7.631 -3.059 14.093
O 7.843 -1.944 13.534
O 7.085 -4.000 13.414
C 11.120 9.154 -7.612
N 11.248 7.995 -6.877
C 11.649 7.006 -7.694
N 11.794 7.513 -8.926
C 11.465 8.845 -8.906
C 12.346 6.800 -10.085
C 13.512 7.586 -10.689
C 11.028 7.914 -5.436
H 11.498 7.012 -5.026
H 9.946 7.900 -5.218
H 11.480 8.802 -4.950
H 11.800 5.958 -7.437
H 11.506 9.454 -9.800
H 10.798 10.098 -7.156
H 12.671 5.799 -9.742
H 11.538 6.652 -10.836
H 13.995 6.996 -11.487
H 13.158 8.529 -11.120
H 14.255 7.819 -9.915
O 1.365 -6.534 9.037
N 1.905 -5.562 9.646
O 2.830 -4.909 9.086
O 1.489 -5.228 10.790
C -6.235 10.796 1.869
N -5.968 11.152 3.168
C -4.638 11.224 3.330
N -4.052 10.913 2.168
C -5.023 10.645 1.237
C -2.602 10.843 1.939
C -2.255 11.066 0.473
C -6.996 11.404 4.179
H -6.588 11.268 5.197
H -7.819 10.695 4.016
H -7.374 12.428 4.081
H -4.122 11.492 4.240
H -4.772 10.399 0.206
H -7.245 10.664 1.506
H -2.145 11.625 2.576
H -2.222 9.855 2.303
H -1.155 11.070 0.326
H -2.694 10.287 -0.167
H -2.650 12.043 0.141
O 18.155 -3.237 5.660
N 18.370 -2.132 6.235
O 17.783 -1.842 7.316
O 19.131 -1.277 5.696
C 13.599 -5.758 -6.479
N 13.036 -5.885 -5.234
C 11.706 -5.779 -5.345
N 11.403 -5.594 -6.638
C 12.567 -5.578 -7.371
C 10.032 -5.412 -7.147
C 10.013 -5.031 -8.625
C 13.790 -6.023 -3.995
H 13.856 -5.026 -3.501
H 14.805 -6.395 -4.225
H 13.280 -6.724 -3.314
H 10.987 -5.816 -4.529
H 12.577 -5.414 -8.457
H 14.679 -5.783 -6.608
H 9.477 -6.364 -6.975
H 9.559 -4.630 -6.533
H 8.997 -4.778 -8.942
H 10.668 -4.166 -8.813
H 10.370 -5.859 -9.258
O -7.922 4.783 10.363
N -8.271 4.451 9.201
O -8.128 3.258 8.805
O -8.729 5.325 8.400
C 0.829 15.593 -1.257
N 1.916 14.821 -1.587
C 1.970 13.775 -0.754
N 0.956 13.866 0.113
C 0.219 14.990 -0.179
C 0.757 12.926 1.225
C 0.559 13.636 2.565
C 2.898 15.088 -2.633
H 2.812 14.337 -3.427
H 3.907 15.043 -2.193
H 2.728 16.104 -3.044
H 2.739 13.006 -0.731
H -0.661 15.263 0.407
H 0.614 16.516 -1.786
H -0.102 12.262 0.986
H 1.659 12.284 1.262
H 0.498 12.877 3.370
H 1.410 14.307 2.772
H -0.373 14.230 2.566
O 13.598 10.736 11.253
N 13.078 11.894 11.219
O 13.192 12.593 10.179
O 12.456 12.345 12.226
C 13.830 17.609 2.953
N 12.482 17.612 3.202
C 11.824 17.386 2.058
N 12.726 17.241 1.075
C 13.986 17.377 1.605
C 12.439 16.977 -0.344
C 12.817 18.159 -1.240
C 11.868 17.688 4.521
H 11.698 16.649 4.875
H 10.892 18.197 4.473
H 12.541 18.197 5.235
H 10.737 17.369 1.954
H 14.875 17.258 0.987
H 14.559 17.775 3.755
H 12.995 16.052 -0.641
H 11.354 16.755 -0.450
H 12.376 18.003 -2.233
H 12.424 19.098 -0.836
H 13.906 18.250 -1.351
O 2.489 -1.024 -2.702
N 3.290 -1.425 -3.588
O 4.063 -0.617 -4.165
O 3.297 -2.653 -3.921
C 12.137 2.072 -12.138
N 11.366 3.156 -11.810
C 12.024 4.271 -12.135
N 13.207 3.933 -12.673
C 13.297 2.560 -12.691
C 14.228 4.876 -13.160
C 15.634 4.284 -13.068
C 10.079 3.148 -11.123
H 10.238 2.905 -10.063
H 9.411 2.385 -11.568
H 9.623 4.143 -11.207
H 11.644 5.281 -11.965
H 14.170 2.053 -13.084
H 11.817 1.032 -11.983
H 13.990 5.145 -14.202
H 14.152 5.801 -12.554
H 16.367 4.971 -13.503
H 15.910 4.100 -12.025
H 15.685 3.331 -13.608
O 0.536 12.764 9.746
N 0.440 11.512 9.628
O 0.433 10.981 8.488
O 0.368 10.782 10.671
C 10.727 2.589 -0.623
N 10.935 3.693 -1.410
C 10.684 4.788 -0.684
N 10.330 4.418 0.554
C 10.348 3.047 0.619
C 9.958 5.359 1.628
C 10.876 6.585 1.634
C 11.273 3.711 -2.829
H 11.827 4.632 -3.067
H 10.330 3.686 -3.410
H 11.868 2.818 -3.098
H 10.769 5.821 -1.036
H 10.075 2.486 1.521
H 10.860 1.566 -1.000
H 8.896 5.673 1.476
H 10.011 4.812 2.586
H 10.475 7.350 2.317
H 11.884 6.318 1.971
H 10.960 7.032 0.621
O 2.915 9.593 -10.665
N 1.990 8.736 -10.651
O 1.700 8.135 -9.571
O 1.346 8.474 -11.704
C 1.622 -7.128 5.546
N 2.364 -6.195 6.221
C 3.261 -6.828 6.989
N 3.113 -8.149 6.815
C 2.089 -8.363 5.922
C 3.927 -9.221 7.407
C 3.035 -10.343 7.943
C 2.175 -4.750 6.129
H 2.799 -4.322 5.314
H 2.480 -4.299 7.087
H 1.122 -4.538 5.919
H 3.950 -6.336 7.667
H 1.769 -9.354 5.611
H 0.802 -6.835 4.888
H 4.609 -9.605 6.614
H 4.563 -8.802 8.213
H 3.613 -11.031 8.567
H 2.222 -9.918 8.547
H 2.580 -10.909 7.121
O 8.444 17.974 -2.945
N 9.519 17.495 -3.423
O 10.407 17.045 -2.636
O 9.683 17.436 -4.670
C 18.264 -4.886 3.154
N 18.767 -5.979 2.489
C 17.774 -6.557 1.793
N 16.653 -5.861 2.006
C 16.925 -4.815 2.853
C 15.320 -6.175 1.473
C 14.340 -6.461 2.610
C 20.170 -6.380 2.442
H 20.546 -6.229 1.420
H 20.274 -7.436 2.712
H 20.746 -5.768 3.140
H 17.835 -7.462 1.192
H 16.147 -4.112 3.170
H 18.861 -4.256 3.805
H 14.973 -5.311 0.873
H 15.420 -7.039 0.790
H 13.301 -6.464 2.250
H 14.556 -7.447 3.063
H 14.440 -5.686 3.391
O -7.530 0.908 -4.926
N -6.800 1.750 -4.335
O -5.820 1.370 -3.643
O -7.061 2.996 -4.443
C 6.049 12.212 -7.008
N 7.380 11.977 -6.786
C 7.785 12.732 -5.764
N 6.744 13.447 -5.314
C 5.643 13.144 -6.080
C 6.793 14.368 -4.162
C 7.014 15.828 -4.568
C 8.214 11.029 -7.513
H 9.263 11.138 -7.182
H 8.137 11.229 -8.600
H 7.884 10.002 -7.295
H 8.798 12.760 -5.344
H 4.675 13.595 -5.909
H 5.494 11.694 -7.784
H 5.854 14.263 -3.600
H 7.611 14.030 -3.512
H 7.143 16.463 -3.669
H 7.936 15.949 -5.182
H 6.153 16.219 -5.147
O 15.434 2.636 9.774
N 15.040 2.988 8.632
O 15.868 3.515 7.812
O 13.844 2.813 8.275
C -3.419 0.319 -10.439
N -3.035 1.280 -11.340
C -1.700 1.258 -11.446
N -1.218 0.305 -10.638
C -2.270 -0.298 -9.996
C 0.205 -0.040 -10.470
C 1.113 1.033 -11.066
C -3.895 2.202 -12.081
H -4.344 2.952 -11.395
H -4.696 1.648 -12.581
H -3.273 2.724 -12.823
H -1.128 1.941 -12.073
H -2.134 -1.089 -9.253
H -4.453 0.141 -10.172
H 0.391 -0.161 -9.389
H 0.386 -1.025 -10.948
H 2.175 0.767 -10.932
H 0.927 1.154 -12.139
H 0.930 2.003 -10.576
O 11.566 10.764 -4.261
N 10.880 11.658 -4.805
O 10.219 12.489 -4.097
O 10.838 11.757 -6.067
C 3.638 10.371 -5.782

N 3.309 9.743 -6.956
C 1.974 9.637 -7.032
N 1.442 10.185 -5.929
C 2.457 10.657 -5.137
C 0.004 10.224 -5.595
C -0.476 11.642 -5.283
C 4.262 9.289 -7.964
H 3.736 9.144 -8.926
H 4.740 8.346 -7.638
H 5.039 10.058 -8.088
H 1.426 9.185 -7.865
H 2.246 11.152 -4.185
H 4.680 10.527 -5.483
H -0.541 9.796 -6.454
H -0.158 9.578 -4.719
H -1.529 11.612 -4.952
H 0.136 12.077 -4.476
H -0.421 12.293 -6.173
O 5.179 8.097 11.122
N 5.484 7.310 10.167
O 6.057 7.771 9.144
O 5.161 6.090 10.226
C 15.378 12.088 -6.246
N 14.192 11.755 -6.851
C 13.640 10.727 -6.193
N 14.434 10.404 -5.164
C 15.530 11.235 -5.179
C 14.169 9.364 -4.153
C 14.361 9.928 -2.743
C 13.586 12.461 -7.975
H 12.847 11.815 -8.457
H 14.358 12.749 -8.694
H 13.087 13.380 -7.606
H 12.684 10.266 -6.438
H 16.315 11.158 -4.438
H 16.003 12.916 -6.603
H 13.130 9.015 -4.304
H 14.849 8.508 -4.345
H 14.375 9.117 -1.985
H 15.305 10.484 -2.682
H 13.531 10.604 -2.483
O 2.744 17.521 5.232
N 3.735 16.753 5.380
O 4.775 16.919 4.672
O 3.706 15.828 6.244
C 10.886 7.777 4.776
N 10.338 8.130 5.979
C 10.989 7.494 6.962
N 11.939 6.723 6.408
C 11.895 6.882 5.043
C 12.861 5.821 7.127
C 14.093 5.508 6.281
C 9.201 9.025 6.139
H 9.026 9.215 7.209
H 8.297 8.558 5.686
H 9.401 9.976 5.625
H 10.775 7.583 8.036
H 12.568 6.349 4.383
H 10.548 8.191 3.826
H 13.151 6.316 8.073
H 12.300 4.898 7.390
H 14.767 4.815 6.820
H 13.801 5.041 5.333
H 14.648 6.435 6.042
O 5.731 8.210 -5.658
N 6.748 8.929 -5.409
O 7.905 8.478 -5.646
O 6.593 10.099 -4.964
C -7.229 -2.926 -3.606
N -6.306 -1.914 -3.515
C -6.167 -1.344 -4.718
N -6.981 -1.965 -5.583
C -7.660 -2.955 -4.912
C -7.207 -1.540 -6.976
C -7.645 -2.695 -7.881
C -5.595 -1.515 -2.302
H -5.249 -0.482 -2.425
H -4.734 -2.191 -2.121
H -6.276 -1.584 -1.435
H -5.497 -0.528 -4.951
H -8.380 -3.591 -5.412
H -7.534 -3.516 -2.742
H -7.967 -0.744 -6.958
H -6.263 -1.102 -7.341
H -8.179 -2.313 -8.756
H -6.768 -3.261 -8.248
H -8.309 -3.382 -7.339
O 11.096 10.039 2.788
N 12.024 10.287 3.607
O 13.224 10.386 3.188
O 11.793 10.351 4.844
C 16.733 11.002 0.142
N 17.884 10.988 0.883
C 18.238 9.718 1.112
N 17.348 8.910 0.517
C 16.391 9.687 -0.092
C 17.424 7.433 0.477
C 18.007 6.916 -0.842
C 18.616 12.165 1.346
H 18.798 12.078 2.439
H 18.011 13.064 1.146
H 19.574 12.239 0.821
H 19.108 9.394 1.684
H 15.535 9.259 -0.625
H 16.256 11.950 -0.122
H 18.081 7.109 1.321
H 16.416 7.032 0.648
H 18.129 5.817 -0.796
H 17.357 7.146 -1.699
H 19.005 7.349 -1.018
O -4.471 -8.786 2.677
N -3.495 -9.588 2.698
O -3.198 -10.199 3.769
O -2.797 -9.782 1.662
C 14.775 14.111 4.388
N 15.448 13.660 3.283
C 16.605 14.329 3.177
N 16.684 15.201 4.193
C 15.561 15.081 4.967
C 17.807 16.107 4.493
C 18.765 15.462 5.501
C 15.031 12.551 2.432
H 15.385 12.732 1.400
H 13.930 12.459 2.459
H 15.482 11.620 2.812
H 17.330 14.183 2.379
H 15.414 15.684 5.867
H 13.787 13.737 4.672
H 18.323 16.334 3.551
H 17.372 17.040 4.894
H 19.672 16.065 5.607
H 18.288 15.378 6.483
H 19.042 14.451 5.169
O 18.282 3.863 -1.423
N 19.019 2.945 -1.935
O 20.259 2.987 -1.771
O 18.481 2.032 -2.615
C 11.571 -8.229 6.863
N 10.849 -7.821 5.769
C 11.445 -8.290 4.660
N 12.529 -8.989 5.020
C 12.631 -8.967 6.389
C 13.454 -9.670 4.096
C 14.277 -10.745 4.800
C 9.675 -6.952 5.825
H 9.693 -6.243 4.979
H 9.689 -6.398 6.787
H 8.736 -7.545 5.765
O 11.122 -8.109 3.632
N 13.436 -9.473 6.906
H 11.288 -7.935 7.880
H 12.841 -10.115 3.288
H 14.126 -8.913 3.628
H 15.007 -11.170 4.106
H 14.818 -10.320 5.655
H 13.625 -11.547 5.166
O 13.706 -0.023 -2.120
N 12.705 0.454 -2.719
O 12.871 1.241 -3.701
O 11.533 0.199 -2.315
C 14.699 4.512 -5.106
N 15.576 4.864 -4.114
C 16.090 3.748 -3.567
N 15.561 2.689 -4.201
C 14.689 3.138 -5.159
C 15.854 1.270 -3.927
C 15.871 0.446 -5.217
C 15.839 6.241 -3.699
H 16.814 6.313 -3.199
H 15.055 6.564 -2.985
H 15.807 6.913 -4.583
H 16.830 3.709 -2.759
H 14.134 2.448 -5.792
H 14.197 5.264 -5.721
H 16.825 1.218 -3.399
H 15.073 0.865 -3.239
H 15.853 -0.630 -4.979
H 14.971 0.672 -5.816
H 16.755 0.660 -5.826
O -2.064 17.696 -4.341
N -1.948 17.137 -5.458
O -0.984 17.453 -6.230
O -2.763 16.248 -5.833
C -2.426 -5.222 11.047
N -1.256 -5.715 11.576
C -0.707 -4.770 12.357
N -1.502 -3.693 12.343
C -2.576 -3.942 11.527
C -1.251 -2.428 13.058
C -2.534 -1.832 13.640
C -0.681 -7.021 11.263
H 0.150 -7.227 11.940
H -0.293 -7.018 10.209
H -1.444 -7.800 11.361
H 0.201 -4.858 12.946
H -3.372 -3.209 11.360
H -3.057 -5.785 10.357
H -0.499 -2.639 13.846
H -0.777 -1.713 12.351
H -2.344 -0.797 13.964
H -3.341 -1.820 12.886
H -2.885 -2.408 14.503
O 2.316 -7.346 -5.857
N 1.072 -7.340 -5.602
O 0.285 -6.690 -6.366
O 0.614 -7.998 -4.641
C -6.587 8.785 6.261
N -7.528 7.868 6.654
C -7.052 6.640 6.423
N -5.823 6.747 5.896
C -5.506 8.078 5.790
C -4.982 5.621 5.468
C -3.685 5.544 6.269
C -8.847 8.167 7.205
H -9.278 7.238 7.599
H -9.492 8.566 6.410
H -8.737 8.911 8.012
H -7.580 5.713 6.642
H -4.554 8.432 5.383
H -6.720 9.870 6.357
H -5.585 4.696 5.573
H -4.760 5.732 4.376
H -3.102 4.653 5.964
H -3.050 6.430 6.084
H -3.870 5.462 7.351
O 10.861 -8.216 -5.039
N 9.626 -8.474 -4.982
O 9.158 -9.175 -4.063
O 8.847 -8.001 -5.891
C 3.137 12.212 8.167
N 4.184 11.570 8.792
C 5.080 12.492 9.180
N 4.630 13.700 8.823
C 3.422 13.556 8.192
C 5.316 14.970 9.106
C 4.320 16.103 9.345
C 4.267 10.130 9.018
H 5.304 9.764 8.890
H 3.612 9.613 8.312
H 3.953 9.864 10.054
H 6.024 12.300 9.681
H 2.869 14.417 7.818
H 2.263 11.674 7.805
H 5.964 14.798 9.981
H 5.982 15.212 8.247
H 4.844 17.057 9.456
H 3.625 16.179 8.488
H 3.730 15.924 10.250
O 16.546 -7.269 -4.627
N 17.139 -6.201 -4.959
O 18.386 -6.088 -4.799
O 16.465 -5.221 -5.402
C 19.460 -1.493 -3.410
N 19.290 -2.804 -3.792
C 17.995 -3.118 -3.678
N 17.324 -2.037 -3.250
C 18.220 -1.009 -3.067
C 15.883 -2.031 -2.927
C 15.072 -2.799 -3.975
C 20.339 -3.735 -4.203
H 20.946 -4.000 -3.327
H 20.976 -3.276 -4.966
H 19.862 -4.643 -4.600
H 17.550 -4.066 -3.976
H 17.930 -0.007 -2.743
H 20.426 -1.009 -3.401
H 15.759 -2.499 -1.930
H 15.535 -0.983 -2.846
H 14.101 -3.145 -3.559
H 14.872 -2.163 -4.848
H 15.625 -3.690 -4.321
O 8.141 14.889 8.328
N 8.253 13.629 8.259
O 9.267 13.050 8.686
O 7.291 12.952 7.742
C 15.027 -3.053 7.367
N 14.700 -3.999 6.431
C 13.381 -3.957 6.207
N 12.848 -3.009 6.989
C 13.853 -2.428 7.724
C 11.413 -2.687 7.063
C 11.166 -1.264 7.557
C 15.626 -4.916 5.775
H 15.278 -5.103 4.742
H 15.670 -5.865 6.324
H 16.629 -4.456 5.749
H 12.835 -4.581 5.491
H 13.658 -1.628 8.427
H 16.062 -2.846 7.653
H 10.982 -2.839 6.065
H 10.928 -3.426 7.749
H 10.081 -1.070 7.626
H 11.595 -1.110 8.560
H 11.612 -0.509 6.880
O -7.050 7.429 -3.719
N -6.980 8.602 -4.247
O -6.742 9.591 -3.532
O -7.159 8.716 -5.492
C -6.515 -4.629 1.125
N -5.371 -3.972 1.503
C -4.922 -4.508 2.653
N -5.752 -5.496 3.011
C -6.755 -5.591 2.079
C -5.630 -6.328 4.220
C -6.873 -6.208 5.107

C -4.789 -2.833 0.795
H -3.885 -2.495 1.324
H -5.540 -2.020 0.756
H -4.507 -3.105 -0.242
H -4.012 -4.236 3.208
H -7.550 -6.320 2.160
H -7.096 -4.347 0.236
H -5.470 -7.381 3.901
H -4.722 -6.020 4.763
H -6.769 -6.865 5.999
H -7.008 -5.180 5.480
H -7.776 -6.499 4.559
O -4.981 -2.123 11.634
N -6.084 -1.515 11.424
O -6.261 -0.356 11.843
O -6.975 -2.097 10.723
C -3.515 -8.950 -3.713
N -2.400 -9.080 -4.509
C -2.262 -7.961 -5.237
N -3.256 -7.120 -4.918
C -4.054 -7.712 -3.978
C -3.507 -5.790 -5.506
C -2.223 -4.976 -5.637
C -1.521 -10.250 -4.536
H -1.189 -10.442 -5.569
H -2.068 -11.123 -4.170
H -0.633 -10.095 -3.900
H -1.447 -7.749 -5.937
H -4.921 -7.212 -3.566
H -3.850 -9.743 -3.057
H -3.975 -5.943 -6.503
H -4.231 -5.277 -4.850
H -2.414 -4.029 -6.171
H -1.813 -4.746 -4.636
H -1.452 -5.541 -6.194
O 6.864 13.340 11.370
N 5.878 13.289 12.160
O 4.709 13.088 11.673
O 6.031 13.389 13.394
C 0.405 3.770 12.245
N 0.414 4.846 13.098
C 1.650 5.005 13.583
N 2.444 4.064 13.049
C 1.688 3.272 12.215
C 3.884 3.890 13.330
C 4.519 5.193 13.800
C -0.754 5.656 13.433
H -1.355 5.141 14.192
H -1.359 5.799 12.522
H -0.430 6.635 13.828
H 1.969 5.800 14.252
H 2.096 2.396 11.707
H -0.506 3.470 11.722
H 4.002 3.099 14.115
H 4.379 3.517 12.413
H 5.588 5.029 14.063
H 4.463 5.970 13.026
H 4.006 5.559 14.709
O -5.743 -7.338 7.765
N -4.716 -6.617 7.839
O -3.958 -6.487 6.840
O -4.432 -6.006 8.923
C 3.893 -0.672 -7.539
N 4.241 -0.981 -8.830
C 4.285 -2.316 -8.957
N 3.994 -2.862 -7.770
C 3.730 -1.862 -6.870
C 3.855 -4.298 -7.481
C 2.375 -4.675 -7.412
C 4.482 -0.005 -9.887
H 5.344 -0.315 -10.501
H 4.706 0.971 -9.433
H 3.587 0.096 -10.527
H 4.529 -2.883 -9.860
H 3.462 -2.080 -5.833
H 3.790 0.357 -7.194
H 4.378 -4.867 -8.278
H 4.356 -4.506 -6.526
H 2.253 -5.728 -7.094
H 1.853 -4.031 -6.685
H 1.896 -4.549 -8.402
O 16.736 14.671 -7.048
N 15.786 15.361 -6.633
O 15.957 16.513 -6.153
O 14.590 14.873 -6.665
C 7.397 -0.280 15.864
N 8.402 0.531 15.401
C 7.988 1.805 15.443
N 6.738 1.829 15.926
C 6.347 0.542 16.206
C 5.875 3.014 16.051
C 5.711 3.457 17.506
C 9.668 0.050 14.858
H 9.475 -0.385 13.859
H 10.083 -0.724 15.508
H 10.377 0.892 14.756
H 8.593 2.677 15.196
H 5.363 0.311 16.594
H 7.510 -1.366 15.907
H 6.314 3.822 15.423
H 4.881 2.748 15.608
H 4.942 4.242 17.558
H 5.398 2.620 18.139
H 6.658 3.865 17.901
O -4.723 -2.221 -8.673
N -3.900 -2.033 -7.743
O -2.758 -2.613 -7.788
O -4.180 -1.296 -6.766
C -7.055 4.638 -7.992
N -6.759 5.629 -7.092
C -7.619 5.558 -6.064
N -8.466 4.542 -6.292
C -8.135 3.954 -7.486
C -9.592 4.136 -5.431
C -9.986 2.679 -5.661
C -5.689 6.616 -7.231
H -5.959 7.529 -6.669
H -5.566 6.861 -8.306
H -4.745 6.217 -6.843
H -7.600 6.222 -5.191
H -8.681 3.101 -7.868
H -6.480 4.494 -8.917
H -9.289 4.294 -4.379
H -10.441 4.812 -5.634
H -10.843 2.414 -5.035
H -10.253 2.511 -6.711
H -9.140 2.010 -5.403
O 3.548 -7.399 -13.338
N 4.782 -7.725 -13.233
O 5.596 -7.384 -14.119
O 5.173 -8.347 -12.203
C -6.040 -2.894 7.342
N -5.287 -2.977 8.491
C -5.845 -3.878 9.312
N -6.928 -4.390 8.711
C -7.073 -3.788 7.480
C -7.818 -5.422 9.271
C -8.531 -6.200 8.166
C -4.076 -2.212 8.768
H -3.890 -2.235 9.858
H -4.206 -1.171 8.421
H -3.216 -2.656 8.231
H -5.472 -4.139 10.293
H -7.882 -4.047 6.808
H -5.821 -2.172 6.548
H -7.205 -6.096 9.884
H -8.545 -4.931 9.938
H -9.182 -6.967 8.595
H -9.140 -5.528 7.549
H -7.786 -6.692 7.514
O 7.737 14.864 -10.333
N 7.499 14.103 -9.350
O 7.711 14.507 -8.172
O 7.040 12.936 -9.549
C 8.952 -6.821 14.660
N 8.405 -6.761 13.400
C 7.080 -6.597 13.518
N 6.764 -6.563 14.820
C 7.917 -6.693 15.556
C 5.417 -6.305 15.364
C 5.313 -4.894 15.951
C 9.164 -6.806 12.152
H 8.609 -7.399 11.393
H 10.138 -7.266 12.331
H 9.326 -5.779 11.764
H 6.355 -6.535 12.690
H 7.921 -6.675 16.637
H 10.014 -6.941 14.822
H 4.695 -6.412 14.538
H 5.188 -7.068 16.120
H 4.259 -4.657 16.152
H 5.894 -4.799 16.874
H 5.691 -4.155 15.225
O -1.288 5.557 -12.995
N -1.655 4.623 -13.782
O -2.228 4.881 -14.843
O -1.373 3.411 -13.455
C 7.308 -10.526 2.642
N 6.203 -10.557 3.455
C 5.144 -10.104 2.766
N 5.548 -9.782 1.532
C 6.892 -10.038 1.423
C 4.702 -9.206 0.472
C 3.929 -10.282 -0.297
C 6.180 -10.982 4.852
H 5.777 -12.000 4.933
H 5.538 -10.292 5.434
H 7.209 -10.970 5.252
H 4.135 -10.002 3.138
H 7.434 -9.845 0.499
H 8.299 -10.807 3.008
H 4.001 -8.489 0.935
H 5.377 -8.647 -0.210
H 3.272 -9.796 -1.050
H 4.611 -10.956 -0.829
H 3.292 -10.869 0.374
O 9.900 1.612 -13.777
N 9.932 0.351 -13.900
O 10.950 -0.291 -13.505
O 8.920 -0.268 -14.333
C 16.513 -6.906 -1.660
N 17.256 -7.984 -2.050
C 16.457 -9.051 -2.144
N 15.206 -8.681 -1.829
C 15.216 -7.345 -1.513
C 14.038 -9.570 -1.730
C 12.792 -8.942 -2.360
C 18.676 -7.934 -2.376
H 18.794 -7.440 -3.362
H 19.086 -8.946 -2.411
H 19.194 -7.329 -1.615
H 16.762 -10.047 -2.427
H 14.316 -6.803 -1.231
H 16.961 -5.914 -1.513
H 14.295 -10.521 -2.214
H 13.876 -9.781 -0.644
H 11.876 -9.444 -2.001
H 12.729 -7.878 -2.084
H 12.808 -9.002 -3.454
O 0.686 -3.994 14.835
N 1.935 -4.201 15.059
O 2.378 -5.361 15.136
O 2.699 -3.201 15.207
C -3.407 12.580 -4.078
N -3.648 12.156 -2.794
C -3.405 13.172 -1.949
N -3.012 14.235 -2.668
C -3.012 13.896 -3.996
C -2.587 15.542 -2.123
C -3.520 16.022 -1.012
C -4.101 10.809 -2.448
H -3.510 10.080 -3.025
H -5.160 10.674 -2.722
H -3.974 10.638 -1.365
H -3.488 13.153 -0.855
H -2.770 14.627 -4.772
H -3.532 11.914 -4.945
H -1.555 15.425 -1.730
H -2.543 16.264 -2.961
H -3.156 16.966 -0.597
H -4.533 16.183 -1.395
H -3.566 15.277 -0.196
O -3.451 4.927 9.395
N -2.575 4.875 10.296
O -1.884 5.921 10.563
O -2.383 3.813 10.943
C 22.041 4.560 1.051
N 20.787 4.837 0.561
C 20.894 5.196 -0.724
N 22.187 5.160 -1.073
C 22.926 4.768 0.021
C 22.724 5.562 -2.382
C 24.011 4.809 -2.722
C 19.530 4.744 1.297
H 18.760 4.335 0.622
H 19.212 5.760 1.632
H 19.675 4.106 2.177
H 20.057 5.478 -1.352
H 24.002 4.663 -0.027
H 22.195 4.255 2.085
H 21.950 5.374 -3.138
H 22.905 6.648 -2.360
H 24.442 5.188 -3.653
H 24.748 4.934 -1.920
H 23.817 3.739 -2.842
O -8.009 8.785 2.901
N -8.392 7.847 3.652
O -7.643 6.804 3.773
O -9.460 7.911 4.286
C 0.677 20.337 -6.862
N 0.255 19.929 -5.617
C 0.919 18.814 -5.285
N 1.770 18.513 -6.274
C 1.630 19.437 -7.282
C 2.701 17.372 -6.283
C 3.764 17.510 -5.187
C -0.821 20.512 -4.818
H -0.413 21.005 -3.928
H -1.501 19.699 -4.503
H -1.367 21.244 -5.418
H 0.827 18.280 -4.345
H 2.221 19.383 -8.204
H 0.268 21.210 -7.353
H 2.120 16.450 -6.144
H 3.147 17.328 -7.297
H 4.598 16.799 -5.343
H 4.192 18.518 -5.187
H 3.314 17.327 -4.189
O -2.983 13.563 3.158
N -2.922 14.113 2.013
O -2.110 15.047 1.810
O -3.653 13.677 1.070
C 18.739 1.143 7.458
N 19.527 1.835 6.568
C 19.533 3.132 6.908
N 18.765 3.286 7.998
C 18.253 2.066 8.357
C 18.471 4.570 8.660
C 18.028 4.368 10.108
C 20.213 1.273 5.406
H 21.006 0.590 5.729
H 20.640 2.094 4.809
H 19.488 0.696 4.797
H 20.053 3.932 6.362
H 17.564 1.964 9.192

H 18.570 0.061 7.375
H 19.369 5.201 8.595
H 17.670 5.065 8.089
H 17.786 5.330 10.569
H 17.127 3.725 10.136
H 18.816 3.890 10.700
O -8.505 -3.696 -0.946
N -8.608 -2.534 -0.489
O -9.686 -1.900 -0.528
O -7.575 -1.981 0.051
C 10.297 -10.154 -0.756
N 10.933 -9.988 0.453
C 10.507 -8.843 1.007
N 9.617 -8.273 0.180
C 9.461 -9.074 -0.922
C 8.939 -6.978 0.411
C 7.458 -7.137 0.755
C 11.970 -10.868 0.983
H 11.967 -10.806 2.087
H 12.962 -10.540 0.610
H 11.781 -11.897 0.668
H 10.834 -8.427 1.962
H 8.780 -8.828 -1.744
H 10.457 -11.019 -1.384
H 9.487 -6.468 1.223
H 9.037 -6.366 -0.507
H 7.003 -6.127 0.826
H 6.924 -7.711 -0.026
H 7.325 -7.651 1.717
O 3.395 9.495 -15.662
N 3.600 8.263 -15.568
O 4.724 7.834 -15.124
O 2.709 7.427 -15.876
C -1.914 -4.324 -10.766
N -1.854 -4.678 -9.440
C -3.097 -4.933 -9.008
N -3.952 -4.753 -10.021
C -3.240 -4.375 -11.132
C -5.411 -4.924 -9.919
C -6.075 -5.011 -11.291
C -0.667 -4.631 -8.594
H -0.770 -5.331 -7.748
H -0.549 -3.608 -8.194
H 0.236 -4.881 -9.178
H -3.376 -5.238 -8.000
H -3.724 -4.171 -12.078
H -1.015 -4.054 -11.333
H -5.587 -5.838 -9.324
H -5.813 -4.063 -9.338
H -7.162 -5.080 -11.182
H -5.844 -4.125 -11.893
H -5.730 -5.895 -11.838
O 15.706 8.003 -6.259
N 14.722 7.846 -7.030
O 14.330 8.791 -7.778
O 14.073 6.757 -7.015
C 11.799 14.997 10.448
N 13.052 15.507 10.212
C 12.987 16.360 9.175
N 11.715 16.415 8.759
C 10.952 15.572 9.530
C 11.203 17.279 7.680
C 10.243 16.515 6.772
C 14.276 15.099 10.897
H 14.020 14.626 11.848
H 14.920 15.967 11.070
H 14.808 14.368 10.263
H 13.833 16.871 8.694
H 9.891 15.405 9.321
H 11.611 14.253 11.225
H 10.692 18.135 8.149
H 12.073 17.679 7.118
H 9.717 17.220 6.100
H 10.781 15.782 6.146
H 9.492 15.977 7.377
O 14.352 14.400 -0.431
N 15.533 14.831 -0.221
O 16.416 14.025 0.215
O 15.800 16.035 -0.413
C -0.307 15.742 5.594
N 0.307 15.484 6.795
C 0.020 14.225 7.165
N -0.762 13.680 6.224
C -0.985 14.601 5.232
C -1.269 12.293 6.240
C -1.170 11.666 4.853
C 1.139 16.429 7.535
H 0.556 16.919 8.323
H 1.538 17.176 6.829
H 1.997 15.895 7.985
H 0.347 13.718 8.084
H -1.606 14.368 4.355
H -0.204 16.694 5.090
H -0.683 11.733 6.992
H -2.317 12.312 6.576
H -1.569 10.641 4.864
H -1.767 12.253 4.126
H -0.126 11.643 4.482
O 16.717 -9.135 0.601
N 15.850 -9.214 1.523
O 16.144 -8.897 2.699
O 14.658 -9.569 1.236
C 4.894 -9.159 -6.073
N 4.142 -10.208 -5.602
C 4.965 -11.183 -5.197
N 6.230 -10.792 -5.417
C 6.215 -9.531 -5.961
C 7.447 -11.547 -5.066
C 8.157 -12.111 -6.304
C 2.690 -10.219 -5.477
H 2.366 -9.360 -4.858
H 2.365 -11.166 -5.008
H 2.216 -10.133 -6.470
H 4.631 -12.119 -4.756
H 7.138 -8.978 -6.160
H 4.436 -8.246 -6.435
H 8.119 -10.860 -4.519
H 7.151 -12.355 -4.386
H 8.976 -12.767 -5.995
H 7.470 -12.693 -6.927
H 8.591 -11.306 -6.922
O 2.029 17.704 -11.312
N 2.481 17.905 -10.168
O 2.246 17.068 -9.223
O 3.190 18.921 -9.904
C -0.347 -3.501 9.029
N -1.062 -4.185 8.078
C -1.432 -3.327 7.112
N -0.951 -2.110 7.426
C -0.271 -2.192 8.612
C -1.178 -0.865 6.664
C -0.881 0.366 7.519
C -1.408 -5.601 8.148
H -1.397 -6.032 7.127
H -2.421 -5.726 8.586
H -0.662 -6.141 8.773
H -1.962 -3.597 6.191
H 0.237 -1.332 9.066
H 0.081 -3.991 9.904
H -0.539 -0.866 5.755
H -2.231 -0.856 6.330
H -1.070 1.276 6.929
H -1.519 0.397 8.408
H 0.175 0.382 7.852
O 1.708 -4.551 -10.522
N 1.389 -3.321 -10.592
O 1.724 -2.529 -9.675
O 0.693 -2.920 -11.571
C -0.460 14.487 -10.105
N -1.240 14.423 -8.977
C -1.416 15.664 -8.499
N -0.757 16.517 -9.295
C -0.152 15.813 -10.304
C -0.679 17.975 -9.105
C -0.774 18.720 -10.437
C -1.743 13.198 -8.367
H -2.812 13.286 -8.151
H -1.200 12.991 -7.426
H -1.575 12.358 -9.067
H -1.978 15.930 -7.597
H 0.469 16.315 -11.047
H -0.236 13.591 -10.679
H -1.482 18.265 -8.414
H 0.286 18.210 -8.606
H -0.698 19.800 -10.277
H 0.052 18.407 -11.096
H -1.724 18.512 -10.940
O 18.427 12.497 4.375
N 17.417 11.761 4.563
O 17.214 10.783 3.753
O 16.616 11.978 5.492
C 1.728 -8.046 -11.087
N 2.360 -7.437 -10.034
C 1.648 -7.645 -8.918
N 0.570 -8.382 -9.234
C 0.598 -8.649 -10.579
C -0.431 -8.912 -8.290
C -0.089 -10.345 -7.876
C 3.622 -6.715 -10.142
H 3.484 -5.811 -10.767
H 4.372 -7.362 -10.633
H 3.966 -6.396 -9.150
H 1.891 -7.262 -7.918
H -0.173 -9.231 -11.066
H 2.173 -8.026 -12.087
H -0.451 -8.244 -7.405
H -1.427 -8.848 -8.765
H -0.807 -10.697 -7.120
H -0.121 -11.028 -8.731
H 0.919 -10.391 -7.428
O 0.906 -12.212 -3.932
N 1.853 -13.052 -3.717
O 1.837 -13.758 -2.684
O 2.814 -13.113 -4.535
C -9.409 -0.469 3.212
N -8.459 -0.241 2.248
C -9.076 0.123 1.115
N -10.397 0.136 1.331
C -10.634 -0.230 2.631
C -11.391 0.523 0.316
C -12.818 0.443 0.853
C -7.015 -0.349 2.426
H -6.609 -1.108 1.729
H -6.787 -0.615 3.471
H -6.547 0.624 2.199
H -8.589 0.375 0.186
H -11.635 -0.290 3.036
H -9.147 -0.771 4.217
H -11.145 1.553 -0.009
H -11.257 -0.147 -0.547
H -13.529 0.744 0.078
H -13.064 -0.578 1.165
H -12.951 1.105 1.715
O 21.227 9.498 0.689
N 20.873 8.316 0.471
O 21.040 7.775 -0.648
O 20.290 7.658 1.414
C 6.425 9.790 -13.564
N 5.664 10.696 -12.870
C 6.437 11.297 -11.951
N 7.675 10.789 -12.043
C 7.697 9.851 -13.041
C 8.831 11.162 -11.210
C 9.447 12.496 -11.648
C 4.240 10.936 -13.090
H 3.641 10.442 -12.295
H 3.945 10.510 -14.069
H 4.034 12.011 -13.074
H 6.141 12.057 -11.234
H 8.598 9.299 -13.279
H 5.993 9.142 -14.339
H 8.483 11.237 -10.160
H 9.557 10.331 -11.281
H 10.376 12.677 -11.099
H 9.678 12.490 -12.718
H 8.759 13.331 -11.435
O 21.123 3.753 3.854
N 21.503 4.830 4.380
O 20.809 5.346 5.329
O 22.524 5.431 3.964
C -1.157 7.793 -14.586
N -1.792 8.464 -13.570
C -1.045 9.521 -13.219
N 0.053 9.540 -13.987
C 0.013 8.471 -14.846
C 1.149 10.515 -13.852
C 0.617 11.932 -13.632
C -3.043 8.062 -12.930
H -3.225 8.716 -12.052
H -2.964 7.014 -12.597
H -3.877 8.156 -13.634
H -1.284 10.246 -12.436
H 0.835 8.247 -15.529
H -1.567 6.878 -15.015
H 1.766 10.201 -12.986
H 1.791 10.437 -14.746
H 1.445 12.625 -13.457
H 0.055 12.284 -14.504
H -0.053 11.957 -12.755
O 0.256 -0.090 4.117
N 0.668 -0.838 3.172
O 0.921 -2.045 3.390
O 0.815 -0.351 2.010
C 0.877 -12.290 -0.266
N 0.459 -10.998 -0.475
C -0.091 -10.529 0.656
N -0.035 -11.491 1.587
C 0.566 -12.601 1.037
C -0.450 -11.344 2.993
C 0.589 -10.533 3.782
C 0.685 -10.225 -1.694
H -0.040 -9.400 -1.742
H 0.598 -10.879 -2.588
H 1.710 -9.789 -1.669
H -0.552 -9.554 0.769
H 0.718 -13.513 1.598
H 1.324 -12.892 -1.072
H -1.439 -10.838 3.016
H -0.574 -12.348 3.418
H 0.169 -10.167 4.736
H 1.477 -11.135 4.008
H 0.911 -9.664 3.189
O 11.389 -4.413 -11.992
N 11.859 -5.245 -11.165
O 11.403 -6.422 -11.104
O 12.768 -4.876 -10.354
C -5.512 11.189 -9.675
N -5.263 10.001 -9.037
C -5.835 10.032 -7.826
N -6.460 11.208 -7.678
C -6.268 11.954 -8.818
C -7.165 11.644 -6.461
C -8.450 12.402 -6.797
C -4.478 8.890 -9.563
H -3.703 8.618 -8.816
H -3.987 9.194 -10.510
H -5.123 7.996 -9.742
H -5.844 9.220 -7.096
H -6.677 12.951 -8.925
H -5.091 11.407 -10.654
H -7.366 10.739 -5.860
H -6.483 12.286 -5.882
H -8.911 12.797 -5.887
H -8.233 13.241 -7.470
H -9.175 11.748 -7.292

O -8.622 4.657 0.815
N -9.288 3.562 0.733
O -9.108 2.680 1.633
O -10.063 3.360 -0.210
C 0.566 -0.144 17.627
N 0.602 -1.339 16.947
C 0.695 -1.088 15.632
N 0.720 0.242 15.458
C 0.637 0.851 16.681
C 0.791 1.003 14.194
C -0.476 0.849 13.345
C 0.549 -2.665 17.559
H -0.309 -2.732 18.235
H 1.467 -2.853 18.127
H 0.457 -3.414 16.757
H 0.720 -1.871 14.867
H 0.649 1.939 16.760
H 0.496 -0.092 18.705
H 0.941 2.058 14.492
H 1.688 0.683 13.618
H -0.591 1.729 12.694
H -0.408 -0.049 12.699
H -1.376 0.757 13.969
O 19.146 -5.746 -0.332
N 19.071 -4.657 -0.992
O 17.923 -4.270 -1.407
O 20.088 -3.994 -1.248
C 6.796 16.647 -0.935
N 7.656 16.933 0.097
C 7.087 16.560 1.252
N 5.878 16.036 0.980
C 5.678 16.072 -0.374
C 4.927 15.488 1.968
C 3.495 15.507 1.434
C 8.957 17.579 -0.049
H 9.650 16.933 -0.642
H 9.381 17.764 0.952
H 8.840 18.522 -0.593
H 7.541 16.686 2.235
H 4.767 15.694 -0.838
H 7.066 16.864 -1.976
H 5.238 14.448 2.191
H 5.007 16.078 2.900
H 2.783 15.178 2.207
H 3.218 16.521 1.096
H 3.396 14.824 0.570
O -3.918 6.050 -10.831
N -5.020 5.576 -10.477
O -5.991 6.354 -10.199
O -5.176 4.324 -10.330
C 1.691 -4.820 -15.085
N 1.705 -5.126 -13.746
C 2.949 -4.953 -13.276
N 3.729 -4.538 -14.284
C 2.971 -4.451 -15.424
C 5.192 -4.364 -14.214
C 5.713 -3.391 -15.269
C 0.559 -5.604 -12.980
H 0.169 -4.781 -12.341
H 0.875 -6.443 -12.333
H -0.223 -5.940 -13.665
H 3.262 -5.079 -12.236
H 3.399 -4.146 -16.371
H 0.795 -4.891 -15.686
H 5.443 -4.025 -13.184
H 5.640 -5.371 -14.343
H 6.814 -3.374 -15.245
H 5.393 -3.699 -16.272
H 5.351 -2.373 -15.090
O 5.153 -9.686 -3.022
N 6.199 -9.866 -2.315
O 6.705 -10.996 -2.205
O 6.703 -8.863 -1.708
C 6.122 17.191 -7.637
N 7.375 17.294 -8.192
C 7.248 17.311 -9.526
N 5.946 17.229 -9.836
C 5.222 17.145 -8.675
C 5.372 17.220 -11.195
C 6.451 17.010 -12.254
C 8.624 17.408 -7.447
H 9.452 17.034 -8.056
H 8.573 16.816 -6.508
H 8.814 18.455 -7.184
H 8.055 17.394 -10.239
H 4.125 17.065 -8.668
H 5.956 17.116 -6.560
H 4.624 16.416 -11.237
H 4.831 18.169 -11.341
H 5.998 16.920 -13.246
H 7.154 17.851 -12.273
H 7.017 16.094 -12.038
O 5.442 -9.169 10.029
N 5.879 -8.410 10.930
O 5.265 -7.342 11.231
O 6.970 -8.680 11.524
C -4.191 -10.253 7.271
N -4.451 -9.449 6.190
C -3.341 -8.770 5.874
N -2.370 -9.121 6.731
C -2.876 -10.051 7.614
C -0.974 -8.643 6.676
C -0.249 -8.790 8.018
C -5.717 -9.354 5.473
H -5.499 -9.119 4.409
H -6.319 -8.535 5.910
H -6.263 -10.297 5.551
H -3.232 -8.042 5.065
H -2.271 -10.482 8.402
H -4.940 -10.898 7.710
H -0.445 -9.235 5.894
H -0.984 -7.582 6.329
H 0.838 -8.895 7.856
H -0.395 -7.903 8.671
H -0.602 -9.681 8.553
O -3.250 10.812 -11.620
N -2.615 11.828 -11.192
O -3.218 12.856 -10.837
O -1.340 11.759 -11.097
C 11.672 10.412 -1.250
N 12.319 10.377 -0.043
C 12.288 11.601 0.505
N 11.637 12.423 -0.335
C 11.230 11.700 -1.428
C 11.396 13.867 -0.151
C 10.309 14.387 -1.092
C 12.983 9.191 0.485
H 13.331 9.401 1.508
H 13.837 8.932 -0.178
H 12.278 8.343 0.486
H 12.696 11.875 1.484
H 10.707 12.152 -2.277
H 11.552 9.521 -1.860
H 11.121 14.043 0.914
H 12.352 14.403 -0.354
H 10.284 15.500 -1.068
H 10.507 14.083 -2.135
H 9.316 14.010 -0.797
O 9.121 -11.654 4.897
N 10.259 -11.250 4.507
O 10.349 -10.514 3.474
O 11.286 -11.540 5.166
C 21.557 10.131 3.310
N 22.059 8.870 3.524
C 21.078 8.095 3.997
N 19.962 8.825 4.104
C 20.231 10.106 3.676
C 18.666 8.279 4.548
C 18.451 6.878 3.970
C 23.411 8.399 3.232
H 23.452 7.321 3.440
H 24.141 8.925 3.857
H 23.646 8.582 2.178
H 21.175 7.043 4.267
H 19.477 10.904 3.662
H 22.157 10.936 2.909
H 18.661 8.244 5.650
H 17.865 8.987 4.244
H 17.445 6.513 4.199
H 18.586 6.877 2.864
H 19.190 6.177 4.398
O -1.766 7.786 5.356
N -2.159 8.397 4.345
O -3.101 9.256 4.435
O -1.657 8.173 3.200
C -4.584 7.047 -0.398
N -4.760 6.846 0.950
C -6.047 7.073 1.258
N -6.697 7.415 0.136
C -5.811 7.413 -0.911
C -8.154 7.645 0.060
C -8.542 8.470 -1.164
C -3.722 6.417 1.883
H -4.197 6.022 2.805
H -3.055 7.257 2.162
H -3.115 5.624 1.406
H -6.511 6.989 2.249
H -6.135 7.637 -1.935
H -3.617 6.867 -0.882
H -8.636 6.643 0.029
H -8.455 8.138 1.002
H -9.627 8.597 -1.206
H -8.077 9.461 -1.141
H -8.210 7.959 -2.091
O 9.004 18.210 2.893
N 8.683 19.080 3.780
O 8.067 20.120 3.433
O 8.956 18.853 4.984
C 9.748 -10.748 9.533
N 9.560 -11.303 8.291
C 8.721 -10.520 7.593
N 8.376 -9.477 8.365
C 9.000 -9.593 9.576
C 7.447 -8.400 7.974
C 7.768 -7.092 8.687
C 10.172 -12.538 7.804
H 10.617 -12.356 6.802
H 9.415 -13.326 7.721
H 10.949 -12.855 8.503
H 8.404 -10.709 6.561
H 8.845 -8.858 10.370
H 10.392 -11.201 10.274
H 7.512 -8.277 6.869
H 6.414 -8.730 8.231
H 6.932 -6.387 8.583
H 7.930 -7.274 9.767
H 8.681 -6.618 8.272
O 1.128 3.671 15.811
N 2.369 3.549 16.063
O 3.056 4.539 16.392
O 2.910 2.401 15.922
C 1.462 4.050 -14.653
N 2.170 5.047 -14.023
C 3.343 5.208 -14.647
N 3.406 4.336 -15.663
C 2.245 3.602 -15.689
C 4.585 4.119 -16.515
C 5.176 5.432 -17.036
C 1.736 5.763 -12.832
H 1.992 5.181 -11.919
H 0.637 5.892 -12.858
H 2.217 6.746 -12.777
H 4.127 5.928 -14.392
H 2.068 2.829 -16.424
H 0.468 3.743 -14.320
H 5.344 3.590 -15.899
H 4.295 3.448 -17.334
H 6.250 5.310 -17.246
H 4.673 5.771 -17.947
H 5.073 6.228 -16.270
O 15.542 17.987 5.439
N 14.887 17.857 6.511
O 13.848 18.537 6.720
O 15.242 16.979 7.365
C 13.116 15.325 -3.093
N 13.873 16.239 -3.790
C 13.356 16.376 -5.019
N 12.287 15.576 -5.127
C 12.116 14.908 -3.940
C 11.576 15.320 -6.391
C 10.149 14.831 -6.173
C 15.067 16.928 -3.299
H 15.815 16.952 -4.106
H 15.461 16.406 -2.414
H 14.811 17.956 -3.001
H 13.743 17.032 -5.785
H 11.308 14.187 -3.786
H 13.345 15.049 -2.054
H 11.590 16.248 -6.981
H 12.175 14.566 -6.952
H 9.662 14.595 -7.128
H 10.140 13.922 -5.541
H 9.539 15.611 -5.668
O 7.003 -8.202 4.945
N 5.858 -7.711 5.183
O 5.739 -6.742 5.985
O 4.833 -8.242 4.672
C 4.127 18.900 1.620
N 5.143 19.670 1.108
C 5.681 20.390 2.102
N 5.037 20.091 3.241
C 4.061 19.166 2.969
C 5.356 20.676 4.559
C 4.785 19.847 5.706
C 5.561 19.678 -0.293
H 6.273 20.489 -0.462
H 4.666 19.807 -0.931
H 6.035 18.712 -0.548
H 6.507 21.080 2.008
H 3.430 18.740 3.756
H 3.551 18.224 0.976
H 6.458 20.738 4.619
H 4.958 21.703 4.583
H 4.963 20.347 6.662
H 3.707 19.688 5.581
H 5.261 18.848 5.737
O -4.693 -7.145 -7.972
N -3.667 -7.838 -8.237
O -3.305 -8.768 -7.469
O -2.952 -7.530 -9.243

Vita

Van Quan Vuong was born in Haiphong, Vietnam. He completed his Bachelor of Science in chemistry at the VNUHCM - University of Science, HCM, Vietnam, in September 2011. He worked for the Institute for Computational Science and Technology (ICST), HCM, Vietnam as an assistant researcher from October 2011 to September 2015. He completed his Master of Science in chemistry at the Nagoya University, Nagoya, Japan, in September 2017. He completed his Doctor of Philosophy in Energy Science and Engineering at the University of Tennessee, Knoxville, US, in July 2021. His Ph.D. dissertation was titled "Development of Density-Functional Tight-Binding Methods for Chemical Energy Science" under the supervision of Dr. Stephan Irle.